U.PORTO Universidade de Aveiro
Departamento de Electrónica, Telecomunicações e Informática,
2018

Isiaka Ajewale Alimi

Otimização do Fronthaul Ótico para Redes de Acesso de Rádio (baseadas) em Computação em Nuvem (CC-RANs)

Optimization of Optical Fronthaul for Cloud Computing Radio Access Networks (CC-RANs)

Universidade de Aveiro
Departamento de Electrónica, Telecomunicações e Informática,
2018

Isiaka Ajewale Alimi

Optimization of Optical Fronthaul for Cloud Computing Radio Access Networks (CC-RANs)

"A new type of thinking is essential if mankind is to survive and move toward higher levels."

— Albert Einstein

Isiaka Ajewale Alimi

Otimização do Fronthaul Ótico para Redes de Acesso de Rádio (baseadas) em Computação em Nuvem (CC-RANs)

Tese apresentada às Universidades de Minho, Aveiro e Porto para cumprimento dos requisitos necessários à obtenção do grau de Doutor em Engenharia Eletrotécnica/Telecomunicações no âmbito do programa doutoral MAP-Tele, realizada sob a orientação científica do Doutor António Luís Jesus Teixeira, Professor Associado do Departamento de Eletrónica, Telecomunicações e Informática da Universidade de Aveiro, e do Doutor Paulo Miguel Nepomuceno Pereira Monteiro, Professor Associado do Departamento de Eletrónica, Telecomunicações e Informática da Universidade de Aveiro.

Apoio financeiro da Fundação para a Ciência e a Tecnologia (FCT) através da bolsa PD/BD/52590/2014.

Isiaka Ajewale Alimi

Optimization of Optical Fronthaul for Cloud Computing Radio Access Networks (CC-RANs)

A thesis submitted to the Unversidade do Minho, Aveiro and Porto in partial fulfilment of the requirements for Doctoral degree in Engenharia Eletrotécnica/Telecomunicações under the MAP-Tele doctoral program. The thesis was conducted under the supervisions of Professor Dr. António Luís Jesus Teixeira, Associate Professor of the Departamento de Eletrónica, Telecomunicações e Informática, Universidade de Aveiro and Professor Dr. Paulo Miguel Nepomuceno Pereira Monteiro, Associate Professor of the Departamento de Eletrónica, Telecomunicações e Informática, Universidade de Aveiro.

This work is supported by the Fundação para a Ciência e a Tecnologia (FCT) under the grant PD/BD/52590/2014.

o júri / the jury

presidente / president

Doutor José Rodrigues Ferreira da Rocha
Professor Catedrático da Universidade de Aveiro (por delegação do Reitor da Universidade de Aveiro)

vogais / examiners committee

Doutor António Luís Jesus Teixeira
Professor Associado com agregação da Universidade de Aveiro (orientador)

Doutor Paulo Miguel Nepomuceno Pereira Monteiro
Professor Associado da Universidade de Aveiro (co-orientador)

Doutor Maria do Carmo Raposo de Medeiros
Professora Associada da Universidade de Coimbra

Doutor Henrique Manuel de Castro Faria Salgado
Professor Associado da Universidade do Porto

Doutor Paulo Sérgio de Brito André
Professor Associado com Agregação do Instituto Superior Técnico

Doutor Mário José Neves de Lima
Professor Auxiliar da Universidade de Aveiro

agradecimentos / acknowledgements

First and foremost, I thank God Almighty for the blessings He has bestowed upon me and for giving me the strength and wisdom in the course of this research work.

I would like to acknowledge the MAP-tele Doctoral Program in Telecommunications being supported by the three Portuguese Universities that have strong tradition in the area of Telecommunications Engineering for initiating my journey to Portugal for a great achievement.

The work presented in this thesis was carried out in the Optical Communications and Photonics Research Group within the Instituto de Telecomunicações (IT), Department of Electronics, Telecommunications and Informatics, Universidade de Aveiro, Portugal. I acknowledge the Institution for the offered conducive atmosphere.

I am sincerely indebted to my supervisor and co-supervisor Professor Luís Jesus Teixeira and Professor Paulo Miguel Nepomuceno Pereira Monteiro, respectively, for the usual guidance, attention, motivation and constant enthusiasm during this work. I am able to weather the trying period through their indispensable opinions, advices and inspirational discussions that helped me to have profound perceptions of different tasks.

I am also using this medium to genuinely thank the Fundação para a Ciência e a Tecnologia for the precious financial support in order to complete this thesis.

I would also like to thank Abdelgader Mahmoud, Ali Shahpari, Vitor Ribeiro, Artur Sousa, Issa Elfergani, Abubakar Hussaini, Daniel Malafaia, João Almeida and Cátia Pinho who are my colleagues at IT, not only for all the fruitful discussions and friendliness but also for sharing their experiences with me.

My family would like to thank Oluyomi Aboderin of Universidade do Porto and his family. Without them, we will not even know about the MAP-tele Doctoral Program.

To conclude, I would like to acknowledge my wife - Biola, and my daughter-Fatima, for the unflinching support, understanding, patience, encouragement and *love* throughout the duration of this work.

Resumo

A proliferação de diversos tipos de dispositivos moveis, aplicações e serviços com grande necessidade de largura de banda têm contribuído para o aumento de ligações de banda larga e ao aumento do volume de trafego das redes de telecomunicações moveis. Este aumento exponencial tem posto uma enorme pressão nos mobile operadores de redes móveis (MNOs). Um dos aspetos principais deste recente desenvolvimento, é a necessidade que as redes têm de oferecer baixa complexidade nas ligações, como também baixo consumo energético, muito baixa latência e ao mesmo tempo uma grande capacidade por baixo usto. De maneira a resolver estas questões, os MNOs têm focado a sua atenção na redes de acesso por rádio em nuvem (C-RAN) principalmente devido aos seus benefícios em termos de otimização de performance e relação qualidade preço. O standard para a distribuição de sinais sem fios por um fronthaul C-RAN é o common public radio interface (CPRI). No entanto, ligações óticas baseadas em interfaces CPRI necessitam de uma grande largura de banda. Estes requerimentos podem também ser atingidos com uma implementação em ligação free space optical (FSO) que é um sistema ótico que usa comunicação sem fios. O FSO tem sido uma alternativa muito apelativa aos sistemas de comunicação rádio (RF) pois combinam a flexibilidade e mobilidade das redes RF ao mesmo tempo que permitem a elevada largura de banda permitida pelo sistema ótico. No entanto, as ligações FSO são suscetíveis a alterações atmosféricas que podem prejudicar o desempenho do sistema de comunicação. Estas limitações têm evitado o FSO de ser tornar uma excelente solução para o fronthaul. Uma caracterização precisa do canal e tecnologias mais avançadas são então necessárias para uma implementação pratica de ligações FSO. Nesta tese, vamos estudar uma implementação eficiente para fronthaul baseada em tecnologia á rádio-sobre-FSO (RoFSO). Propomos expressões em forma fechada para mitigação das perdas de propagação e para a estimação da capacidade do canal de maneira a aliviar a complexidade do sistema de comunicação. Simulações numéricas são também apresentadas para formatos de modulação adaptativas. São também considerados esquemas como um sistema hibrido RF/FSO e tecnologias de transmissão apoiadas por retransmissores que ajudam a alivar os requerimentos impostos por um backhaul/fronthaul de C-RAN. Os modelos propostos não só reduzem o esforço computacional, como também têm outros méritos, tais como, uma elevada precisão na estimação do canal e desempenho, baixo requisitos na capacidade de memória e uma rápida e estável operação comparativamente com o estado da arte em sistemas analíticos (PON)-FSO. Este sistema é implementado num recetor em tempo real que é emulado através de uma field-programmable gate array (FPGA) comercial. Permitindo assim um sistema aberto, interoperabilidade, portabilidade e também obedecer a standards de software aberto. Os esquemas híbridos têm a habilidade de suportar diferentes aplicações, serviços e múltiplos operadores a partilharem a mesma infraestrutura de fibra ótica.

Keywords

Atmospheric turbulence, backhaul, channel capacity, cloud radio access network (C-RAN), diversity techniques, free space optical (FSO) communication, fronthaul, next-generation networks (NGNs), passive optical network (PON), relay-assisted transmission, repetition coding, hybrid RF/FSO technology, scintillation, space-time coding.

Abstract

The proliferation of different mobile devices, bandwidth-intensive applications and services contribute to the increase in the broadband connections and the volume of traffic on the mobile networks. This exponential growth has put considerable pressure on the mobile network operators (MNOs). In principal, there is a need for networks that not only offer low-complexity, low-energy consumption, and extremely low-latency but also high-capacity at relatively low cost. In order to address the demand, MNOs have given significant attention to the cloud radio access network (C-RAN) due to its beneficial features in terms of performance optimization and cost-effectiveness. The de facto standard for distributing wireless signal over the C-RAN fronthaul is the common public radio interface (CPRI). However, optical links based on CPRI interfaces requires large bandwidth. Also, the aforementioned requirements can be realized with the implementation of free space optical (FSO) link, which is an optical wireless system. The FSO is an appealing alternative to the radio frequency (RF) communication system that combines the flexibility and mobility offered by the RF networks with the high-data rates provided by the optical systems. However, the FSO links are susceptible to atmospheric impairments which eventually hinder the system performance. Consequently, these limitations prevent FSO from being an efficient standalone fronthaul solution. So, precise channel characterizations and advanced technologies are required for practical FSO link deployment and operation. In this thesis, we study an efficient fronthaul implementation that is based on radio-on-FSO (RoFSO) technologies. We propose closed-form expressions for fading-mitigation and for the estimation of channel capacity so as to alleviate the system complexity. Numerical simulations are presented for adaptive modulation scheme using advanced modulation formats. We also consider schemes like hybrid RF/FSO and relay-assisted transmission technologies that can help in alleviating the stringent requirements by the C-RAN backhaul/fronthaul. The propose models not only reduce the computational requirements/efforts, but also have a number of diverse merits such as high-accuracy, low-memory requirements, fast and stable operation compared to the current state-of-the-art analytical based approaches. In addition to the FSO channel characterization, we present a proof-of-concept experiment in which we study the transmission capabilities of a hybrid passive optical network (PON)-FSO system. This is implemented with the real-time receiver that is emulated by a commercial field-programmable gate array (FPGA). This helps in facilitating an open system and hence enables interoperability, portability, and open software standards. The hybrid schemes have the ability to support different applications, services, and multiple operators over a shared optical fiber infrastructure.

— To the memory of
my dear parents.

Contents

Contents i

List of Figures v

List of Tables vii

List of Acronyms viii

1 Introduction 1
- 1.1 Cellular Base Station Architectural Evolution . . . 2
  - 1.1.1 Conventional Macro BS Architecture . . . 2
  - 1.1.2 Distributed BS Architecture . . . 3
  - 1.1.3 Centralized RAN Architecture . . . 3
- 1.2 Cloud Computing-Based RANs (CC-RANs) . . . 4
  - 1.2.1 Cloud Radio Access Network (C-RAN) . . . 4
    - 1.2.1.1 Mobile Backhaul (MBH) . . . 5
    - 1.2.1.2 Mobile Fronthaul (MFH) . . . 7
  - 1.2.2 Heterogeneous Cloud Radio Access Network (H-CRAN) . . . 7
  - 1.2.3 Fog Radio Access Network (F-RAN) . . . 8
- 1.3 Motivation and Justification . . . 10
- 1.4 Aim and Objectives . . . 11
- 1.5 Thesis Organization . . . 11
- 1.6 Main Research Contributions . . . 13
- 1.7 List of Publications . . . 14
  - 1.7.1 Book Chapters . . . 14
  - 1.7.2 Journal Papers . . . 15
  - 1.7.3 Conference Papers . . . 16
  - 1.7.4 Posters . . . 16

2 Mobile Fronthaul Transport Solutions 17
- 2.1 Introduction . . . 17
  - 2.1.1 CPRI Concepts and Requirements . . . 18
    - 2.1.1.1 CPRI Data-rate . . . 18
    - 2.1.1.2 Latency in the Fronthaul . . . 20
  - 2.1.2 Fronthaul Transport Technologies . . . 20
    - 2.1.2.1 Dedicated Fiber . . . 21
    - 2.1.2.2 Microwave . . . 21

2.1.2.3 Optical Transmission Network (OTN) . . . 22
2.1.2.4 CPRI over Ethernet (CoE) . . . 22
2.1.2.5 Wavelength based Systems . . . 22
2.1.2.6 Passive Optical Network (PON) . . . 24
2.2 PON Architectures . . . 25
2.2.1 Gigabit-class PON (GPON) . . . 25
2.2.2 10 Gigabit-class PON (XG-PON) . . . 26
2.2.3 Next-generation PON stage 2 (NG-PON2) . . . 26
2.3 Optical Access Technologies . . . 27
2.3.1 Time Division Multiplexed PON (TDM-PON) System . . . 27
2.3.2 Wavelength Division Multiplexed PON (WDM-PON) System . . . 28
2.3.3 Time and Wavelength Division Multiplexed PON (TWDM-PON) System 29
2.4 Centralized RAN Architecture Modifications . . . 31
2.4.1 Split-processing . . . 31
2.4.2 Bandwidth Compression Techniques . . . 32
2.4.3 Radio over Ethernet (RoE) . . . 32
2.5 Evolution towards Efficient Fronthaul for the 5G Network and Beyond . . . 34
2.5.1 Radio-over-Fiber (RoF) Technologies . . . 34
2.5.1.1 Analog RoF . . . 35
2.5.1.2 Digitized RoF . . . 35
2.5.2 D-IFoF with Bandpass Sampling Technique . . . 38
2.5.3 Broadband OFDM Transmission in Fiber-Wireless Links . . . 38
2.5.4 Frequency-Division Multiplexed Radio-over-Fiber (FDM RoF) . . . 39
2.5.5 MFH Interface Based on Aggregated RoF/CW . . . 39
2.5.6 Software-Defined Fronthaul (SDF) . . . 41
2.6 Research Contributions . . . 42
2.7 Conclusion . . . 42

3 Free Space Optical Communication Systems 44
3.1 Introduction . . . 44
3.2 Block Diagram of OWC System . . . 46
3.3 Safety and Regulations . . . 47
3.4 OWC System Classification . . . 48
3.4.1 Visible Light Communication (VLC) Systems . . . 49
3.4.1.1 Huge Bandwidth . . . 49
3.4.1.2 Low Power Consumption . . . 49
3.4.1.3 Low Cost . . . 49
3.4.1.4 No Health Concerns . . . 50
3.4.1.5 Ubiquitous Computing . . . 50
3.4.1.6 Inherent Security . . . 51
3.4.1.7 Indoor Localization . . . 51
3.4.2 Terrestrial Free Space Optical (FSO) Communications . . . 51
3.5 Radio-on-free space optical (RoFSO) . . . 53
3.6 Optical System and Channel Model . . . 54
3.6.1 Atmospheric Attenuation . . . 54
3.6.2 Pointing Error or Misalignment Fading . . . 55
3.6.3 Atmospheric Turbulence . . . 56

3.6.3.1 Log-normal Distribution (LN) . . . 56
3.6.3.2 Gamma-Gamma (ΓΓ) Distribution . . . 57
3.6.3.3 Málaga ($\mathcal{M}$)-Distribution . . . 59
3.6.4 Combined Attenuation Statistics . . . 60
3.7 Performance Analysis . . . 61
3.7.1 BER . . . 61
3.7.2 Ergodic Channel Capacity . . . 62
3.8 Simulation Results and Discussions . . . 63
3.9 Research Contributions . . . 65
3.9.1 First Contribution . . . 65
3.9.2 Second Contribution . . . 65
3.10 Conclusion . . . 66

4 FSO Turbulence-Induced Fading Mitigation 67
4.1 Introduction . . . 67
4.2 System Model . . . 68
4.3 FSO Link with Diversity Techniques . . . 70
4.3.1 Modified OSTBCs for FSO Communication . . . 70
4.3.2 Repetition Coding for FSO Communication . . . 71
4.4 Approximate Closed-Form Expressions . . . 72
4.4.1 Approximate Expression for Modified OSTBCs . . . 72
4.4.2 Approximate Expression for Repetition Coding . . . 73
4.5 Numerical Results and Discussions . . . 74
4.6 Research Contributions . . . 76
4.6.1 First Contribution . . . 76
4.6.2 Second Contribution . . . 76
4.7 Conclusion . . . 77

5 Computational-Efficient Estimation of MIMO-FSO System Capacity 78
5.1 Introduction . . . 78
5.2 Spatial Interpolation System Models . . . 79
5.2.1 Barycentric Lagrange interpolation . . . 79
5.2.2 Precomputed B-spline Weights . . . 82
5.3 Power Series Representation System Model . . . 83
5.4 Model Validation and Simulation Speed Analysis . . . 85
5.5 Research Contributions . . . 87
5.5.1 First Contribution . . . 87
5.5.2 Second Contribution . . . 87
5.6 Conclusion . . . 88

6 Technologies for Performance Enhancement 89
6.1 Introduction . . . 89
6.2 Hybrid RF/FSO Technology . . . 90
6.3 Relay-assisted FSO Transmission . . . 91
6.4 System and Channel Models . . . 92
6.5 Performance Analysis . . . 93
6.5.1 Outage Probability . . . 93

6.5.2 Average Symbol Error Probability (ASEP) . . . 95
6.5.3 Ergodic Channel Capacity . . . 95
6.6 Results and Discussion . . . 96
6.6.1 Outage Performance for $\mathcal{M}$-distributed Fading . . . 96
6.6.2 Outage Performance for $\Gamma\Gamma$-distributed Fading . . . 97
6.6.3 ASEP with $\Gamma\Gamma$-distributed Fading . . . 99
6.6.4 Ergodic Channel Capacity with $\Gamma\Gamma$-Distributed Fading . . . 99
6.7 Research Contributions . . . 100
6.8 Conclusion . . . 100

7 Channel Characterization and Hybrid PON-FSO System 101
7.1 Introduction . . . 101
7.2 Channel Measurement and Characterization . . . 103
7.2.1 Experimental Setup . . . 103
7.2.2 Experimental Results . . . 103
7.3 Real-Time Coherent PON OWC based on Dual-Polarization for the Mobile Backhaul/Fronthaul . . . 105
7.3.1 Experimental Setup . . . 105
7.3.2 Experimental Results . . . 106
7.4 Research Contributions . . . 107
7.4.1 First Contribution . . . 107
7.4.2 Second Contribution . . . 107
7.5 Conclusion . . . 108

8 Conclusion 109
8.1 Concluding Remarks . . . 110
8.2 Future Work . . . 112
8.2.1 Link Adaptation Technology . . . 112
8.2.2 Multi-Hop High-Altitude Platform FSO Communication . . . 112

List of Figures

1.1 Schematic of C-RAN architecture. 6
1.2 Schematic of (a) MBH architecture for D-RAN (b) MFH architecture for C-RAN. 6
1.3 Schematic of H-CRAN architecture. 8
1.4 Schematic of F-RAN architecture. 9

2.1 Implementations of CWDM networks for separating BSs from ONUs (a) with CWDM splitter (b) with CWDM over standard PON to form virtual PONs. . 23
2.2 Implementation of DWMD feeder network using dedicated wavelength channels assigned to each BS and ONU. 24
2.3 PON architecture. 25
2.4 MFH based on TDM-PON System. 28
2.5 MFH based on WDM-PON System. 30
2.6 MFH based on TWDM-PON and DWDM-PON overlay sharing the same ODN simultaneously. 30
2.7 Schematic of (a) existing RE and REC (b) native RoE RE and existing REC (c) existing RE and native RoE REC (d) native RoE RE and REC 33
2.8 Schematic of (a) RoF (b) IFoF (c) BBoF (d) D-RoF (e) D-IFoF (f) DSP-RoF transport scheme. 36

3.1 Block diagram of a terrestrial OWC system. 46
3.2 Response of the human eye at different wavelengths. 48
3.3 Electromagnetic spectrum. 50
3.4 Optical wireless communication system classification 50
3.5 A scenario for OWC system deployment for access networks. 52
3.6 Atmospheric turbulence mitigation techniques 53
3.7 Log-normal pdf for different values of log-irradiance variance using (a) linear scale and (b) logarithmic scale. 57
3.8 Gamma-gamma pdf for weak-strong turbulence regimes using (a) linear scale and (b) logarithmic scale. 59
3.9 (a) Average BER versus SNR for BPSK under different turbulence conditions at 1550 nm, (b) BER against average received irradiance with different wavelength values, (c) BER against average received irradiance with different constellation sizes, (d) BER against average received irradiance with different refractive index values, (e) BER against average received irradiance with different refractive index values and constellation sizes, (f) Average channel capacity of FSO link versus average electrical SNR. 64

4.1 Block diagram of modified OSTBCs for FSO communication. 71
4.2 (a) Performance comparison of OSTBC for different number of transmit apertures and standard deviation, (b) Performance comparison of RC for different number of transmit apertures and standard deviation, (c) Performance comparison of diversity schemes for different number of transmit apertures, (d) Performance comparison of diversity schemes for different number of transmit apertures, (e) Performance comparison of spatial diversity scheme with spatial correlation among the apertures. 75

5.1 Block diagram of $M \times N$ MIMO FSO system. L: laser, C: collimator, PD: photodetector, Tx: transmitter, Rx: receiver. 80
5.2 Average channel capacity versus the average SNR for (a) $2 \times N$, (b) $10 \times N$ schemes, (c) $2 \times N$, (d) $10 \times N$. EE: exact expression, SL: second order Lagrange, QS: quadratic spline, TL: third order Lagrange, CS: cubic spline. . 85
5.3 Average channel capacity versus the average SNR for (a) $10 \times N$, (b) $M \times N$. 86

6.1 Diagram of a mixed RF/FSO dual-hop communication system. 92
6.2 Outage performance of a mixed RF/FSO wireless communication system with Rayleigh and $\mathcal{M}$-distributed fading considering (a) scattering power coupled to the LOS component, (b) pointing errors at the FSO links, (c) pointing errors at the FSO links and different $N_s \times N_d$ combinations. 97
6.3 A dual-hop multiuser mixed RF/FSO wireless communication system (a) outage performance considering the impact of pointing errors at the FSO links, (b) outage performance considering different atmospheric conditions. 98
6.4 A dual-hop multiuser mixed RF/FSO wireless communication system (a) ASEP considering different atmospheric conditions (b) Ergodic channel capacity considering different atmospheric conditions. 99

7.1 Experimental setup. The inset presents the picture of outdoor FSO setup, ILMZ: Integrated Laser Mach Zehnder. 104
7.2 Histogram of normalized irradiance with log-normal and gamma-gamma fits under different scintillation index values. 104
7.3 (a) Experimental setup for 20×625 Mbaud DP-QPSK signal; (b) Overall spectrum (PBS: polarization beam splitter; BPD: balanced photodetector; CoRX: coherent receiver). 106
7.4 Receiver sensitivity in terms of BER measured for DP-QPSK signals. 107

List of Tables

2.1 List of CPRI interface rates/options with applications 19
2.2 Timing and latency requirements for CPRI and 3GPP specifications 21
2.3 CPRI vs. Ethernet 32
2.4 Comparison of RoF transport schemes features 40
2.5 Innovative fronthaul interfaces 41
2.6 Experimental efforts toward an efficient MFH 42

3.1 Approximations required for generating different distribution models from $\mathcal{M}$-distribution model 60

5.1 Computation time (s) analysis of the models 87
5.2 NMSE (dB) for MIMO FSO configurations 87
5.3 NMSE for different MIMO FSO aperture configurations. 87

List of Acronyms

10G-EPON	10Gigabit Ethernet PON
3GPP	3rd Generation Partnership Project
5G	Fifth Generation
ADC	Analog to Digital Conversion
a-MFH	analog Mobile Fronthaul
AR	Adaptive-Rate
ARQ	Automatic Repeat Request
ASEP	Average Symbol Error Probability
AWG	Arbitrary Waveform Generator
AWGN	Additive White Gaussian Noise
B2B	Back-to-Back
B^2**LUT**	B-spline and Barycentric Lagrange interpolation Lookup Table
BBU	Base Band Unit
BER	Bit Error Ratio
BPSK	Binary Phase-Shift Keying
BS	Base Station
BTS	Base Transceiver Station
CA	Carrier Aggregation
CAPEX	Capital Expenditure
CC-RAN	Cloud Computing-based RAN
CO	Central Office
CO_2	Carbon Dioxide
CoE	CPRI over Ethernet

CoMP	Coordinated Multiple Point
CPRI	Common Public Radio Interface
C-RAN	Cloud Radio Access Network
CRRM	Cooperative Radio Resource Management
CRSP	Collaboration Radio Signal Processing
CW	Control Word
CWDM	Coarse Wavelength-Division Multiplexing
D2D	Device-to-Device
DAC	Digital to Analog Conversion
DAS	Distributed Antenna System
DBA	Dynamic Bandwidth Allocation
DLC	Data Link Control
d-MFH	digital Mobile Fronthaul
DP	Dual-Polarization
DP-QPSK	Dual-Polarization Quadrature Phase Shift Keying
DPt	Demarcation Point
D-RoF	Digital Radio over Fiber
DS	Downstream
DSP	Digital Signal Processing
DSP-ARoF	Digital Signal Processing Analog RoF
DU	Digital Unit
DWBA	Dynamic Wavelength and Bandwidth Allocation
DWDM	Dense Wavelength-Division Multiplexing
e2e	End-to-End
ECL	External Cavity Laser
EE	Energy Efficiency
eICIC	enhanced Inter-Cell Interference Cancellation
eNB	evolved Node B
EPC	Evolved Packet Core

EPON	Ethernet-PON
F-APs	Fog-computing-based Access Points
FBA	Fixed Bandwidth Allocation
FEC	Forward Error Correction
FPGA	Field-Programmable Gate Array
F-RAN	Fog Computing Based Radio Access Network
FSAN	Full Service Access Network
FSO	Free Space Optical
FTTH	Fiber To The Home
GPON	Gigabit-PON
G-PON	Gigabit-capable PON
GPS	Global Positioning System
HAP	High-Altitude Platform
H-CRAN	Heterogeneous Cloud Radio Access Network
HD-FEC	Hard-Decision Forward Error Correction
HetNet	Heterogeneous Network
hybrid PON-FSO	hybrid Passive Optical Network Free Space Optics
IEEE	Institute of Electrical and Electronics Engineers
ILMZ	Integrated Laser Mach Zehnder
IM/DD	Intensity-Modulation/Direct-Detection
IoT	Internet of Things
IQM	IQ modulator
ITU	International Telecommunication Union
ITU-T	ITU Telecommunication Standardization Sector
LD	Laser Diode
LED	Light-Emitting Diode
LO	Local Oscillator
LPNs	Low Power Nodes
LTE	Long Term Evolution

LTE-A	LTE Advanced
Massive MIMO	Massive Multiple-Input Multiple-Output
MBH	Mobile Backhaul
MBS	Macro Base Station
MEC	Mobile Edge Computing
MeNB	Master eNB
MFH	Mobile Fronthaul
MIMO	Multiple-Input Multiple-Output
mixed RF/FSO	mixed Radio Frequency/Free Space Optical
MME	Mobility Management Entity
mm-wave	Millimeter-Wave
MNOs	Mobile Network Operators
mobile DBA	mobile Dynamic Bandwidth Allocation
M-QAM	M-ary Quadrature Amplitude Modulation
NFV	Network Function Virtualization
NGNs	Next-Generation Networks
NG-PON2	Next-Generation Passive Optical Network stage 2
NG-PON3	Future Next Generation PON System
NRZ	Non-Return-to-Zero
OAM	Operation, Administration, and Maintenance
OAN	Optical Access Networks
OBSAI	Open Base-Station Initiatives
ODN	Optical Distribution Network
OFDM	Orthogonal Frequency Division Multiplexing
OLT	Optical Line Terminal
OMCI	ONU Management Control Interface
ONT	Optical Network Terminal
ONU	Optical Network Unit
OOK	ON–OFF-Keying

OPEX	Operational Expenditure
OSTBC	Orthogonal Space-Time Block Code
OTN	Optical Transmission Network
OWC	Optical Wireless Communication
PAPR	Peak-to-Average Power
PAs	Power Amplifiers
PBC	Polarization Beam Combiner
PD	Photo-Detector
PHY	Physical
PON	Passive Optical Network
PRBS	Pseudo Random Bit Sequence
PS	Power Supply
PtMP	Point-to-MultiPoint
PtP	Point-to-Point
PtP WDM	Point-to-Point Wavelength Division Multiplexed
QAM	Quadrature Amplitude Modulation
QoE	Quality of Experience
QoS	Quality of Service
RAN	Radio Access Network
RAU	Remote Antenna Unit
RC	Repetition Code
RE	Radio Equipment
REC	Radio Equipment Controller
RF	Radio Frequency
RoE	Radio over Ethernet
RoF	Radio over Fiber
RoFSO	Radio-on FSO
RRH	Remote Radio Head
RSP	Radio Signal Processing

RU	Radio Unit
SDF	Software-Defined Fronthaul
SDN	Software-Defined Networking
SE	Spectral Efficiency
SeNB	Secondary eNB
S-GW	Serving Gateway
SISO	Single-Input Single-Output
SNI	Service Node Interface
SNR	Signal-to-Noise-Ratio
SSMF	Standard Single-Mode Fiber
T/H	Track-and-Hold
TCO	Total Cost of Ownership
TDM	Time Division Multiplexing
TDMA	Time-Division Multiple Access
TDM-PON	Time Division Multiplexed PON
TIA	TransImpedance Amplifiers
TSN	Time Sensitive Networking
TWDM-PON	Time and Wavelength Division Multiplexed PON
UDN	Ultra-Dense Network
UDWDM	Ultra-Dense WDM
UE	User Equipment
UNI	User Network Interface
US	Upstream
VLC	Visible Light Communication
VOA	Variable Optical Attenuators
WDM	Wavelength-Division Multiplexing
WDM-PON	Wavelength Division Multiplexed PON
WiMAX	Worldwide interoperability for Microwave Access
XG-PON	10 Gigabit-PON
XG-PON2	10 Gigabit-PON2

Chapter

Introduction

There have been a notable increase in trends for high-bandwidth transmission systems in the cellular mobile networks. The development can be attributed to the high increase in the broadband connections as well as the resulting traffic on yearly basis [1]. The Fifth Generation (5G) wireless system has been noted to be a remarkable technology for supporting the huge system capacity growth and coverage in an efficient manner [2–4]. Moreover, one of the key technologies for the realization of 5G network requirements is Cloud Radio Access Network (C-RAN). C-RAN is an evolving architecture in which cloud computing is being integrated into the Radio Access Network (RAN) [5, 6]. In addition, the C-RAN is a centralized system in which the baseband processing is achieved in the Base Band Unit (BBU) pool. Furthermore, another important component of the C-RAN is the Remote Radio Head (RRH). A number of densely deployed RRHs are connected to the BBU pool by the aids of the fronthaul links. C-RANs have the capacity for enabling cooperative spectrum sensing, improving shared spectrum access, as well as facilitating Device-to-Device (D2D) communications [5]. Additionally, C-RANs are futuristic technologies that have high capabilities for achieving considerable gains in Spectral Efficiency (SE) and Energy Efficiency (EE) for the 5G cellular networks and beyond. However, the majority of C-RAN's challenges are based on the constrained fronthaul. Mainly, the stringent requirements for facilitating centralized processing in the BBU pool are the employment of high bandwidth and low latency fronthaul for the network elements interconnection. Nevertheless, in reality, fronthaul links are capacity and time-delay constrained. Consequently, this eventually results into significant degradations on the C-RAN performance [5, 6].

In general, Common Public Radio Interface (CPRI) or Open Base-Station Initiatives (OBSAI) interface is employed for digital fronthauling in the C-RAN architecture [7, 8]. Nonetheless, large bandwidth is needed by the optical fronthaul in which these interfaces are employed. This is due to the high-resolution bits that are essential for digitalization process of the Radio Frequency (RF) samples [9]. Hence, the related bandwidth inefficiency could limit or make C-RANs impractical to meet the performance requirements of the 5G wireless systems in which Massive Multiple-Input Multiple-Output (Massive MIMO) antenna

systems are envisaged to be integrated [10], [11]. For instance, with Carrier Aggregation (CA) of Long Term Evolution-Advanced (LTE-A) of five 20 MHz mobile signals with 3 sectors, as well as 8×8 Multiple-Input Multiple-Output (MIMO) antennas, about 147.5 Gb/s fronthaul data rate will be needed by the CPRI [12], [13]. Subsequently, for the realization of bandwidth-efficient mobile fronthaul, innovative measures can be implemented. One of such is the implementation of analog optical transmission technique that is based on Radio over Fiber (RoF) technology [7, 11, 14].

The RoF is a scheme whose deployment depends mainly on the availability of the installed optical fiber cables between a number of network elements. Conversely, when cell densification is considered, optical fiber deployment will be capital-intensive and time-consuming. This is even more demanding for installations that involve trenching. Furthermore, acquisition of right-of-way for Base Station (BS) locations could be one of the limiting factors for appropriate network deployment. Therefore, these challenges, in addition to the limited amount of installed optical fiber cables, bring about the recognition of the viability of Free Space Optical (FSO) communication system.

The FSO is a feasible technology that can be used for RF signal transmission without the necessity for the installation of fiber cables. The idea of transmitting the RF signals over FSO channel that is generally known as Radio-on FSO (RoFSO), exploits the high transmission capacity offered by the optical technologies and the ease of deployment of wireless systems [15]. In spite of the fact that FSO is a practical optical technology with various applications, the trade-off between the required data rates and limitations of the atmospheric channel are the main implementation challenges in the access networks. Consequently, these challenges prevent FSO from being a proficient standalone fronthaul solution in the network [15]. Therefore, schemes like relay-assisted transmission technologies can be employed so as to address the associated limitations and enhance the performance of FSO communication in the access networks. This PhD work is an effort to study different enabling technologies for an efficient mobile fronthaul network. Furthermore, it is intended for the optimization of the cloud RAN by profiling viable solutions for alleviating the stringent requirements of the mobile fronthaul.

1.1 Cellular Base Station Architectural Evolution

Mobile networks have progressed from the analog BS technologies into digital radio technologies. Besides, current developments in cellular technologies require substantial upgrading in the mobile network architectures. Therefore, Mobile Network Operators (MNOs) and equipment vendors have been inventing more effective and proactive ways of meeting the stringent network requirements. Fundamentally, the BS performs tasks such as baseband processing and radio functionalities. This section presents the ways by which the architectural evolution splits the functionalities and placement of network elements.

1.1.1 Conventional Macro BS Architecture

The traditional Macro Base Station (MBS) comprises two functional electronic subsystems that are normally located at the base of the tower or in the building. The typical radio electronic subsystems are the Radio Equipment Controller (REC) or Digital Unit (DU) which is also known as the BBU. Also, the other electronic is the Radio Equipment (RE) or Radio Unit (RU). In the traditional MBS architecture, the RU and the BBU are usually placed on

the ground at the base of the BS's mast. Furthermore, the RUs are typically connected to the antennas by heavy and large diameter coaxial feeder cables. This BS architecture has a number of drawbacks such as high deployment costs, large equipment footprint, and high overall power consumption [16]. Furthermore, substantial amount of transmitted power is lost in the coaxial cable.

1.1.2 Distributed BS Architecture

An alternative architecture of the traditional MBS physically splits the BS into two parts which are the BBU and the RRH [17]. The RRHs comprise the RF transmit and receive electronic units such as duplexers, Power Amplifiers (PAs), and low noise amplifiers. Besides, the RRHs help in frequency conversion in addition to Analog to Digital Conversion (ADC) and Digital to Analog Conversion (DAC) [18]. Moreover, the RRHs need compact Power Supply (PS) which helps in reducing the overall power consumption of the BSs [16, 19]. The RRHs are usually mounted and distributed on the mast, consequently, they require short coaxial jumpers to connect them to the antennas [16]. Nevertheless, the connections between the BBU and the RRHs are primarily based on optical fiber, although, microwave connections can be used as well [18]. The process of replacing copper cabling with fiber cabling offers substantial improvements such as better noise interference immunity, higher bandwidth, lower power requirements, and better network coverage [20]. Consequently, in the distributed BS architecture, integration of optical fiber and wireless networks has been an outstanding development in realizing high-speed and cost-effective wireless broadband access networks. Technologies such as the 3rd Generation Partnership Project (3GPP) Long Term Evolution (LTE) and LTE Advanced (LTE-A) have been exploiting lower Capital Expenditure (CAPEX) and Operational Expenditure (OPEX) of the distributed architecture.

1.1.3 Centralized RAN Architecture

The tremendous emergent in the number of mobile subscribers, the proliferation of prevailing applications as well as mobile devices result in the deployment of more BSs by the MNOs. This is done with the aim of meeting the network service requirements. Nonetheless, with an increase in the number of BSs, there is a corresponding upsurge in the energy required by the system. Then, the increase in the energy consumption is not in line with the idea of green communications in which energy efficiency in cellular networks is of utmost importance. In addition, the increase in the harmful greenhouse gas emissions such as Carbon Dioxide (CO_2) emissions, is associated with the off-grid sites which are usually powered by diesel generators. The off-grid sites offer the necessary coverage for the remote areas. Consequently, the quest to minimize the CO_2 emissions and the OPEX have prompted broad research into green communications [21].

It is essential for the distributed BS architecture to realize the goals of green communication networks in cost-effective manners for next-generation wireless networks. The realization of this brought about a new architecture that takes advantage of the optical fibers in the current infrastructure between the Base Transceiver Station (BTS) site and the Central Office (CO). The architecture moves the BBUs from the BSs to the CO or point of concentration. Therefore, this entails shifting specific amount of the radio network control functions from the BS to the CO. This configuration is known as BBU centralization or BBU hosteling with stacking. Generally, the BBU stacking needs a BBU for managing all the RRHs located at

a BTS. For that reason, management of multiple RRHs with a BBU reduces the MNOs' and service providers' expenditures. Moreover, the BBU can communicate with each other within the BBU hostel through the standardized X2 interface [16]. Subsequently, with this arrangement, RRHs can simply be mounted on lampposts or rooftops which brings about an efficient cooling scheme. Moreover, the energy consumption required for air-conditioning and other on-site equipment can be conserved [18].

Additionally, system centralization aids network coordination and management. The impact of this can be appreciated in the inter-cell interference cancellation in the cellular networks based on Coordinated Multiple Point (CoMP) transmission and reception as well as network-MIMO [7, 22, 23]. The CoMP offers cooperative transmission from multiple BSs to a User Equipment (UE) and essentially alleviates interference and transforms it into cooperation gain [24]. Furthermore, there are other advanced centralized RAN implementations that have been presented in order to enhance system performance. We discuss the concepts in the next section.

1.2 Cloud Computing-Based RANs (CC-RANs)

In recent times, there are several research efforts on how RAN SE and EE performances can be further improved. So, an attractive paradigm implementation for the RAN called Cloud Computing-based RAN (CC-RAN) has been presented. The CC-RAN is able to give high SE and EE performances by embedding cloud computing into wireless communication system. The application models of CC-RANs are C-RAN, Heterogeneous Cloud Radio Access Network (H-CRAN), and Fog Computing Based Radio Access Network (F-RAN) [25, 26].

1.2.1 Cloud Radio Access Network (C-RAN)

One of the cost-effective and energy-efficient means of addressing the traffic explosion being experienced in the networks is wireless network densification based on the small-cell concepts. The small-cell systems have various advantages such as more coverage and frequency reuse between small-cell, which eventually lead to system capacity enhancement. Consequently, various advanced technologies such as Distributed Antenna System (DAS), femtocells, Heterogeneous Network (HetNet), picocells, and relay schemes have been implemented in the cellular mobile networks to increase the system coverage and capacity.

The development in the HetNet architecture significantly aids small-cell systems in further enhancement in the system capacity. This is due to the architectural decoupling of control and user planes for better functionalities. Conceptually, HetNet is structured on the deployment of heterogeneous small-cell networks such as femtocells, picocells, and relays overlay on the conventional MBSs. Besides, the HetNet architecture permits deployment of very dense and low-power-small-cells. This implementation results in further effective spatial spectrum reuse. In general, it improves the cellular network performance by enabling deployment of Low Power Nodes (LPNs). Furthermore, deployment of LPNs gives high system capacity and relatively lessen the associated challenges of densely deployed MBSs in the mobile networks. Nevertheless, densely deployed small-cell exhibits a number of challenges concerning inter-cell/inter-tier interference and management issues. This may happen when MBSs and LPNs reuse the same spectral resources as envisaged in the 5G networks and beyond [22, 27, 28]. To address the problems, the C-RAN architectures support effective implementation of innovative Radio Signal Processing (RSP) methods such as CA, CoMP, and enhanced Inter-Cell

Interference Cancellation (eICIC). Consequently, C-RAN architecture facilitates suppression of intra-tier/inter-tier interference [22]. Additionally, C-RAN helps significantly in the reduction of the CAPEX and OPEX of the cellular networks [10]. Hence, C-RANs have gained considerable research interests and have been recognized as an essential part of the 5G network [19, 22, 27–30].

Figure 1.1 depicts the schematic of C-RAN architecture. Generally, the C-RAN architecture is made up of a substantial number of densely deployed as well as distributed low-power and low-cost RRHs. The RRHs are low-complexity network elements that are normally employed for only RF functionalities such as digital to analog conversion, frequency filtering, and power amplification [8]. The centralized BBU is another notable component of C-RAN. The BBUs are clustered as a pool in the C-RAN system architecture. Also, the BBUs comprise high-performance processors as well as real-time virtualization and management technologies [7, 22, 28]. Moreover, the pool aggregates all the BSs' computational resources and manages huge number of RRHs located at different antenna sites. Furthermore, the advancement in the BBU hosteling results in new high-speed and low-latency transmission segments that connect the RRHs on the cell site to the BBUs in the CO. The ensuing connectivity segment is known as fronthaul links [8, 16, 22, 23, 28–31]. So, at this stage, we delve into network connectivity segments such as Mobile Backhaul (MBH) and Mobile Fronthaul (MFH) that are usually employed to support small-cell BSs in the cellular network.

1.2.1.1 Mobile Backhaul (MBH)

In the mobile cellular networks, MBH connects the BSs to the core network typically through an IP/Ethernet based network. Moreover, the evolved Node B (eNB) that signifies the BS in LTE is connected to the other eNB by the X2 interfaces. Furthermore, the eNBs are connected by the backhaul link, S1 interface, to the Evolved Packet Core (EPC). Generally, the connection between the eNB and the Mobility Management Entity (MME) is by means of S1-MME interface. Also, the connection between the eNB and the Serving Gateway (S-GW) is by S1-U interface as depicted in Fig. 1.2 [32]. The S1 interface, being a logical interface, offers a many-to-many relation between the MMEs/S-GWs and the eNBs. The backhaul link acts as the transmission medium for both user data as well as Control and Management (C&M) data between the eNB and the EPC [33]. Furthermore, the backhaul links enable transmission of data, that are exchanged between eNBs for handover and coordinated transmission schemes [32]. In order to permit inter cell cooperation between the BSs, higher layer BS functions are normally concentrated in the master BS, whereas, the lower layer functions are distributed. Consequently, this architecture is called distributed RAN (D-RAN). For example, in LTE, the Master eNB (MeNB) is connected to the Secondary eNB (SeNB) via the X2 interface [33]. Figure 1.2(a) illustrates the MBH based architecture.

One of the major requirements of the next-generation wireless access network is the need for high-speed in addition to low-latency inter-BS communications channels. This enables co-processing operations which are utilized so as to increase the bandwidth by inter-cell interference mitigation via CoMP. The S1, as well as X2 interfaces, require consideration in an LTE deployment for multi-cell joint signal processing. In the C-RAN architectural implementation, the coordination function occurs within the pool of resources. This approach provides substantial simplification of the required synchronization between the eNodeB's [34].

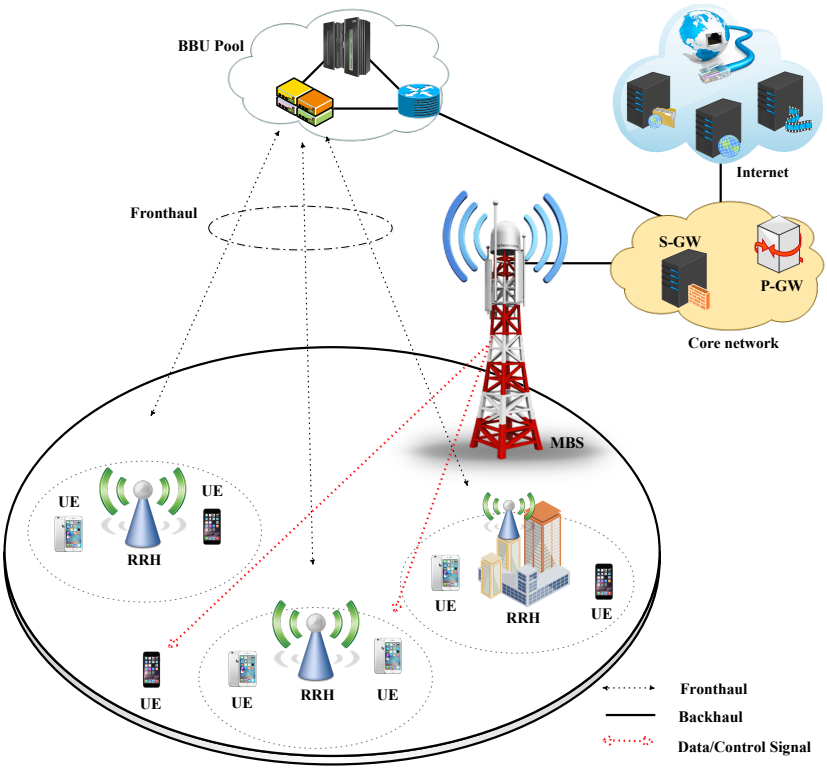

Figure 1.1: Schematic of C-RAN architecture.

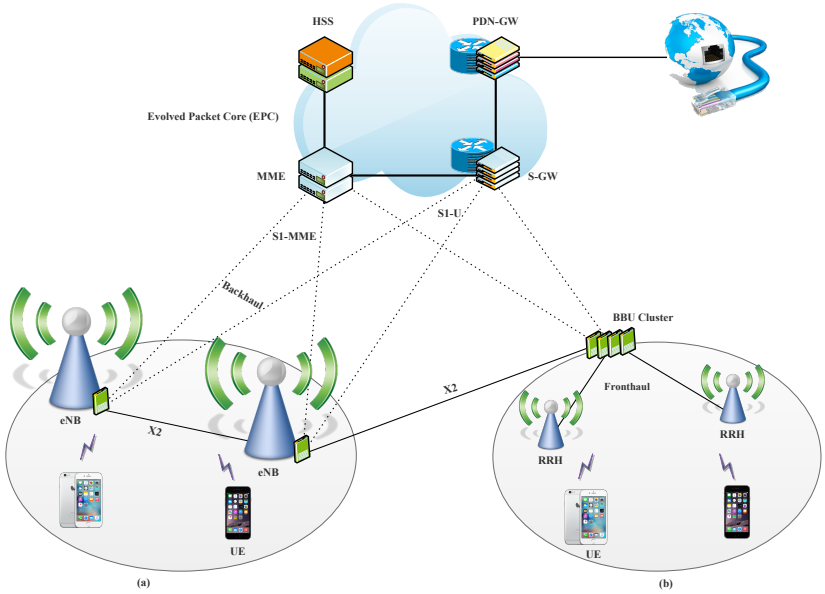

Figure 1.2: Schematic of (a) MBH architecture for D-RAN (b) MFH architecture for C-RAN.

1.2.1.2 Mobile Fronthaul (MFH)

Figure 1.2(b) depicts the MFH based architecture. In the MFH architecture, the BSs baseband signal processing functions are centralized so as to simplify the operation of remote antennas. Furthermore, the architecture supports advanced cooperation between the cells [35–39]. Fundamentally, fiber-optic MFH can be classified into digital Mobile Fronthaul (d-MFH) and analog Mobile Fronthaul (a-MFH) [40]. It should be noted that the transmission between the BBU and the RRHs is usually based on Digital Radio over Fiber (D-RoF) technology in the d-MFH [17]. The de facto standard for connecting the BBU to the RRHs is the CPRI protocol [33]. Nevertheless, the 5G RANs are envisaged to incorporate 100 MHz channels with Massive MIMO. This result in huge capacity demand in the fronthaul network. The demand is highly challenging for the CPRI-based optics and can eventually results in the implementation of the traditional analog radio-over-fiber (A-RoF) transmission technology. With the implementation of A-RoF, expensive ADC and DAC are kept in the centralized DU site [40]. Chapter 2 on page 17 provides a detailed explanation on different transport solutions that can be used for the MFH. Furthermore, the related technical challenges of their implementations are considered.

In the C-RAN architecture, stringent requirements are generally placed on the fronthaul concerning latency, jitter, and bandwidth for multiple duplex radio transmissions. The conditions are even more challenging with the implementation of CoMP scheme [11,19,31]. This condition can be attributed to the fact that, CoMP implementation requires further processing and bandwidth that limit the amount of RRHs that can access the same BBU pool at a time. In order to attend to the aforementioned fronthaul constraints, equipment vendors, MNOs, and research institutions have been proposing various system architectures. The innovative architectures are expected to exploit potential advantages of C-RAN and cloud computing technology. One of such architectures is the H-CRAN which is a promising 5G solution [22].

1.2.2 Heterogeneous Cloud Radio Access Network (H-CRAN)

The RRHs according to C-RAN architectural specification are mainly designed for high capacity in specific areas but not really meant for coverage. However, the MBSs of HetNets are primarily intended for backward compatibility and seamless coverage in wireless networks. Furthermore, the MBSs help in efficient coexistence of multiple RANs and alleviate transportation of control signaling in the network. Consequently, H-CRAN architectures are proposed to integrate MBSs into the C-RANs so as to take advantages of both the HetNets and the C-RANs. This integration enables exploitation of cloud computing technologies, so that the related challenges of HetNets can be attended to [28].

The schematic of H-CRAN architecture is shown in Fig. 1.3. The high-power nodes (HPNs) are employed for seamless coverage and interference mitigation across the network nodes in the H-CRAN architecture [6]. Furthermore, unlike the C-RAN, the HPNs connect with the BBU pool so as to mitigate cross-tier/inter-tier interference across the HPNs and the RRHs. The mitigation is achieved by employing centralized cooperative processing techniques such as cloud-computing-based CoMP (CC-CoMP), large-scale cooperative multiple antenna (LS-CMA), and cloud-computing-based cooperative radio resource management (CC-CRRM). Besides, utilization of HPN alleviates the fronthaul limitations between the RRHs and the BBU pool. Furthermore, the control functionalities of the BBU pool and the RRHs are moved to the HPNs so as to alleviate the fronthaul requirements regarding the ca-

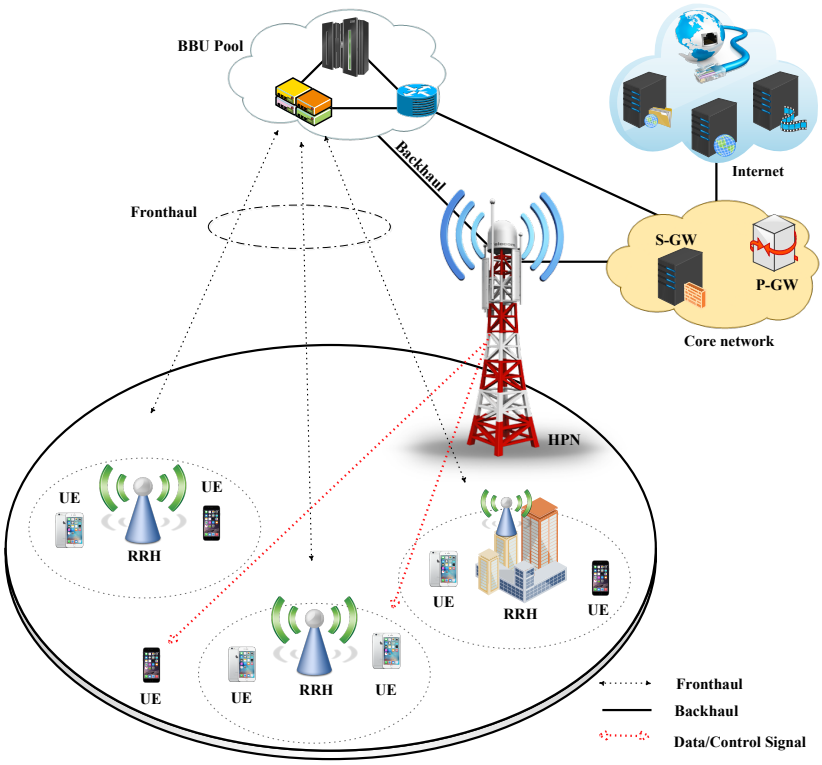

Figure 1.3: Schematic of H-CRAN architecture.

pacity and latency constraints. This can be achieved by supporting control signals, services, and applications with low data rate or high mobility on the heterogeneous HPNs for seamless coverage in the system. Moreover, high data rate or low mobility services and applications are dedicated to the ultra-dense RRHs. In addition, unnecessary handover between BSs can be avoided with the assistance of HPNs [6]. Also, the architecture supports MIMO schemes integration with the HPNs so that system coverage and capacity can be improved [22, 27, 28]. However, the H-CRAN performance is limited by the lack of ability to exploit processing and storage capabilities in the edge devices. Likewise, further burdens are imposed on the backhaul/fronthaul links by the persistent surge in the redundant information in the emerging networks. Therefore, the fronthaul constraints for information exchange between the edge users are worsened. As a result, these challenges lead to the idea of fog RAN (F-RAN) which is an alternative advanced CC-RAN technology [6, 26, 27, 41].

1.2.3 Fog Radio Access Network (F-RAN)

The envisioned stringent requirements like high capacity demand, ultra-low latency, experience continuity, and high reliability for the 5G wireless networks and beyond instigate the necessity for additional localized services within RANs. Furthermore, the service localization has to be in very close proximity to the wireless mobile subscribers. Therefore, this initiates the idea of Mobile Edge Computing (MEC). The MEC intends to combine telco, information technology (IT), and cloud computing with the intention of delivering cloud services straight from the network edge. This concept not only enhances the cloud services availability and

reachability but also minimizes network latency. Conceptually, MEC is based on techniques of extending cloud resources such as computing, storage, and caching to the edge of the networks. This can be realized by deploying cloud servers within or adjacent to the BS. Consequently, the MEC strategy aids in reducing the end-to-end latency as well as enhancing the broadband experiences of the mobile users [42, 43].

Correspondingly, the fog network consists several devices that are accessing the Internet and form a number of small clouds at the edge of the network [27]. Figure 1.4 illustrates the schematic of F-RAN architecture. With the intention of alleviating the challenges of H-CRANs, fog-computing is integrated into the edge devices in the F-RAN. This is achieved by upgrading the traditional RRHs into Fog-computing-based Access Points (F-APs). The upgrade is realized by equipping the F-APs with specific caching, Collaboration Radio Signal Processing (CRSP), and Cooperative Radio Resource Management (CRRM) capabilities. Accordingly, part of radio signal processing as well as resource management can be accomplished locally. In addition, this allows edge devices like F-APs and "smart" user equipment (F-UEs) to exhibit processing potentials for a specific operation. Also, other operations that cannot be effectively executed by the edge devices are managed in the cloud. This idea enables neighboring devices to efficiently share resources such as computing and storage capabilities. Moreover, a group of edge devices with highly correlated traffic to be sent to the cloud can transport it through one of the edge devices. Besides, the cloud with highly correlated traffic which is meant for multiple edge devices can just send it to one edge entity which in turn distributes the traffic to the others [5, 6]. Therefore, this approach reduces the End-to-End (e2e) latency and the network traffic volume to be supported by the MFH and the MBH links [27].

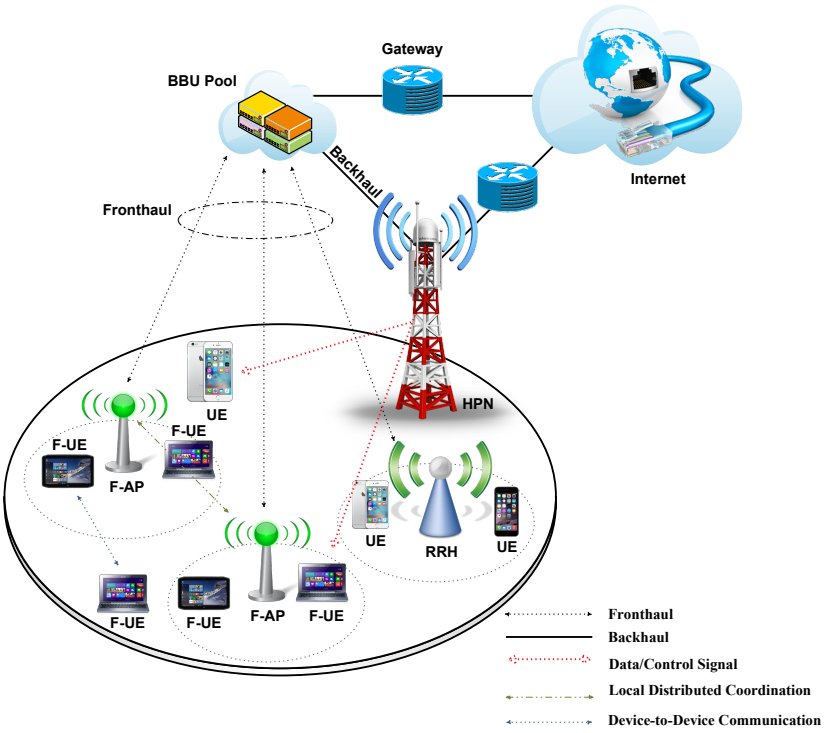

Figure 1.4: Schematic of F-RAN architecture.

Consequently, the spectral utilization and EE of the constrained fronthaul are enhanced. Furthermore, the heavy burdens that full-centralized architecture imposed on the computing resources of the BBU pool, as well as the fronthaul, can be alleviated by the F-RANs. This is due to the fact that certain group of edge devices do not need direct access to the BBU pool. Nevertheless, the reliability of data delivery and mobility management in the network needs further research. Similarly, lack of efficient resource coordination between edge devices may results in interference and can hinder system performance accordingly [6, 27]

Generally, the C-RAN, H-CRAN, and F-RAN are encouraging CC-RAN technologies for accomplishing the requirements of the 5G networks. Nonetheless, owing to the huge amount of heterogeneous devices to be served, considerable traffic burdens are imposed on the MFH and MBH links. This situation limits CC-RAN application efficiency in real-life scenarios. Therefore, effective digital radio signal transmission and reception necessitate compatible and standard interface for connecting the RRHs to the BBU pool by means of an optical fiber.

In practice, the C-RAN architecture demands each RRH with a dedicated connection to the centralized BBU and D-RoF based CPRI is the primary means of distributing baseband samples in the C-RAN fronthaul. However, in 5G networks and beyond, a massive number of RRHs may be deployed at locations that are extremely challenging to be reached by fiber. Therefore, dedicated wired links between individual RRH to the BBU may be impractical. Consequently, an optical wireless fronthaul solution can be a viable complementary and/or alternative technology for better flexibility, high cost-efficiency, and easier deployment of the RRHs [26, 44]. Consequently, FSO communication systems as discussed in Chapter 3 on page 44 are applicable in certain areas within the mobile cellular networks where physical connections by optical fiber cables are impracticable or in the rural area with the shortage of optical fiber infrastructure.

1.3 Motivation and Justification

There have been remarkable influx of various bandwidth-intensive smart devices and applications in the wireless communication systems. For the MNOs to provide ubiquitous wireless access for the vast subscribers, more BSs have to be sited in relation to the small-cell concept. However, studies have shown that the architectural design of BS results in high expenditures which might be quite a limitation for mobile operators in the future. Therefore, implementation of small-cell requires some technical questions such as; how can a cost-effective small-cell architecture be designed and deployed? What are the enabling technologies for providing cost-effective solutions for high-speed fronthaul networks? What is the most efficient way to transport radio information over fiber? What are the technologies that can be employed for backward compatibility for multi-service and multi-operator to coexist in a shared infrastructure? How can we have an adequate system reliability and protection? Consequently, the motivation for this PhD work is how to achieve the envisioned coverage, capacity, and energy-efficiency objectives of the next generation systems with cost-effective architectures and with reduced complexity. This will enable the MNOs to minimize their expenditures while enhancing the Quality of Service (QoS). Moreover, it will make the offered QoS commensurate with the Quality of Experience (QoE) enjoyed by subscribers. To achieve this goal, this PhD work considers the aim and objectives in the next section.

1.4 Aim and Objectives

The aim of this PhD work is to analyze enabling technologies to provide cost-effective solutions for high-speed optical networks and their seamless convergence with wireless networks for the next generation networks. This aim will be achieved through the following objectives which are to:

1. Study enabling technologies to provide cost-effective solutions for the high-speed fronthaul networks;
2. Analyze the most efficient way to transport information in microwave-photonics networks that will support multi-service and multi-operator operations;
3. Evaluate the most relevant sources of transmission impairments on the considered microwave-photonics networks;
4. Consider transmission impairment compensation schemes so as to enhance the system performance in terms of network coverage and capacity;
5. Investigate the proficiency of multiple aperture system in improving the system performance and propose computational-efficient models for optimization of the next-generation networks;
6. Study viable transmission technologies that can be employed for performance optimization of the considered system in the networks;
7. Verify experimentally the turbulence induced fading effect on the system performance and develop an experimental test-bed to validate the concept implementation.

1.5 Thesis Organization

In order to accomplish the aforementioned objectives, the thesis is divided into the enumerated Chapters:

Chapter 2 reviews the state-of-the-art in terms of mobile fronthaul transport solutions. It presents possible methods that can be employed for CPRI transportation. Then, it focuses on the Passive Optical Network (PON) implementations for cost-effective integration of small cells into the network. Moreover, the centralized RAN architectural modifications such as split-processing, bandwidth compression, and Radio over Ethernet that can be employed to address the bandwidth required for digital signal transportation are discussed. Furthermore, evolution towards efficient fronthauls for the 5G network and beyond through different RoF Technology implementations are discussed. Efforts towards Software-Defined Fronthaul (SDF) are considered as well.

Chapter 3 presents Optical Wireless Communication (OWC) as an alternative and/or complementary technology for the wireless RF/fiber solutions. Also, the basic block diagram of OWC system is discussed for clear perception about the concept. Furthermore, the chapter takes into consideration, eye/skin safety from optical radiation and the international standard bodies that regulate optical beam emissions. Moreover,

the chapter focuses on the terrestrial FSO communications and present the concept of RoFSO. Optical system and channel models are presented considering factors such as atmospheric attenuation, misalignment fading, and different atmospheric turbulence conditions. In addition, performance analysis of the considered system is presented.

Chapter 4 addresses the FSO turbulence-induced fading mitigation by presenting performance optimization schemes. Efficient methods for alleviating the turbulence-induced fading and subsequently enhancing the system performance that are based on spatial diversity techniques are presented. Furthermore, the chapter considers effects of spatial correlation between the transmit apertures on the system performance. System models for the studied diversity schemes are presented. In addition, simple approximate closed-form expressions for performance evaluation are proposed. Numerical results and discussions are also presented in this chapter.

Chapter 5 studies ways of realizing computational-efficient MIMO-FSO systems ergodic channel capacity estimation. To achieve this, spatial interpolation system and power series representation models are presented. Furthermore, model validation and simulation speed analysis are considered to show the efficiency of the proposed models.

Chapter 6 focuses on performance optimization schemes for the FSO system implementations. It presents schemes like hybrid RF/FSO and relay-assisted transmission technologies that can be implemented to enhance the performance of FSO technology in the access networks. Moreover, system and channel models for a mixed RF/FSO dual-hop relay system are presented. The chapter also considered different metrics for performance evaluation. In addition, the simulation results are comprehensively discussioned.

Chapter 7 describes means of realizing accurate FSO channel measurements for different weather conditions. To achieve this, Experimental Setup for Channel Measurement and Characterization are presented. Furthermore, results of FSO channel samples are discussed. The chapter considers hybrid schemes that have the ability to support different applications over a shared optical fiber infrastructure. To demonstrate this, an experimental work on a proof-of-concept gigabit-capable, long-reach, hybrid real-time coherent PON and OWC for the mobile backhaul/fronthaul are also presented.

Chapter 8 summarizes the main findings of the research work with concluding comments. In addition, recommendations for future work are outlined.

As enumerated in the following section, most of the concepts discussed in this PhD thesis were either published or submitted for consideration in relevant scientific journals [J1]–[J6]. Furthermore, others are either presented in international conferences [C1]–[C2] or local conferences [C3]. It is noteworthy that, related state-of-the-art are thoroughly discussed in the book chapter [B1] as well as in the tutorial journal [J6]. Consequently, the thesis is written comprehensively in order to complement the published manuscripts that contain largely the information therein. Furthermore, it is noteworthy that all the numerical simulations are implemented in MATLAB® programming language.

1.6 Main Research Contributions

This PhD work has contributed beyond the state-of-the-art on potential solutions for efficient C-RAN fronthauls for the Next-Generation Networks (NGNs) such as the 5G network and beyond. Furthermore, the thesis focuses on feasible means of reducing system complexity, cost, bandwidth requirements, and latency in the fronthaul. Majority of the presented work is published in a book chapter (1 manuscript), six scientific journals (8 papers), two international conferences (2 papers), and a national conference (1 paper) which focused on optical communications and related topics.

- A comprehensible tutorial journal written in a way that is easy to understand by the upcoming researchers and readers outside the specialty of the field is presented. Moreover, the tutorial will be of great help to specialists that are aiming to have better perception of the concepts of the C-RAN MFH. This effort is in an attempt to realize objectives 1 and 2 of this thesis. The work is presented in the journal paper [J6].

- Furthermore, the most relevant sources of transmission impairments on the considered networks are identified. Also, effects of different parameters such as constellation size, wavelength, and refractive index on RoFSO transmissions are suitably classified. Moreover, effects of transmission impairments on different modulation formats for adaptive modulation scheme are characterized under different operating conditions. These activities are based on the fulfilment of objective 3 of this thesis. The work is presented in the conference papers [C1] and [C3].

- In addition, we consider spatial diversity techniques for mitigating turbulence-induced fading in the FSO systems. To distinguish our contributions from others, we derive simple as well as accurate approximate closed-form expressions for the error probability of the turbulence-induced FSO links with Intensity-Modulation/Direct-Detection (IM/DD). This approach helps in preventing the associated analytical complexity of multi-dimensional numerical integration. It also serves as preventive measure for controlling the related upper limit truncation of the multi-dimensional numerical integration. Furthermore, another significant contribution is that we study the effects of spatial correlation between the transmit apertures on the system performance and demonstrated that, realization of the envisioned diversity gains by spatial diversity is contingent on effective separation between the apertures so as to alleviate the associated spatial correlation. This effort is in an attempt to achieve objective 4 of this thesis. The work is presented in the journal paper [J5].

- Moreover, we propose a novel adaptive multivariate precomputed statistical models and a power series representation based model for estimating the ergodic capacity of MIMO FSO system under generalized atmospheric turbulence channels. The models have a number of advantages such as high-accuracy, low memory requirement, fast, and stable operation. They also enhance modeling efficiency considerably without trade-off in accuracy nor complexity. Additionally, the proposed models can reduce the computational time by up to fifteen orders of magnitude and beyond without loss of fidelity compared to the existing models which are based on time-consuming numerical integration. In addition, the models are appropriate for real-time applications in FSO system deployment for fast performance evaluation and system optimization. This effort is in an attempt

to realize objective 5 of this thesis. The work is presented in the journal papers [J3] and [J4].

- Furthermore, considering the small-cell network architectures, we present multiuser mixed RF/FSO relay schemes as feasible ways for realizing optical-wireless convergence in dual-hop communication systems for the cloud-based RANs. We demonstrate that the schemes are viable solutions for wireless system performance optimization. Likewise, we establish that the schemes can efficiently address the last-mile transmission bottleneck and be of great help in alleviating the associated stringent requirement by C-RAN backhaul/fronthaul. These activities are based on the fulfilment of objective 6 of this thesis. The work is presented in the journal papers [J1] and [J2].

- Furthermore, through experimental channel measurements, we characterized the Single-Input Single-Output (SISO) FSO link. Also, based on the measurements, the scintillation effects on the system performance are analyzed over different turbulence conditions for MIMO FSO communication systems. We also present a proof-of-concept experiment on the transmission capabilities of a hybrid Passive Optical Network Free Space Optics (hybrid PON-FSO) system. The experiment is in an effort to validate FSO application in sensitive or hazardous environments where the implementation of RF technology is not permitted. The idea is also relevant in the mobile cellular networks where physical connections through optical fiber cables are unviable or in rural area that lacks fiber infrastructure. In addition, the system implementation on real-time Optical Network Unit (ONU) receiver that is emulated by a commercial Field-Programmable Gate Array (FPGA) enables an open system and hence supports interoperability, portability, and open software standards. This is in an effort to accomplish objective 7 of this thesis. The work is presented in the journal paper [J3], book chapter [B1] and conference paper [C1].

1.7 List of Publications

The following manuscripts are prepared for publication considerations during the course of the PhD work:

1.7.1 Book Chapters

B1 **I. Alimi**, A. Shahpari, A. Sousa, R. Ferreira, P. Monteiro and A. Teixeira, "Challenges and opportunities of optical wireless communication technologies," in *Optical Communication Technology*, P. Pinho, Ed. Rijeka: InTech, 2017, ch. 02.

B2 **I. A. Alimi**, A. M. Abdalla, J. Rodriguez, P. P. Monteiro and A. L. Teixeira, "Energy Efficiency in Cloud Radio Access Network (C-RAN)-Based Green 5G Mobile Wireless Systems: Opportunities and Challenges," to be submitted (the proposal has been accepted by Wiley).

B3 **I. A. Alimi**, N. J. Muga, A. M. Abdalla, J. Rodriguez, P. P. Monteiro and A. L. Teixeira, "Towards a Converged Optical-Wireless Mobile Fronthaul/Backhaul Solutions for the 5G Networks," to be submitted (the proposal has been accepted by Wiley).

1.7.2 Journal Papers

J1 **I. A. Alimi**, P. P. Monteiro, A. L. Teixeira, "Analysis of Multiuser Mixed RF/FSO Relay Networks for Performance Improvements in Cloud Computing-Based Radio Access Networks (CC-RANs)," *Optics Communications*, vol. 402, pp. 653-661, 2017.

J2 **I. A. Alimi**, P. P. Monteiro, A. L. Teixeira, "Outage Probability of Multiuser Mixed RF/FSO Relay Schemes for Heterogeneous Cloud Radio Access Networks (H-CRANs)," *Wireless Personal Communications*,vol. 95, no. 1, pp. 27-41, Jul 2017.

J3 **I. Alimi**, A. Shahpari, V. M. C. Ribeiro, A. Sousa, P. Monteiro, A. Teixeira, "Channel characterization and empirical model for ergodic capacity of free-space optical communication link," *Optics Communications*, vol. 390, pp. 123-129, May, 2017.

J4 **I. A. Alimi**, A. M. Abdalla, J. Rodriguez, P. P. Monteiro and A. L. Teixeira, "Spatial Interpolated Lookup Tables (LUTs) Models for Ergodic Capacity of MIMO FSO Systems," *IEEE Photonics Technology Letters*, vol. 29, no. 7, pp. 583-586, April, 2017.

J5 **I. A. Alimi**, A. Shahpari, P. P. Monteiro and A. L. Teixeira, "Effects of Diversity Schemes and Correlated Channels on OWC Systems Performance," *Journal of Modern Optics*, vol. 64, no. 21, pp. 2298-2305, 2017.

J6 **I. A. Alimi**, A. L. Teixeira and P. P. Monteiro, "Towards an Efficient C-RAN Optical Fronthaul for the Future Networks: A Tutorial on Technologies, Requirements, Challenges, and Solutions," In Press, *IEEE Communications Surveys Tutorials*, 2017.

J7 A. N. Sousa, **I. A. Alimi**, R. M. Ferreira, A. Shahpari, M. Lima, P. P. Monteiro and A. L. Teixeira, "Real-Time Dual-Polarization Transmission based on Hybrid Optical Wireless Communications," *Optical Fiber Technology*, vol. 40, pp. 114-117, Jan 2018.

J8 **I. A. Alimi**, A. O. Mufutau, A. L. Teixeira and P. P. Monteiro, "Performance Analysis of Space-Air-Ground Integrated Network (SAGIN) over an Arbitrarily Correlated Multivariate FSO Channel," In Press, *Wireless Personal Communications*.

J9 **I. A. Alimi**, P. P. Monteiro, A. L. Teixeira, "Effects of Correlated Multivariate FSO Channel on Outage Performance of Space-Air-Ground Integrated Network (SAGIN)," submitted to Physical Communication (Elsevier).

J10 **I. A. Alimi**, P. P. Monteiro, A. L. Teixeira, "Ubiquitous and On-demand Communication based on WiFSO Convergence," to be submitted to Physical Communication (Elsevier).

J11 **I. Alimi**, A. Sousa, A. Almeida, A. Shahpari, P. Monteiro and A. Teixeira, "Gigabits Capable Mobile Backhaul/Fronthaul Networks based on optical FiWi communication Systems," to be submitted.

J12 **I. A. Alimi**, A. M. Abdalla, J. Rodriguez, P. P. Monteiro and A. L. Teixeira, "A Dynamic Programming Model for Ergodic Capacity of MIMO FSO Systems on a Multicore Architecture," to be submitted.

1.7.3 Conference Papers

C1 **I. Alimi**, A. Shahpari, V. Ribeiro, N. Kumar, P. Monteiro and A. Teixeira, "Optical wireless communication for future broadband access networks," *21st European Conference on Networks and Optical Communications (NOC)*, Lisbon, 2016, pp. 124-128.

C2 C. Pinho, A. Shahpari, **I. Alimi**, M. Lima and A. Teixeira, "Optical transforms and CGH for SDM systems," *18th International Conference on Transparent Optical Networks (ICTON)*, Trento, 2016, pp. 1-4.

C3 **I. Alimi**, P. Monteiro, A. Teixeira, "Analysis of Atmospheric Effects on RF Signal Transmission over the Optical Wireless Communication Links," *XIII Symposium on Enabling Optical Networks and Sensors (SEONS)*, Covilhã, Portugal, 2016, pp. 35-38.

1.7.4 Posters

Po1 **I. Alimi**, P. Monteiro and A. Teixeira, "Optimization of Mobile Fronthaul for Cloud Radio Access Network (C-RANs)," *MAP-Tele Workshop*, Universidade do Minho-Guimarães, Braga, 2015, pp. 10.

Po2 **I. Alimi**, P. Monteiro and A. Teixeira, "Optimization of Mobile Fronthaul for Cloud Radio Access Network (C-RANs)," *students & teachers @deti*, Lisbon, 2016.

Po3 **I. Alimi**, P. Monteiro and A. Teixeira, "Optical Wireless Communication for Future Broadband Access Networks," *MAP-Tele Workshop*, Faculdade de Engenharia da Universidade do Porto, 2016, pp. 10.

Po4 **I. Alimi**, P. Monteiro and A. Teixeira, "Analysis of Atmospheric Effects on RF Signal Transmission over the Optical Wireless Communication Links," *XIII Symposium on Enabling Optical Networks and Sensors (SEONS)*, Covilhã, Portugal, 2016.

Po5 **I. Alimi**, P. Monteiro and A. Teixeira, "Optical Wireless Communication for Future Broadband Access Networks," *Research Day*, Rectory Building University of Aveiro, 2017.

Po6 **I. Alimi**, P. Monteiro and A. Teixeira, "Hybrid RF/FSO Communication System for 5G MFH/MBH," *MAP-Tele Workshop*, Instituto de Telecomunicações (IT), Universidade de Aveiro, 2017.

Chapter

Mobile Fronthaul Transport Solutions

The notable increase in the broadband connection requires high-capacity and high-speed communication links so as to support a number of bandwidth-intensive applications and services. Due to its huge aggregate bandwidth, optical link can efficiently support the high bit rate wireless signals in the network. Moreover, the high bandwidth allows multiple wireless services to share the same optical network infrastructure. The inherent bandwidth of optical networks can be efficiently exploited by the RoF so as to give the high throughput required by the CC-RAN's MFH. In addition, RoF has a number of features that support centralized network control and simple Remote Antenna Unit (RAU). These features are in line with the concept of CC-RANs and enable easy maintenance, flexible upgrade, and efficient sharing of resources. Consequently, in this chapter, based on the manuscript [45], comprehensive overview of the MFH transport solutions are discussed. Also, we present different centralized RAN architectural modifications that are required for bandwidth reduction in the MFH. Then, it expatiates on the required evolution towards efficient fronthaul for the 5G network and beyond.

2.1 Introduction

The advent of centralized baseband processing, ease the installation of wireless BSs in different places. The connection between the BBUs and RRHs is normally realized by the digital radio interface which enables the signal transmission over the optical fiber. Furthermore, the introduction of CoMP scheme also results in a new digital interface for connecting the network elements via optical fiber [46]. The RRHs are connected to the BBUs through a high-speed digital fronthaul protocol which is responsible for transmitting the digitized IQ waveforms of the wireless signals. Also, it is used in transmitting the control words (CWs) which are employed for equipment C&M purposes. The two types that are defined by radio equipment manufacturers are CPRI and OBSAI specifications [23]. Both of them contain

vendor-specific elements, therefore, full interoperability is not guaranteed [47]. Also, CPRI specifies the interface between the REC and the RE using layer 1 and layer 2 protocols, whereas OBSAI offers system modularity and interoperability by specifying the internal BS modules. It also specifies the required interface for communication between the modules. The four protocol layers that OBSAI accounts for are the physical, data link, transport and application layers [13, 17].

Furthermore, the European Telecommunications Standards Institute (ETSI) has initiated a new Industry Specification Group (ISG) called open radio interface (ORI) [48]. It is developed in order to have an interface specification which can support multi-vendor interoperability between elements of BSs of the cellular mobile network equipment [47, 49]. However, up to now, CPRI is the widely adopted specification for the fronthaul interface by vendors because of its efficient mapping methods. It is a serial constant bit rate (CBR) interface in which the PHY layer is usually optical fiber and is based on small form pluggable (SFP) connectivity. Also, it is based on the implementation of the digital radio over fiber (D-RoF) concept [23]. In this subsection, we discuss different network requirements using CPRI as a case study.

2.1.1 CPRI Concepts and Requirements

CPRI defines the existing specification for the key internal interface of radio BSs between the Radio Equipment Control (REC) and the Radio Equipment (RE). So, it specifies the PHY layer (L1) and data link layer (L2) for transporting digitized radio information between the REC and the RE. The REC/RE functional split defined by the CPRI is given in [23]. The entire operations above, as well as most of those of the PHY, are executed by the REC. Functionality such as radio signal generation, sampling, and transmission of the resulting data to the RE are performed by the REC. The REC/RE functional split ensures that virtually no digital processing functions are required at the RRHs. So, this approach makes the RRHs to be very small and cheap. Furthermore, the centralized signal processing in the BBU facilitates adoption of advanced schemes like CoMP, which enables concurrent processing of radio signal of several RRHs. Additional study on the main design features, transmission of user plane data, implementation, and requirements of CPRI are presented in [23].

2.1.1.1 CPRI Data-rate

CPRI is a digital protocol which is use for the encapsulation of radio samples between a radio and a digital baseband processing unit. It is not a packet-based interface but signals are multiplexed in a low-latency timeslot-like fashion. Therefore, CPRI specifies a near zero jitter, maximum latency, and near zero bit error rate [48], [57], [58]. CPRI data-rates is from 614.4 Mbit/s (option 1) up to 24.33024 Gbit/s (option 10) over several kilometer distances between the RRHs and the BBU [16], [20], [48], [57]. The interface rates/options for CPRI version 7.0 is shown in Table 2.1. Therefore, the required rate at the fronthaul for the connection between the BBU and RRH depends on the employed technology [59]. The reference configurations that should be supported by the CPRI specification are given in [50]. In the CPRI specification, information such as the digitized radio signals (IQ data), C&M data, signaling, and synchronization required for Global System for Mobile communications (GSM), Worldwide Interoperability for Microwave Access (WiMAX), Universal Mobile Telecommunications System (UMTS), and LTE radio access technologies are defined [47]. Moreover, in

Table 2.1: List of CPRI interface rates/options with applications

Option	Line bit rate (Gbps)	Length of word (bit)	Line coding	Transport Capacity (#WCDMA AxC)	Transport Capacity (#20MHz LTE AxC)	Application (Configuration)	Reference
1	0.6144	8	8B/10B	4	-	• 2G/3G Radios • 10 MHz 1T1R LTE	[50–55]
2	1.2288	16	8B/10B	8	1	• 10 MHz LTE, 2T2R LTE • 20 MHz LTE 1T1R LTE • Small Cells	[50–55]
3	2.4576	32	8B/10B	16	2	• 10MHz 4T4R LTE • 20MHz 2T2R LTE • Small Cells	[50–55]
4	3.0720	40	8B/10B	20	2	• 2×20MHz LTE • Small Cells • 5CA	[50, 51, 55]
5	4.9152	64	8B/10B	32	4	• 10MHz 8T8R LTE • 20MHz 4T4R • 2CA + 2×2 MIMO	[50–55]
6	6.1440	80	8B/10B	40	5	• 5×20MHz LTE	[50, 51, 55]
7	9.8304	128	8B/10B	64	8	• 20MHz 8T8R LTE • 2CA + 4×4 MIMO	[50, 52–55]
7A	8.1100	128	64B/66B	64	8	• 20MHz 8T8R LTE • 4CA + 2×2 MIMO	[50, 55]
8	10.1376	160	64B/66B	80	10	• Carrier aggregation of 5×20MHz 2T2R LTE • 10×20MHz	[50, 51, 53–56]
9	12.1651	192	64B/66B	96	12	• 12×20MHz LTE • 3 CA + 4×4 MIMO	[50–53, 55]
10	24.3302	384	64B/66B	192	24	• 20×20MHz LTE	[50, 51, 55]

principle, multiple radio access technologies (RATs) with multiple antennas are normally employed by different MNOs in the fronthaul network. So, the bit rates can be aggregated into multiple tens of Gbit/s with many RRHs connected to a common BBU cluster by the CPRI. Therefore, the achievable data rate depends on factors such as the RAT that is employed, the carrier bandwidth, and the number of multiple antennas in use. The CPRI data-rate for multi-sector and multi-antenna configurations is expressed as [48], [59]

$$Data\ Rate\ \ (R_D) = S_n\, M\, f_s\, N\, 2C_w\, C, \tag{2.1}$$

where S_n denotes the number of sector, M represents the number of antennas per sector, f_s denotes the sampling rate used for digitization (sample/s/carrier), N is the sample width (bits/sample), (2) denotes a multiplication factor of two introduced to account for the (IQ) data, C_w is the factor of CPRI control word (CW) and C is a coding factor (either 10/8 for $8B/10B$ code or 66/64 for $64B/66B$ code).

The CPRI specification does not only offers sampling rates values conforming to different RATs with respect to the associated channel bandwidths but also with regard to the minimum and maximum values for uplink and downlink I/Q sample width [48]. Also, in line with the CPRI specification, the bit error ratio (BER) on the fronthaul link should be lower than 10^{-12} [48].

2.1.1.2 Latency in the Fronthaul

Another factor to be considered is the latency constrained by the RAT in the fronthaul transport. The transmission latency represents the round-trip time (RTT) between the RRH and BBU, the transmission time over the fiber, and the signal processing time in the optical equipment. The fiber length between BBU and RRH is subject to the optical transmission technology being employed. This is normally restricted to be lower than 20 km [47]. In addition, due to the fact that the RRHs generate their clocks in accordance with the receive CPRI signal, it is completely important that the CPRI signal possess low jitter. About 65 ns maximum variation in delay (Jitter) is required. Table 2.2 illustrates the timing and latency requirements for CPRI and 3GPP specifications. However, in some cases, the CPRI requirements can be relaxed from those presented in Table 2.2 as they vary from MNOs to MNOs [51]. Comparatively, LTE imposes the most stringent conditions on transport latency. This is as a result of the uplink hybrid automatic repeat request (UL-HARQ) process being employed for error-control in data transmission. Furthermore, the constraints on transport latency by the 5G radio networks will be more stringent than the ones imposed by the LTE networks [47]. Therefore, to address the stringent requirements by the fronthaul, efficient transport scheme should be employed. The next section presents different transport methods that can be employed in the MFH. Also, the associated technical challenges of their implementations are discussed.

2.1.2 Fronthaul Transport Technologies

There are a number of existing transportation approaches for the CPRI. The techniques are categorized into an active and passive solutions. An active solution means that, the CPRI traffic is encapsulated by another protocols and multiplexed on the fronthaul. Furthermore, the Demarcation Point (DPt) at the cell site requires PS. The passive solution depends on passive multiplexing and demultiplexing of the CPRI links. Additionally, the DPt does

Table 2.2: Timing and latency requirements for CPRI and 3GPP specifications

Parameter	Standard body	Requirement	Reference
Jitter & wander	3GPP	• $< \pm$ 50 ppb at radio • $< \pm$ 16 ppb at line (below 1 kHz)	[51]
	CPRI	• $< \pm$ 2 ppb (below 300 Hz)	[60,61]
Latency	3GPP	• $<$ 3 ms (HARQ budget)	[51,52,55]
	CPRI	• 150-200 μs • 5 μs (excl. cable)	[60,61]
One way latency	3GPP	• $< 15\mu s$ (No FEC) • $< 25\mu s$ (with FEC)	[51]
Round trip delay accuracy	3GPP CPRI	• $\pm$ 130 ns (T_{ADV}) • $\pm$ 16 ns	[51,61]
Error Vector Magnitude (EVM)	3GPP	• TM2:$<$ 8% (64QAM) • TM3.1:$<$ 8% (64QAM) • TM3.2:$<$ 12.5% (16QAM) • TM3.3:$<$ 17.5% (QPSK)	[51]
BER	CPRI	• 10^{-12}	[51,60–62]
Digital data compression	CPRI	• 50%	[51]
Synchronization time	CPRI	• 10 s	[61]

not require any PS, however, monitoring can be achieved with active equipment at the CO DPt [48]. Furthermore, dedicated fiber and other possible methods can be employed for the CPRI transportation [58].

2.1.2.1 Dedicated Fiber

The use of dedicated fiber alternatives occurs when an operator has a sufficient number of fibers installed for its needs. It is also a suitable option in conditions where it is more cost-effective to lease fiber than to deploy an optical transport element at the cell site. However, the cost associated with the new fiber deployment and restrictions on the number of fibers per duct limits the extensive applicability of the dedicated fiber option [58]. Section 2.5 on page 34 discusses a number of broadband optical and wireless transport schemes that can be utilized in the telecommunication infrastructure to accomplish a converged optical wireless access network.

2.1.2.2 Microwave

Microwave transport is an encouraging option that can be used for line-of-sight short distance (1 km or less) transmission. Presently, microwave transport scheme supports a subset of the CPRI interface bit-rate options. So, the supported CPRI bit-rate options are just up to the CPRI Option 3 [53]. Consequently, this relatively leads to bandwidth limitation [63].

Moreover, another remarkable challenge is that, microwave transport option is sensitive to weather fading [51].

2.1.2.3 Optical Transmission Network (OTN)

The Optical Transmission Network (OTN) is an active and scalable transport solution that can substantially increase the range of optical networks. The CPRI traffic is encapsulated by means of OTN and multiplexed on the fronthaul. Moreover, OTN has Forward Error Correction (FEC) that helps in alleviating the link sensitivity to the bit errors. Therefore, it assists in increasing the reach of metro optical networks. Nevertheless, FEC and other features that have been employed in the OTN lead to an increase in the latency for CPRI transportation [58, 63]. The cases for OTN MFH capabilities are comprehensively discussed in [51].

2.1.2.4 CPRI over Ethernet (CoE)

The current Ethernet cable infrastructure can be utilized for the encapsulation and transportation of the CPRI data from the BBU pool to the RRH. This implementation reduces the cost considerably and facilitates system convergence. Moreover, it offers some notable benefits such as statistical multiplexing, infrastructure sharing, and optimized performance through probe-based monitoring and Software-Defined Networking (SDN). Furthermore, the Ethernet Operation, Administration, and Maintenance (OAM) capabilities permit standardized methods of managing, troubleshooting, and monitoring the performance of the network. Consequently, with CPRI over Ethernet (CoE), the OAM functions that are unaccounted for in the CPRI can be provided by the Ethernet [56]. However, ultra-high-bit-rate needed by multiple antenna systems, joint processing demand, as well as low latency and jitter to meet delay requirements are challenging. It is remarkable that transportation of CPRI data on the link is not continuous. It is transported as discrete Ethernet 802.3 frames. To meet requirements such as latency and jitter, CoE sometimes needs dedicated Ethernet links between the BBU pool and the RRH. It is worth mentioning that, the CoE cabling architecture requires CPRI-Ethernet mapping guidelines in addition to the integrated Ethernet monitoring capabilities. This aids in maintaining the stringent jitter and latency requirements, that are not integrated into the CPRI standard [63]. Moreover, further information on the Ethernet based approach is presented in Section 2.4 on page 31.

2.1.2.5 Wavelength based Systems

The Wavelength-Division Multiplexing (WDM) alternative offers the prospect of serving high capacity metro and low cost access networks. Moreover, the WDM is an auspicious solution that permits a suitable combination of features for the CPRI transportation [58]. In addition, Coarse Wavelength-Division Multiplexing (CWDM) is a low-cost optical multiplexing technology for the access as well as metro networks. This is owing to its reduced footprint, simplicity, low delay, and high reliability [47]. Moreover, the associated high throughout, cost-effectiveness and its adaptability to outdoor deployment makes it an appropriate solution for the unpredictable nature of RRHs placement. It can also be employed for short term fronthaul deployments based on 2.5 or 5 Gbit/s CPRI interfaces [48]. Figure 2.1 on the next page shows the implementations of CWDM networks. As illustrated in Fig. 2.1(a), CWDM splitter can be employed for separating a set of BSs from ONUs. Likewise, as shown in Fig.

2.1(b), CWDM can be employed over standard PON to form virtual PONs for separating BSs and ONUs. There are notable efforts by the International Telecommunication Union (ITU) on the CWDM implementations. For instance, the ITU Telecommunication Standardization Sector (ITU-T) defines 18 CWDM channels with 20 nm channel spacing. The broader channel spacing of CWDM schemes allow less sophisticated and therefore cheaper transceiver designs. Additionally, CWDM is compatible with industrial temperature range and can scale up 10 Gbit/s CPRI [48]. However, from the network operation and migration perspectives, it is not extensively deployed due to the fixed wavelength assignment in the commercial CWDM solutions. Also, the number of channels proposes by the CWDM may not be enough in network scenarios in which many RRHs are connected to a central BBU cluster [48], [47].

In case of applications that demand additional number of channels than those that can be accomplished by a CWDM PON network, a dedicated Dense Wavelength-Division Multiplexing (DWDM) network can be used to supply the feeder network as illustrated in Fig. 2.2. In addition, for Millimeter-Wave (mm-wave) RoF applications, specific amount of DWDM spectrally efficient multiplexing and demultiplexing approaches can be utilized. It is noteworthy that, the SE of DWDM is much better than that of CWDM due to the denser channel spacing implementation. The usual channel spacing values for DWDM are 0.2 nm (25 GHz grid), 0.4 nm (50 GHz grid), 0.8 nm (100 GHz grid), and 1.6 nm (200 GHz grid). The number of channels for 200 GHz, 100 GHz, 50 GHz, and 25 GHz frequency grids are 20, 40, 80, and 160 channels, respectively. Consequently, there is a need for more stable wavelength or frequency in DWDM schemes compared with CWDM schemes because of the closer spacing between the wavelengths. Besides, DWDM channels can be inserted into the CWDM infrastructure for

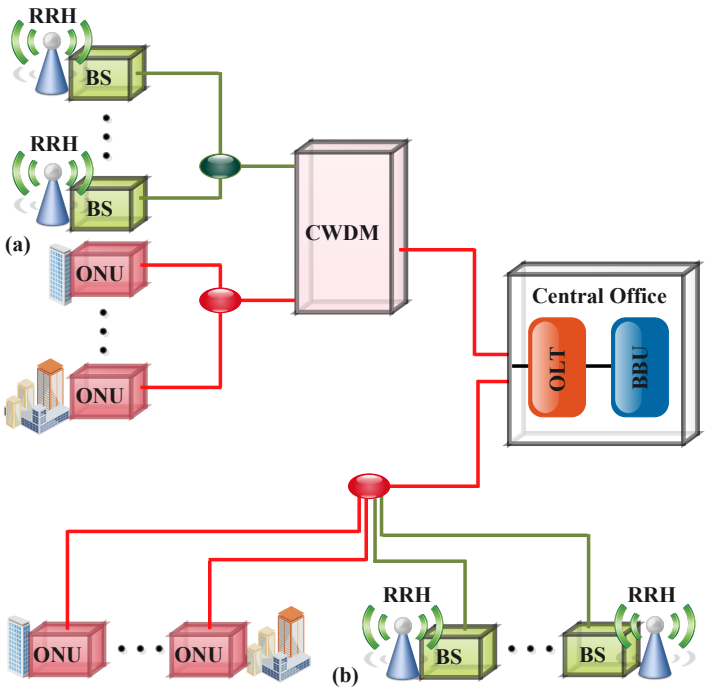

Figure 2.1: Implementations of CWDM networks for separating BSs from ONUs (a) with CWDM splitter (b) with CWDM over standard PON to form virtual PONs.

smooth migration in case of higher density antenna sites [48]. Additionally, a pure DWDM fronthaul network can be used, however, the requirement for low cost transmitters and the industrial temperature requirement demand further attentions so that the cost-effective benefits of the centralized RAN idea will not be hindered. Basically, DWDM technology has to be compliant with the cost figures and operational requirements for managing the Optical Access Networks (OAN) [47, 48, 64, 65].

2.1.2.6 Passive Optical Network (PON)

The PON is a viable solution for CPRI transportation in high traffic areas. The associated low cost and inherent centralized system make it a good candidate for the small cell deployments [37, 66]. Furthermore, MNOs prefer and value the passive nature provided by the PON architecture. Moreover, the PON architecture offers an applicable platform for cost-effective integration of small cells into the current network. Nevertheless, implementation of PON system needs a cautious design so as to prevent further latency and power loss that can limit the cell radius. In addition, the main weakness of this solution is that not all standards are supported at the fronthaul. This is due to the huge bandwidth required by the new technologies such as LTE-A. In Section 2.2 on the following page, we give comprehensive discussions on the PON architectural evolution and their salient features.

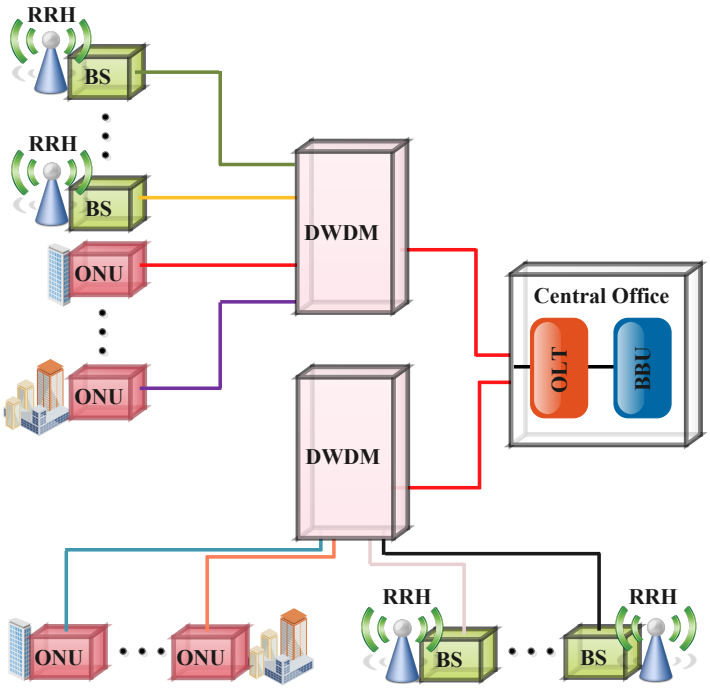

Figure 2.2: Implementation of DWMD feeder network using dedicated wavelength channels assigned to each BS and ONU.

2.2 PON Architectures

Figure 2.3 depicts the basic PON architecture. Fundamentally, PON system comprises of elements such as Optical Line Terminal (OLT), ONU, and Optical Distribution Network (ODN). The OLT is the PON headend that is usually located in the CO. The OLT connects the system to the metro/core network by means of Service Node Interface (SNI). Furthermore, the ONU equally called an Optical Network Terminal (ONT), is normally placed at the subscriber's premises. It connects the user to the network via the User Network Interface (UNI). The ODN connects the OLT and ONU to each other. The ODN consists of optical fiber as well as a passive optical splitter [67].

It should be noted that, the robustness of ODN is highly important for its implementation in the MFH. As a result, it is essential to automatically detect fiber-fault remotely and be capable of localizing the faults in the network. This approach proffers proactive as well as reactive monitoring solutions in the MFH. This is due to the fact that; it enables shorter service delivery downtime. Furthermore, parameters such as completeness, comprehensiveness, high sensitivity, neutrality to traffic flow, and accuracy are entirely vital for a resilient ODN [40]

In addition, there are various PON architectures such as Gigabit-PON (GPON), 10 Gigabit-PON (XG-PON), and the Next-Generation Passive Optical Network stage 2 (NG-PON2) that can be employed for the fixed access as well as backhaul networks [68].

2.2.1 Gigabit-class PON (GPON)

The GPON is established on the ITU-T Recommendations G.984.x standard. It has an aggregate bandwidth of about 2.5 Gbit/s for the Downstream (DS) and Upstream (US) directions [9]. When deployed for residential use, the typical splitting ratio is 1:32 or 1:64. The DS wavelengths range from 1480 nm to 1500 nm, while the US wavelengths range between 1260 nm and 1360 nm. Furthermore, the GPON ONUs do not need tunable receivers and transmitters. This is because the wavelengths are fixed [68]. However, apart from the associated latency, GPON is impractical for the MFH applications due to the limited bandwidth exhibited in both DS and US directions. Examples of GPON systems that have been stan-

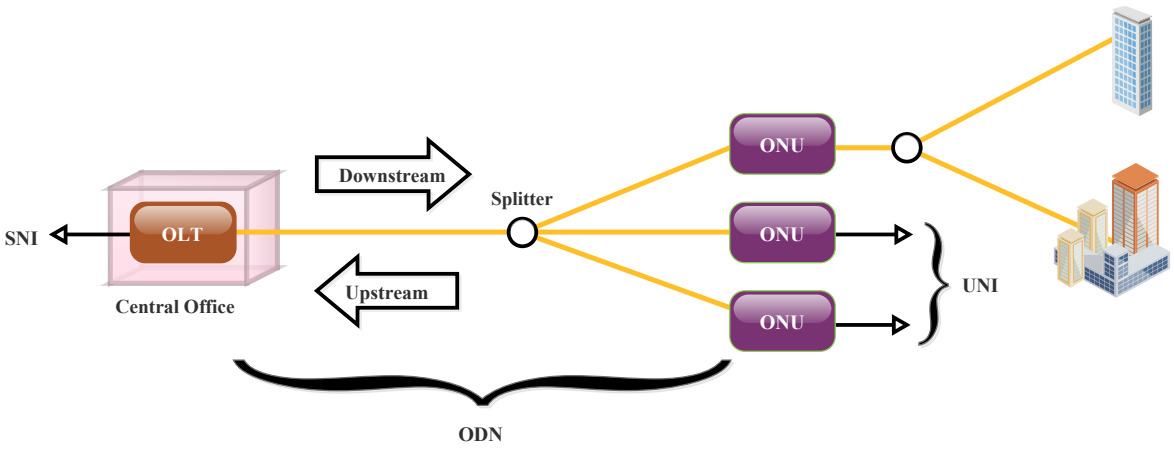

Figure 2.3: PON architecture.

dardized by the ITU-T and the Institute of Electrical and Electronics Engineers (IEEE) are Gigabit-capable PON (G-PON) and Ethernet-PON (EPON), respectively [67, 69–71].

2.2.2 10 Gigabit-class PON (XG-PON)

The XG-PON has the capability of addressing the DS demand by supporting rates of 10 Gbit/s, however, the US transmission is limited to 2.5 Gbit/s. Furthermore, the 10 Gigabit-PON2 (XG-PON2) standard provides symmetric rates of 10 Gbit/s [9]. The wavelengths normally employed in XG-PON are 1577 nm for the DS and 1270 nm for the US. Also, similar to the GPON and in view of the fact that the wavelengths are fixed, there is no requirement for tunable components at the ONUs. Likewise, the XG-PON is backward compatible with the GPON, consequently, identical infrastructure and splitters can be employed. The compatibility ensures cost-effective migration policy for the existing GPON service providers. Moreover, its normal features are contingent on the ITU-T G.987.1 and G.987.2 recommendations. In addition, features such as QoS, Dynamic Bandwidth Allocation (DBA), transmission convergence traffic management, layer principles, and remote operation of ONUs through the ONU Management Control Interface (OMCI) are inherited from the current GPON systems. Moreover, XG-PON presents enhanced security mechanisms, enhanced power saving options, and performance monitoring [68]. Furthermore, an alternative XG-PON is 10Gigabit Ethernet PON (10G-EPON) [67, 69, 71, 72].

2.2.3 Next-generation PON stage 2 (NG-PON2)

In an effort to address the higher bandwidth demands being experienced by the MNOs, Full Service Access Network (FSAN) and ITU-T are considering optical fiber network schemes that are capable of offering improved capacities compared with XG-PON in the access network [73]. Therefore, FSAN initiated the NG-PON2 project [70, 74, 75]. Additionally, the main requirements of NG-PON2 are to present at least 40 Gb/s aggregate rate in the DS or US, 1:64 split ratio, 40 km reach, and at least 1 Gb/s access rate per ONU. The NG-PON2 is based on ITU-T Recommendation G.989.x and provides considerable bandwidth enhancement compared to other current standards [69, 76].

The NG-PON2 has been acknowledged as a potential solution for the high capacity links demanded by the C-RAN MFH for the transportation of the in-phase and quadrature-phase (IQ) samples between the RRH and the BBU with strict latency requirements [69]. Moreover, the major attribute that distinguishes the NG-PON2 system from the existing PON systems is that, it permits multiple wavelengths per direction. In addition, it is compatible with power-splitter-based ODN [75]. Moreover, it is noteworthy that, all of the aforementioned PON standards employ different access technologies. Nevertheless, the access technology proposed for the NG-PON2 supports legacy infrastructure and facilitates a smooth transition for services providers so as to avoid service disruption for the customers that are currently on the legacy PON systems [13, 68, 69, 74]. Basically, NG-PON2 is anticipated to be highly reliable, flexible, scalable, and efficient regarding the bandwidth and power consumption [69]. In Section 2.3 on the following page, we review optical access technologies for the PON systems. Furthermore, their implementation requirements in terms of latency and capacity are discussed.

2.3 Optical Access Technologies

The NGNs are expected to support clusters of densely deployed small-cells which are anticipated to address demands in high traffic areas. It is remarkable that, deployment of dedicated optical fiber will not be cost-effective in this type of scenario. Therefore, the PON architecture presents a suitable solution for cost-effective integration of small-cell network with the OAN [33]. The two main PON optical access technologies are Time Division Multiplexed PON (TDM-PON) and Wavelength Division Multiplexed PON (WDM-PON) [77].

2.3.1 Time Division Multiplexed PON (TDM-PON) System

The gigabit class of TDM-PON systems like GPON and EPON systems, are commonly deployed to provide economical Fiber To The Home (FTTH) broadband services. Moreover, another variety of TDM-PON is the 10 Gigabit class such as XG-PON and 10G-EPON systems that have been developed for the next generation systems. Optical infrastructure as well as network equipment can be shared by TDM-PON systems for the purpose of reducing the associated CAPEX and OPEX. Consequently, Time Division Multiplexing (TDM)-based transmission can provide a lower cost solution for bit rates of up to 10 Gb/s. Furthermore, it can be utilized in small-cell clusters with lowest Total Cost of Ownership (TCO). However, the cost effectiveness of TDM-PON is not so high for a lightly deployed small-cell network [33].

Figure 2.4 on the next page illustrates the TDM-PON system in which optical fiber and network OLT are shared between ONUs in order to offer lower TCO compared with the Point-to-Point (PtP) systems [33]. The DS data for the respective ONU is multiplexed and transmitted by broadcast from the OLT. Moreover, a Time-Division Multiple Access (TDMA) scheme is used for scheduling and multiplexing of the US data packets of each ONU. In addition, an efficient US transmission can be realized by implementing a DBA algorithm [33]. It should be noted that, the TDM-PON systems have asymmetric latency with US latency being dominant (>1 ms).

Furthermore, in the next-generation wireless MFH networks, a low latency transmission will be highly important for the optical network. The associated DS latency of the TDM-PON technology is appropriate for the MFH application. Nevertheless, the US latency is unsuitable for the MFH in the conventional state. This is as a result of the US latency that exceeds the global standard. The main reason for the latency in the TDM-PON can be attributed to the DBA algorithm for the US transmission. The implementation of DBA algorithm makes the latency to be of the order of milliseconds. This time frame is significantly greater than the one required for an efficient operation of the MFH [77]. Consequently, the US MFH requirements regarding latency, as well as capacity, cannot be fulfilled with the current TDM-PON. Therefore, to enable this option to be feasible for the MFH, a number of efficient enhancement algorithms are essential for the TDM-PON deployment [33].

The US transmission latency can be improved by implementing some innovative bandwidth allocation algorithms. One of such is the application of the Fixed Bandwidth Allocation (FBA) algorithm. The fixed bandwidth mode of operation guarantees consistent bit rates on the client interfaces and prevents jitter accumulation which is as a result of random access to the PON. Consequently, multiple time slots per Physical (PHY) layer frame can be allotted to an individual ONU (RRH). Therefore, this approach reduces the buffer time in the end equipment to few tens of microseconds [33], [47]. However, the disadvantage of FBA algorithm is that, fixed bandwidth is allocated to each connection. Thus, this does not

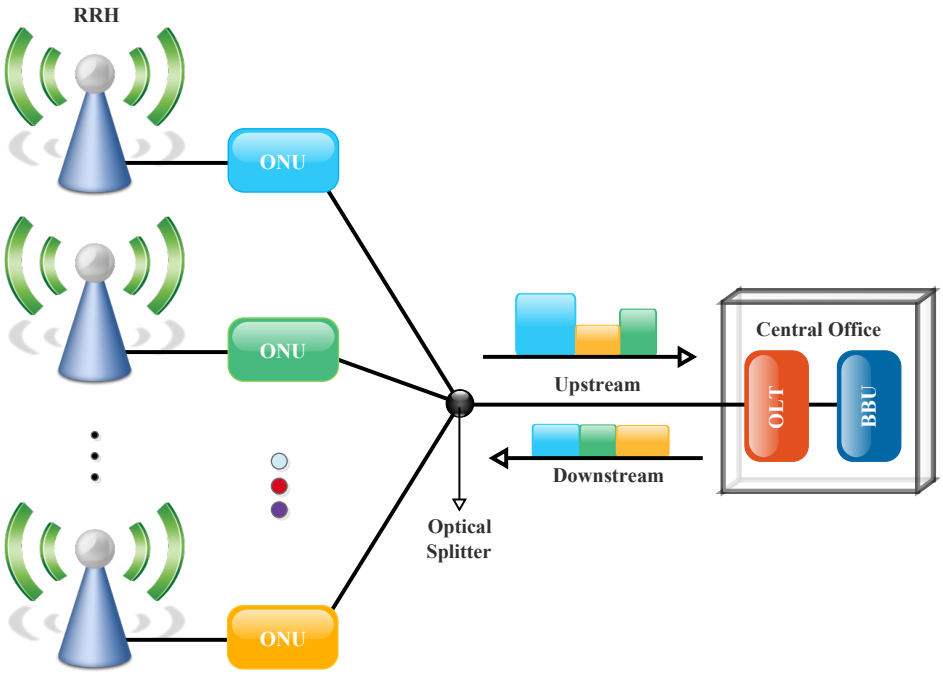

Figure 2.4: MFH based on TDM-PON System.

encourage efficient bandwidth allocation that is based on statistical multiplexing. Furthermore, a mobile Dynamic Bandwidth Allocation (mobile DBA) algorithm that is based on mobile bandwidth allocation can be implemented to improve the system performance [77]. In addition, the uplink scheduling information of the mobile system can be utilized to minimize the latency of TDM-PON [33].

2.3.2 Wavelength Division Multiplexed PON (WDM-PON) System

The WDM-PON uses wavelength for multiple access to the shared optical infrastructure and permits multiple PtP physical links. Furthermore, it possesses benefits such as high flexibility in terms of protocol and transmission data rate. Also, it helps in the realization of high capacity and low latency link. Consequently, it is a good alternative for the next-generation MFH network that demands high capacity and low latency for effective operation. Technically, these requirements can be simply attended to with the WDM PtP connections for the Master evolved NodeB (MeNB). Moreover, WDM-PON is a good option for small cell clusters. Furthermore, the fiber deployment and management costs can be considerably reduced by the WDM overlay of the existing PON systems [33].

The capability of WDM-PON for transporting the CPRI traffic makes its employment encouraging for the C-RAN. Each of its wavelength can support up to 9830.4 Gb/s [78]. Furthermore, it can support CPRI streams at different bit-rate and data streams from different protocols simultaneously. This benefit can be attributed to the stream segregation and protocol transparency features of the WDM-PON. In addition, it has high fiber SE. This is majorly due to its ability for reusing the same wavelength for the US and DS traffic over the same optical fiber infrastructure [78].

Figure 2.5 on the following page illustrates a basic WDM-PON system in which the optical infrastructure is shared by ONUs. Also, in the WDM-PON scheme, each wavelength connection is PtP [33]. By means of this configuration, high flexibility with regard to protocol and data rate of the connections can be accomplished. However, optical infrastructure sharing has just slight cost benefit due to the high cost of WDM-PON equipment such as transceivers and WDM multiplexers/demultiplexers. Therefore, this may limit deployment of the WDM-based system for the MFH [19]. Consequently, the choice between TDM-PON and WDM-PON based systems is determined by the mobile network cell density. In addition, a hybrid implementation can be realized by combining the TDM and WDM-PON based systems as in the case of NG-PON2.

2.3.3 Time and Wavelength Division Multiplexed PON (TWDM-PON) System

In April 2012, a novel optical access technology was selected by the FSAN for the standardization of the NG-PON2 [74]. The access technology is based on a hybrid Time and Wavelength Division Multiplexed PON (TWDM-PON) system with an optional Point-to-Point Wavelength Division Multiplexed (PtP WDM) overlay extensions designed for the NG-PON2 [9, 70, 73, 76, 79]. The scheme takes advantage of both time and wavelength multiplexing schemes in order to improve the system performance. The DWDM provides multiple unshared PtP connections, while, the TDM offers Point-to-MultiPoint (PtMP) connections on a separate set of DWDM channels [80]. Nevertheless, both of the schemes operate concurrently on the shared ODN infrastructure as depicted in Fig. 2.6. In addition, the MNOs requirements for business and MFH services can be accomplished with the PtP WDM overlay in the NG-PON2 technology. This can be realized by dedicating a wavelength (λ)-channel to each ONU [69].

The TWDM-PON can give flexible use of large bandwidth with the implementation of Dynamic Wavelength and Bandwidth Allocation (DWBA) scheme. Furthermore, it supports legacy infrastructures being deployed in the network [33], [68]. It is anticipated to deliver 40 Gb/s bandwidth [33]. The basic idea of TWDM-PON is to increase the aggregate PON rate via stacks of XG-PONs by multiple pairs of wavelengths. In view of the fact that an XG-PON can offer access rates of 10 Gb/s in the DS and 2.5 Gb/s in the US, then, a TWDM-PON architecture with four pairs of wavelengths can deliver 40 Gb/s aggregate DS capacity and 10 Gb/s in the US [69], [74]. In general, the system can be configured to operate at different bit rates so as to best address a particular service requirements. Moreover, the NG-PON2 basic requirement for compatibility with power-splitter-based ODN implies that, wavelength-tunable optics are essential at the transmitter and receiver of the ONU. As a result, one of the challenges of the TWDM-PON application is the means of achieving the ONU tunable transceiver at a reasonable cost [75], [79].

Furthermore, another effort on enhanced architecture was presented in the COCONUT project. The project architectures consider the cost, power consumption, and migration scenarios for the system. The project proposed an Ultra-Dense WDM (UDWDM) access scheme that utilizes basic coherent technology with the intention of enhancing the system performance compared to the standardized technologies. This is realized by operating in a very narrow spectral band due to the 6.25 – 12.5 GHz wavelength channel. Moreover, COCONUT has been presented as an attractive solution for aiding advanced features in NG-PON2 or for the Future Next Generation PON System (NG-PON3) [81].

Generally, to support the 5G network, transport networks have to offer extensive range of service requirements and diverse transport services. The transport networks have to be capable of sustaining the envisioned massive connections with sufficiently high capacity. They also have to support radio interference coordination between Ultra-Dense Network (UDN) and offer cost-effective RAN deployment for several functional split. Furthermore, to satisfy the vision of Networked Society, system automation and the capability for network elements integration are very important. These can be easily realized with the aids of Network Function Virtualization (NFV) and SDN. These innovative technologies will assist transport networks in offering efficient and flexible platforms for resource sharing/management. With these, multiple MNOs can conveniently coexist on the shared infrastructures. This will allow each operator to access the network resources through the APIs [82, 83]. Therefore, different

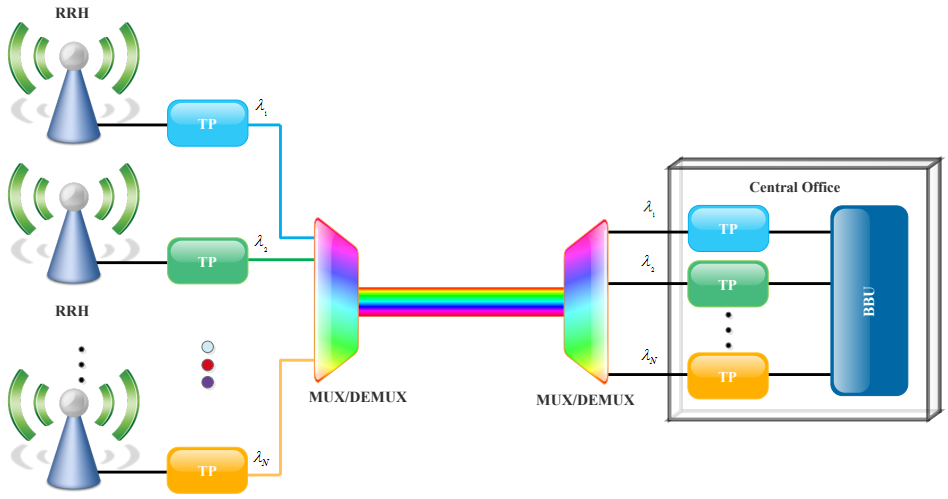

Figure 2.5: MFH based on WDM-PON System.

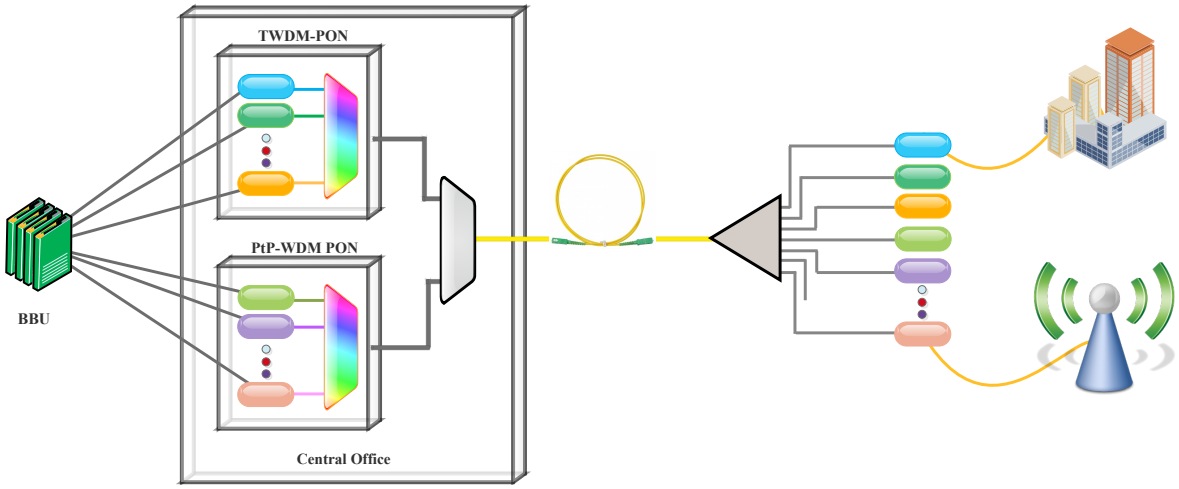

Figure 2.6: MFH based on TWDM-PON and DWDM-PON overlay sharing the same ODN simultaneously.

transport schemes will be needed to fulfill the network requirements based on the deployment areas and economics.

In addition, integrated photonics is anticipated to play a vital role in the 5G transport owing to its advantages such as low cost, low footprint, and reduced power consumption. New generation of optical components based on integrated photonics are transforming the traditional perspective of optical network of being a physical layer entity just for transmission of huge data between two network nodes with constrained flexibility and prohibitive cost. An improved amount of flexibility offered by the optical components can give additional degrees of freedom in the transport layer. Moreover, the inherent transparent feature of optical networks can aid in the simplification of upper layers' migration, stratification of layers, and implementation of fixed/mobile convergence scenario on shared infrastructure.

Nevertheless, certain modifications may be necessary in the C-RAN architecture for an effective transportation of CPRI traffic over the system. The modifications are considered in the subsequent section.

2.4 Centralized RAN Architecture Modifications

The current RAN fronthauling is generally realized by the optical links with the supports of CPRI protocol. In reality, fixed line rate, digitized analogue radio signals are required for transmission over the transport link irrespective of the actual amount of the users‘ information being conveyed. Nonetheless, the bandwidth needed to convey digital radio signals with this method is comparatively high. Moreover, attainment of the required bit rates by the CPRI fronthaul is viable and could be cost-effective using PtP and WDM optical technology in a scenario with limited number of sites [46]. Conversely, in a complex scenario with numerous antenna elements and large spectral width, the CPRI fronthaul approach demands modifications owing to the continuous increase in the need for radio bandwidths and creation of new services and technologies in the 5G networks [46], [47]. This is due to the fact that, the CPRI based approach implementation will continue to pose various economical and technical challenges. For instance, the expenditure that will be incurred in providing high CPRI bandwidth hinders the cost-effectiveness of the C-RAN architecture in the long run [57]. Therefore, in this section, we discuss possible modifications such as split-processing, bandwidth compression, and Radio over Ethernet, so as to attend to the bandwidth demand of digital signal transportation.

2.4.1 Split-processing

A practical way of addressing the cost challenge is to exploit the current fiber resources or the low-cost multichannel WDM technologies. Nevertheless, in a scenario where both are not available, a dynamically shared network that corresponds to TDM-PON can be used. This dynamic network splits the processing chain, so that, the system can take advantage of statistical multiplexing. This also helps in achieving a relaxed latency constraint. This method is known as split-processing or dual-site processing [46, 47, 57]. The idea of the split-processing approach is that; the baseband processing functions are in part executed in the centralized BBU pool as well as in the remote site. The techno-economic analysis of the processing chain splitting is properly reviewed in [46].

2.4.2 Bandwidth Compression Techniques

The stringent requirements concerning high-bandwidth, low-latency, and strict synchronization, as well as being a serial constant bit rate interface, make it really challenging to have CPRI traffic and other traffic sources over the same link. Therefore, bandwidth reduction technique is very essential for multiplexed transmission [84, 85]. This problem can be addressed by bandwidth compression techniques with the intention of reducing the link load. Furthermore, data compression technique for wireless waveform data helps in increasing the number of RRHs that can be supported efficiently by the MFH within an allowable latency [84]. A number of compression schemes and the associated trade-off are effectively discussed in [18, 86].

Furthermore, the bandwidth compression can be regarded as a road map with regard to packetization of the CPRI data. The packetization can be achieved through the Ethernet framing. However, plain Ethernet is asynchronous and based on the best effort approach. Consequently, plain Ethernet is unsuitable solution for the CPRI traffic transportation [23]. Table 2.3 compares different attributes of CPRI and Ethernet-based transport networks. As a consequence of the limitations of plain Ethernet, the Time Sensitive Networking (TSN) Task Group of IEEE 802.1 is aiming at creating innovative extensions that will support Ethernet traffic forwarding with delay and jitter guarantees. In addition, mechanisms such as frame preemption, jitter reduction techniques, and expedited traffic forwarding are to be investigated. Moreover, besides the present high-precision timing protocols (IEEE 1588) over Ethernet that guarantees synchronization via the time-stamped packets exchange [56], new methods that employ frequency adjustable oscillators or Global Positioning System (GPS) signals are under study for attending to the timing issue [23]. In [84], a prototype of a CPRI over Ethernet-based TDM-PON system in which the CPRI signals are packetized into PON frames for transmission is reported.

2.4.3 Radio over Ethernet (RoE)

It is remarkable that, CPRI does not offer specifications for well-defined optical layer. Therefore, transport OAM and networking functions are not well-defined. To address this challenge, IEEE is working on stipulating an optical transport layer for the fronthaul by

Table 2.3: CPRI vs. Ethernet

	Features										
Solution	**Synchronous**	**Symmetric link**	**Intermittent stream**	**Idle link**	**Energy efficient**	**Periodic sync bit**	**Cost effective**	**Best-effort**	**Statistical multiplexing gains**	**Dedicated media**	**OAM functionalities**
CPRI	√	√				√				√	
Ethernet			√	√	√		√	√	√		√

considering Ethernet technologies. This is envisioned to reduce the equipment costs. Also, it will enable convergence of wireline and wireless services on a common transport platform that is based on Ethernet networking. Similarly, IEEE Groups are working toward Radio over Ethernet (RoE), Encapsulations, as well as Mappings. Also, they are supposed to define a native RoE format [23]. This includes RoE encapsulation and mappings of digitized radio *IQ* payload, potential vendor specific and control data channels. In addition, flows into an encapsulating Ethernet frame payload field should also be considered. Moreover, the header formats for the structure-aware and the structure-agnostic encapsulation of the existing digitized radio transport formats have to be specified.

Furthermore, the engagement focuses on establishment of rules for mapping the CPRI frames into the payload of Ethernet packets. Similarly, concurrent transmission of data over switched Ethernet networks with other best-effort-type traffic in the same network is being considered [47]. Figure 2.7 illustrates different structures that can be implemented in RoE-based transport networks. Figure 2.7(a) supports legacy systems, therefore, it needs mapper frontends and RoE Encapsulations (Encaps)/Decapsulations (Decaps) for the current RE and REC. Likewise, Fig. 2.7(b) has native RoE RE but demands RoE Encaps/Decaps and mapper frontend for the current REC. In addition, Fig. 2.7(c) has native RoE REC but requires RoE Encaps/Decaps and mapper frontend for the existing RE. Finally, Fig. 2.7(d) is based on native RoE RE and REC [87].

In addition, recent study shows that, Ethernet networks with enhanced traffic schedule and a well-defined schedule algorithm can meet CPRI jitter requirement. Nevertheless, neither shared nor dedicated Ethernet networks with or without frame preemption, can meet the CPRI jitter requirement [88].

It is noteworthy that, all the modifications discussed so far show that, 5G network and beyond will require innovative measures for an efficient fronthaul. The efforts toward an efficient MFH for the NGNs are considered in the next section.

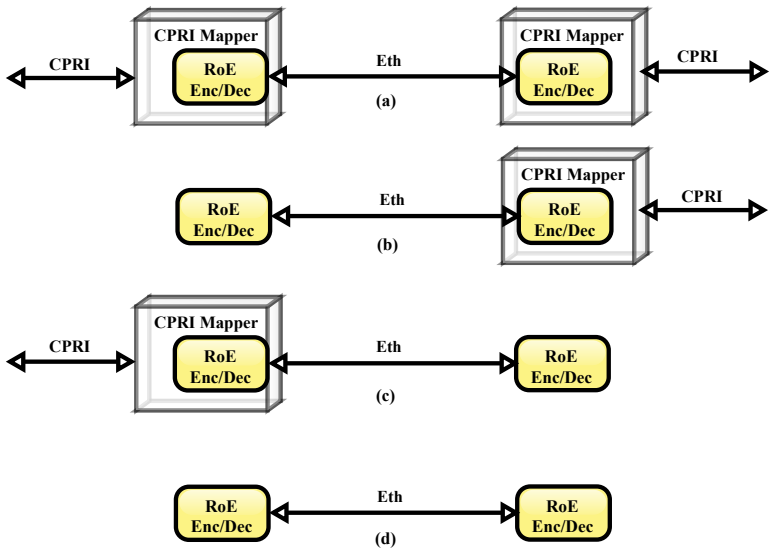

Figure 2.7: Schematic of (a) existing RE and REC (b) native RoE RE and existing REC (c) existing RE and native RoE REC (d) native RoE RE and REC (adapted from [87]).

2.5 Evolution towards Efficient Fronthaul for the 5G Network and Beyond

There are different ways of accomplishing a viable MFH in the C-RAN, nevertheless, the high-capacity and low latency requirements make optical fiber connections an encouraging solution. Also, adoption of optical fiber for ultra-dense deployment of RRHs renders C-RAN implementations less flexible and cost-intensive. This is even more challenging when trenching is required. There are some research efforts that are aiming at meeting the 5G RAN requirements with a realistic MBH/MFH. One measure is to evolve the current backhaul such as microwave, optical fiber, and copper, in order to meet the 5G expectations. An alternative means is to incorporate innovative wireless technologies for instance mm-wave, in-band links (reuse the radio access spectrum), and FSO [89, 90].

In addition, the transmission capacity would be constrained when wireless communications in microwave bands is implemented due to the limited available bandwidths. Likewise, the implementation of mm-wave would results in low dynamic range owing to the associated free-space loss and atmospheric attenuation. Additionally, in the C-RAN architecture, the fundamental means of distributing wireless signal in the fronthaul is to transmit digital baseband oversampled IQ streams using CPRI or OBSAI interface [7]. Nonetheless, besides the strict control of jitter, synchronization, and latency that are required, optical link based on these interfaces requires large bandwidth which is as a result of high resolution bits needed for the digitalization process of the RF samples [9, 29]. Consequently, this bandwidth inefficiency might limit or make them impractical for the next generation mobile system in which Massive MIMO antenna system is expected to be incorporated [10, 11, 91, 92].

The requirements for transporting high number of radio channels, multi-RRH joint processing, channel monitoring and estimation, will demand for huge bit-rate in the order of Tbit/s [13], [66]. For instance, with CA of five 20 MHz LTE-A mobile signals with 3 sectors, and 8×8 MIMO antennas, about 147.5 Gb/s fronthaul data rate will be required by the CPRI. Therefore, a substantial amount of high-speed optical ON–OFF-Keying (OOK) transceivers will be needed to support the high-data rate MFH implementation [12]. In order to address the bandwidth and flexibility limitations, implementation of innovative measures is essential to realize bandwidth-efficient MFHs [12]. One of such is the use of analog optical transmission technology based on RoF technology as a mobile fronthauling technique [7, 11, 12, 93–95].

2.5.1 Radio-over-Fiber (RoF) Technologies

The RoF technologies are means of transmitting RF signal that is modulated onto optical carriers over the low loss optical fibers [96], [97]. Moreover, RoF has been an efficient means of achieving optical-wireless convergence in which wireless signal can be conveyed directly over the optical carrier [98]. The huge amount of bandwidth offered by the optical link enables multiple wireless services to share the same optical network fronthaul. Another advantages of RoF such as support for centralized network control and simple RAU, permit easier maintenance, upgrade, and sharing of resources [99].

In RoF technology, wireless signal transmission over the optical fiber link can be achieved by analog and digital means. Digitized wireless transport technologies are digitized RF-over-fiber (D-RoF) and digitized intermediate frequency-over fiber (D-IFoF). Furthermore, the analog wireless transport technologies are analog RoF (A-RoF) and intermediate frequency-over-fiber (IFoF) [99–101]. Depending on the application, each technology has its merits and

demerits as explained in the subsequent subsections.

2.5.1.1 Analog RoF

The analog-RoF or simply, RoF, employs analog optical transmission by directly modulating the optical carrier with microwave signals. The schematic of RoF is shown in Fig. 2.8(a). RoF facilitates centralized control, wireless signal transparency, and multi-band wireless support [102]. Furthermore, it presents a bandwidth efficient solution that can coexist with D-RoF in the fronthaul and complies with the elastic optical networking [66]. Employment of RoF helps in realizing a simplified BS architecture with reduced operational functionalities. It is highly essential for the optical-to-electrical (O-E) and electrical-to-optical (E-O) to be low loss and very linear in order to realize a high performance in RoF. It is remarkable that, directly modulated lasers (DMLs) can be employed for low frequency signal transmission, however, for higher microwave as well as millimeter-wave frequencies, external modulators such as Mach–Zehnder modulators (MZMs) are required. For the latter application, single sideband modulators are preferable for better performance in order to prevent the effects of dispersion induced power penalty. Furthermore, with multiple frequencies, the RoF link is prone to intermodulation distortions (IMD) caused by nonlinearity of both microwave and optical components of the optical link. One of the factors that significantly affect the overall system performance of an external modulator based link is the modulator's nonlinearity. Currently, commercial products are available with capability to support RoF transmission with good IMD performance. However, they are appropriate for common microwave frequencies. So, to handle IMD at higher frequencies or bandwidths, specialized techniques may be needed. This results in an increase in complexity and reduction in cost-effectiveness of an optical link. Furthermore, the RoF implementation leads to the optical link having a limited dynamic range. The limitation is due to dynamic range that decreases linearly with an increase in the length of the link. This effect can be attributed to the attenuation of the optical fiber. Moreover, another constrain of the RoF links is that, the bandwidth of the link have to be adequately greater than the highest microwave signal frequency irrespective of the signal message bandwidth [103]. In general, impairments such as fiber non-linearity, chromatic dispersion, and noise cause performance degradation of an analog optical fiber link [9, 66, 99, 101].

Moreover, Fig. 2.8(b) shows a schematic of IFoF. In this scheme, the wireless signal is transmitted at a lower IF over an optical fiber. This relaxes the requirements for high-speed optoelectronic hardware that is associated with the RoF technique. Similarly, fiber chromatic dispersion effect can be significantly reduced with optical distribution of the IF signal. Nonetheless, this presents more complexity in the BS antenna design. This is due to the requirements for a stable Local Oscillator (LO) and mixers which are employed for frequency translation purposes [100].

2.5.1.2 Digitized RoF

Figure 2.8(c) shows an architecture of baseband-over-Fiber (BBoF) scheme in which the wireless signal is transported optically as baseband data. This results in the complete wireless signal processing at the antenna BS. The BBoF scheme is compatible with the existing optical networks in which data are transmitted mainly at the information level in digital domain. Consequently, the optical domain of transmission makes the CO design to be as simple as

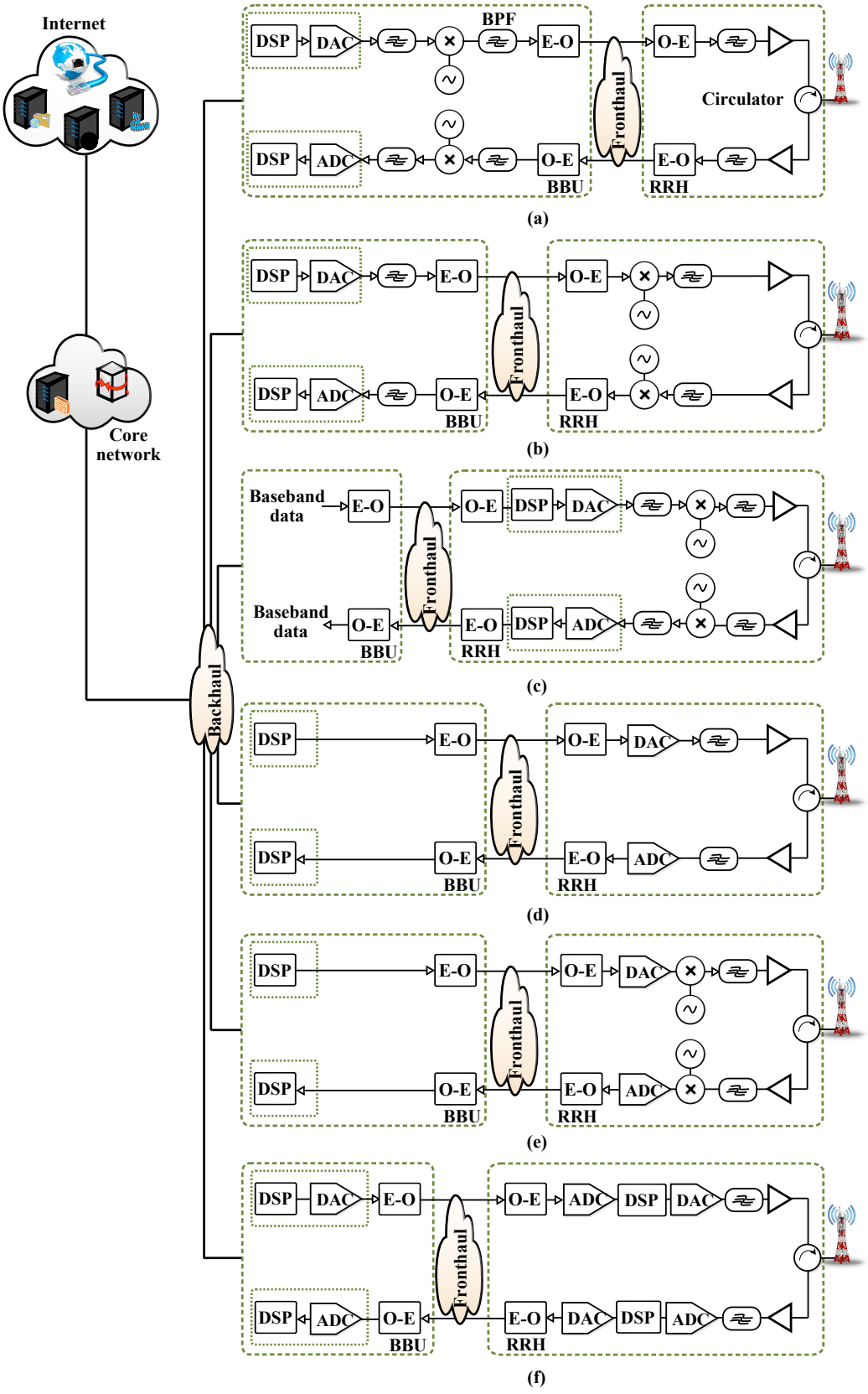

Figure 2.8: Schematic of (a) RoF (b) IFoF (c) BBoF (d) D-RoF (e) D-IFoF (f) DSP-RoF transport scheme.

possible. Notwithstanding, the BBoF scheme BS has to house extra hardware in order to process the wireless signal electronically. Therefore, this approach not only increase the BS complexity but also decrease the link transparency. In order to address these challenges, an innovative transport scheme that is based on digitization of the wireless signals has been presented. The scheme maintains comparatively simple BS design and still exploits digital optical links inherent features. Compare to the BBoF scheme, in the digitized scheme, the wireless signal is digitized before the actual optical transportation. This helps in the BS design simplification as well as improving the link transparency [100]. An architecture of D-RoF is illustrated in Fig. 2.8(d)

Unlike analog optical transmission scheme, in the D-RoF transport approach, ADC and DAC functions are executed at the BS. The generated sampled digital signal can be employed to directly modulate the laser for further transmission over an optical fiber. With this approach, minimal amount of the front-end hardware components are required in the transceiver functions of the BS while all signal processing functionalities are executed at the CO [103].

The associated impairments of RoF can be reduced by the D-RoF which makes transmission of digital signal over the optical link relatively reliable. So, the sampled digital signal in D-RoF system minimizes the nonlinear effects that is caused by the optoelectronic conversion in the analog transmission. This enables the system to maintain its dynamic range independent of the fiber length, until the received signal goes below the link sensitivity when error-free transmission is lost [9], [66], [100]. Consequently, it offers sustainable and high dynamic range over long distances compared to the RoF links. Moreover, wireless signal transmission based on digitized RoF enables implementation of low-cost transceiver. As a result, implementation of D-RoF in the network not only leads to simpler CO and BSs subsystems with digitized RF interfaces but also offers higher performance subsystems [103]. On the other hand, D-RoF scheme requires band-pass sampling, more ADC, and DAC, which cause impairments such as aliasing, quantization and jitter noise. Also, the requirements of D-RoF scheme make remote unit to have more circuitry [99], [100]. Moreover, these requirements become more stringent for wireless signals operating at frequency that is above the microwave bands. Another associated issue of D-RoF is that, because of the band-pass sampling employed, when the D-RoF signal processing blocks are designed for a specific RF frequency range, application of the same blocks for frequency ranges outside the specified ranges will be highly challenging without changing the sampling frequencies of the ADC and the DAC [104]. In order to address this drawback, D-IFoF is presented for down-conversion of the wireless signal to an IF frequency so as to address the limitations of the existing ADC technology [100]. A schematics of D-IFoF is shown in Fig. 2.8(e).

Furthermore, an architecture of Digital Signal Processing Analog RoF (DSP-ARoF) is depicted in Fig. 2.8(f). Unlike other analog schemes already presented, the DSP-ARoF has additional components such as Digital Signal Processing (DSP) and a DAC/ADC at the RRH. Also, like other analog schemes, analog waveforms are also transmitted in the optical domain. This enables DSP-ARoF in maintaining the SE of the wireless channels. Furthermore, it permits efficient aggregation of traffic that originates from different RRH. However, due to the high-speed DAC/ADC and the DSP required, the DSP-ARoF based schemes are subjected to higher cost and power consumption. These may introduce implementation issues in the C-RAN [105].

Generally, development of simplified BSs based on D-RoF interfaces reveal the prospect of backbone network design based on the distribution of digitized RF signals. This approach en-

ables easy integration of existing and future broadband optical and high-speed networks [103]. In the C-RAN, the baseband digital processing is accomplished in the BBU that interconnects the corresponding RRH by optical fiber using a D-RoF transmission system specified either by the CPRI or OBSAI protocol [17], [23], [92], [94], [100]. In wireless applications such as Worldwide interoperability for Microwave Access (WiMAX) and 3G in which information bandwidths are small fractions of their carrier frequency, bandpass sampling can be effectively employed for RF signal digitization. The resulting digital baseband signal can be efficiently transmitted over digital optical communication infrastructure. Signal digitization for wireless applications in the millimeter-wave frequency bands can be realized by converting the frequency to an IF frequency. The digitization process is then carried out on the IF frequency. However, D-RoF applications for ultra-broadband wireless access by means of mm-wave frequency bands are more challenging. In general, the realizable cost-effectiveness of the system majorly depends on maximum of the RF frequency and the product of sampling rate and resolution needed for signal digitization [103].

2.5.2 D-IFoF with Bandpass Sampling Technique

Analog bandpass signals can be downconverted to baseband or low IF digital signals without analog mixers with the aids of bandpass sampling technique [106]. Furthermore, compared to direct sampling, bandpass sampling technique offers better performance as the speed requirement on the ADC technology can be further relaxed. Moreover, the amount of digital memory required to capture a given time interval of a wireless information signal is reduced [107].

Furthermore, the bandpass sampling exploits the fact that, the required information bandwidths of most of the wireless applications are just small fractions of the wireless carrier frequency. Consequently, the wireless information signal can be sampled in accordance with its bandwidth. This enables the use of lower sampling frequency compared to when wireless carrier frequency is considered. However, care should be taken in choosing an appropriate sampling frequency to prevent spectral replica overlaps that can result in spectral aliasing [106, 107]. An appropriate bandpass filter can be employed to recover the wireless signal. In essence, with the implementation of bandpass sampling technique, frequency translation can be realized without the need for LO and mixers. Consequently, system complexity is significantly reduced [106]. This advantage manifests itself in the uplink path in which frequency translation stage is not required. Therefore, the BS design is further simplified. In the next subsection, we give comprehensive explanation on these schemes and discuss their applications to the transmission of broadband Orthogonal Frequency Division Multiplexing (OFDM) over fiber-wireless links.

2.5.3 Broadband OFDM Transmission in Fiber-Wireless Links

In practice, to improve the transmission capacity of a link, advanced modulation formats can be used together with the OFDM. This is because, OFDM has inherent advantages such as immunity to multipath fading, resilience to intersymbol interference (ISI), high-SE, efficient implementation using fast Fourier transform (FFT), and dispersion tolerance [108]. Due to this merits, it has been adopted by various existing wireless standards such as LTE and LTE-A standards for the cellular communications. It also finds application in IEEE802.11a/g/n/ac standards for wireless local area networks [109]. Also, it is employed for delivering high-

speed wireless personal area networks (WPANs) in the ultrawideband (UWB) spectrum by the WiMedia Alliance. Moreover, it has been adopted in Europe and Asia for terrestrial broadcast of digital television such as digital video broadcasting-Handheld (DVB-H), digital video broadcasting-terrestrial (DVB-T), and terrestrial-digital multimedia broadcasting (T-DMB) [110, 111]. For high-speed rate delivery and cost-efficiency in the future ultra-high speed wireless communication, an efficient delivery of the broadband OFDM signal at high frequency with cost-effective BS design is essential [112]. However, multi-carrier systems such as OFDM requires linear transmission link with the capability to handle high Peak-to-Average Power (PAPR) [100, 113, 114]. This will enable the high-PAPR signals in the system to be efficiently amplified by the BS PAs in order to meet the stringent linearity requirements by the wireless standards [115]. Analog RoF, digitized RoF, and sampled RoF transport schemes can be employed in the distribution of OFDM signals.

2.5.4 Frequency-Division Multiplexed Radio-over-Fiber (FDM RoF)

There might be strong justification for the analogue fronthaul links over fibers in the 5G cellular networks in which mm-wave and Massive MIMO technologies are envisioned to be integrated into the BSs. It is challenging and economically unattractive to provide CPRI links for massive number of antenna elements or for broad spectra of the mm-wave carriers. Therefore, a bandwidth-efficient MFH can be realized by transmitting multiple mobile channels through frequency-division multiplexing (FDM) in a single wavelength channel. This can be achieved by analog signal processing which includes frequency conversion and RF combining/splitting [12]. The spectral bandwidths of aggregated multiple wireless signals transmission over the optical channel might not change. Therefore, this results in more improved bandwidth efficiency compared to the CPRI based approach. Furthermore, for seamless control and management of the fronthaul equipment and/or to be compatible with CPRI, synchronous transmission of IQ waveforms of wireless signals and Control Word (CW) is essential. This leads to the concept of aggregated RoF/CW. Besides, an efficient DSP is required for channel aggregation and de-aggregation [12]. In the next subsection, we present comprehensive explanations on MFH transmission based on aggregated RoF/CW.

2.5.5 MFH Interface Based on Aggregated RoF/CW

Seamless transitions from the existing generational network to 5G require efficient MFHs in order to support key technologies such as UDN, carrier-aggregation, and Massive MIMO radio configurations. In this subsection, we give comprehensive explanations on MFH transmissions which are based on channel aggregation. The techniques can be employed to achieve bandwidth-efficient and cost-effective ultra-broadband access services in the 5G network and beyond. The concept of aggregated RoF entails transmission of multiple wireless signals that have been aggregated into one wavelength channel over the fronthaul. Moreover, for effective channel aggregation and de-aggregation, DSP can be employed. Since the existing MFH is mainly based on the CPRI, further transmission of CWs which are typically employed for C&M purposes are required for the aggregated RoF scheme to be compatible with the CPRI. Furthermore, synchronous transmission of IQ waveforms of wireless signals and CWs can be achieved in the MFH with the aid of frequency-division multiple access (FDMA). This is known as FDMA-based RoF/CW [12]. Another approach is the employment of time-division multiple access (TDMA) for the synchronous transmission and it is known as TDMA-based

RoF/CW [116].

The concept of a CPRI-based interface is that, in the downlink transmission, the generated wireless signals in the CO are aggregated and then converted into an optical signal with the aids of an optical transmitter. Furthermore, the subsequent optical signal is transmitted via an optical fiber based fronthaul link to the remote site. At the remote site, wireless signals which are designated for different antenna-carriers (AxCs) are de-aggregated and then delivered to their specified antennas for transmission. Similarly, the uplink transmission is typically a reverse process of the downlink transmission. Apart from the CPRI-based interface that is primarily employ in the MFH, FDMA-based RoF/CW and TDMA-based RoF/CW can also be employed for an effective performance [12, 116].

In general, Table 2.4 presents comparative analysis of the consider RoF transport schemes regarding the signal format, chromatic dispersion, transmission distance, BS simplification, linearity, optoelectronic device cost, and link performance. It is remarkable that, out of the schemes, analog RoF link offers the simplest BS configuration, however, it demands the use of costly optoelectronic devices. Similarly, occurrence of nonlinear distortion and chromatic dispersion in the system hinders its performance. So, it is only effective for supporting short distance transmission. On the other hand, sampled RoF transport scheme can employ narrow-bandwidth low-cost O-E/E-O converters, nonetheless, its performance is hindered by the nonlinear distortion. Furthermore, digitized RoF transport scheme compared to the analog transport scheme, results in more complex structure for the BS. Similarly, its implementation leads to higher cost of O-E/E-O converters relative to the sampled transport scheme. However, it offers the best link performance compared to the others.

Table 2.4: Comparison of RoF transport schemes features (adapted from [112])

	Analog RoF	**Sampled RoF**	**Digitized RoF**
Signal format	RFoF	IFoF	BBoF
Nonlinear distortion	Not good from O-E/E-O	Not good from O-E/E-O	✓Good from ADC
Chromatics dispersion	Not good	✓Good	✓Good
Transmission distance	Short	✓Long	✓Long
O-E/E-O cost	High	✓Low	Medium
BS simplification	✓Good	Medium	Medium
Link performance	Not good (20km) Good(b2b)	Medium	✓Good

It is noteworthy that, the wide adoption of any generation network depends among other factors on the backward compatibility with other networks. The fact that we are not expected to think about the 5G as any other existing networks does not mean that certain contemporary concepts will not be adopted for the 5G network. The current broadband networks such as 3G and 4G rely mainly on fiber, microwave or mm-wave approaches for BSs connections. It is noteworthy that, deployment of RoF technology depends on the availability of the installed optical fiber cables between different network facilities. However, for cell densification, fiber deployment is cost intensive and time consuming especially when trenching is required. Moreover, acquisition of right-of-way permits for BSs location might be one of the limiting factors for appropriate system deployment [117]. Because of these challenges and the limited amount

of installed fiber cables, the viability of FSO communication system has been recognized. The FSO scheme concepts are comprehensively discussed in the next chapter.

2.5.6 Software-Defined Fronthaul (SDF)

It is noteworthy that, even though C-RAN decouples the BBUs from the RRHs regarding the physical placement, a one-to-one logical mapping between the entities still exist. For instance, a BBU can be assigned tentatively for generating/receiving signal to/from an RRH. The mapping helps in the generation of distinct frame for individual cell in order to improve network capacity when technique such as dynamic fractional frequency reuse (FFR) or CoMP is implemented. Nonetheless, a fixed one-to-one mapping concept limits the C-RANs performance and can be attended to by deploying switching hardware in the fronthaul for flexible mapping of the BBUs and RRHs connections. Not only that this approach aids traffic optimization in the RAN but also helps in the energy optimization in the BBU pool. The concept of programmable fronthaul network is known as software-defined fronthaul (SDF). Means of realizing SDF, its potential and challenges are discussed in [24]. Furthermore, Table 2.5 presents different innovative fronthaul interfaces. Also, in Table 2.6 we present some experimental efforts toward an efficient MFH.

Table 2.5: Innovative fronthaul interfaces

Key Concept	Challenges	Method of Solution	Reference
• Next-generation fronthaul interface (NGFI) • Fronthaul-lite • NGFI: xHaul • Software-defined fronthaul (SDF) • FluidNet • 5G-Crosshaul	• Latency • Synchronization • Communication protocol • Switching method • Heterogeneity • Operational cost • Reliability • Flexibility • Scalability	• High-performance switching techniques • Functional split • Radio protocols evolution • Efficient bandwidth utilization • Logical configurations • Ethernet network support • Common frame format • Forwarding abstraction • Crosshaul slices • Unified management	[24, 56, 118–125]

Table 2.6: Experimental efforts toward an efficient MFH

	Processes												
Reference	**SDN**	**Fiber monitoring**	**Multiplexing scheme**	**DSP-based data-mapping**	**IF signal transmission**	**Microwave**	**mm-wave**	**m-MIMO**	**FDM RoF/CW**	**TDMA RoF/CW**	**Crosstalk cancellation**	**Virtual tone-based DSP**	**Hybrid RF/FSO**
[126, 127]			√	√				√					
[128]	√		√										
[129]			√			√	√						
[40, 130–132]		√	√										
[12, 112, 116, 129, 133–136]			√	√	√								
[12, 137]			√	√	√				√				
[116, 138]			√	√	√					√			
[139]			√								√		
[140]			√									√	
[93, 141, 142]			√		√								
[143, 144]			√			√							√

2.6 Research Contributions

Based on the manuscript [45], this chapter presents comprehensive overview of the MFH transport solutions. Furthermore, it offers different centralized RAN architectural modifications that are necessary for bandwidth reduction in the MFH. In addition, a number of optical technologies that can facilitate flexibility and multiple system operational functionalities in the MFH are presented. The chapter then expatiates on the required evolution towards efficient fronthauls for the 5G networks and beyond.

2.7 Conclusion

The 5G networks are envisioned to be heterogeneous communication systems that have the capabilities of supporting a number of advanced wireless technologies, services and applications. C-RAN is an attractive and feasible solution for efficient realization of the envisaged goals of the 5G network. This is as a result of its appealing features in terms of performance optimization and cost-effectiveness. However, the C-RAN architecture imposes stringent requirements on the fronthaul link in order to achieve seamless connectivity between the network elements. This chapter has presented comprehensive overview of the key technologies, architectures, requirements, and challenges of the C-RAN MFH. Moreover, some related open-ended issues are considered and the proffered prospective solutions on means

of realizing an efficient C-RAN MFH for the NGNs are well discussed. In addition, current fronthaul solutions and their limitations in the 5G cellular networks in which mm-wave and Massive MIMO technologies are envisaged to be integrated are considered. Also, the chapter has presented potential modifications to address the bandwidth required for digital signal transportation in the MFH network. Additionally, different methods of achieving an efficient MFH as well as technologies for the access network performance enhancement have been presented. Schemes that can help in reducing the system complexity, cost, bandwidth requirement, and latency in the MFH have been discussed. In addition, different optical technologies that facilitate flexibility and multiple system operational functionalities in the fronthaul network have been discoursed. Furthermore, the related technical challenges of their applications are deliberated. Moreover, potentials of SDF for an efficient, automatic network management, and provisioning have been outlined.

Chapter

3

Free Space Optical Communication Systems

The FSO communication has been gaining significant attention as an attractive broadband access technology that offers high-speed and enhanced capacity. Furthermore, OWC is a promising technology in sensitive or hazardous environments where the implementation of the RF technology is not permitted. Also, OWC contributes to green communications and networking as the required components consume low power compared to the RF options that demand high power consumption for the signal processing and transmission. Consequently, it has been considered as an alternative and/or complementary technology for the current wireless RF solutions. In this chapter, based on manuscripts [14, 145, 146], comprehensive overview of FSO communication systems are presented. Furthermore, we study the effects of different parameters such as constellation size, wavelength, and refractive index on the RoFSO transmissions. Moreover, different modulation formats for adaptive modulation scheme are considered under different operating conditions.

3.1 Introduction

The Internet is experiencing high growth with varieties of bandwidth-intensive mobile applications on an unprecedented scale. One of the potential reasons for the growth is the Internet of Things (IoT) technologies that have brought exceptional revolutions into the number of devices in the network. Conceptually, IoT entails ubiquitous existence of a variety of *things* such as mobile phones, sensors, actuators, and RF identification (RFID) tags. These entities are capable of interacting with each other as well as cooperating with their neighbors in order to accomplish common goals via unique addressing scheme [147]. It is envisaged that by the year 2020, billions of devices with an average of 6-7 devices per person will be connected to the Internet [148]. The 5G wireless communication systems in which mm-wave and Massive MIMO antenna technologies are expected to be integrated are the promising solutions for supporting the huge amount of anticipated devices. However, the RF-based

wireless mobile technologies transmission speeds are limited by the available RF spectrum in the regulated RF spectrum. This is due to various innovative wireless technologies and standards like WiMAX (IEEE 802.16), UWB (IEEE 802.15), Wi-Fi (IEEE 802.11), iBurst (IEEE 802.20), the cellular based 3G and 4G [146]. Moreover, because of various advanced technologies being employed in the optical communications, there have been considerable advancements in the optical system capacity, network reach, and number of supported users. For example, the optical-fiber based broadband network architectures like FTTH and fiber to the building (FTTB) present commercial solutions to the communication barriers by progressively rendering services closer to the customers via the PON technologies such as, GPON, XG-PON, and EPON. Currently, one of the major challenges is the capability to support various service requirements so as to achieve elastic and ubiquitous connections [149]. Consequently, convergence of wireless and optical networks is highly essential for cost-effective and pervasive network penetration for the NGNs. The convergence will help in exploiting the mobility benefit offered by the wireless connectivity and the inherent bandwidth provided by the optical systems. This will help in achieving the anticipated capacity and energy-efficiency objectives of the NGNs [146]. Furthermore, OWC system is one of attractive broadband access technologies that offers high-speed as well as improved capacity. Consequently, the OWC can attend to the bandwidth requirements of different services and applications of the NGNs at relatively low cost [146, 150].

The OWC can be an alternative and/or complementary technology for the current wireless RF solutions. For instance OWC operating at 350-1550 nm wavelength band can offer high-data rate of about 30 Gb/s data rate. This advantage makes it an attractive solution for addressing the prevailing “last mile” and “last-leg” problems in the access network. Furthermore, in mobile communication, resources re-use is an important requirement in order to enhance the network coverage and capacity. OWC technology is able to meet this requirement with the aids of spatial diversity [150, 151]. OWC link can be of different configurations such as

1. Directed line-of-sight (LOS)
2. Non-directed LOS
3. Diffuse
4. Quasi diffuse
5. Multi-spot LOS

Out of these configurations, the LOS links have the highest data rates, lowest bit error rate (Bit Error Ratio (BER)) performance, and less complex protocol. These features make LOS link the extensively employed configuration in the outdoor applications. Nevertheless, the major deficiencies of the LOS link are lack of mobility and susceptibility to blockage. The diffuse and non-directed LOS configurations, on the other hand, give better mobility advantages and are less susceptible to shading. However, noise, path loss, and multi-path induced dispersion relatively hinder their achievable data rate for high-speed links. IM/DD is the most widely used scheme in OWC systems. Furthermore, coherent scheme can also be employed to enhance channel usage. The implementation of coherent scheme relatively improve system performance at the expense of increased system complexity. This can be attributed to the fact that, precise wave-front matching between the incoming signal and

the LO is required to guarantee efficient coherent reception. Furthermore, DD application is uncomplicated as just low-cost transceiver devices are required without the necessity for the intricate high-frequency circuit designs relative to coherent systems [150, 151].

In this chapter, we present a comprehensive overview of OWC systems and RoFSO transmission schemes. Moreover, we study the effects of different parameters such as constellation size, wavelength, and refractive index on RoFSO transmissions. Furthermore, different modulation formats for adaptive modulation scheme are considered under different operating conditions.

With the need for OWC systems being presented, in Section 3.2, block diagram of OWC system is discussed. Section 3.3 on the following page highlights safety and regulations for optical beam transmissions as well as the associated international standard organizations. In Section 3.4 on page 48, OWC system classifications are comprehensively discussed. Also, in Section 3.5 on page 53 RoFSO is presented for enhancing the system performance and extending broadband connectivity. Section 3.6 on page 54 presents optical system and channel models with parameters such as atmospheric attenuation, pointing error, and atmospheric turbulence being considered. We analyze the system performance in Section 3.7 on page 61. In Section 3.8 on page 63, simulation results are presented with comprehensive discussions. We discuss research contributions in Section 3.9 on page 65 and concluding remarks are given in Section 3.10 on page 66.

3.2 Block Diagram of OWC System

A terrestrial OWC system consist of the transmitter, channel, and receiver. Figure 3.1 illustrates a schematic of a terrestrial OWC system. The source at the transmitter generates information waveforms which are modulated onto an optical carrier. The optical field produced is then radiated over the atmospheric channel to the destination. The optically collected field at the receiver is then transformed to an electrical current. The detected electrical current is processed in order to recover the original transmitted information [152]. However,

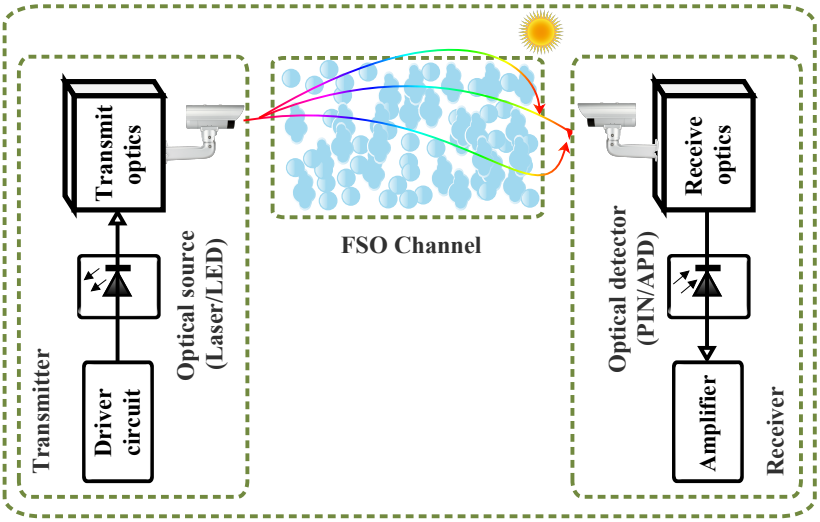

Figure 3.1: Block diagram of a terrestrial OWC system.

the received information may not be an exact replica of the original transmitted information because of the transmission loss experienced over the channel by the signal. This factor significantly limits the performance of wireless communications systems.

The transmission loss is mainly due to the resultant effects of scattering and absorption which are being introduced by the molecular constituents and aerosols along the transmission path. Therefore, scattering and wavelength dependent absorption are the key components of atmospheric attenuation. Since absorption is a function of wavelength and wavelength selective, there are a range of wavelength windows that experience comparatively minimal absorptions.

In general, the wavelength ranges 780-850 nm and 1520-1600 nm commonly used in the current OWC equipment are located in the atmospheric transmission windows where molecular absorption is negligible. This helps in mitigating the atmospheric absorption losses. Furthermore, certain wavelength windows that are located in the region of four specific wavelengths such as 850, 1060 nm, 1250 nm, and 1550 nm normally experience an attenuation of less than 0.2 dB/km. It is noteworthy that, the 850 nm and 1550 nm transmission windows coincide with the standard transmission windows of fiber communication systems. For this reason, majority of commercial OWC systems operates at these two windows in order to encourage the use the available off-the-shelf components. Also, wavelengths like 10 μm and ultraviolet (UV) have also been considered for the OWC systems. The 10 μm wavelength has better fog transmission characteristics, whereas, the UV wavelength is more robust against impairment such as pointing errors and beam blockage. Also, the UV wavelength is less susceptible to solar and other background interferences [152].

Furthermore, it is noteworthy that, 1520-1600 nm wavelengths are compatible with erbium-doped fiber amplifier (EDFA) technology. This is highly essential in order to achieve high-power and high-data rate systems. Moreover, 1520-1600 nm wavelengths enable transmission of about 50-65 times more average output power than can be transmitted at 780-850 nm for a specified eye safety classification. This can be attributed to the low transmission of the human eye at these wavelengths [153].

3.3 Safety and Regulations

One of the key factors for the laser transmitter design is the safety issue. The infrared (IR) light sources can be likely safety threats to human if they are operated inappropriately. Also, exposure to certain optical beams may injure human skin and eye. However, the likely harm to the eye is comparatively more severe due to the eyes ability to focus and concentrate optical energy. For instance, the eye can focus wavelength range 0.4-1.4 μm on the retina with enough intensity to damage it; however, other wavelengths can be absorbed by the front part of the eye before being focused on the retina. It should be noted that, laser that is deemed to be "eye-safe" is also "skin-safe" [150, 153].

Moreover, it has been shown that, the absorption coefficient at the front part of the eye is considerably greater for longer wavelengths (>1400 nm). Consequently, the permissible average transmission power for lasers operating at 1550 nm is relatively higher. Therefore, they are usually employed for longer transmission range [150, 153].

Figure 3.2 depicts the response of the eye at different wavelengths. At 700-1000 nm spectral range, the cost of optical sources and detectors are relatively low, however, the eye safety regulations are mainly strict. The maximum permissible exposure (MPE) at 900 nm

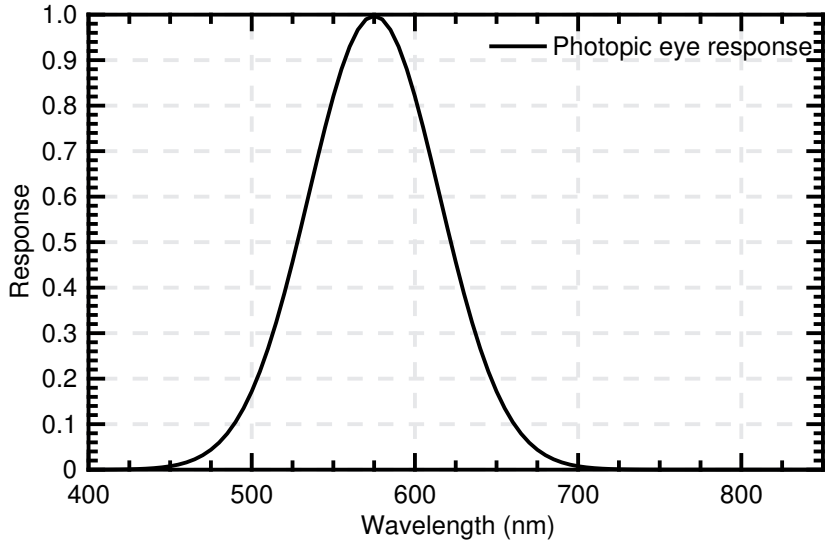

Figure 3.2: Response of the human eye at different wavelengths (adapted from [150, 153]).

wavelength is ∼143 mW/sr. On the other hand, at longer wavelengths (≥1500 nm), the eye safety regulations are relatively less stringent, however, devices operating in these wavelengths are comparatively expensive. The guidelines on safety of optical beams have been specified by several international standard organizations such as [150, 153]

1. International Electrotechnical Commission (IEC)
2. Center for Devices and Radiological Health (CDRH)
3. European Committee for Electrotechnical Standardization (CENELEC)
4. American National Standards Institute (ANSI)
5. Laser Institute of America (LIA)

The aforementioned organizations have established mechanisms for categorizing lasers in accordance with their type and power. Generally, the classification is based on four groups which are Class 1 through Class 4. Comparatively, Class 1 is the least powerful whereas Class 4 is the most powerful. Also, each of the classes is specified by the accessible emission limits (AEL) metric. The AEL is determined by the optical source wavelength, the emitter geometry, and the source intensity [150, 153]. Consequently, the AEL varies from one OWC category to another. In the next section, we present the major OWC categories.

3.4 OWC System Classification

There have been growing research interests in the OWC system as a viable solution to attend to the NGNs requirements in cost-effective ways. The two generic groups of OWC are indoor and outdoor optical wireless communications. The unlimited bandwidth offers by the OWC can be attributed to different bands such as IR, Visible (VL), and UV being employed

for communication purposes. Figure 3.3 shows the electromagnetic spectrum for different applications. Furthermore, the spectrum illustrates the frequency and wavelength ranges being occupied by the bands in OWC. The indoor OWC employs IR or VL light for an in-building wireless solutions. It is of high importance especially in scenarios in which the probability of offering network connectivity through physical wired connections are challenging. Moreover, the indoor OWC systems can be categorized into four broad configurations such as tracked, diffused, non-directed LOS, and directed line-of-sight (LOS). Furthermore, the outdoor OWC employs optical carrier for transporting information from one point to another over an unguided channel that could be an atmosphere or a free space. So, this OWC technology is also known as a FSO communication system. The FSO communication systems operate at the near IR frequencies and are classified into terrestrial and space optical links. These consist of building-to-building, satellite-to-ground, ground-to-satellite, satellite-to-satellite, and satellite-to-airborne platforms (unmanned aerial vehicles (UAVs) or balloons) [154]. The tree diagram in Fig. 3.4 shows the OWC system classification.

3.4.1 Visible Light Communication (VLC) Systems

The current enhancement of Light-Emitting Diode (LED) chip design with swift nanosecond switching times and extensive deployment of LEDs for energy efficiency pave the way for Visible Light Communication (VLC) system [155, 156]. So, the VLC system has become an attractive technology for addressing challenges such as energy efficiency, bandwidth limitation, electromagnetic radiation, and safety in wireless communications [157, 158]. The VLC system operates in the wavelength range of $\sim$ 390-750 nm. The concurrent support for communication and illumination by the VLC offer the following advantages over the RF communications:

3.4.1.1 Huge Bandwidth

It exhibit almost unlimited and unlicensed bandwidth which approximately ranges from 380-780 nm. Therefore, VLC has 350 THz that can support multi-gigabit-per-second data rates with LED arrays in a MIMO configuration [156]. This makes VLC a good alternative to the indoor IR that operates at 780-950 nm for the access technologies [151].

3.4.1.2 Low Power Consumption

The VLC provides both communication and lighting, giving Gbps data rates with only unsophisticated LEDs and Photo-Detector (PD)s that consume low power compared to costly RF alternatives that demand high power consumption for sampling, processing, and transmitting Gbps data [156].

3.4.1.3 Low Cost

The required optical components such as LEDs and PD are inexpensive, compact, lightweight, amenable to dense integration, and have very long lifespan [155]. Moreover, with large unlicensed optical spectrum, as well as much lower power-per-bit cost compared to the RF communications, the VLC is relatively cheaper.

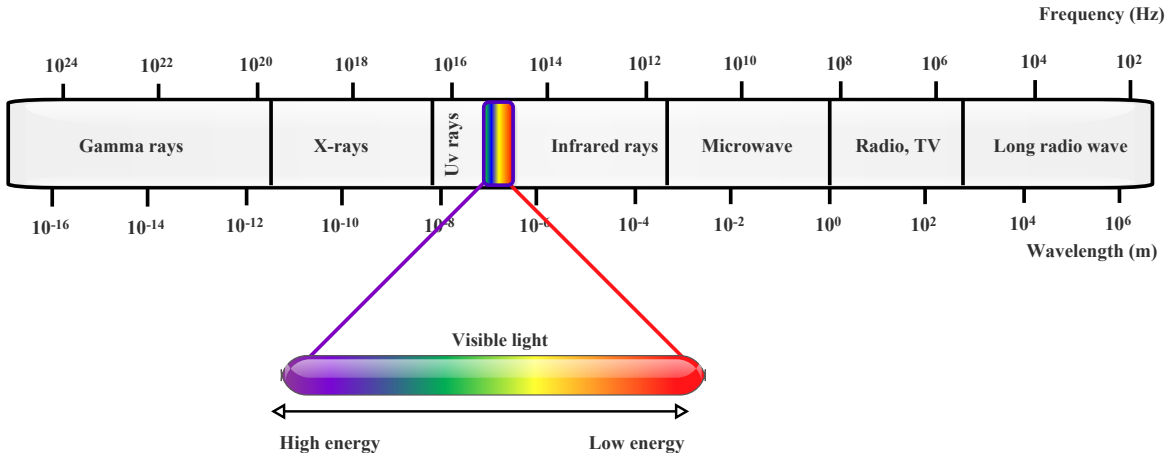

Figure 3.3: Electromagnetic spectrum.

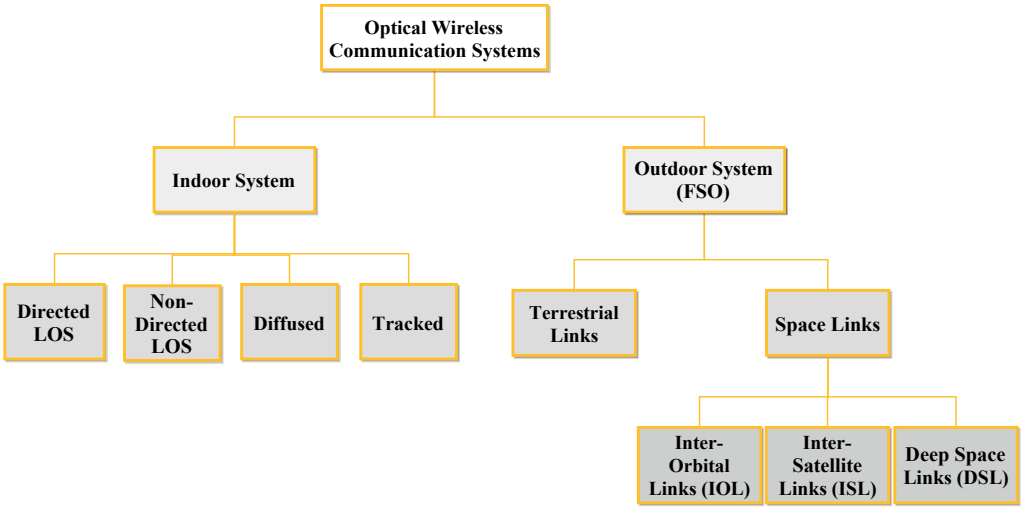

Figure 3.4: Optical wireless communication system classification (adapted from [154]).

3.4.1.4 No Health Concerns

The VLC does not generate radiation that leads to public health concern. Besides, it lowers the carbon dioxide emission owing to the little extra power consumption for communication purposes [159].

3.4.1.5 Ubiquitous Computing

Due to the fact that there are various luminous devices like traffic signs, commercial displays, indoor/outdoor lamps, TVs, car headlights/taillights, etc. being used everywhere, VLC can be employed for wide range of network connectivity [160].

3.4.1.6 Inherent Security

The VLC offers comparatively higher security due to the fact that, it is highly intricate for a network intruder that is outside to pick up the signal [156].

3.4.1.7 Indoor Localization

The existing RF based GPS gives inadequate or no network coverage in the indoor and underground (e.g. tunnel) environment. This is as a result of high attenuation, multipath, and the safety regulation. These factors lead to an accuracy of only up to a few meters for the RF based GPS. The VLC based indoor positioning can be employed to attend to the issues in the enclosed environments. So, the VLC based indoor navigation services offer very high accuracy to within a few centimeter. In essence, VLC offers good indoor localization system using the white LEDs. Furthermore, LEDs give better light source that is more than 400 lux. This is sufficient for high speed data transmission compared to the incandescent and fluorescent sources. Moreover, LEDs have longer lifespan that results in ecological and financial benefits [151].

In addition, VLC is an alternative technology in sensitive or hazardous environments like airplanes, hospitals, and industrial gas production plants where the employment of RF technology is not permitted. The worldwide research community through bodies like the Wireless World Research Forum, the IEEE standardization body, the VLC consortium, the UK research council, and the European OMEGA project has embraced the indoor short range VLC as a promising scheme because of the associated excellent attributes [151].

However, simultaneous employment of light sources for the data communication, as well as illumination, cause certain challenges that require consideration for the VLC system implementations to be viable. Flicker mitigation and dimming support are the two major challenges of visible light spectrum [156, 161]. In the contemporary lighting systems, the light sources are equipped with dimming control functionality that enables the users to control the average brightness of light sources to their preferred level. Flicker is the variation in the brightness of light perceived by the human naked eye. Flicker is as a result of continuous switching on and off of the light source during data transmission. It is essential to mitigate any possible flicker because, it can instigate negative/harmful physiological changes in humans. Flicker can be prevented by making the changes in brightness be within the maximum flickering time period (MFTP). The MFTP is the maximum time period within which the light intensity can be changing without any perception by the human eye [156]. Also, various modulation formats have been recommended for VLC in view of dimming control and flicker mitigation. For instance, the IEEE 802.15.7 standard proposes variable pulse position modulation (VPPM) for the VLC system because of its notable ability to control dimming. It integrates the pulse position modulation (PPM) and pulse width modulation (PWM) in order to support communication with dimming control [156,161]. Furthermore, other challenges are high path losses, multipath induced intersymbol interference (ISI), artificial light induced interference, and blocking. Moreover, LED electro-optic response nonlinearity has to be taken into consideration [151].

3.4.2 Terrestrial Free Space Optical (FSO) Communications

There have been much more research effort in the terrestrial FSO partly because of some successful field trials and commercial deployments [64, 162–165]. Figure 3.5 on the following

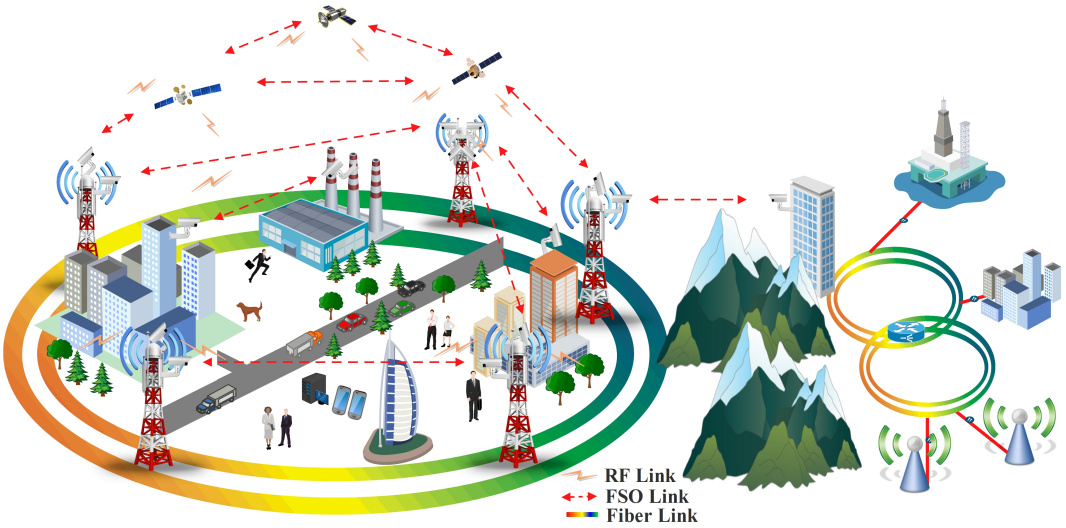

Figure 3.5: A scenario for OWC system deployment for access networks.

page shows a scenario for the FSO system deployment as a universal platform for a nippy, as well as an efficient ubiquitous wireless service provision, for the future broadband access networks. The significant attentions being attracted by the FSO systems are primarily due to their inherent advantages such as cost-effectiveness, lower power consumption (high energy efficiency-green communication), ease of deployment, higher bandwidth/capacity, more compact/low mass equipment, reduced time-to-market, immunity to EMI, high degree of security against eavesdropping, license-free operation, as well as better protection against interferences, compared with the traditional RF communication systems [166, 167]. These salient features make FSO communication systems very appealing for variety of applications in disaster recovery, radio astronomy, remote sensing/surveillance/monitoring, metropolitan area network extension, high definition TV transmission, sharing of medical imaging in real-time, fronthaul and backhaul for wireless cellular networks [146, 152]. Moreover, apart from being used for establishing terrestrial links, they are applicable for launching high speed interplanetary space links such as inter-satellite/deep space, and ground-to-satellite/satellite-to-ground links [154].

In spite of the advantages of FSO communication and diverse application, its extensive use is hindered by some challenges in real-life scenarios. For instance, the FSO links are susceptible to scattering caused by adverse weather conditions like snow, rain, and fog [152, 167]. Moreover, building-sway caused by factors such as thermal expansion, wind loads, and weak earthquakes also impairs the FSO link performance [167]. Also, atmospheric turbulence-induced fading has been recognized as the main contributor of the FSO link impairment [167, 168]. Consequently, the system performance is impeded as a result of atmospheric effects which cause loss of spatial coherence, beam spreading, and temporal irradiance fluctuation known as scintillation or fading [152, 169]. Scintillation manifests as temporal and spatial variation in the light intensity along the transmission path. This is due to the random changes in the refractive index which is as a result of the inhomogeneties in the air temperature and pressure [152, 166]. For these reasons, the dispersive nature of the link needs considerable attention when modeling an FSO system. This will help in supporting the stringent require-

ments of various bandwidth-intensive mobile applications of the NGNs [146]. The FSO link impairment modelings are discussed in Section 3.6. The tree diagram in Fig. 3.6 presents different atmospheric turbulence mitigation techniques.

3.5 Radio-on-free space optical (RoFSO)

The RoF involves transmission of RF signals using optical fiber links and has been employed as a cost-effective and high-capacity solution in order to simplify the wireless access. Nevertheless, its implementation depends significantly on the availability of fiber cable infrastructure. Consequently, in an environment without fiber cable installations, FSO links can be employed for appropriate RF signals transmissions. This scheme is similar to RoF scheme but it requires no fiber medium like RoF. Therefore, the concept of transmitting the RF signals by means of FSO links is referred to as RoFSO. The RoFSO scheme integrates advantages of high transmission capacity offered by optical technologies as well as ease of deployment of wireless links. The RoFSO systems are generally deployed for last-mile access solutions in terrestrial communications. The implementation helps in extending broadband connectivity to poorly served areas. It can also serve as a backup link for both fiber and RF links as discussed in Chapter 6 on page 89. Nevertheless, the performance of RoFSO link can be hindered by factors such as rain, fog, atmospheric turbulence, as well as non-ideal characteristics of optical transmitters and receivers. [14, 146, 170]

OFDM has been adopted in a number of high-speed digital communication standards. This is due to its remarkable advantages such as narrow-band interference, robustness against frequency selective fading, and high channel efficiency. In general, the baseband OFDM signal

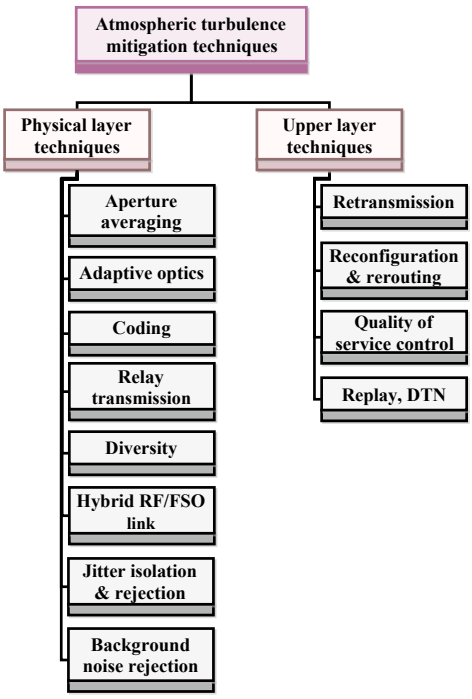

Figure 3.6: Atmospheric turbulence mitigation techniques (adapted from [154]).

is complex and bipolar. Conversely, OFDM transmission over optical link using IM/DD scheme requires a real and positive RF signal for driving the Laser Diode (LD). Consequently, Hermitian symmetry can be implemented on the input vector to the transmitter inverse fast Fourier transform (IFFT) block so as to generate the real OFDM signal. Moreover, OFDM signal can be transformed into unipolar by adding a direct current (DC) bias to the OFDM signal (DC-OFDM). This process ensures that the subsequent signal is positive. In order to prevent clipping and distortion in the optical domain, the DC bias has to be sufficiently large. Generally, IM/DD multiple-subcarrier modulation (MSM) systems have major disadvantages such as average optical power inefficiency that is due to the large added DC bias and distortions that is due to the LD and optical channel nonlinearity [170].

3.6 Optical System and Channel Model

Assuming a practical FSO link with IM/DD using OOK modulation, the data is modulated onto the instantaneous intensity of an optical beam at the transmitter. The optical power emanated from the transmit aperture into the free space is assumed to be affected by factors such as misalignment fading (pointing errors), atmospheric turbulence induced fading, and background noise or ambient noise before reaching the receive aperture. These factors lead to the signal intensity fluctuation. Consequently, the subsequent received electrical signal, r at the receive aperture can be modeled as [146, 169, 171, 172]

$$r = \eta_e h x + n, \tag{3.1}$$

where $x \in \{0, 1\}$ denotes the transmitted information bit, η_e is the effective photoelectric conversion ratio of the receiver, n is Additive White Gaussian Noise (AWGN) with zero mean and variance $\sigma_n^2 = N_0/2, N_0$ is a one-sided noise power spectral density in watts/Hz, and $h = h_\ell h_\mathrm{a} h_\mathrm{p}$ represents the irradiance that influences the channel state. The channel irradiance in Eq. (3.1) is a product of the deterministic path loss, h_ℓ; the random attenuation (i.e. atmospheric turbulence-induced fading), h_a; as well as the random attenuation (due to geometric spread and pointing errors), h_p. The h_a and h_p are random variables with probability density functions (pdfs) $f_{h_\mathrm{a}}(h_\mathrm{a})$ and $f_{h_\mathrm{p}}(h_\mathrm{p})$, respectively.

3.6.1 Atmospheric Attenuation

When an optical beam passes through the atmosphere, it experiences atmospheric loss. The attenuation suffered by the signal power according to the exponential Beers-Lambert law is given by [171–173]

$$h_\ell(\lambda, z) = \frac{P(\lambda, z)}{P(\lambda, 0)} = \exp(-\sigma(\lambda) z) \tag{3.2}$$

where $h_\ell(\lambda, z)$ denotes the loss that is a function of propagation path of length z at wavelength λ, $P(\lambda, z)$ and $P(\lambda, 0)$ are the signal power and the emitted power at distance z, respectively. The attenuation coefficient or the total extinction coefficient, $\sigma(\lambda)$ per unit of length, is given by [171]

$$\sigma(\lambda) = \alpha_m(\lambda) + \alpha_a(\lambda) + \beta_m(\lambda) + \beta_a(\lambda), \tag{3.3}$$

where α_m and α_a represent molecular and aerosol absorption coefficients, respectively. Also β_m and β_a denote molecular and aerosol scattering coefficients, respectively.

The attenuation h_ℓ is assumed to be a constant scaling factor over a long time period, so, there is no haphazard behavior. Moreover, it is subject to the distribution and size of the scattering particles as well as the wavelength employed. It can be expressed in terms of visibility, which can be measured directly from the atmosphere. Empirically, attenuation can be defined in terms of visibility as [145, 171]

$$\sigma(\lambda) = \frac{3.912}{V}\left(\frac{\lambda}{550}\right)^{-q}, \tag{3.4}$$

where V is the visibility (in kilometers) and q is a parameter that depends on the particle size distribution in the atmosphere expressed by the Kruse model as [145, 171]

$$q = \begin{cases} 1.6 & V > 50 \text{ km} \\ 1.3 & 6 \text{ km} < \text{V} < 50 \text{ km} \\ 0.585V^{1/3} & V < 6 \text{ km} \end{cases} \tag{3.5}$$

Furthermore, Kim presents an extended model in order to achieve a better accuracy at lower visibility scenarios. The Kim model is expressed as [145, 171]

$$q = \begin{cases} 1.6 & V > 50 \text{ km} \\ 1.3 & 6 \text{ km} < \text{V} < 50 \text{ km} \\ 0.16V + 0.34 & 1 \text{ km} < \text{V} < 6 \text{ km} \\ V - 0.5 & 0.5 \text{ km} < \text{V} < 1 \text{ km} \\ 0 & V < 0.5 \text{ km} \end{cases} \tag{3.6}$$

3.6.2 Pointing Error or Misalignment Fading

The FSO link is a LOS communication with narrow optical beamwidth that brings stringent pointing accuracy requirements for an efficient performance and the reliability of optical systems. The pointing errors and signal fading normally occur at the receiver because of the wind loads and thermal expansions that lead to random building sways. Assuming a Gaussian spatial intensity profile of beam waist w_z at the receiver plane, located at distance z away from the transmitter. Also, suppose a circular aperture of radius r, the collected power fraction owing to the geometric spread with radial displacement α, from the detector origin can be approximated as the Gaussian form [145, 172, 173]

$$h_{\text{p}}(\alpha) \approx A_0 \exp\left(-\frac{2\alpha^2}{w_{z_{eq}}^2}\right) \tag{3.7}$$

where $w_{z_{eq}}^2 = w_z^2\left[\sqrt{\pi}\text{erf}(\upsilon)\right] / \left[2\upsilon\exp\left(-\upsilon^2\right)\right]$, $\upsilon = \sqrt{\pi}r/\sqrt{2}w_z$, $A_0 = \left[\text{erf}(\upsilon)\right]^2$, $w_{z_{\text{eq}}}$ is the equivalent beamwidth, and $\text{erf}(\cdot)$ denotes the error function given by [145, 174]

$$\text{erf}(x) = (2/\sqrt{\pi})\int_0^x e^{-u^2}du \tag{3.8}$$

If we assume that the elevation and the horizontal sway are independent and identical Gaussian distributions, then the radial displacement, α, follows a Rayleigh distribution. Then, the $f_{h_{\text{p}}}(h_{\text{p}})$ can be defined as [145, 172, 173]

$$f_{h_\mathrm{p}}(h_\mathrm{p}) = \frac{\gamma^2}{A_0^{\gamma^2}} h_\mathrm{p}^{\gamma^2-1}, \quad 0 \leq h_\mathrm{p} \leq A_0 \tag{3.9}$$

where $\gamma = w_{z_{eq}}/2\sigma_s$ represents the ratio between the equivalent beam radius and the standard deviation (jitter) of the pointing error displacement at the receiver and σ_s^2 is the jitter variance at the receiver.

3.6.3 Atmospheric Turbulence

The intensity fluctuation over the FSO channel has been defined by several statistical models in the literature for different turbulence regimes. One of such model is the log-normal (LN) distribution that has been extensively employed because of its significant match with the experimental measurements. This is discussed further in chapter 7 on page 101. Some of the other widely employed models are gamma-gamma ($\Gamma\Gamma$), negative exponential, K distribution, and I-K distribution. However, in this work, we focus on the LN, $\Gamma\Gamma$, and generic Málaga ($\mathcal{M}$)-distribution models.

3.6.3.1 Log-normal Distribution (LN)

In general, the LN model is only suitable for weak turbulence conditions and for link range that is less than 100 m [175]. So, the intensity fluctuation pdf for the weak turbulence modeled by the LN distribution is given by [145, 146, 169]

$$f_{h_\mathrm{a}}(h_\mathrm{a}) = \frac{1}{2h_\mathrm{a}\sqrt{2\pi\sigma_x^2}} \exp\left(-\frac{(\ln(h_\mathrm{a}) + 2\sigma_x)^2}{8\sigma_x^2}\right), \tag{3.10}$$

where $\sigma_x^2 = \sigma_l^2/4$ represents the log-amplitude variance defined for plane wave and spherical waves, respectively as [145, 146, 169]

$$\sigma_x^2|_{\mathrm{plane}} = 0.307 C_n^2 k^{7/6} L^{11/6}, \tag{3.11a}$$

$$\sigma_x^2|_{\mathrm{spherical}} = 0.124 C_n^2 k^{7/6} L^{11/6}, \tag{3.11b}$$

$$\sigma_l^2|_{\mathrm{plane}} = 1.23 C_n^2 k^{7/6} L^{11/6}, \tag{3.11c}$$

$$\sigma_l^2|_{\mathrm{spherical}} = 0.50 C_n^2 k^{7/6} L^{11/6}, \tag{3.11d}$$

where σ_l^2 is the log-irradiance variance, $k = 2\pi/\lambda$ represents the optical wave number, L denotes the distance, and C_n^2 is the altitude-dependent index of refraction structure parameter. The C_n^2 is a main parameter for distinguishing the amount of refractive index fluctuation in the atmospheric turbulence. It is a function of the atmospheric altitude, wavelength, and temperature. There are a number of C_n^2 profile models being proposed in the literature, however, the extensively used one in terms of altitude is the Hufnagle-Valley model given by [145, 146, 150, 169, 174]

$$C_n^2(h) = 0.00594(v_w/27)^2(10^{-5}h)^{10}\exp(-h/1000) + 2.7\times10^{-16}\exp(-h/1500) + \hat{A}\exp(-h/100), \tag{3.12}$$

where h signifies the altitude in meters (m) and $\hat{A}$ represents the nominal value of $C_n^2(0)$ at the ground level in $m^{-2/3}$. The value of C_n^2 for the FSO links near the ground level is

approximately 1.7 $\times 10^{-14} m^{-2/3}$ and $8.4 \times 10^{-15} m^{-2/3}$ during the daytime and at the night, respectively. Generally, C_n^2 ranges from $10^{-13} m^{-2/3}$ for the strong turbulence to $10^{-17} m^{-2/3}$ for the weak turbulence. Its typical average value is $10^{-15} m^{-2/3}$ [150, 174]. The v_w denotes the root mean square (rms) wind speed (pseudowind) in meters per second (m/s) with most usual value of 21 m/s, but, it can be described by [174]

$$w = \left[\frac{1}{15 \times 10^3} \int_{5\times10^3}^{20\times10^3} V^2(h) dh \right]^{1/2}, \tag{3.13}$$

where $V(h)$ is normally defined by the Bufton wind model that can be expressed as [145, 174]

$$V(h) = \omega_s h + V_g + 30 \exp\left[-\left(\frac{h - 9400}{4800} \right)^2 \right] \tag{3.14}$$

where V_g denotes the ground wind speed and ω_s signifies the *slew rate* that is related to the satellite movement regarding the observer on the ground.

We substitute different values of the log-irradiance variance i.e. $\sigma_l^2 \in (0.01, 0.1, 0.4, 0.9)$ in eq. (3.11) on page 56 into eq. (3.10) on page 56 in order to estimate the intensity fluctuation pdf for the LN distribution. The LN pdf plot can be easily achieved by using a linear scale, however, we also present results of a logarithmic scale implementation. This is to ensure uniformity in this chapter because, we are going to use the logarithmic scale to present experimental results of irradiance fluctuation in Chapter 7 on page 101. Moreover, logarithmic scale has the ability to respond to skewness towards the large values. So, it is more appropriate for illustrating how the measured samples would fit with the distributions at their tails. Figure 3.7 shows the LN pdf for different values of log-irradiance variance. In Fig. 3.7(a) linear scale is employed whereas in Fig. 3.7(b), we use logarithmic scale. It is crystal clear that, detail insight of the tails of the plots are presented in Fig. 3.7(b). Furthermore, it should be noted that, as the value of σ_l^2 increases, the distribution is getting more and more tilted. This signifies the magnitude of the irradiance fluctuation of the system.

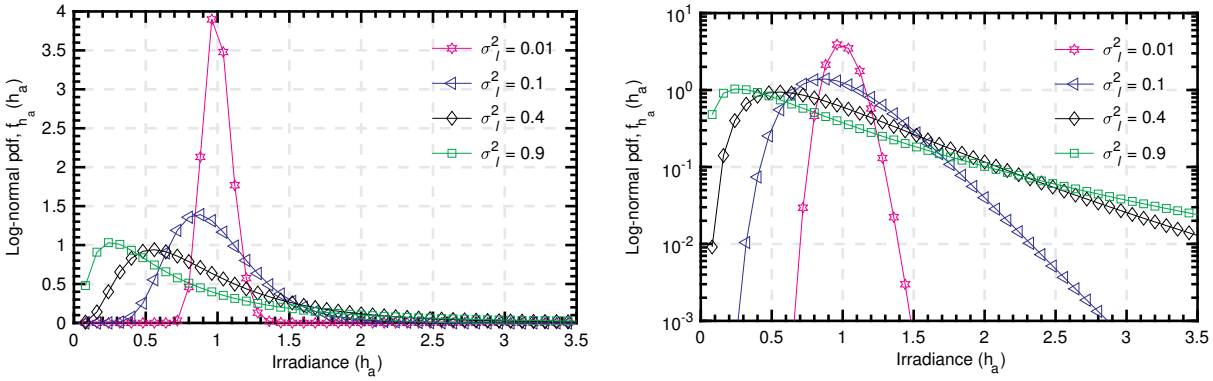

Figure 3.7: Log-normal pdf for different values of log-irradiance variance using (a) linear scale and (b) logarithmic scale.

3.6.3.2 Gamma-Gamma ($\Gamma\Gamma$) Distribution

In most cases, in the strong turbulence regimes in which the LN distribution characterization does not valid, the $\Gamma\Gamma$ distribution is normally employed in modeling the scintillation effects. Also, the $\Gamma\Gamma$ model can be used in characterizing the fading gains from the weak to the strong turbulence scenarios. The pdf of h_{a} using the $\Gamma\Gamma$ distribution is given by [146, 150, 169, 174]

$$f_{h_{\mathrm{a}}}(h_{\mathrm{a}}) = \frac{2(\alpha\beta)^{(\alpha+\beta)/2}}{\Gamma(\alpha)\Gamma(\beta)}(h_{\mathrm{a}})^{\frac{(\alpha+\beta)}{2}-1}\mathrm{K}_{\alpha-\beta}(2\sqrt{\alpha\beta h_{\mathrm{a}}}), \tag{3.15}$$

where $\Gamma(\cdot)$ represents the gamma function, $K_\nu(\cdot)$ is the modified Bessel function of the second kind of order ν, α and β are the effective number of large-scale and small-scale eddies of the scattering process, respectively. The parameters α and β are defined respectively for the plane wave as [145, 146, 150, 169, 174]

$$\alpha = \left[\exp\left(\frac{0.49\sigma_R^2}{(1+1.11\sigma_R^{12/5})^{7/6}}\right) - 1\right]^{-1}, \tag{3.16a}$$

$$\beta = \left[\exp\left(\frac{0.51\sigma_R^2}{(1+0.69\sigma_R^{12/5})^{5/6}}\right) - 1\right]^{-1}, \tag{3.16b}$$

and for the spherical wave, they can be expressed as [145, 169]

$$\alpha = \left[\exp\left(\frac{0.49\sigma_R^2}{(1+0.18d^2+0.56\sigma_R^{12/5})^{7/6}}\right) - 1\right]^{-1}, \tag{3.17a}$$

$$\beta = \left[\exp\left(\frac{0.51\sigma_R^2(1+0.69\sigma_R^{12/5})^{-5/6}}{(1+0.9d^2+0.62d^2\sigma_R^{12/5})^{5/6}}\right) - 1\right]^{-1}, \tag{3.17b}$$

where $d \triangleq (kD^2/4L)^{1/2}$, D represents the diameter of the receiver aperture, σ_R^2 denotes the Rytov variance which is a metric for the strength of the turbulence fluctuations. The σ_R^2 is defined for the plane and the spherical waves, respectively, as [145, 150, 169, 174]

$$\sigma_R^2|_{\mathrm{plane}} = 1.23\ C_n^2\ k^{7/6}\ L^{11/6}, \tag{3.18a}$$

$$\sigma_R^2|_{\mathrm{spherical}} = 0.492\ C_n^2\ k^{7/6}\ L^{11/6}, \tag{3.18b}$$

Apart from different values of σ_l^2 being employed, that is $\sigma_l^2 \in (4.0, 1.5, 0.5)$, we substitute different values of the effective number of large- and small-scale eddies of the scattering process i.e. α and $\beta \implies \alpha \in (4.3, 4.1, 6.0)$ and $\beta \in (1.3, 2.0, 4.4)$ in eq. (3.16) into eq. (3.15) to estimate the $\Gamma\Gamma$ pdf. The results of both linear and logarithmic scales are depicted in Fig. 3.8. The figure shows turbulence regimes that correspond to the weak, moderate, and strong atmospheric scenarios. The results show that, an increase in the turbulence from the weak regime to the strong regime leads to corresponding increase in the distribution spreading.

The normalized variance of the irradiance also known as the scintillation index (σ_N^2) can be expressed in terms of σ_x^2 and eddies of the scattering process (α and β), respectively,

as [145, 169, 174]

$$\sigma_N^2 \triangleq \frac{\langle h_{\rm a}^2\rangle - \langle h_{\rm a}\rangle^2}{\langle h_{\rm a}\rangle^2} \tag{3.19a}$$

$$= \frac{\langle h_{\rm a}^2\rangle}{\langle h_{\rm a}\rangle^2} - 1 \tag{3.19b}$$

$$= exp\left(4\sigma_x^2\right) - 1 \tag{3.19c}$$

$$= 1/\alpha + 1/\beta + 1/(\alpha\beta), \tag{3.19d}$$

where $\langle . \rangle$ denotes the average over the scintillation.

3.6.3.3 Málaga ($\mathcal{M}$)-Distribution

The $\mathcal{M}$-distribution is a generic model that is appropriate for defining the entire turbulent regimes. Table 3.1 on the next page shows the means of generating the existing atmospheric turbulence models from the $\mathcal{M}$-distribution model [176]. The $\mathcal{M}$-distributed fading model is based on components such as U_L, U_S^C, and U_S^G which represent the LOS component; the scattered component by the eddies on the propagation axis that is coupled to the LOS contribution; and the scattered component to the receiver by the off-axis eddies, respectively. The average power of the LOS component, as well as that of the total scatter components, are $\Omega = E[|U_L|^2]$ and $2b_0 = E[|U_S^C|^2 + |U_S^G|^2]$, respectively. In addition, the average power of the coupled-to-LOS scattering component and that of the scattering component received by off-axis eddies are $E[|U_S^C|^2] = 2\rho b_0$ and $E[|U_S^G|^2 = (1-\rho)2b_0]$, respectively. The parameter $0 \leq \rho \leq 1$, represents the amount of scattering power coupled to the LOS component [145,176,177]. The pdf of the optical channel gain $h_{\rm a}$ for the $\mathcal{M}$-distribution can be written as [176–179]

$$f_{h_{\rm a}}(h_{\rm a}) = A \sum_{k=1}^{\beta} a_k h_{\rm a}^{\frac{\alpha+k}{2}-1} K_{\alpha-k}\left(2\sqrt{\frac{\alpha\beta h_{\rm a}}{\mu\beta+\Omega'}}\right) \tag{3.20}$$

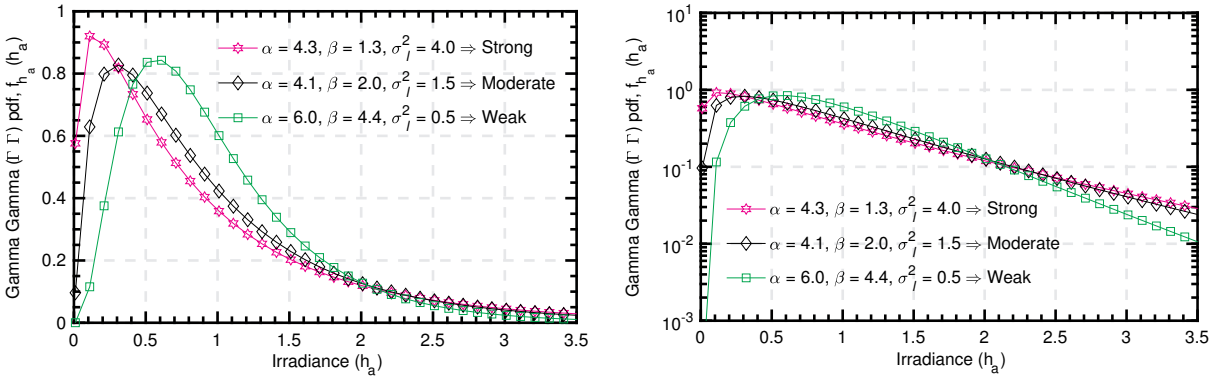

Figure 3.8: Gamma-gamma pdf for weak-strong turbulence regimes using (a) linear scale and (b) logarithmic scale.

Table 3.1: Approximations required for generating different distribution models from $\mathcal{M}$-distribution model (adapted from [176])

	Generation									
Distribution model	ρ	Var $[\lvert U_L \rvert]$	Var [G]	X	Ω'	Var [X]	γ	Ω	α	β
Rice-Nakagami	0	0								
Gamma	0						0			
Homodyned K (HK)	0		0	γ						
Gamma-gamma	1				1		0			
Shadowed-Rician						0				
Log-normal	0	0					$\to 0$			
K	0							0		
Exponential	0	0						0	$\to \infty$	
Gamma-Rician										$\to \infty$

where $\mu = E[|U_S^C|]^2 = (1-\rho)2b_0$, $\Omega' = \Omega + 2\rho b_0 + 2\sqrt{2\rho b_0 \Omega} cos(\varphi_A - \varphi_B)$, φ_A and φ_B represent the deterministic phases of the LOS and the coupled-to-LOS component, respectively; α denotes a positive parameter that depends on the effective number of large-scale cells of the scattering process, β is a natural number which represents the amount of fading parameter, $K_v(\cdot)$ represents the modified Bessel function of the second kind with order v, A and a_k can be expressed respectively, as [176–179]

$$A \triangleq \frac{2\alpha^{\frac{\alpha}{2}}}{\mu^{1+\frac{\alpha}{2}}\Gamma(\alpha)} \left(\frac{\mu\beta}{\mu\beta + \Omega'}\right)^{\beta+\frac{\alpha}{2}} \tag{3.21}$$

$$a_k \triangleq \binom{\beta}{k} \frac{(\mu\beta + \Omega')^{1-\frac{k}{2}}}{(k-1)!} \left(\frac{\Omega'}{\mu}\right)^{k-1} \left(\frac{\alpha}{\beta}\right)^{\frac{k}{2}} \tag{3.22}$$

3.6.4 Combined Attenuation Statistics

The pdf of $h = h_\ell h_\mathrm{a} h_\mathrm{p}$ that constitutes the aforementioned factors of the propagation channel can be defined as [145, 172, 173]

$$f_h(h; w_z) = \int f_{h|h_\mathrm{a}}(h|h_\mathrm{a}) f_{h_\mathrm{a}}(h_\mathrm{a}) dh_\mathrm{a} \tag{3.23}$$

where $f_{h|h_\mathrm{a}}(h|h_\mathrm{a})$ is the conditional probability given a turbulence state h_a and its distribution can be written as [172, 173]

$$f_{h|h_\mathrm{a}}(h|h_\mathrm{a}) = \frac{1}{h_\mathrm{a} h_\ell} f_{h_\mathrm{p}}\left(\frac{h}{h_\mathrm{a} h_\ell}\right) = \frac{\gamma^2}{A_0^{\gamma^2} h_\mathrm{a} h_\ell} \left(\frac{h}{h_\mathrm{a} h_\ell}\right)^{\gamma^2 - 1}, \qquad 0 \le h \le A_0 h_\mathrm{a} h_\ell. \tag{3.24}$$

Therefore, $f_h(h; w_z)$ can be written as [172]

$$f_h(h; w_z) = \frac{\gamma^2}{(A_0 h_\ell)^{\gamma^2}} h^{\gamma^2-1} \int_{h/A_0 h_\ell}^{\infty} h_{\rm a}^{-\gamma^2} f_{h_{\rm a}}(h_{\rm a}) dh_{\rm a}. \tag{3.25}$$

3.7 Performance Analysis

3.7.1 BER

The channel state distribution $f_h(h; w_z)$ can be calculated by employing an appropriate model for the atmospheric turbulence regimes in eq. (3.25) as follows:

1. **For a weak turbulence** ($\sigma_{\rm R}^2 < 0.3$)
   In this regime, $f_{h_{\rm a}}(h_{\rm a})$ follows LN distribution, so, $f_h(h; w_z)$ can be expressed as [145, 172]

$$f_h(h; w_z) = \frac{\gamma^2}{2(A_0 h_\ell)^{\gamma^2}} h^{\gamma^2-1} \times \operatorname{erfc}\left(\frac{\ln\left(\frac{h}{A_0 h_\ell}\right) + \mu}{\sqrt{8}\sigma_x} \right) e^{\left(2\sigma_x^2 \gamma^2 (1+\gamma^2)\right)}. \tag{3.26}$$

2. **For a strong turbulence**
   This regime is characterized by the $\Gamma\Gamma$ distribution, so, $f_h(h; w_z)$ can be written as [145, 172, 173]

$$f_h(h; w_z) = \frac{2\gamma^2 (\alpha\beta)^{(\alpha+\beta)/2}}{(A_0 h_\ell)^{\gamma^2} \Gamma(\alpha)\Gamma(\beta)} h^{\gamma^2-1} \times \int_{h/A_0 h_\ell}^{\infty} h_{\rm a}^{(\alpha+\beta)/2-1-\gamma^2} {\rm K}_{\alpha-\beta}\left(2\sqrt{\alpha\beta\ h_{\rm a}}\right) dh_{\rm a}. \tag{3.27}$$

where ${\rm K}_\nu(\cdot)$ can be expressed in terms of the Meijer's G-function $G_{p,q}^{m,n}[\cdot]$ as [169]

$${\rm K}_\nu(x) = \frac{1}{2} G_{0,2}^{2,0}\left[\frac{x^2}{4} \middle|_{(\nu/2), -(\nu/2)}^{-} \right]. \tag{3.28}$$

So, from eq. (3.28), ${\rm K}_{\alpha-\beta}\left(2\sqrt{\alpha\beta h_{\rm a}}\right)$ can be expressed as [169]

$${\rm K}_{\alpha-\beta}\left(2\sqrt{\alpha\beta h_{\rm a}}\right) = \left(\frac{1}{2}\right) {\rm G}_{0,2}^{2,0}\left[\alpha\beta h_{\rm a} \middle| \begin{matrix} - \\ \frac{\alpha-\beta}{2}, \frac{\beta-\alpha}{2} \end{matrix} \right]. \tag{3.29}$$

Therefore, $f_h(h)$ can be written as [173]

$$f_h(h) = \frac{\alpha\beta\gamma^2}{A_0 h_l \Gamma(\alpha)\Gamma(\beta)} \left(\frac{\alpha\beta h}{A_0 h_l}\right)^{(\alpha+\beta/2)-1} \times G_{1,3}^{3,0}\left[\frac{\alpha\beta}{A_0 h_l} h \middle| \begin{matrix} 1 - \frac{\alpha+\beta}{2} + \gamma^2 \\ -\frac{\alpha+\beta}{2} + \gamma^2, \frac{\alpha-\beta}{2}, \frac{\beta-\alpha}{2} \end{matrix} \right]. \tag{3.30}$$

The average BER, $P(e)$, in term of $f_h(h)$ can be expressed as [173]

$$P(e) = \int_0^\infty P(e|h) f_h(h) dh. \tag{3.31}$$

Furthermore, for an OFDM signal over the FSO link, assuming that the Gray-coded mapping is employed at the transmitter, the average bit error probability per subcarrier $\langle P_{b,n} \rangle$ can be expressed as [170]

$$\langle P_{b,n} \rangle = \frac{1}{\mathrm{Log}_2(M)} \langle P_{s,n} \rangle, \tag{3.32}$$

where $\langle P_{s,n} \rangle$ represents the average symbol error probability per subcarrier defined by [170]

$$\langle P_{s,n} \rangle = (1 - \sqrt{M}^{-1}) \frac{2^{\alpha+\beta-1}}{\pi\sqrt{\pi}\Gamma(\alpha)\Gamma(\beta)} \; G_{5,2}^{2,4} \left(\frac{2^3 A (m_n \rho P_{r,0})^2}{(\langle \sigma_N^2 \rangle + \langle \sigma_{\mathrm{IMD}}^2 \rangle)(\alpha\beta)^2} \Big|_{0,\; \frac{1}{2}}^{\frac{1-\alpha}{2}, \frac{2-\alpha}{2}, \frac{1-\beta}{2}, \frac{2-\beta}{2}, 1} \right), \tag{3.33}$$

where $A = 3/[2(M-1)]$, $M = 2^k$, k is an even number, $m_n = \frac{m_{\mathrm{Total}}}{\sqrt{N}}, \quad n = 0, 1, \ldots, N-1$ denotes the modulation index, m_{Total} represents the optical modulation index (OMI), $P_{r,0}$ is the received optical power in the absence of turbulence, ρ is the responsivity of the PD, σ_{IMD}^2 is the third order intermodulation distortion (IMD3) [170]

3.7.2 Ergodic Channel Capacity

Another main figure of merit for characterizing the communication link performance is the achievable average (ergodic) channel capacity. Consequently, the channel capacity is one of the main performance metrics in the design of FSO systems that needs significant attention. The capacity of a MIMO FSO system with M lasers and N PDs in $bits/s/Hz$ can be expressed as [145, 168, 180, 181]

$$C = \log_2 \left[det \left(\boldsymbol{I}_M + \frac{\gamma_{\mathrm{inst}}}{M} \; \boldsymbol{R} \right) \right], \tag{3.34}$$

where $\boldsymbol{R} = \begin{cases} \boldsymbol{H}\boldsymbol{H}^\dagger & \text{if } N < M \\ \boldsymbol{H}^\dagger\boldsymbol{H} & \text{if } N \leq M \end{cases}$, $\boldsymbol{H}$ denotes an $N \times M$ channel state matrix, $(\cdot)^\dagger$ corresponds to the Hermitian transpose, $\boldsymbol{I}_M$ is an $M \times M$ identity matrix, $\gamma_{\mathrm{inst}} = \eta_e^2 \mathrm{h}^2/N_0$ denotes the instantaneous electrical Signal-to-Noise-Ratio (SNR) whose average $\xi_a = \eta_e^2 \mathbb{E}\langle \mathrm{h} \rangle^2/N_0$.

The ergodic capacity, C_{erg}, of MIMO FSO link can be define by the expected value of the instantaneous mutual information C, between the transmit and receive apertures. Hence, the C_{erg} of FSO system, is a random variable and a function of SNR. The C_{erg} can be estimated using numerical integration approach as [168, 169, 180, 182]

$$C_{\mathrm{erg}} \triangleq \mathbb{E}\langle C \rangle = \int_0^\infty \log_2(1 + \gamma_{\mathrm{inst}}) f_{\gamma_{\mathrm{inst}}}(\gamma_{\mathrm{inst}}) d\gamma_{\mathrm{inst}}, \tag{3.35}$$

where $\mathbb{E}(\cdot)$ denotes the expectation operator and $f_{\gamma_{\mathrm{inst}}}(\gamma_{\mathrm{inst}})$ is the pdf of γ_{inst}.

It should be noted that, most of the models for ergodic capacity evaluation are based on numerical integration. However, integration based approach requires comparatively more computational time. This is even more challenging in the strong turbulence regimes analysis. The consequence can be attributed to the Bessel function that is usually expressed in terms of the Meijer's G-function for an easier evaluation [168]. In [168] and [169], computational-efficient approaches are presented in order to reduce the associated high computational time of

the integration based approach. This enables faster performance evaluation over a wide range of SNR. Computational-efficient approaches such as power series and spatial interpolation lookup are discussed in Chapter 5 on page 78.

3.8 Simulation Results and Discussions

This section presents results of the analyses of atmospheric effects on the BER performance of the Binary Phase-Shift Keying (BPSK) and M-ary Quadrature Amplitude Modulation (M-QAM) under different turbulence conditions by simulation. Also, simulation result on the average channel capacity of FSO link are presented. In the simulation, effects of different parameters such as constellation size, wavelength and the refractive index are analyzed on the system performance for different operation conditions for the FSO with a link range of 1 km and 10 $Gbps$ bit rate.

Figure 3.9(a) shows the average BER in terms of the average SNR for BPSK over different values of turbulence strength. In this analysis, only the atmospheric turbulence effect is assumed when eq. (3.31) on page 62 is considered. The atmospheric turbulence parameters $\alpha \in (4.34, 4.05, 5.98, 204.64)$, $\beta \in (1.31, 1.98, 4.40, 196.03)$, and $\sigma_l^2 \in (4.00, 1.50, 0.50, 0.01)$ which represent weak to strong turbulence conditions are employed in order to estimate the system BER performance at 1550 nm window. It is observed that, the SNR required to achieve a specific BER increases with an increase in the atmospheric turbulence strength. For instance to achieve a BER of 10^{-6} in a channel with $\sigma_l^2 = 0.01$, the required SNR is about 18 dB, however, for fading strength of $\sigma_l^2 = 0.50$, the required SNR increases to 28 dB. Furthermore, at this BER, for $\sigma_l^2 = 0.01$ and $\sigma_l^2 = 0.50$ additional 2 dB and 12 dB, respectively, are required compared to the ideal channel in which there is no turbulence. This shows that the BER increases as turbulence strength becomes stronger.

Initially, a refractive index of $1.7 \times 10^{-15}\mathrm{m}^{-2/3}$ is employed so as to study the BER performance for different wavelengths for 8-Quadrature Amplitude Modulation (QAM). Figure 3.9(b) presents the BER performance as a function of the average received irradiance for different values of λ for 8-QAM. According to the results, we observed that, to attain a BER of 10^{-6}, an average received irradiance of about -22 dBm, -21 dBm, and -20.5 dBm are needed for the optical wavelength windows 1550 nm, 850 nm, and 650 nm, respectively. Furthermore, it is noted that, 1550 nm window is comparatively the least susceptible to the fading effects of the fluctuation. So, we consider 1550 nm window in the rest of this work because of its associated advantage and the fact that, it coincides with the standard transmission window of fiber communication systems.

Moreover, we analyzed the BER performances for different constellation sizes of the M-QAM so as to demonstrate the effects of atmospheric turbulence condition on the modulation formats. Figure 3.9(c) depicts the BER performance for different constellation sizes under the influence of an atmospheric turbulence condition. We observed that, to achieve a BER of 10^{-6}, with $M = 4, 8$, and 16, about -23 dBm, -22 dBm, and -21 dBm are required, respectively. This shows that reducing the constellation size is a good option in order to minimize the effect of impairments caused by the atmospheric turbulence and the noise.

Furthermore, the BER performance for different refractive index values are studied. Figure 3.9(d) shows the BER performance for various values of C_n^2. In the study, we observed that, to realize a BER of 10^{-6}, with the $C_n^2 = 1.7 \times 10^{-16}\mathrm{m}^{-2/3}$ about -23 dBm is needed. Nevertheless, this eventually increased to about $-22dBm$, for the same BER for $C_n^2 = 1.7 \times$

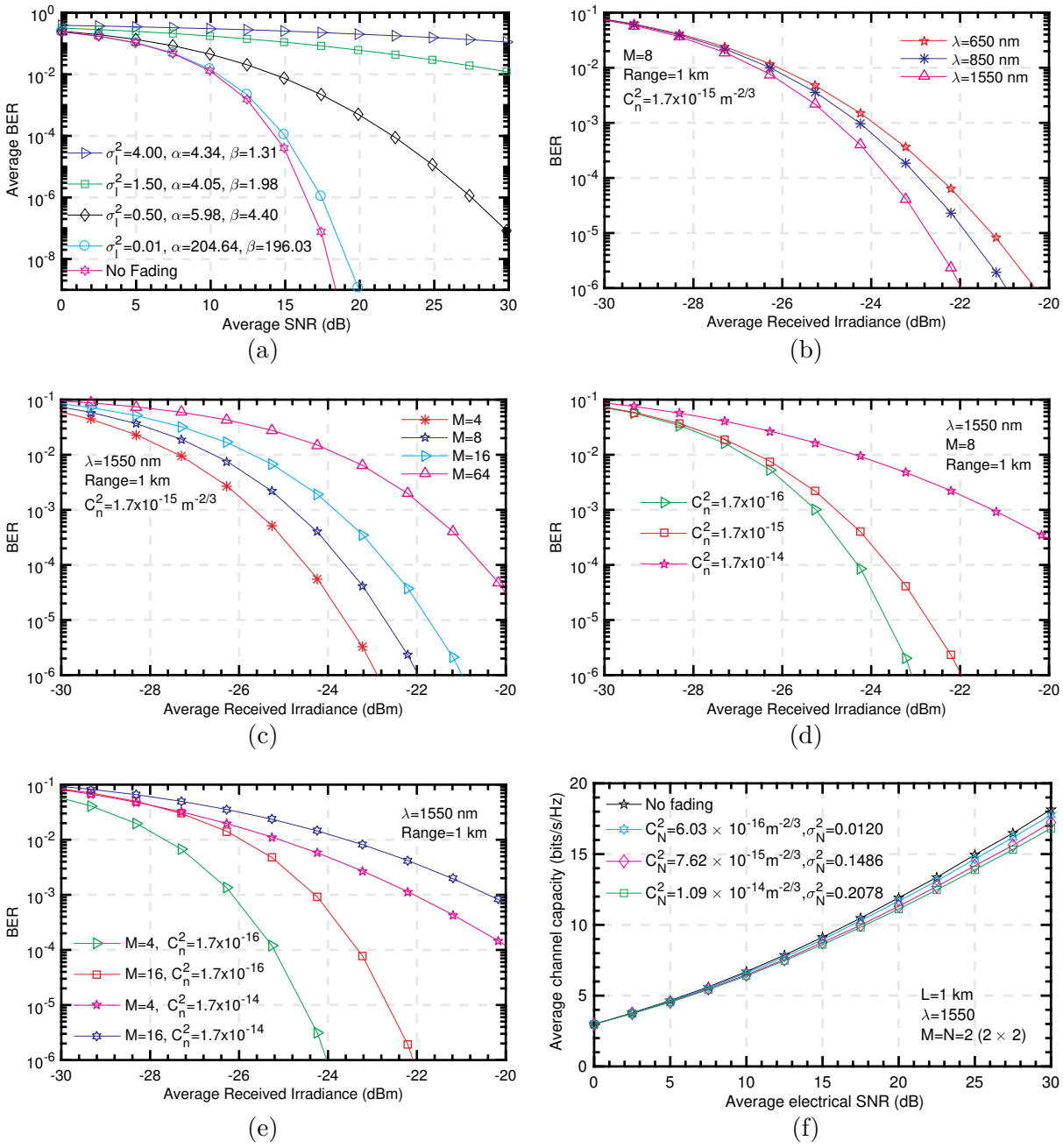

Figure 3.9: (a) Average BER versus SNR for BPSK under different turbulence conditions at 1550 nm, (b) BER against average received irradiance with different wavelength values, (c) BER against average received irradiance with different constellation sizes, (d) BER against average received irradiance with different refractive index values, (e) BER against average received irradiance with different refractive index values and constellation sizes, (f) Average channel capacity of FSO link versus average electrical SNR.

$10^{-15}\mathrm{m}^{-2/3}$ that shows an increase in the atmospheric turbulence.

Furthermore, we analyze the BER performance of the 4-QAM and 16-QAM with different refractive index values. Figure 3.9(e) depicts the effects of different refractive index values on the constellation sizes. We discerned that, for $C_n^2 = 1.7 \times 10^{-16}\mathrm{m}^{-2/3}$ the 4-QAM requires about -24 dBm, whereas the 16-QAM requires about -22 dBm to achieve the same BER of 10^{-6}.

Figure 3.9(f) shows the average channel capacity of FSO link as a function of average electrical SNR for different values of turbulence strength. The atmospheric turbulence parameters $\sigma_N^2 \in (0.0120, 0.1486, 0.2078)$ result in $C_N^2 \in (6.03 \times 10^{-16}m^{-2/3}, 7.62 \times 10^{-15}m^{-2/3}, 1.09 \times 10^{-14}m^{-2/3})$ which correspond to the weak, moderate, and strong turbulence conditions, respectively. Moreover, the capacity of the non-turbulent channel condition (no fading) is presented for benchmarking. Obviously, the ergodic capacity of FSO link significantly depends on the atmospheric turbulence strength. Comparatively, the ergodic channel capacity for the weak turbulence condition is considerably more than in the cases of moderate and strong turbulence conditions. Moreover, the channel condition with no fading offers the highest capacity. This shows that the atmospheric turbulence-induced fading results in severe impairment on the FSO link performance. This can eventually result in recurrent link failures. Consequently, optical wireless technologies are not as reliable as the conventional optical fiber technologies. In order to address the challenges, innovative technologies can be employed to enhance the system performance.

3.9 Research Contributions

The contributions of this chapter as reported in the manuscripts [14,145,146] are enumerated in the following subsections.

3.9.1 First Contribution

Based on the book chapter [145], we present various opportunities of optical wireless communication technologies implementations in each sector of optical communication networks. Moreover, challenges of optical-wireless network applications are presented. The book chapter is written in an understandable way for easy understanding by the future researchers and readers outside the specialty of the topic. Additionally, it will help researchers to have better view about the concepts of OWC systems.

3.9.2 Second Contribution

Based on [146] and [14] we have been able to demonstrate the atmospheric turbulence effects on the RF signal transmission over the FSO (i.e. RoFSO) links considering different optical wavelength windows. In the analyses, we consider BER performance of M-QAM regarding the average received irradiance. We present results that can be helpful in the adoption of adaptive modulation scheme in order to enhance the system SE. Also, we showed that, reducing the constellation size is a good option for minimizing the associated effects of impairments of the atmospheric turbulence as well as noise when the channel state is poor. Moreover, we demonstrated that the 1550 nm window is comparatively less susceptible to the fading effects of the fluctuation. Furthermore, the presented results can be useful in

the evaluation, optimization, and prediction of RoFSO system performance in the real-life scenario deployments.

3.10 Conclusion

In this chapter, we have presented various opportunities of the OWC technologies implementations in different sectors of optical communication networks. Furthermore, challenges of optical-wireless network applications have been presented. Also, we have presented simulation results on the atmospheric effects on RF signal transmission over the FSO links. The presented results can be useful in the adoption of adaptive modulation scheme that helps in enhancing the system spectral efficiency. Moreover, the results can be suitable for the evaluation, optimization, and prediction of RoFSO system performance in the real-life scenario deployments.

Chapter

FSO Turbulence-Induced Fading Mitigation

The significant attributes and benefits of FSO communication system are attractive for various applications in different communication divisions. Despite the benefits and various applications of FSO system, its extensive implementation is hindered by the atmospheric turbulence-induced fading in the real-life situations. One of efficient methods for alleviating the turbulence-induced fading and subsequently enhancing the system performance is spatial diversity techniques. In this chapter, based on the article [183], we study the spatial diversity techniques for alleviating turbulence-induced fading in the FSO systems. In the study, the BER is employed as a performance metric. The methods employed are based on the Orthogonal Space-Time Block Code (OSTBC) and Repetition Code (RC). The log-normal FSO links with IM/DD are employed and simple approximate closed-form expressions for the error probability are derived for the considered links. Moreover, effects of spatial correlation between the transmit apertures on the system performance are considered. To realize this, we employ the exponential model for analyzing the correlations between the apertures. The results show that the proposed BER expressions are capable of quantifying the effects of spatial diversity schemes as well as spatial correlations on the system.

4.1 Introduction

FSO systems have gained significant attentions because of the related benefits like ease of deployment, higher bandwidth, license-free operation, and better protection against interferences [152, 167, 184, 185]. However, FSO systems are prone to atmospheric impairments that consequently hinder the system error rate performance and reliability [146, 168, 186, 187]. As a result, for the system to be deployed and operated efficiently, efficient fading-mitigation methods are essential [169, 188].

A number of techniques have been widely employed for mitigating fading in the literature [185]. An example of such approach is the use of repetition code that was demonstrated

in [189–191]. In the analyses, it was shown that unlike the wireless RF communication counterparts, the RC can be used for exploiting additional degrees of freedom of the spatial dimension in the FSO communication links with IM/DD. Besides, the study in [189] considered the viability of OSTBC implementation. Moreover, in [192], error control coding (ECC) in conjunction with interleaving were presented. Nonetheless, to achieve reasonable coding gains, large-size interleavers are generally require in order to address turbulence-induced fading with the ECC approach. This is due to the inherent capacity and high transmission rates of optical links that present high temporal correlation [167,193]. Moreover, a maximum likelihood sequence detection (MLSD) was presented in [194] as an alternative mitigation technique. The study was based on the statistical properties of turbulence-induced fading in the FSO. Nevertheless, even with a simple and low-order modulation format like OOK, the associated intricacy of MLSD may be excessive for practical implementations. This is as a result of the complicated multidimensional integrations that are related with the MLSD based fading mitigation approach [167, 193]. In order to avoid the associated computational complexity of MLSD, sub-optimal temporal-domain approaches were reported in [193, 195]. Unlike the method that was implemented in [195], the approach in [193] is independent of the channel's fading statistics. Furthermore, a viable method for alleviating turbulence-induced fading is spatial diversity techniques. In spatial diversity, multiple transmit/receive apertures are deployed so as to establish and exploit additional degrees of freedom in the spatial dimension [168, 196]. In addition, spatial diversity is a fascinating method because of its inherent redundancy [167, 193]. Moreover, the detrimental effects of spatial correlation on the system performance are studied in [167].

In this chapter, we extensively study the BER performance of FSO communication links over log-normal atmospheric turbulence channels presented in eq. (3.10) on page 56. In the study, different spatial diversity schemes are considered. By employing the BER as performance metric, we derive simple approximate closed-form expressions for the error probability of the log-normal FSO links with IM/DD. In addition, the effects of spatial correlation between the transmit apertures on the system performance are taken into consideration. The analysis of spatial correlation is achieved by employing the exponential model for determining the correlations between the apertures. We observed that the proposed BER expressions are able to quantify the effects of spatial diversity schemes and spatial correlations on the system.

Having presented the associated impairments of the FSO communication systems as well as the state-of-the-art on various efficient fading-mitigation techniques, in Section 4.2, we present the system model for the FSO communication system with IM/DD. Furthermore, comprehensive clarifications on the diversity schemes considered are given in Section 4.3 on page 70. The proposed approximate closed-form expressions are analyzed in Section 4.4 on page 72. In addition, Section 4.5 on page 74, presents numerical results with comprehensive discussions. In Section 4.6 on page 76, we discuss the research contributions towards the FSO turbulence-induced fading mitigation and concluding remarks are given in Section 4.7 on page 77.

4.2 System Model

In this section, we consider an $M \times N$ FSO communication system with IM/DD. In the system, the information bit $s \in \{0, 1\}$ is transmitted via M apertures and received by N apertures in order to satisfy the unipolar requirement of an IM/DD. Also, we assume OOK

and high SNR regime so as to use Gaussian noise model [167]. The received signal at the nth receive aperture can be defined as [167, 184, 197]

$$r_n = s\eta \sum_{m=1}^{M} I_{mn} + v_n, \qquad n = 1, \ldots, N, \tag{4.1}$$

where η represents the optical-to-electrical conversion coefficient, v_n denotes the additive white Gaussian noise with zero mean and variance $\sigma_{v_n}^2 = N_0/2$. The signal irradiance from the mth transmit aperture to the nth receive aperture can be written as [167, 196]

$$\begin{aligned} I_{mn} &= I_0 \exp(2X_i) \\ &= I_0(h_i) \end{aligned} \tag{4.2}$$

where I_0 denotes the signal irradiance without turbulence, h_i are the channel irradiance, and X_i are the fading log-amplitudes and are modeled as identically but not necessarily independently distributed normal random variables with mean μ_x and variance σ_x^2 [167, 189]. Therefore, I_{mn} follow a log-normal distribution with the pdf expressed by eq. (3.10) on page 56.

With the intention of preventing fading from attenuating or amplifying the average power, the fading coefficients are normalized such that, $E[|I_{mn}/I_0\,|] = 1$, this means that $\mu_x = -\sigma_x^2$ [167, 189].

The subsequent cumulative density function (CDF) of eq. (3.10) on page 56 can be expressed as [198]

$$F(I_{mn}) = 1 - Q\left(-\frac{\ln(I_{mn}/I_0) - 2\mu_x^2}{2\sigma_x^2}\right). \tag{4.3}$$

where $Q(\cdot)$ is the Gaussian-Q function defined as [167, 197, 198]

$$Q(y) \triangleq 1/\sqrt{2\pi} \int_y^{\infty} \exp(-t^2/2)\mathrm{d}t, \tag{4.4}$$

There are a number of determinants of performance enhancement, one of such is the spatial correlation between the apertures. Moreover, an increase in the correlation brings about subsequent increase in the performance loss which is as a result of reduction in diversity gains. The effect of correlation become comparatively severe when the apertures are not well spaced. In this work, we employ exponential model for modeling the correlations between the transmit apertures. The spatial correlation matrix $\mathbf{R}$, can be accurately modeled as [199–201]

$$\mathbf{R}_{[i,j]} = \begin{cases} \rho^{|i-j|} & \text{if } i \geq j \\ \\ (\rho^*)^{|i-j|} & \text{if } i < j \end{cases}, \tag{4.5}$$

where i and j denote the row and the column indices of the matrix coefficients, $|\cdot|$ represents the absolute value, $(\cdot)^*$ represents a complex conjugate, and $\rho = ae^{j\theta}$ denotes the correlation coefficient of $\mathbf{R}$ with $0 \leq a < 1$. Moreover, ρ is a function of the separation between transmit apertures.

The spatial covariance matrix, $\mathbf{\Gamma} = \sigma_x^2\mathbf{R}$, can be used in the spatial correlation modeling [167]. Consequently, $\mathbf{\Gamma}$ can be written as

$$\mathbf{\Gamma}_{[i,j]} = \begin{cases} \sigma_x^2 \rho^{|i-j|} & \text{if } i \geq j \\ \\ \sigma_x^2 (\rho^*)^{|i-j|} & \text{if } i < j \end{cases}, \tag{4.6}$$

4.3 FSO Link with Diversity Techniques

The performance of SISO FSO link is impeded by the turbulence-induced signal fading which results to requirement for extra power margin. The associated power penalty that is caused by signal fading can be alleviated by increasing the transmission power and also by frequency diversity. The former approach is comparatively costly and impractical because of the eye safety regulations. Likewise, the latter is limited by the higher costs of broadband components [150]. In addition, other methods such as ECC in conjunction with interleaving, aperture averaging, spatial and time diversities and MLSD have been presented in the literature [150, 167, 190]. The wide implementation of MLSD is limited by the associated high computational complexity whereas the aperture averaging approach requires stringent condition that is intricate to accomplish in the FSO system [150]. Furthermore, to be efficient, ECC needs to be robust for detecting and correcting random errors in addition to burst errors. Nonetheless, the need for large-size interleavers to realize the coding gains is a limiting factor for the ECC implementation [167, 193].

We consider transmit diversity schemes in this chapter because of the fact that, it is very cost-effective to deploy additional equipment at the base stations rather than at the remote units [202]. The key application challenges of the receive diversity method are the related cost, size, and power of the remote units. Employment of multiple apertures renders remote units larger and more expensive. Consequently, transmit diversity techniques have been widely used for enhancing the data rate, error performance, and capacity of wireless communication systems [202]. Therefore, in this chapter we consider transmit diversity techniques such as the modified OSTBCs and RCs.

4.3.1 Modified OSTBCs for FSO Communication

In [202], a simple, practical, and effective transmit diversity scheme is proposed in order to address the effect of multipath fading in the system. Part of notable features of the scheme is that it does not require any additional power or any sacrifice in bandwidth and has reasonable computation complexity. Nevertheless, for Alamouti's code to be appropriate in the FSO communication with DD in which unipolar modulation formats such as OOK and pulse-position modulation are typically implemented, modification of the conventional Alamouti code originally proposed in [202] is essential [189]. The concept is that, in the first bit interval, t, transmit aperture 1 transmits x_1 while aperture 2 transmits x_2 where x_1 and x_2 each range over the signal set (s_1, s_2). Moreover, in the second bit interval, $t+T$, aperture 1 transmits $\overline{x_2}$ whereas aperture 2 transmits x_1 [203, 204]. The complement of x_2 which is achieved by reversing the role of on and off bits is expressed as $\overline{x_2}$. The process is illustrated in Fig. 4.1 for a multiple-input single-output (MISO) system.

The instantaneous received electrical SNR for the OSTBC can be expressed as [189]

$$\gamma_{\text{OOK}}^{\text{OSTBC}} = \frac{\eta^2 I_0^2}{2M^2 N_0} \sum_{i=1}^{M} h_i^2. \tag{4.7}$$

Substituting eq. (4.2) on page 69 into eq. (4.7) on page 70 implies that

$$\gamma_{\mathrm{OOK}}^{\mathrm{OSTBC}} = \frac{\eta^2}{2M^2 N_0} \sum_{i=1}^{M} I_i^2 \tag{4.8}$$

Moreover, conditional BER performance of OSTBC can be expressed as [189]

$$\begin{aligned} P_{\mathrm{e|h}}^{\mathrm{OSTBC}} &= Q\left(\sqrt{\frac{\eta^2}{2M^2 N_0} \sum_{i=1}^{M} I_i^2}\right) \\ &= Q\left(\frac{\eta}{M\left(2N_0\right)^{1/2}} \sqrt{\sum_{i=1}^{M} I_i^2}\right) \end{aligned} \tag{4.9}$$

The average bit error probability of OSTBC can be defined as [166, 167]

$$P_{\mathrm{e}}^{\mathrm{OSTBC}} = \int_0^{\infty} \mathfrak{f}(I_m) P_{\mathrm{e|h}}^{\mathrm{OSTBC}} dI \tag{4.10}$$

4.3.2 Repetition Coding for FSO Communication

The major motive for wide employment of the RC is the simplicity of its application. Implementation of RC across lasers so as to transmit the same signal pattern on each symbol results in limitation on the system. This constrains the permissible rate of information transfer compared with an unrestrained set of patterns [191]. This can be attributed to the resulting transmitted signal that requires a bit interval that is m times smaller than the uncoded type. The decrease in the bit interval shows that, the transmitted energy/bit reduces by a factor of m. This eventually results in an increased error probability at the receiver. Generally, the RC offers a bad trade-off between BER and data rate. Moreover, implementation of error control coding could create substantial processing delays and efficiency degradation in view of the number of redundant bits that will be required [150]. This can be attributed to the majority logic detection algorithms being employed in the system that needs relatively huge decoding time [205]. Studies in [189–191] have established the viabilities of RC in accomplishing transmit diversity in FSO systems. The aim is to transmit the same OOK signal from M apertures in such a way that, the intensities received from independent transmitters are combined [189]. The concept involves adding redundancy to the data at the transmitter

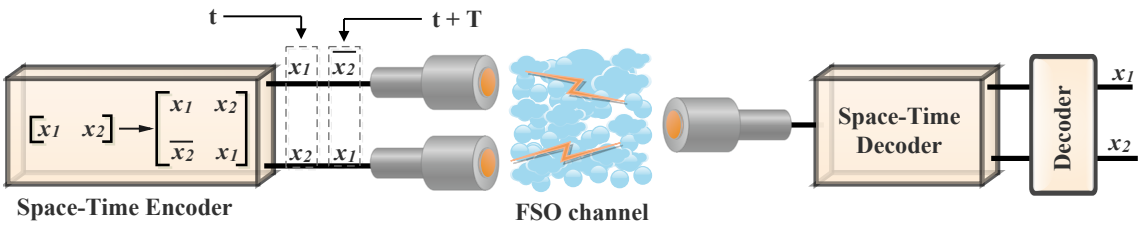

Figure 4.1: Block diagram of modified OSTBCs for FSO communication.

to permit error detection or correction at the receiver. Generally, an (m, k) code employs m channel bits in transmitting k data bits at the code rate of $R = k/m$.

The instantaneous received electrical SNR with the implementation of RC can be expressed as [189]

$$\gamma_{\text{OOK}}^{\text{RC}} = \frac{\eta^2 I_0^2}{2M^2 N_0} \left(\sum_{i=1}^{M} h_i \right)^2. \tag{4.11}$$

Substituting eq. (4.2) on page 69 into eq. (4.11) infers that, the conditional BER performance of RC can be defined as

$$\begin{aligned} P_{\text{e|h}}^{\text{RC}} &= Q\left(\sqrt{\frac{\eta^2}{2M^2 N_0} \left(\sum_{i=1}^{M} I_i \right)^2} \right) \\ &= Q\left(\frac{\eta}{M\left(2N_0\right)^{1/2}} \sum_{i=1}^{M} I_i \right) \end{aligned} \tag{4.12}$$

4.4 Approximate Closed-Form Expressions

It is noteworthy that, the integral stated in eq. (4.10) on page 71 can be evaluated by means of multi-dimensional numerical integration which could bring about truncating its upper limit. However, it is really difficult if not impossible to be evaluated in a closed-form [167, 197, 206]. Consequently, in order to prevent the analytical complexity involved in resolving eq. (4.10) on page 71, we propose an approximate closed-form expressions for the error probability estimation.

4.4.1 Approximate Expression for Modified OSTBCs

In order to estimate the error probability of the OSTBC, we substitute eq. (4.9) on page 71 into eq. (4.10) on page 71 resulting in

$$P_{\text{e}}^{\text{OSTBC}} = \int_0^{\infty} Q\left(\frac{\eta}{M\left(2N_0\right)^{1/2}} \sqrt{\sum_{i=1}^{M} I_i^2} \right) \mathfrak{f}(I) dI \tag{4.13}$$

From eq. (3.10) on page 56 for a log-normal PDF, assuming a function $\mathfrak{f}(I_m)$ express as

$$\mathfrak{f}(I_m) \triangleq \frac{1}{2I_m} \frac{e^{-s(I_m/I_0)}}{\sqrt{2\pi\sigma_x^2}} \exp\left[-\frac{\left(\ln(I_m/I_0) - 2\mu_x\right)^2}{8\sigma_x^2} \right] dI. \tag{4.14}$$

Furthermore, substituting eq. (4.14) into eq. (4.13) implies that, the BER of OSTBC over the lognormal irradiance fluctuation can be written as

$$\begin{aligned} P_{\text{e}}^{\text{OSTBC}} = \int_0^{\infty} Q\left(\frac{\eta}{M\left(2N_0\right)^{1/2}} \sqrt{\sum_{i=1}^{M} I_i^2} \right) \frac{1}{I_m} \frac{e^{-s(I_m/I_0)}}{\sqrt{8\pi\sigma_x^2}} \\ \times \exp\left(-\frac{\left(\ln(I_m/I_0) - 2\mu_x\right)^2}{8\sigma_x^2} \right) dI. \end{aligned} \tag{4.15}$$

By employing a change of variable $x = \frac{\ln(I_m/I_0)-2\mu_x}{2\sqrt{2}\sigma_x}$, we express the $P_{\mathrm{e}}^{\mathrm{OSTBC}}$ as

$$\begin{aligned} P_{\mathrm{e}}^{\mathrm{OSTBC}} &= \int_{-\infty}^{\infty} \frac{1}{\sqrt{\pi}} Q\left(\frac{\eta}{M\left(2N_0\right)^{1/2}}\sqrt{\sum_{i=1}^{M} I_i^2}\right) \exp\left(-x^2\right) \exp\left[-sI_0 e^{2\sqrt{2}\sigma_x x} e^{2\mu_x}\right] dx \\ &= Q\left(\frac{\eta}{M\left(2N_0\right)^{1/2}}\sqrt{\sum_{i=1}^{M} I_i^2}\right) \int_{-\infty}^{\infty} \frac{1}{\sqrt{\pi}} \exp\left(-x^2\right) \exp\left[-sI_0 e^{2\sqrt{2}\sigma_x x} e^{2\mu_x}\right] dx \end{aligned} \tag{4.16}$$

In order to solve eq. (4.16), Gauss-Hermite integration approximation is employed. The integral approximation is defined as [150]

$$\int_{-\infty}^{+\infty} f(x)\exp(-x^2)dx \cong \sum_{i=1}^{M} w_i f(x_i), \tag{4.17}$$

where $[w_i]_i^M$ and $[x_i]_i^M$ represent the weight factors and the zeros of an mth-order Hermite polynomial $H_M(x)$, respectively. The weight factors can be defined as [207]

$$w_i = 2^{M+1}M!\sqrt{\pi}/[H'_M(x_i)]^2 \tag{4.18}$$

So, using eq. (4.17), $P_{\mathrm{e}}^{\mathrm{OSTBC}}$ can be written as

$$P_{\mathrm{e}}^{\mathrm{OSTBC}} \cong \frac{1}{\sqrt{\pi}} \sum_{i=1}^{M} w_i f(x_i) Q\left(\frac{\eta}{M\left(2N_0\right)^{1/2}}\sqrt{\sum_{i=1}^{M} I_i^2}\right) \tag{4.19}$$

where $f(x_i) \triangleq \exp\left[-sI_0 e^{2\sqrt{2}\sigma_x x} e^{2\mu_x}\right]$.

Moreover, eq. (4.19) can be defined as

$$P_{\mathrm{e}}^{\mathrm{OSTBC}} \cong \frac{1}{\sqrt{\pi}} \sum_{i=1}^{M}\sum_{k=1}^{M} w_i \frac{(\mathfrak{I})^{-1+2k}\,(2k-\mathfrak{I})}{(2k)\,!} Q\left(\frac{\eta}{M\left(2N_0\right)^{1/2}}\sqrt{\sum_{i=1}^{M} I_i^2}\right) \tag{4.20}$$

where $(\cdot)!$ denotes a factorial function and $\mathfrak{I}$ can be represented as

$$\mathfrak{I} = \exp\left[-2\left(\mu_x + \sqrt{2}\sigma_x x\right)\right] sI_0 \tag{4.21}$$

4.4.2 Approximate Expression for Repetition Coding

Furthermore, to estimate the error probability of the RC, we employ eq. (4.10) on page 71 and then follow the procedures in eq. (4.13) on page 72 - eq. (4.20)). The resulting $P_{\mathrm{e}}^{\mathrm{RC}}$ can be written as

$$P_{\mathrm{e}}^{\mathrm{RC}} \cong \frac{1}{\sqrt{\pi}} \sum_{i=1}^{M}\sum_{k=1}^{M} w_i \frac{(\mathfrak{I})^{-1+2k}\,(2k-\mathfrak{I})}{(2k)\,!} Q\left(\frac{\eta}{M\left(2N_0\right)^{1/2}}\sum_{i=1}^{M} I_i\right) \tag{4.22}$$

It is noteworthy that, the argument of Q function in Eq. (4.20) is less than that of Eq. (4.22). This indicates that the RC gives an improved performance over the log-normal atmospheric turbulence-induced fading channels than the OSTBC scheme counterpart.

4.5 Numerical Results and Discussions

In this section, we present results of numerical calculations of the BER performance of FSO links for transmit diversity schemes. Also, we employ 1550 nm wavelength window due to the fact that it coincides with the standard transmission window of fiber communication systems and comparatively less susceptible to the fading effects of the fluctuation [146, 152]. Furthermore, we assume a receive aperture of size $D_o = 5$ cm and link distance of 2 km. Similarly, as the case may be, lognormal fading but independent channels with standard deviation of $\sigma_x = 0.1$ and $\sigma_x = 0.3$ are assumed. Furthermore, for diversity, we consider $M =$ 2, 3, and 4 transmit apertures performances along with that of SISO FSO link for benchmark purpose.

Figure 4.2(a) illustrates the BER performance of OSTBC with OOK modulation over the lognormal fading channel with different values of standard deviation. We observe that, the system performance increases as the number of transmit apertures increases with the implementation of OSTBC as regards SISO FSO scheme. For instance, to achieve a BER of 10^{-8} for the case of $\sigma_x = 0.1$, $\approx$ 23 dB and 21 dB are required for the SISO FSO scheme and the MIMO FSO with $M = 4$ transmit apertures, respectively. Therefore, for the considered turbulence level, OSTBC achieves about 2 dB gain. Similarly, for the same BER but considering $\sigma_x = 0.3$, $\approx$ 38 dB and 28 dB are required for the SISO FSO scheme and the $M = 4$ transmit apertures, respectively. So, for this turbulence level, OSTBC achieves about 10 dB gain. Furthermore, we deduce that, the required power increases with increase in turbulence and that increase in the transmit apertures enables OSTBC to effectively mitigate the turbulence-induced signal fading.

Figure 4.2(b) shows the BER performance of RC for OOK modulation over a lognormal fading channel with different values of standard deviation. Like OSTBC implementation, we observe an increase in system performance as the number of transmit apertures increases with regard to SISO FSO scheme. For instance, to achieve a BER of 10^{-8} for the case of $\sigma_x = 0.1$, $\approx$ 23 dB and 19 dB are required for the SISO FSO scheme and the $M = 4$ transmit apertures, respectively. Therefore, for the considered turbulence level, RC achieves about 4 dB gain. Likewise, for the same BER but for $\sigma_x = 0.3$, $\approx$ 38 dB and 25 dB are required for the SISO FSO scheme and the $M = 4$ transmit apertures, respectively. Hence, for the stated turbulence level, RC achieves about 13 dB gain. Also, we infer that the RC is able to achieve additional 3 dB gain compared to the OSTBC.

Figure 4.2(c) shows the BER performance for the considered diversity schemes with $\sigma_x =$ 0.1. The figure gives a clearer comparison of the schemes. We observed that the RC schemes outperform the OSTBC schemes significantly. For instance, to achieve a BER of 10^{-8} when $M = 2$, $\approx$ 21 dB and 20 dB are required for the OSTBC and RC, respectively. This shows that the RC gives about 1 dB performance improvement for the considered scenario.

Figure 4.2(d) depicts the BER performance for the considered diversity schemes with $\sigma_x = 0.3$. We observed that the RC schemes outperform the OSTBC schemes significantly. For instance, to achieve a BER of 10^{-8} when $M = 3$, $\approx$ 29 dB and 27 dB are required for the OSTBC and RC schemes, respectively. This shows that the RC gives about 2 dB performance improvement for the considered instance. Furthermore, it shows that as the turbulence increases, performance improvement of the RC schemes manifests more compared to that of the OSTBC schemes.

For more insight into the study, we drop the idea of independent channel and consider spatial correlation among the apertures. We examine different transmit apertures which are

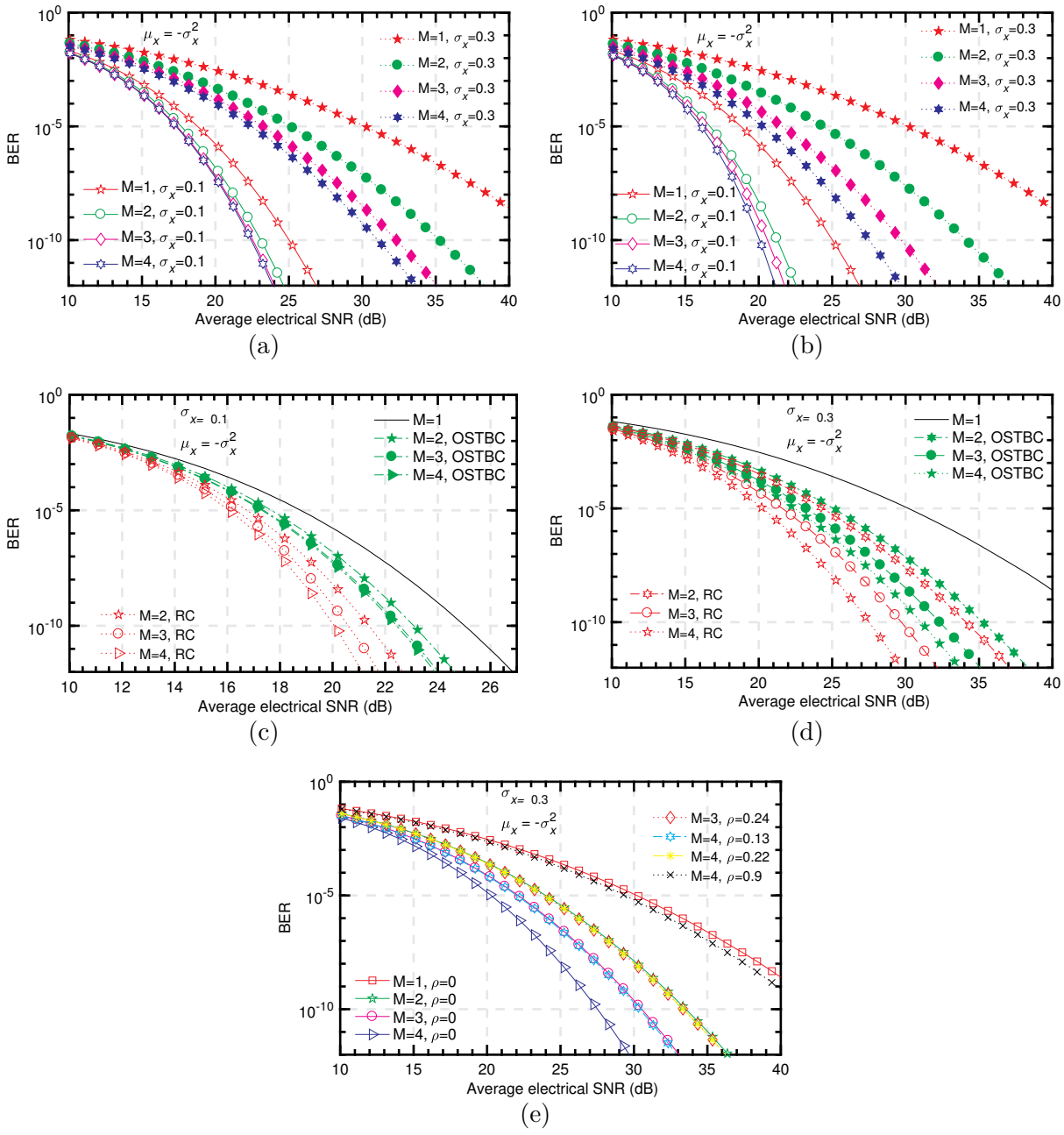

Figure 4.2: (a) Performance comparison of OSTBC for different number of transmit apertures and standard deviation, (b) Performance comparison of RC for different number of transmit apertures and standard deviation, (c) Performance comparison of diversity schemes for different number of transmit apertures, (d) Performance comparison of diversity schemes for different number of transmit apertures, (e) Performance comparison of spatial diversity scheme with spatial correlation among the apertures.

equidistant from each other and with different correlation values. As benchmarks, we also consider transmit apertures that are spatially independent. Figure 4.2(e) depicts the BER performance with spatial correlation among the apertures for standard deviation $\sigma_x = 0.3$. We observe that, for a spatially correlated channel scenario in which $M = 4$ and $\rho = 0.13$, the achievable performance corresponds to that of a situation for spatially independent channel in which $M = 3$ and $\rho = 0$. This means that a diversity order of 1 has been lost due to the correlation. Also, we noticed that, as the correlation increases, the performance loss becomes more severe. For instance, when $M = 4$ and $\rho = 0.9$, the observed performance is very similar to that of SISO FSO which means that virtually 3 diversity orders have been lost. Furthermore, another interesting observation that shows the importance of effective separation between the apertures is that, scenarios in which $M = 3$ and $\rho = 0.24$, and $M = 4$ and $\rho = 0.22$ have the anticipated performance of a situation in which $M = 2$ and $\rho = 0$. The scenario in which $M = 3$ experienced reduction in the diversity order by 1 despite the fact that it has higher correlation ($\rho = 0.24$). However, for $M = 4$ and with relatively lower correlation ($\rho = 0.22$), diversity order of 2 is lost. This is due to smaller separation between the apertures compared with the former. This demonstrates that, achievement of the envisaged diversity gains of spatial diversity depends significantly on effective separation between the apertures.

4.6 Research Contributions

The impacts of this chapter regarding reducing the computational complexity of the spatial diversity techniques in the FSO systems are stated in the following subsection.

4.6.1 First Contribution

In this chapter, based on [183] we have studied the BER performance of FSO communication links over the log-normal atmospheric turbulence channels. In the study, we consider spatial diversity techniques such as OSTBC and RC for mitigating turbulence-induced fading in the FSO systems. We use the BER as a performance metric and derive simple as well as accurate approximate closed-form expressions for the error probability of the log-normal FSO links with IM/DD. This approach helps in preventing the analytical complexity that is involved in solving the multi-dimensional numerical integration. It also helps in checking the associated upper limit truncation of the multi-dimensional numerical integration. The results show that the proposed BER expressions are capable of quantifying the effects of spatial diversity schemes on the considered FSO communication links. Furthermore, based on the proposed models, we have been able to show that the RCs schemes give considerable better performance than the OSTBCs schemes.

4.6.2 Second Contribution

Another remarkable contribution in this chapter is that, we study the effects of spatial correlation between the transmit apertures on the system performance. We employ the exponential model for determining the correlations between the apertures in the analysis. Furthermore, we have demonstrated that the realization of the envisioned diversity gains by spatial diversity is contingent on effective separation between the apertures so as to alleviate the associated spatial correlation.

4.7 Conclusion

In this chapter, we have studied the BER performance of OWC system links over log-normal atmospheric turbulence channels with different diversity schemes being considered. We observed that, an increase in the channel variance subsequently results in an increase in the signal impairment. Moreover, it is observed that the considered diversity schemes can be employed to reduce the detrimental effect of the channel variance. In addition, we have compared the BER performance of OSTBC with that of the RC schemes. The numerical analyses and results presented have shown that, both RCs and OSTBCs diversity schemes are effective for fading mitigation. Nevertheless, the RCs schemes significantly offer improved performance in relation to the OSTBCs schemes. Moreover, we have demonstrated that, realization of the envisaged diversity gains of the spatial diversity depends extensively on effective separation between the apertures to mitigate the associated spatial correlation.

Chapter

Computational-Efficient Estimation of MIMO-FSO System Capacity

This chapter is based on articles [168] and [169]. The chapter presents computational-efficient means of estimating the ergodic channel capacity of MIMO-FSO systems. This can be achieved by the spatial interpolation and power series representation approaches. In [168], we present the spatial approach that is based on B-spline and Barycentric Lagrange interpolation Lookup Table (B^2LUT). The B^2LUT models can be employed for the estimation of MIMO FSO system ergodic capacity over general turbulence conditions. It is noteworthy that the simplicity of the B^2LUT can be attributed to the fact that, the model selects just few precomputed weights in creating the LUTs. The chosen precomputed weights are then utilized for spatial interpolation. This approach results in a very low memory requirement for an efficient operation of the system. Furthermore, the B^2LUT facilitates faster (up to fifteen orders of magnitude and beyond) and stable performance evaluation compared to the current state-of-the-art analytical based approaches [168]. Furthermore, in [169], we present an empirical model for determining ergodic channel capacity of MIMO FSO communication systems. The model is based on power series representation and enables faster performance estimation compared to the existing numerical integration based models. Moreover, the model gives considerable perception of the effects of atmospheric turbulence-induced channel fading on the system performance.

5.1 Introduction

FSO communication systems are broadband access technologies with various remarkable benefits. However, FSO links are susceptible to turbulence-induced fading. As a result, the achievable ergodic capacity, which is one of the major figure of merits for characterizing

the communication link performance is impaired [169]. Consequently, the dispersive nature of FSO channel has to be addressed by employing different cutting edge schemes such as diversity techniques. Spatial diversity technique with MIMO FSO system is one of feasible means of alleviating fading in the FSO links. MIMO FSO system not only mitigates the atmospheric turbulence-induced fading but also enhances the FSO links reliability [169,176,208]. However, evaluation of ergodic channel capacity of MIMO FSO system based on numerical integration requires relatively more computational time. This is even more demanding for the strong turbulence regimes analysis [177]. This is can be attributed to the Bessel function that is generally defined in terms of the Meijer's G-function given in eq. (3.29) on page 61 for easier estimation [177].

The resulting impairment of MIMO FSO system can be appropriately expressed with behavioral model. Behavioral model involves the engagement of black box models for relating the input and output signals. Memory polynomials are typically used for building the behavioral model algorithm based lookup tables (LUTs) [209]. Furthermore, implementation of fast and low memory basis (B)-spline LUT have been employed for enhancing the effectiveness of behavioral model. Also, the LUT weight changing approach have been demonstrated in order to improve the behavioral modelling efficiency [210, 211]. Additionally, standard optimization software such as DAKOTA uses Barycentric Lagrange interpolation for efficient global optimization of stochastic black-box systems. Implementation of Barycentric Lagrange interpolation helps in reducing the computational effort for interpolant estimations from $O(n^2)$ to $O(n)$ [212].

With insights on B^2LUT models being presented, in section 5.2, we present B^2LUT models for the estimation of ergodic capacity of MIMO FSO system under general turbulence conditions. Section 5.3 on page 83 presents the power series representation approach for capacity estimation. Model validation and simulation speed analysis are discussed in section 5.4 on page 85. In section 5.5 on page 87, research contributions on efficient capacity estimations are presented and concluding remarks are given in section 5.6 on page 88

5.2 Spatial Interpolation System Models

The B^2LUT models with data set of the form $\{\gamma_i, f(\gamma_i)\}_{i=0}^{n}$ for function f, corresponding to the C_{erg}, of a SISO system at a specific scintillation index σ_N^2, and refractive index C_n^2, can be constructed by representing the univariate (precomputed B-spline and Barycentric Lagrange weights) interpolating polynomial to f in the nodal points $\gamma_0, \cdots, \gamma_i$. Furthermore, both spatial interpolation approaches can be reformulated so as to build and achieve the identification quality of interpolated LUTs for ergodic channel capacity of a MIMO FSO system. This is implemented by considering the M transmit apertures and the N receive apertures under the effect of the channel matrix $\boldsymbol{H}$ as depicted in Fig. 5.1. The analysis can be initiated by building the FSO system capacity that is based on the SNR through the multivariate piecewise Barycentric Lagrange LUT in accordance with the tensor product from the univariate model of each aforementioned variable (i.e. M, N, σ_N^2) [168].

5.2.1 Barycentric Lagrange interpolation

It is worth mentioning that, the conventional Lagrange interpolation has some limitations that makes it a bad option for practical computations. For example, to improve the sys-

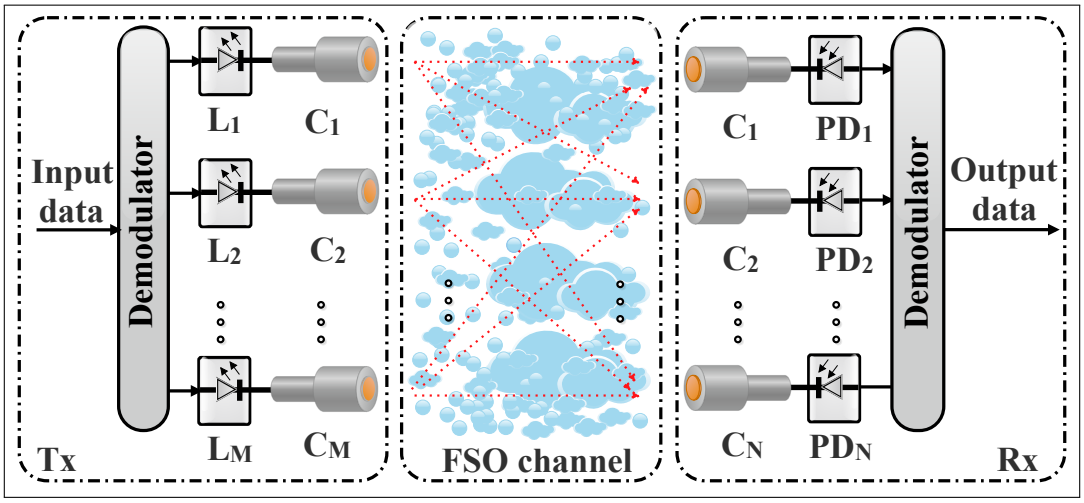

Figure 5.1: Block diagram of $M \times N$ MIMO FSO system. L: laser, C: collimator, PD: photodetector, Tx: transmitter, Rx: receiver.

tem accuracy by adding new data pairs, a new set of calculations are needed for the whole LUTs [213]. The flaws make the scheme to be numerically unstable, this is even worst for higher order systems. Moreover, estimation of each interpolation needs $O(n^2)$ additions and multiplications. Consequently, we adopt Barycentric Lagrange interpolation due to the fact that it is fast and stable [213]. The exhibited beneficial features are as a result of the pre-computed techniques of the Barycentric weights that ease its computational complexity to $O(n)$ compared to $O(n^2)$ operations when the conventional Lagrange is employed [212, 213].

The Barycentric Lagrange is a special Lagrange with symmetric weights w_j that exist in the numerator and denominator but without the data factors f_j in the denominator. This implies that, the common factor in the weights w_j may be canceled without affecting the value of the polynomial $p(x)$.

Let $\prod_n$ represent the vector space of all the polynomials with degree at most n. Therefore, to find the polynomial $p \in \prod_n$ that interpolates f at the points x_j, implies

$$p\left(x_j\right) = f_j \qquad j = 0, \cdots, n \ , \tag{5.1}$$

In practice, for $n+1$ mutually distinct nodes $x_0, x_1, \cdots, x_n$ and functions $f_0, f_1, \cdots, f_n$, the univariate Barycentric Lagrange for $p(x)$ can be written as [212–216].

$$p\left(x\right) = \frac{\sum\limits_{j=0}^{n} \frac{w_j}{x - x_j} \ f_j}{\sum\limits_{j=0}^{n} \frac{w_j}{x - x_j}} \qquad j = 0, \cdots, n \ , \tag{5.2}$$

where w_j denotes the pre-computed Barycentric weights which can be expressed as [168]

$$w_j = \left[\prod_{\substack{k=0 \\ k \neq j}}^{n} \left(x_j - x_k\right) \right]^{-1} . \tag{5.3}$$

For a multivariate system, assume that

$$\prod_{\gamma_M}^{a} = \{\gamma_t | t = 1, 2, \ldots, a\} \subset (\gamma_{M_t}, \gamma_{M_c}), \quad \gamma_1 < \gamma_2 < \ldots < \gamma_a, \tag{5.4a}$$

$$\prod_{\gamma_N}^{b} = \{\gamma_r | r = 1, 2, \ldots, b\} \subset \left(\gamma_{N_r}, \gamma_{N_q}\right), \quad \gamma_1 < \gamma_2 < \ldots < \gamma_b, \tag{5.4b}$$

$$\prod_{\gamma_{\sigma_N^2}}^{m} = \{\gamma_p | p = 1, 2, \ldots, m\} \subset \left(\gamma_{\sigma^2_{N_p}}, \gamma_{\sigma^2_{N_v}}\right), \quad \gamma_1 < \gamma_2 < \ldots < \gamma_m. \tag{5.4c}$$

$$\therefore \prod_{\gamma_{M,N,\sigma_N^2}}^{a,b,m} = \{(\gamma_t, \gamma_r, \gamma_p) | t = 1, 2, \ldots, a; r = 1, 2, \ldots, b; p = 1, 2, \ldots, m\} \subset \times (\gamma_{M_t}, \gamma_{M_c}) \times \left(\gamma_{N_r}, \gamma_{N_q}\right) \times \left(\gamma_{\sigma^2_{N_p}}, \gamma_{\sigma^2_{N_v}}\right), \tag{5.5}$$

where

$$f(\gamma_t, \gamma_r, \gamma_p) = f_{t,r,p}\,(t = 1, 2, \ldots, a; r = 1, 2, \ldots, b; p = 1, 2, \ldots, m). \tag{5.6}$$

Also, let

$$\Psi\left(\gamma|_{M,N,\sigma_N^2}\right) = \frac{\sum_{t=1}^{a} \frac{w_{t,a}(\gamma|_M)}{\varphi_t(M-M_t)} \mathcal{F}_t\left(\gamma|_{M,N,\sigma_N^2}\right)}{\sum_{t=1}^{a} \frac{w_{t,a}(\gamma|_M)}{\varphi_t(M-M_t)}} \qquad w_{t,a}\left(\gamma|_M\right) \neq 0, \tag{5.7a}$$

$$\mathcal{F}_t\left(\gamma|_{M,N,\sigma_N^2}\right) = \frac{\sum_{r=1}^{b} \frac{w_{r,b}(\gamma|_N)}{\varphi_r(N-N_r)} \mathcal{J}_{t,r}\left(\gamma|_{M,N,\sigma_N^2}\right)}{\sum_{r=1}^{b} \frac{w_{r,b}(\gamma|_N)}{\varphi_r(N-N_r)}} \qquad w_{r,b}\left(\gamma|_N\right) \neq 0, \tag{5.7b}$$

$$\mathcal{J}_{t,r}\left(\gamma|_{M,N,\sigma_N^2}\right) = \frac{\sum_{p=1}^{m} \frac{w_{\mathcal{P},m}\left(\gamma|_{\sigma_N^2}\right)}{\varphi_{\mathcal{P}}\left((\sigma_N^2)-(\sigma_N^2)\right)} f_{t,r,p}\left(\gamma|_{M,N,\sigma_N^2}\right)}{\sum_{p=1}^{m} \frac{w_{\mathcal{P},m}\left(\gamma|_{\sigma_N^2}\right)}{\varphi_p\left((\sigma_N^2)-(\sigma_N^2)\right)}} \qquad w_{\mathcal{P},m}\left(\gamma|_{\sigma_N^2}\right) \neq 0. \tag{5.7c}$$

Furthermore, consider a multivariate Barycentric Lagrange interpolation (BLI) for a continuous function f, i.e. $C_{ij} = f(\gamma_{ij}|_{(M,N,\sigma_N^2)})$ for $i = 1, \cdots, n$ and $j = 1, \cdots, k$, then, the capacity of MIMO FSO system can be defined as [168]

$$C\left(\gamma|_{\left(M,N,\sigma_N^2\right)}\right) = \frac{\sum_{t=1}^{a}\sum_{r=1}^{b}\sum_{p=1}^{m} f\left(\gamma_{ij}|_{\left(M_t,N_r,(\sigma_N^2)_p\right)}\right)\mathfrak{A}}{\sum_{t=1}^{a}\sum_{r=1}^{b}\sum_{p=1}^{m}\mathfrak{A}}, \tag{5.8}$$

where $\mathfrak{A} = w_{trp}\left(\gamma|_{\left(M,N,\sigma_N^2\right)}\right)/\varphi_{trp}\left(\gamma|_{\left(M,N,\sigma_N^2\right)}\right)$, $\varphi_{trp}(\cdot) = \varphi_t(M - M_t)\,\varphi_r(N - N_r)\,\varphi_p \times \left((\sigma_N^2) - (\sigma_N^2)_p\right)$, and $w_{trp}(\cdot)$ represents the tensor product of barycentric weights expressed

as [168]

$$w_{trp}(\gamma|_{(M,N,\sigma_N^2)}) = w_{t,a}(\gamma|_M) w_{r,b}(\gamma|_N) w_{p,m}(\gamma|_{\sigma_N^2}) \\ 0 \leq c \leq a,\ 0 \leq q \leq b,\ 0 \leq v \leq m, \quad (5.9)$$

where $w_{t,a}(\cdot)$, $w_{r,b}(\cdot)$, and $w_{p,m}(\cdot)$ denote the subsets of the precomputed barycentric weights for the transmit apertures, receive apertures, and σ_N^2, respectively and they are expressed as [168]

$$w_{t,a}(\gamma|_M) = \frac{1}{\prod_{\substack{t=1 \\ t\neq c}}^{a} M_t - M_c}, \quad (5.10a)$$

$$w_{r,b}(\gamma|_N) = \frac{1}{\prod_{\substack{r=1 \\ r\neq q}}^{b} N_r - N_q}, \quad (5.10b)$$

$$w_{p,m}(\gamma|_{\sigma_N^2}) = \frac{1}{\prod_{\substack{p=1 \\ p\neq v}}^{m} (\sigma_N^2)_p - (\sigma_N^2)_v}. \quad (5.10c)$$

5.2.2 Precomputed B-spline Weights

The multivariate LUTs for the estimation of channel capacity of MIMO FSO system can be built by reformulating the De Boor's algorithm with precomputed B-spline weights [168]. The precomputation process involves finding the closest precomputed weight in the LUT. The coefficients can then be looped over their corresponding precomputed weights. Implementation of this approach ensures that the computation of the weights is realized just once for the interpolated LUT construction [211]. The LUT can be interpolated in a such a way that, just few weights are precomputed and stored for the process. This approach prevents precomputation and storage of all the weights. Consequently, the approach eases the computational cost by reducing the lookup table size without loss of fidelity. Furthermore, the trade-off between the LUT size, as well as the approximation accuracy, can be effectively controlled by choosing the (over) sampling rate of the precomputed weights in accordance with the control point grid [168].

The multivariate spline interpolation LUT model can be built by combining three univariate piecewise B-spline into the data set given by [168]

$$\left\{ M_t, N_r, (\sigma_N^2)_p, f_{trp} \right\}_{t=r=p=1}^{m_1,m_2,m_3}. \quad (5.11)$$

The univariate De Boor's algorithm of the B-spline interpolation for estimating the spline of $\mathcal{N}(x)$ for parameter $x \in [u_l, u_{l+1}]$ can be expressed as [217]

$$S(x) = \sum_{i=l-n}^{l} d_i \mathcal{N}_i^n(x), \quad (5.12)$$

where $\mathcal{N}_i^n(x)$ is the basis expressed recursively as [218]

$$\mathcal{N}_i^0 = \begin{cases} 1 & \text{if } x_i \leq x \leq x_{i+1} \\ 0 & \text{otherwise.} \end{cases} \quad (5.13)$$

$$\mathcal{N}_i^n(x) = \frac{x - x_i}{x_{i+n} - x_i}\mathcal{N}_i^{n-1}(x) + \frac{x_{i+n+1} - x}{x_{i+n+1} - x_{i+1}}N_{i+1}^{n-1}(x), \tag{5.14}$$

and d_i is the precomputed control points of S defined as

$$d_i^{([k])} = S_i[d_{(l-n)}, d_{(l-n+1)} \dots d_i], \quad i = j - n, \dots, j, \tag{5.15}$$

The initial d_i weight precomputation process of the De Boor's algorithm commences by setting $d_i^{[0]} = \mathcal{N}_i^{[0]}(x)$ for $i = l - n, \dots, l$. Subsequently, the procedure continues up till

$$d_i^{[k]} = (1 - \alpha_{k,i})\, d_{i-1}^{[k-1]} + \alpha_{k,i} d_i^{[k-1]}, \tag{5.16}$$

where α is defined as

$$\alpha_{k,i} = \frac{x - u_i}{u_{i+n+1-k} - u_i}, \tag{5.17}$$

Furthermore, the tensor-product counterpart of eq. (5.8) on page 81 with the B-spline interpolated LUT for the MIMO FSO channel capacity is of the form [168]

$$C\left(\gamma|_{(M,N,\sigma_N^2)}\right) = \sum_{t=1}^{m_1}\sum_{r=1}^{m_2}\sum_{p=1}^{m_3} \omega\left(\gamma|_{\sigma_N^2}\mathfrak{I}_p, \cdots, \mathfrak{I}_{p+h}\right) \times \psi\left(\gamma|_N \mathfrak{D}_r, \cdots, \mathfrak{D}_{r+\ell}\right) \phi\left(\gamma|_M \mathfrak{S}_t, \cdots, \mathfrak{S}_{t+s}\right) \mathfrak{M}_{t,r,p}, \tag{5.18}$$

where $\mathfrak{I} = (\mathfrak{I}_p, \cdots, \mathfrak{I}_{p+h})$, $\mathfrak{D} = (\mathfrak{D}_r, \cdots, \mathfrak{D}_{r+\ell})$, and $\mathfrak{S} = (\mathfrak{S}_t, \cdots, \mathfrak{S}_{t+s})$ are the knot sequences and $(\mathfrak{M}_{t,r,p} : t = 1, \cdots, m_1; r = 1, \cdots, m_2; p = 1, \cdots, m_3)$ are coefficient arrays. They are precomputed weights with respect to the control point grid with weight in the range $[0, 1]$, as defined by the aforementioned De Boor's algorithm. Moreover, the $\omega(\cdot), \psi(\cdot), \phi(\cdot)$ are the univariate piecewise B-spline for M, N , and σ_N^2, respectively.

In this work, the normalized mean square error (NMSE) metric is used in an attempt to offer a quantitative measure of the accuracy of the models for MIMO FSO systems. The NMSE can be expressed as [219, 220]

$$\text{NMSE (dB)} = 10\log_{10}\left[\frac{\sum_{m=1}^{M}|y(t_m) - \hat{y}(t_m)|^2}{\sum_{m=1}^{M}|y(t_m)|^2}\right]. \tag{5.19}$$

where $y(t_m)$ is the simulated ergodic capacity, C_{erg}, of FSO system and $\hat{y}(t_m)$ is the estimated ergodic capacity, $\langle C \rangle$, using the proposed MIMO FSO model.

5.3 Power Series Representation System Model

The power series approach employed is based on polynomial fitting. In the analysis, we employ third-order polynomial fitting due to the fact that the second-order polynomial is not sufficient to offer precise fitting whreas the fourth-order polynomial equation does not provide considerable improvement in the accuracy and also presents more computational complexity.

Therefore, in the analysis, we observed that, the ergodic capacity fitting for SISO FSO follows the power series of the form [221, 222]

$$\sum_{n=0}^{\infty} a_n \ \mathcal{X}^n = a_0 + a_1 \ \mathcal{X} + a_2 \ \mathcal{X}^2 + a_3 \ \mathcal{X}^3 + \cdots \ , \tag{5.20}$$

where a_n denotes the coefficient of the nth term and $\mathcal{X} = k_1\gamma$, k_1 denotes a coefficient whose value is one and the unit is in $b/s/Hz$. The sum of the series can be expressed in term of a function as [169]

$$f\left(\mathcal{X}\right) = a_0 + a_1 \ \mathcal{X} + a_2 \ \mathcal{X}^2 + \cdots + a_n \ \mathcal{X}^n + \cdots \ . \tag{5.21}$$

As mentioned earlier, third-order polynomial can offer a good compromise concerning accuracy and complexity, consequently, the first few terms of the series are sufficient to acquire precise results. Hence, the series can be summarized in a single big $\mathcal{O}$ notation as [223, 224]

$$f\left(\mathcal{X}\right) = a_0 + a_1 \ \mathcal{X} + a_2 \ \mathcal{X}^2 + a_3 \ \mathcal{X}^3 + \mathcal{O}\left(\mathcal{X}^4\right). \tag{5.22}$$

The reason for the summarization is that, as the order of $\mathcal{X}$ increases, the absolute-value of the error is close enough to 0 (zero) and employment of higher order increases the system computational complexity. Therefore, it implies that [169]

$$f\left(\mathcal{X}\right) - \left(a_0 + a_1 \ \mathcal{X} + a_2 \ \mathcal{X}^2 + a_3 \ \mathcal{X}^3\right) \approx 0 \ . \tag{5.23}$$

Hence, it implies that [169]

$$f\left(\mathcal{X}\right) = a_0 + a_1 \ \mathcal{X} + a_2 \ \mathcal{X}^2 + a_3 \ \mathcal{X}^3 \ , \tag{5.24}$$

The coefficients of the nth term for a given scintillation index, σ_N^2, are achieved by mapping the coefficients of the third-order polynomial fitting discussed in Chapter 7 on page 101 to the variance of irradiance. As a result, the coefficients are defined as [169]

$$a_0 = 0.13\pi k_1 \Re, \tag{5.25a}$$
$$a_1 \ = 0.66\Re, \tag{5.25b}$$
$$a_2 \ = 1.45 \times 10^{-3}\Re, \tag{5.25c}$$
$$a_3 \ = -1.73 \times 10^{-5}\Re, \tag{5.25d}$$

where $\Re = \pi exp\left(\sigma_R^2 - \sigma_N^2\right) = \pi \sum_{k=0}^{\infty} \frac{(-\sigma_N^2 + \sigma_R^2)}{(k)!}$.

The parameter $\Re$ that signifies the effect of an atmospheric turbulence is employed for shaping the slope of eq. (5.24) to be in accordance with that of experimental measurement.

The average channel capacity of MIMO FSO systems in the presence of atmospheric turbulence and weather condition using eq. (5.24) can be defined as [169]

$$\langle C \rangle = f\left(\mathcal{X}\right) = \psi\mathcal{A}\left(a_0 + a_1 \ \mathcal{X} + a_2 \ \mathcal{X}^2 + a_3 \ \mathcal{X}^3 \ \right) \ , \tag{5.26}$$

where $\psi = \pi/4$ and $\mathcal{A} = \min\left\{M, N\right\}$ is the minimum number of transmit or receive apertures.

5.4 Model Validation and Simulation Speed Analysis

We estimate the ergodic channel capacity of MIMO FSO communication systems using the proposed models and the obtained results are validated by Monte Carlo simulation. We use scintillation index $\sigma_N^2 = 0.0120$ and refractive-index $C_n^2 = 6.0 \times 10^{-16} m^{-2/3}$ in the models. The average channel capacity versus the average SNR in the presence of turbulence conditions are shown in Fig. 5.2 for different $M \times N$ schemes. In the plot, we use analytical model (exact expression) for benchmarking. We obtain an approximate fit of the system capacity when we employ quadratic spline and second order Lagrange as shown in Figs 5.2(a) and 5.2(b) for the considered $M \times N$ schemes. To ensure accurate evaluation of the system capacity, we then use cubic spline and third order Lagrange with results depicted in Figs 5.2(c) and 5.2(d). The cubic spline and third order Lagrange shown in the figure give rise to an exact fit and show a good compromise regarding accuracy and complexity.

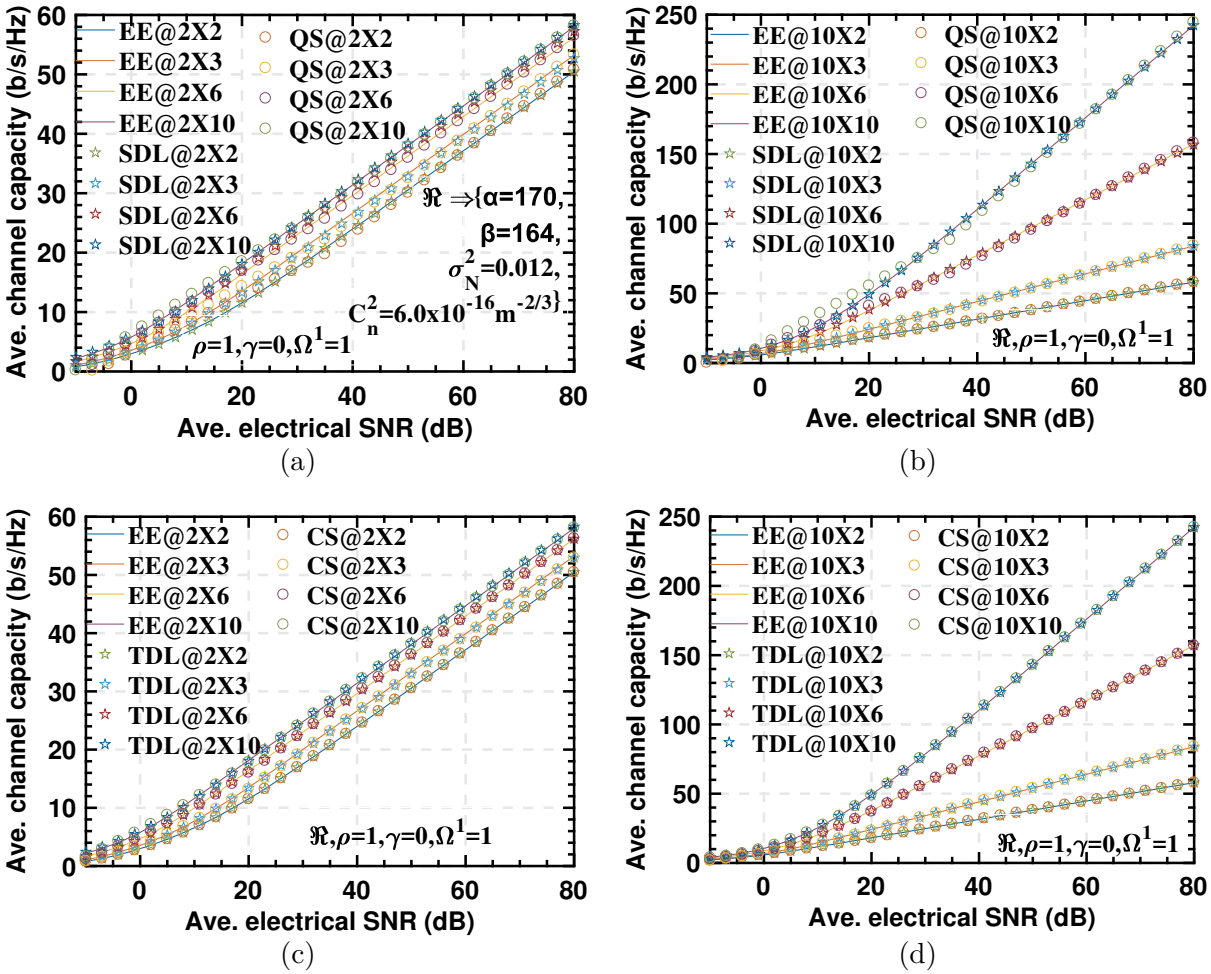

Figure 5.2: Average channel capacity versus the average SNR for (a) $2 \times N$, (b) $10 \times N$ schemes, (c) $2 \times N$, (d) $10 \times N$. EE: exact expression, SL: second order Lagrange, QS: quadratic spline, TL: third order Lagrange, CS: cubic spline.

Furthermore, we use different values of σ_N^2 that correspond to low-strong turbulence regimes to observe their effects on the system performance. The results presented in Fig. 5.3(a) show that, an increase in the atmospheric turbulence has relative adverse effects on system performance. It should be noted that, the effect of fading decreases with the increase in the number of apertures. Figure 5.3(b) shows the feasibility of the proposed models with higher combinations of transceiver apertures.

We compare the performance of the proposed models and the analytical model in terms of computational time. Our simulations are implemented on a 64-bit windows 10 operating system with 2.10GHz Intel® Core™ i3-2310M processor and 8GB RAM. Table 5.1 on the following page shows that the proposed models can enhance the speed by up to fifteen orders of magnitude and beyond considering the multiple transmitter and receive apertures under the effect of the channel matrix, H for different σ_N^2 and refractive index C_n^2 compared to the analytical model.

Moreover, we evaluate the performance of the proposed models for different MIMO FSO aperture configurations. We observe, that the proposed models maintain the NMSE values within a close range for the MIMO configurations under consideration. Table 5.2 on the next page shows the results of the NMSE in dB for the proposed models. The results are similar for most Lagrange and spline orders. This good agreement between the analytical and the developed interpolated LUT behavioral models confirms that the proposed models improve modeling efficiency greatly without trade-off in accuracy nor complexity.

Furthermore, it is noteworthy to add that, both models offer high accuracy, however, the Barycentric Lagrange LUT is more computationally efficient. Moreover, due to the reduced computational effort of the Barycentric Lagrange interpolation, its computational time is consequently lower than that of the B-spline as depicted in Table 5.1 on the following page.

The performance of the power series model is evaluated in Table 5.3 on the next page for different MIMO FSO aperture configurations. It is observed that, the proposed model maintains NMSE in a close range for the MIMO configurations under consideration. This shows the model potential in managing different MIMO FSO aperture configurations.

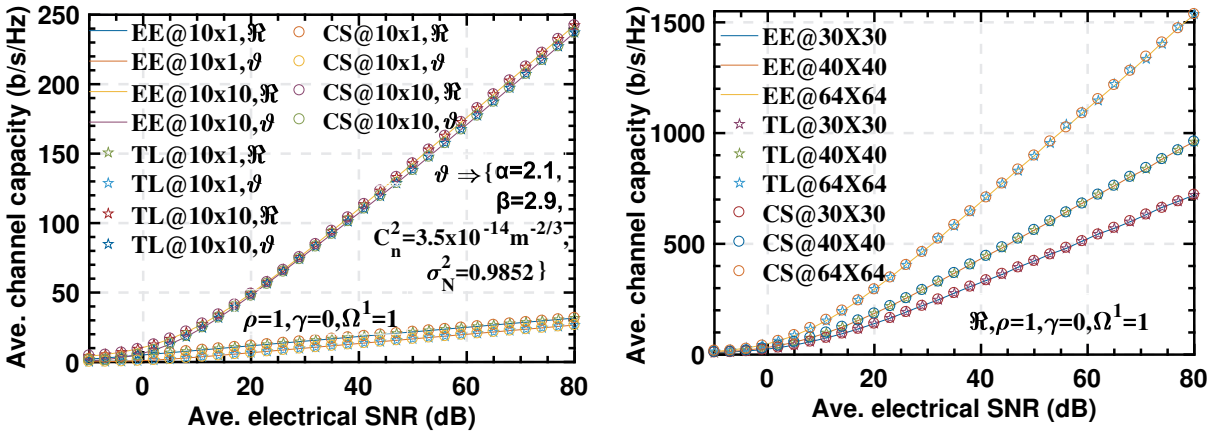

Figure 5.3: Average channel capacity versus the average SNR for (a) $10 \times N$, (b) $M \times N$.

Table 5.1: Computation time (s) analysis of the models [168]

Model	2×10	5×10	10×10
Analytical	93.678	106.379	126.3467
Barycentric Lagrange	2.579	4.852	6.4583
Spline	3.891	6.791	8. 2040

Table 5.2: NMSE (dB) for MIMO FSO configurations [168]

Order	**Barycentric Lagrange**		**Spline**	
	$2 \times N$	$10 \times N$	$2 \times N$	$10 \times N$
2	-45.3185	-50.1216	-45.6876	-60.8972
3	-65.9963	-79.8614	-67.8069	-77.1585

Table 5.3: NMSE for different MIMO FSO aperture configurations [169].

Aperture configuration	**NMSE(dB)**
1×1	-69.1596
2×2	-36.3084
3×3	-34.4037
4×4	-38.9964

5.5 Research Contributions

The contributions of this chapter based on the estimation of ergodic channel capacity of MIMO FSO systems are enumerated in the following subsection.

5.5.1 First Contribution

In [168] we proposed low complexity and adaptive multivariate precomputed B^2LUT statistical models for the estimation of ergodic channel capacity of MIMO FSO systems over generalized $\mathcal{M}$-distributed atmospheric turbulence channels. The models significantly reduced the size of the lookup table, consequently, easing the computational cost. Besides, the B^2LUT models have a number of merits such as high-accuracy, low memory requirement, fast and stable operation. The advantages are attributed to the precomputed weights that are exploited for creating the LUTs for spatial interpolation. Furthermore, the models significantly improved modeling efficiency without a trade-off in accuracy nor complexity. Moreover, the models enhanced the speed by up to fifteen orders of magnitude and beyond without loss of fidelity compared with the current analytical models. The B^2LUT models are appropriate for real-time applications in FSO system deployment for fast performance evaluation and system optimization.

5.5.2 Second Contribution

In [169] we analyzed different diversity schemes and propose a closed-form expression for the estimation of ergodic channel capacity of MIMO FSO communication systems over atmospheric turbulence fading channels. The proposed empirical model is based on SISO

FSO channel characterization discussed in Chapter 7. The model is also based on power series representation and enables faster performance evaluation compared to the existing models which are based on time-consuming numerical integration. Furthermore, the model presents significant understanding of the effects of atmospheric turbulence fading channels on the system performance. In addition, based on the proposed model, scintillation effects on the system performance can be effectively analyzed. The model is useful in the FSO system deployment as the required capacity for distinct SNR can be analyzed easily. Also, the maximum data rate that can be reliably transmitted can be determined for different operating conditions.

5.6 Conclusion

In this chapter, we have presented adaptive multivariate precomputed B^2LUT statistical models for estimating the ergodic capacity of MIMO FSO system under generalized $\mathcal{M}$-distributed atmospheric turbulence channels. The B^2LUT models have a number of advantages such as high-accuracy, low memory requirement, fast, and stable operation. The benefits are as a result of the precomputed weights that are being exploited for the LUTs for the spatial interpolation creation. The good agreement between the analytical and our models validates that the B^2LUT models enhance modeling efficiency significantly without trade-off in accuracy nor complexity. Additionally, the proposed models can improve the speed by up to fifteen orders of magnitude and beyond without loss of fidelity. The B^2LUT models are appropriate for real-time applications in FSO system deployment for fast performance evaluation and system optimization.

Chapter

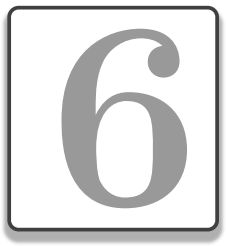

Technologies for Performance Enhancement

FSO is a promising optical technology that can be employed for different application. However, the trade-off between the required high data rates as well as the limitations of atmospheric channel are the major challenges for reliable implementation of FSO technologies in the access networks. Therefore, the problems inhibit the FSO system from being an effective and reliable standalone fronthaul technology. In this chapter, based on manuscripts [26] and [225], schemes like hybrid RF/FSO and relay-assisted transmission technologies that can be implemented to enhance the performance of FSO technology in the access networks are presented.

6.1 Introduction

For an efficient management of the NGNs and the associated evolving complexity, C-RAN has been envisioned as an encouraging model for the next generation access network. This is due to its valuable features in terms of performance optimization and cost-effectiveness [22,73]. In the C-RAN architecture, the main approach for signal transmission in the fronthaul is by digital baseband oversampled IQ streams. This can be realized with the aids of CPRI or OBSAI interface [7]. However, optical links that are based on these interfaces require huge bandwidth which is as a result of the high resolution bits required for the digitalization process of the RF samples [9]. So, the bandwidth inefficiency could limit or make C-RANs impractical for the next generation mobile system in which Massive MIMO antenna system is envisaged to be integrated [10], [11]. For instance, take into consideration the CA of LTE-A of five 20 MHz mobile signals with 3 sectors, and 8 $\times$ 8 MIMO antennas. This configuration needs about 147.5 Gb/s fronthaul data rate for the CPRI implementation [12], [13]. Consequently, in order to accomplish a bandwidth-efficient mobile fronthaul, an implementation of advanced measures is required. One of such is the employment of analog optical transmission technique which is based on RoF technology [7, 11, 14].

It is should be noted that, deployment of RoF technology is contingent mainly on the accessibility of the installed optical fiber cables between different network facilities. However, for cell densification, fiber deployment is capital–intensive and time-consuming especially when trenching is needed. Moreover, acquisition of right-of-way for BSs locations could be one of limiting factors for an appropriate system deployment. As a consequence of these challenges and the limited number of the installed fiber cables, the viability of FSO communication system has been acknowledged. Similar to RoF, the FSO can be employed in RF signal transmission with the significant benefit that, installation of fiber cables is not required. The concept of transmitting RF signals over FSO (i.e. RoFSO) exploits high transmission capacity offers by the optical technologies and ease of deployment of wireless systems [15].

As discussed in Chapter 3 on page 44, despite the fact that, FSO is an appealing optical technology with various applications, the trade-off between the required high data rates, as well as the limitations presented by the atmospheric channel, are the major application challenges in the access networks. Consequently, these limitations prevent FSO from being an efficient standalone fronthaul solution [15]. Nevertheless, schemes like hybrid RF/FSO and relay-assisted transmission technologies can be utilized so as to make FSO a better communication system.

With the need for FSO communication systems along with the associated impairments, as well as the state-of-the-art on the subject matter being presented, in Section 6.2, we give comprehensive overviews of a hybrid RF/FSO technology. The relay-assisted FSO transmission schemes are presented in Section 6.3 on the following page. Section 6.4 on page 92 describes the system and channel models. We present performance metrics such as outage probability, average symbol error probability (ASEP), and ergodic channel capacity in Section 6.5 on page 93. In Section 6.6 on page 96, results and discussion are presented. Research contributions are discussed in Section 6.7 on page 100 and finally, Section 6.8 on page 100 concludes this chapter.

6.2 Hybrid RF/FSO Technology

It should be noted that RF wireless technologies that operate above approximately 10 GHz frequencies are adversely affected by rain, whereas, fog has insignificant effect on them. On the other hand, FSO systems are highly susceptible to fog, whereas, effect of rain on them are negligible. Therefore, it is of high importance to improve the link reliability to alleviate the adverse effects of the meteorological and weather conditions. An attractive way of addressing the challenge is a simultaneous employment of the RF and FSO links for transmission. It is remarkable that, fog and rain rarely occur concurrently in nature. Consequently, the two links can function in a complementary way. This concept influences the hybrid RF/FSO scheme. The RF/FSO is a hybrid scheme that combines the benefits of the inherent high transmission capacity of optical technologies and the ease of deployment of wireless links. Moreover, the idea of hybrid RF/FSO system is to concurrently attend to the related drawbacks and take advantages of both technologies. This will help in the reliable transmission of heterogeneous wireless services [152, 226].

In a hybrid RF/FSO technology, there are two parallel links between the transmitter and the receiver. Moreover, subject to deployment scenario and application, both parallel links of the hybrid technology have the capability to transmit data. Nevertheless, based on the weather conditions as well as the EMI levels, either of the links can be used for data

transmission [227]. For instance, under adverse atmospheric condition (i.e. fog), the hybrid RF/FSO scheme ensures that the RF link serves as a back-up in case of FSO link outage. However the resultant data rate of the RF link is less than that of the actual FSO link [152,226]

6.3 Relay-assisted FSO Transmission

A realistic approach for turbulence-induced fading mitigation is spatial diversity technique. In this technique, multiple transmit/receive apertures are employed in order to create and exploit additional degrees of freedom in the spatial domain. The spatial diversity is an appealing technique for fading mitigation because of its typical redundancy. However, utilization of multiple apertures presents different challenges such as, an increase in the system complexity as well as cost. In addition, the distance between the apertures has to be large enough in order to inhibit detrimental effects of spatial correlation. A simplified way of implementing spatial diversity is the dual-hop relaying which has been considerably employed in the RF communication systems. The dual-hop relaying implementation helps substantially in extending the network coverage area, as well as improving the quality of the receive signal [228].

Furthermore, the concept of relay-assisted transmission is based on creating a virtual multiple-aperture system in order to realize advantages of MIMO techniques. This is achieved by exploiting both RF and FSO characteristics in order to have an efficient system in a real-life situation. Additionally, a relay-assisted transmission is also known as a mixed Radio Frequency/Free Space Optical (mixed RF/FSO) dual-hop communication scheme. The dual-hop entails the links from the source to the relay which are RF links and the links between the relay and the destination which are FSO links. In essence, RF transmission is utilized at one hop and the FSO transmission is employed at the other. It is remarkable that, in principle, the mixed RF/FSO dual-hop relay scheme is comparatively different from the hybrid RF/FSO technology. In the latter, parallel RF and FSO links are normally used for the same path [228]. Furthermore, in the mixed RF/FSO dual-hop scheme, the main purpose of the FSO link is to enable the RF users to communicate with the backbone network. This helps in bridging the connectivity gab between the backbone and the last-mile access networks [177, 229].

The mixed RF/FSO dual-hop model efficiently addresses the last-mile transmission bottleneck of the system. This is achieved by enabling multiplexing of multiple users with RF capabilities as well as their aggregation in a particular high-speed FSO link so as to exploit the inherent optical capacity [177, 228]. Moreover, this implementation stalls any form of interference due to the fact that, RF and FSO operate on completely different frequency bands. Therefore, the mixed RF/FSO dual-hop model offers better performance compared to the traditional RF/RF transmission system [228, 229]. In a mixed RF/FSO system, the source comprises multiple RF users, each equipped with an antenna. Furthermore, at the destination, there is an FSO detector that is equipped with an aperture. In addition, the source and the destination are connected by a relay that is usually mounted on a high platform. The relay node performs RF to FSO conversion. Also, the relay has a receive antenna and a transmit aperture that are assigned for the RF signal reception and optical signal transmission, respectively.

6.4 System and Channel Models

In this section, a mixed RF/FSO dual-hop relay system that comprises the source nodes which transmit information to the destination nodes with the help of a relay node as depicted in Fig. 6.1 is considered. Direct link between the source and destination nodes is assumed to be weak enough and consequently, it is ignored. Additionally, the links from the source nodes to the relay are considered to be the RF links whereas the links between the relay and the destination are assumed to be the FSO links. Moreover, the RF and the FSO links are assumed to experience a Rayleigh fading distribution and $\mathcal{M}$-distribution, respectively. Furthermore, the source nodes and the destination nodes are assumed to be equipped with N_s antennas and N_d apertures, respectively. Moreover, the relay node is assumed to be equipped with N_{sr} receive antenna for the RF signal reception and N_{rd} transmit aperture for optical signal transmission. Also, it is assumed that $N_{sr} = N_{rd} = 1$.

At the first hop, the symbol vector $s \in \mathbb{C}^{N_s}$ is transmitted from the source to the relay node and the signal $y_R \in \mathbb{C}^{N_r}$ received at the relay can be expressed as [230]

$$y_R = \sqrt{\frac{P_s}{N_s}} \sum_{n=1}^{N_s} h_{sr} s + n_r, \tag{6.1}$$

where P_s represents the transmit power of the source node, $h_{sr} \in \mathbb{C}^{N_{sr} \times N_s}$ denotes the source-relay channel that represents the Rayleigh fading channel, and $n_r \in \mathbb{C}^{N_r}$ is the AWGN vector at the relay node whose components are independent and identically distributed (i.i.d.) with zero mean and variance σ_r^2.

At the second hop, we employ a subcarrier intensity modulation (SIM) scheme for converting the input RF signal to optical signal for retransmission to the destination through FSO links. The optical intensity at the relay node can be written as [231]

$$s_R = G(1 + \eta y_R), \tag{6.2}$$

where the G represents the relay gain and the η denotes the electrical-to-optical conversion coefficient.

The received optical signal at the destination aperture can be expressed as [178, 231–233]

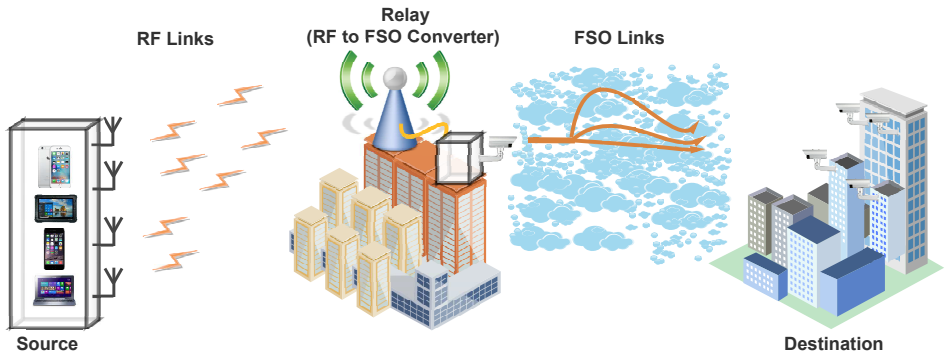

Figure 6.1: Diagram of a mixed RF/FSO dual-hop communication system.

$$y_m = \xi I_m G \left[1 + \eta \left(\sqrt{\frac{P_s}{N_s}} \sum_{n=1}^{N_s} h_{sr} s + n_r\right)\right] + n_m, \qquad m = 1, \ldots, N_d \tag{6.3}$$

where ξ is the optical-to-electrical conversion coefficient, I_m is a random variable (RV) between the relay aperture and the mth receive aperture of the FSO link which follows an $\mathcal{M}$-distribution model discussed in section 3.6.3 on page 56, and n_m is an AWGN term over the FSO link, with zero mean and variance σ_m^2.

Furthermore, the received signal after removing the DC bias can be written as

$$y_m = \xi I_m G \eta \left(\sqrt{\frac{P_s}{N_s}} \sum_{n=1}^{N_s} h_{sr} s + n_r\right) + n_m, \qquad m = 1, \ldots, N_d. \tag{6.4}$$

6.5 Performance Analysis

In this section, performance metrics such as outage probability, Average Symbol Error Probability (ASEP), and ergodic channel capacity are adopted in the analysis of the mixed RF/FSO dual-hop communication for improving the system performance.

6.5.1 Outage Probability

The outage probability is the probability that the instantaneous SNR falls below a specific SNR threshold γ_{th}. In general, outage probability is an essential performance metric for the system characterization in the quasi-static fading channels. It is a significant metric because, a system with a sufficient average BER can temporarily suffer from an increase in the error rate due to deep fades. The 'short outages' cannot be modelled sufficiently by the average BER. As a result, an alternative performance metric is the probability of outage that is due to the presence of atmospheric turbulence [150].

In addition to the attenuation due to atmospheric turbulence, effects of attenuation due to geometric spread as well as pointing errors I_p on the system performance require further attention. Using the pdf of I_p given in eq. (3.9) on page 55 and the $\mathcal{M}$-distribution given in eq. (3.20) on page 59, the combined pdf of I can be expressed in terms of the Meijer's G-function $\mathrm{G}_{p,q}^{m,n}[\cdot]$ as [178, 234]

$$f_{I_m}(I) = \frac{g^2 A}{2} I^{-1} \sum_{k=1}^{\beta} a_k \left(\frac{\alpha\beta}{\gamma\beta + \Omega'}\right)^{\frac{-(\alpha+k)}{2}} \mathrm{G}_{1,3}^{3,0}\left[\frac{\alpha\beta}{\gamma\beta + \Omega'} \frac{I}{A_0}\Big|_{g^2,\alpha,k}^{g^2+1}\right] \tag{6.5}$$

Similarly, the CDF can be defined as [178]

$$F_{I_m}(I) = \frac{g^2 A}{2} \sum_{k=1}^{\beta} a_k \left(\frac{\alpha\beta}{\gamma\beta + \Omega'}\right)^{\frac{-(\alpha+k)}{2}} \mathrm{G}_{2,4}^{3,1}\left[\frac{\alpha\beta}{\gamma\beta + \Omega'} \frac{I}{A_0}\Big|_{g^2,\alpha,k,0}^{1,g^2+1}\right] \tag{6.6}$$

The outage probability can be estimated using the upper bound of the e2e instantaneous SNR γ_{e2e} as [178]

$$P_{out} \approx F_{\gamma_1}(\gamma_{th}) + F_{\gamma_2}(\gamma_{th}) - F_{\gamma_1}(\gamma_{th}) F_{\gamma_2}(\gamma_{th}) \tag{6.7}$$

where $\gamma_1 = P_s ||\mathbf{h}||^2/(N_s N_0) = \overline{\gamma}_1 ||\mathbf{h}||^2$, $\gamma_2 = (\xi\eta P_r I_{max})^2/N_0 = \overline{\gamma}_2 {I_{max}}^2$, $\overline{\gamma}_1$ and $\overline{\gamma}_2$ are the average SNRs. Also, $F_{\gamma_1}(\gamma_{th})$ and $F_{\gamma_2}(\gamma_{th})$ can be defined respectively as [178]

$$F_{\gamma_1}(\gamma_{th}) = 1 - exp(-\frac{\gamma_{th}}{\overline{\gamma}_1}) \sum_{t=0}^{N_s-1} \frac{1}{t!}(\frac{\gamma_{th}}{\overline{\gamma}_1})^t \tag{6.8}$$

$$F_{\gamma_2}(\gamma_{th}) = \left[F_{I_m}\left(\sqrt{\frac{\gamma_{th}}{\overline{\gamma}_2}}\right)\right]^{N_d} \tag{6.9}$$

The asymptotic outage performance at high SNRs can be defined with the Meijer G-function and eq. (6.6) on page 93. Therefore, eq. (6.9) can be asymptotically expressed as

$$F_{\gamma_2}(\gamma_{th}) \rightarrow \left(\frac{g^2 A}{2}\right)^{N_d} \left[\sum_{k=1}^{\beta} a_k \left(\frac{\alpha\beta}{\gamma\beta + \Omega'}\right)^{\frac{-(\alpha+k)}{2}} \left(\frac{A_1}{\overline{\gamma}_2^{\frac{g^2}{2}}} + \frac{A_2}{\overline{\gamma}_2^{\frac{\alpha}{2}}} + \frac{A_3}{\overline{\gamma}_2^{\frac{k}{2}}}\right)\right]^{N_d} \tag{6.10}$$

Additionally, scenarios in which opportunistic schedule transmission is employed are considered. In principle, opportunistic scheduling scheme can be implemented to select and enable user with the best SNR to transmit at a specific period of time. Therefore, based on this transmission, the CDF $F_{\gamma_{\mathrm{Sel},r}}(\gamma)$ over the RF hop and the CDF $F_{\gamma_{r,d}}(\gamma)$ over the FSO hop defined by the $\Gamma\Gamma$ distribution in eq. (3.15) on page 58 can be expressed respectively as [235–237]

$$F_{\gamma_{\mathrm{Sel},r}}(\gamma_{th}) = \sum_{k=0}^{K} \frac{(-1)^k}{k!} \sum_{n_1,\cdots,n_k}^{K} \exp\left(-\sum_{t=1}^{k} \lambda_{n_t,r}\gamma_{th}\right), \tag{6.11a}$$

$$F_{\gamma_{r,d}}(\gamma_{th}) = \frac{r^{(\alpha+\beta-2)}\zeta^2}{(2\pi)^{r-1}\Gamma(\alpha)\Gamma(\beta)} \mathrm{G}_{r+1,3r+1}^{3r,1}\left[\frac{(\alpha\beta)^r}{r^{(2r)}\bar{\gamma}_{r,d}}\gamma_{th}\middle|_{\chi_2,0}^{1,\chi_1}\right], \tag{6.11b}$$

where $\bar{\gamma}_{r,d} = \eta\xi P_r \mu_{r,d}/(N_{02})$, μ represents the mean power of $|I_m|^2$, $\chi_1 = \frac{\zeta^2+1}{r}, \ldots, \frac{\zeta^2+r}{r}$, $\chi_2 = \frac{\zeta^2}{r}, \ldots, \frac{\zeta^2+r-1}{r}, \frac{\alpha}{r}, \ldots, \frac{\alpha+r-1}{r}, \frac{\beta}{r}, \ldots, \frac{\beta+r-1}{r}$, where ζ denotes the ratio between the equivalent beam radius and the pointing error displacement standard deviation at the receiver, parameter r represents the type of detection technique being employed in the system (i.e., $r = 1$ and $r = 2$ denotes heterodyne detection and IM/DD), respectively.

Furthermore, the asymptotic outage performance at high SNRs can be expressed as [235]

$$P_{\mathrm{out}}^{\infty} = \begin{cases} \left[\frac{\bar{\gamma}_{u,r}}{\gamma_{\mathrm{out}}}\right]^{-K} & \text{weak turbulence} \\ \left[\frac{\Lambda^{-\frac{2}{\nu}}}{\gamma_{\mathrm{out}}}\bar{\gamma}_{r,d}\right]^{-\frac{\nu}{2}} & \text{strong turbulence} \end{cases} \tag{6.12}$$

where $\bar{\gamma}_{u,\mathrm{r}}$ denotes the average SNR for identical channels case, $\nu = \min\{\zeta^2, \alpha, \beta\}$, and Λ can be written as [235, 236]

$$\Lambda = \frac{r^{(\alpha+\beta-2)}\zeta^2}{(2\pi)^{r-1}\Gamma(\alpha)\Gamma(\beta)} \sum_{k=1}^{6} \frac{\prod_{j=1,j\neq k}^{6}\Gamma(b_j - b_k)\Gamma(b_k)}{\prod_{j=2}^{3}\Gamma(a_j - b_k)\Gamma(1 + b_k)} \left(\frac{(\alpha\beta)^r}{r^{(2r)}}\right)^{b_k/2}, \tag{6.13}$$

where $a_j = \chi_1(j)$ for $j = 1, \ldots, 3$, $b_j = \chi_2(j)$ for $j = 1, \ldots, 6$, and $b_k = \nu$

6.5.2 Average Symbol Error Probability (ASEP)

It should be noted that the ASEP of various digital modulation schemes over the fading channels can be estimated by using the moment generating function (MGF) based approach. Nevertheless, derivation of a closed-form expression for the output SNR MGF is difficult. This is due to the fact that; no analytical expression is readily available for the received SNR pdf [238]. Alternatively, the Meijer's G-function can be employed for expressing the ASEP for several modulations schemes [239]. Therefore, the ASEP, P_e, can be defined in terms of the CDF of the received SNR, γ_{e2e}, denoted by $F_{\gamma_{e2e}}$ as [177, 240]

$$P_e = \varrho \int_0^{\infty} \frac{e^{-b\gamma}}{\sqrt{\gamma}} F_{\gamma_{e2e}}(\gamma)\, d\gamma, \tag{6.14}$$

where $\varrho = \frac{a\sqrt{b}}{2\sqrt{\pi}}$, parameters a and b are modulation-specific constant terms such that for binary phase-shift keying, $a = b = 1$, for M-ary phase-shift keying $a = 2, b = \sin^2(\pi/M)$, and for M-ary quadrature amplitude modulation, $a = 4(M^{1/2} - 1)/M^{1/2}, b = 3/(2(M - 1))$ [177].

Therefore, the $F_{\gamma_{e2e}}(\gamma)$ can be expressed as [235]

$$\begin{aligned} F_{\gamma_{e2e}}(\gamma) = & \sum_{k=0}^{K} \frac{(-1)^k}{k!} \sum_{n_1,\ldots,n_k}^{K} \exp\left(-\sum_{t=1}^{k} \lambda_{n_t,r}\gamma_{th}\right) \left\{ \frac{(\alpha\beta)^r}{r^{(2r)}\bar{\gamma}_{r,d}} \left(1 - \frac{r^{(\alpha+\beta-2)}\zeta^2}{(2\pi)^{r-1}\Gamma(\alpha)\Gamma(\beta)} \mathrm{G}_{r+1,3r+1}^{3r,1}\right) \right. \\ & \left. \times \left[\frac{(\alpha\beta)^r}{r^{(2r)}\bar{\gamma}_{r,d}} \gamma \middle| \begin{matrix} 1,\chi_1 \\ \chi_2,0 \end{matrix}\right] \right\} + \frac{r^{(\alpha+\beta-2)}\zeta^2}{(2\pi)^{r-1}\Gamma(\alpha)\Gamma(\beta)} \mathrm{G}_{r+1,3r+1}^{3r,1} \left[\frac{(\alpha\beta)^r}{r^{(2r)}\bar{\gamma}_{r,d}} \gamma \middle| \begin{matrix} 1,\chi_1 \\ \chi_2,0 \end{matrix}\right], \end{aligned} \tag{6.15}$$

So, the P_e can be written as

$$\begin{aligned} P_e = & \varrho \left[\sum_{k=0}^{K} \frac{(-1)^k}{k!} \sum_{n_1,\ldots,n_k}^{K} (b + \sum_{t=1}^{k} \lambda_{n_t,r})^{-\frac{1}{2}} \right. \\ & \times \left\{ \Gamma(1/2) - \frac{r^{(\alpha+\beta-2)}\zeta^2}{(2\pi)^{r-1}\Gamma(\alpha)\Gamma(\beta)} \mathrm{G}_{r+2,3r+1}^{3r,2} \left[\frac{(\alpha\beta)^r}{(b + \sum_{t=1}^{k} \lambda_{n_t,r}) r^{(2r)}\bar{\gamma}_{r,d}} \middle| \begin{matrix} \frac{1}{2},1,\chi_1 \\ \chi_2,0 \end{matrix} \right] \right\} \\ & \left. + \frac{r^{(\alpha+\beta-2)}\zeta^2}{(2\pi)^{r-1}\Gamma(\alpha)\Gamma(\beta)} b^{-\frac{1}{2}} \mathrm{G}_{r+2,3r+1}^{3r,2} \left[\frac{(\alpha\beta)^r}{r^{(2r)}\bar{\gamma}_{r,d} b} \middle| \begin{matrix} \frac{1}{2},1,\chi_1 \\ \chi_2,0 \end{matrix} \right] \right]. \end{aligned} \tag{6.16}$$

6.5.3 Ergodic Channel Capacity

In addition, another notable performance metric that quantifies the maximum achievable transmission rate under which errors are recoverable is the ergodic channel capacity C_{erg}. The C_{erg} can be mathematically expressed in terms of the pdf of γ_{e2e} as [168, 169, 235, 241]

$$C_{\text{erg}} \triangleq \mathbb{E}\langle C \rangle = \frac{1}{\ln(2)} \int_0^{\infty} \ln(1 + \gamma) f_{\gamma_{e2e}}(\gamma) d\gamma. \tag{6.17}$$

So, C_{erg} can be expressed as

$$
\begin{aligned}
C_{\text{erg}} =& \frac{1}{\ln(2)} \Bigg\{ \sum_{k=0}^{K} \frac{(-1)^k}{k!} \sum_{n_1,\ldots,n_k}^{K} \Bigg[\exp\left(\sum_{t=1}^{k} \lambda_{n_t,r} \right) \mathbb{E}_i \left(- \sum_{t=1}^{k} \lambda_{n_t,r} \right) \\
& - \frac{r^{(\alpha+\beta-2)} \zeta^2}{(2\pi)^{r-1} \Gamma(\alpha) \Gamma(\beta)} \Bigg(\mathrm{G}_{1,0:2,2:r,3r}^{0,1:1,2:3r,0} \left[\frac{1}{\sum_{t=1}^{k} \lambda_{n_t,r}}, \frac{(\alpha\beta)^r \sum_{t=1}^{k} \lambda_{n_t,r}}{r^{(2r)} \bar{\gamma}_{\mathsf{r},\mathsf{d}}} \middle| \begin{matrix} 1 \\ - \end{matrix} \middle| \begin{matrix} 1,1 \\ 1,0 \end{matrix} \middle| \begin{matrix} \chi_1 \\ \chi_2 \end{matrix} \right] \\
& - \left(\sum_{t=1}^{k} \lambda_{n_t,r} \right)^2 \mathrm{G}_{1,0:2,2:r+1,3r+1}^{0,1:1,2:3r,1} \left[\frac{1}{\sum_{t=1}^{k} \lambda_{n_t,r}}, \frac{(\alpha\beta)^r \sum_{t=1}^{k} \lambda_{n_t,r}}{r^{(2r)} \bar{\gamma}_{\mathsf{r},\mathsf{d}}} \middle| \begin{matrix} 2 \\ - \end{matrix} \middle| \begin{matrix} 1,1 \\ 1,0 \end{matrix} \middle| \begin{matrix} 1,\chi_1 \\ \chi_2,0 \end{matrix} \right] \Bigg) \Bigg] \\
& + \frac{r^{(\alpha+\beta-2)} \zeta^2}{(2\pi)^{r-1} \Gamma(\alpha) \Gamma(\beta)} \mathrm{G}_{r+2,3r+2}^{3r+2,1} \left[\frac{(\alpha\beta)^r}{r^{(2r)} \bar{\gamma}_{\mathsf{r},\mathsf{d}}} \middle| \begin{matrix} 0,1,\chi_1 \\ \chi_2,0 \end{matrix} \right] \Bigg\},
\end{aligned} \tag{6.18}
$$

where $\mathrm{G}\left[Z_1, Z_2 | . | . | .\right]$ denotes the extended generalized bivariate Meijer G-function.

6.6 Results and Discussion

In this section, we present numerical simulation results of the outage performance for $\mathcal{M}$-distributed fading. Furthermore, apart from the result of outage performance of the $\Gamma\Gamma$-distributed fading, we present ASEP and ergodic channel capacity results as well for the mixed RF/FSO dual-hop communication.

6.6.1 Outage Performance for $\mathcal{M}$-distributed Fading

In this section, we present the outage performance of the considered mixed RF/FSO wireless communication system. In our analysis, we use normalized average optical power $E[|I_m|] = \Omega + 2\rho b_0 = 1$. Also, the values of channel parameters that we use are $\alpha = 4.8$ and $\beta = 2$. However, we vary the values of g and ρ depending on the situation under consideration.

Initially, we consider the effect of the amount of scattering power coupled to the LOS component on the outage performance of dual-hop RF/FSO communication system. We assume that the FSO links are subjected to the generalized atmospheric fading channels with different values of ρ (i.e. $\rho = 0, 0.5, 0.8, 1$) employed as the channel parameter. We use SNR threshold $\gamma_{th} = 5\ dB$ and $N_s = N_d = 4$ in our analysis. We present the resultant plot of the outage performance in Fig. 6.2(a). We observe that, the system performance improves with an increase in ρ which is reasonable because, an increase in ρ leads to a decrease in the scintillation index $\sigma_{I_m}^2$. It is noteworthy that, $\rho = 0$ and $\rho = 1$ match the special cases of K and Gamma-Gamma distribution, respectively.

Furthermore, we study the effect of varying the ratio between the equivalent beam radius and the pointing error displacement standard deviation in order to analyze the resultant effects of the atmospheric turbulence and pointing errors on the system performance. We use $N_s = N_d = 4$, $\rho = 1$, and different values of g (i.e. $g = 0.5, 0.75, 0.9, 1$) in our analysis. The plot of outage curves for the analysis is depicted in Fig. 6.2(b). We observe that, an increase in g enhances the outage performance significantly.

Also, we study the effect of different diversity schemes on the performance of RF/FSO communication system. We use $g = 0.9$, $\rho = 1$, and different combinations of $N_s \times N_d$ in our analysis. The plot of the outage performance is shown in Fig. 6.2(c). We observe that, employment of multiple antennas at the source as well as multiple apertures at the destination

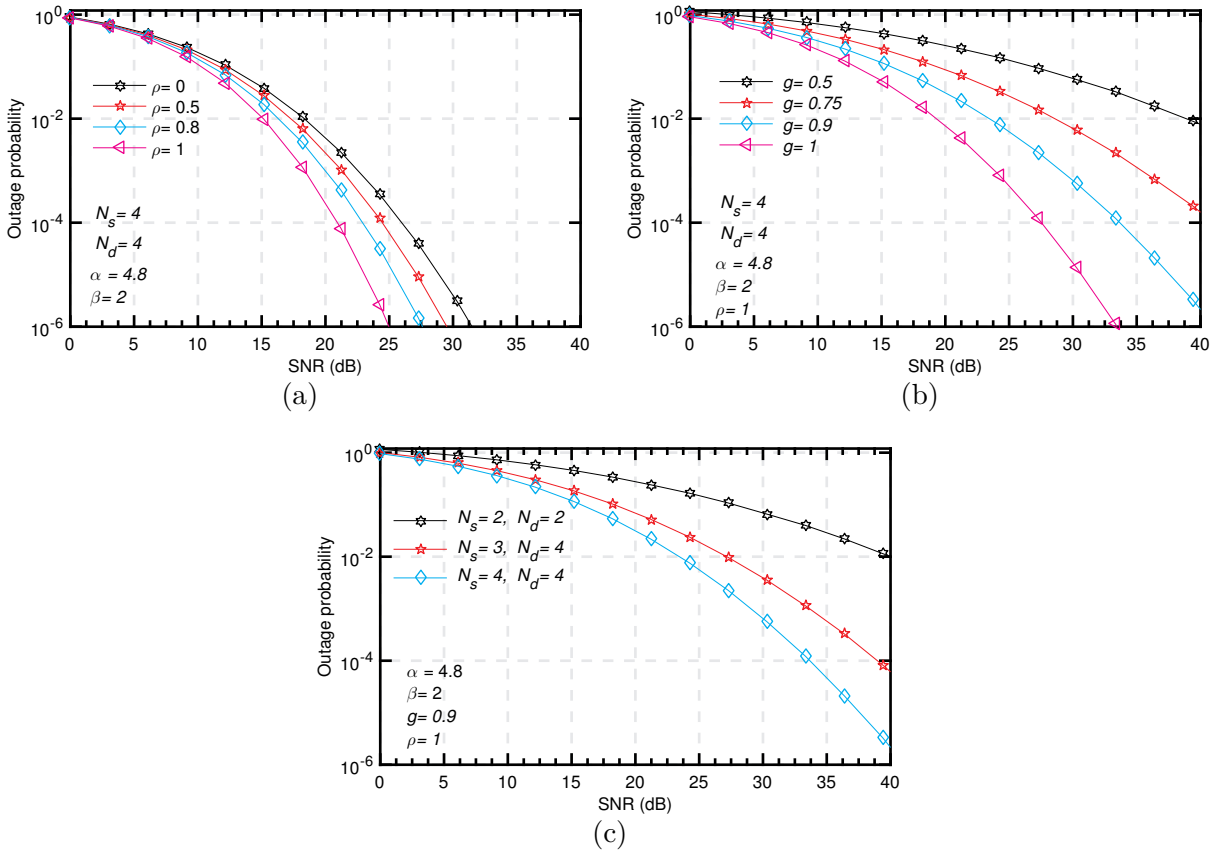

Figure 6.2: Outage performance of a mixed RF/FSO wireless communication system with Rayleigh and $\mathcal{M}$-distributed fading considering (a) scattering power coupled to the LOS component, (b) pointing errors at the FSO links, (c) pointing errors at the FSO links and different $N_s \times N_d$ combinations.

enhances the system performance considerably. For instance, we observe that, to achieve an outage probability of 10^{-2} with 4×4 system, about 23 dB is required whereas for 2×2 system at the same outage probability, about 40 dB is required.

6.6.2 Outage Performance for $\Gamma\Gamma$-distributed Fading

In this section, we present results of our studies on the e2e outage probability, ASEP, and ergodic channel capacity of the considered mixed RF/FSO wireless communication system. We study the effect of varying the ratio between the equivalent beam radius and the pointing error displacement standard deviation in order to analyze the resultant effects of pointing errors and atmospheric turbulence on the system outage performance. Initially, we consider strong turbulence conditions with channel parameters $\alpha = 0.8$ and $\beta = 1.5$. Furthermore, for a $\gamma_{th} = 5$ dB and two users, we employ different values of ζ (i.e. $\zeta = 0.5, 0.7, 0.9, 1.5, 2.1$). Figure 6.3(a) shows the plot of outage probability for different values of average SNR/hop and ζ. We observed that, as ζ increases, the detrimental effect of pointing error on the system

performance decreases, so, the outage performance improves significantly. The observation is due to the fact that, as the value of ζ increases, the effect of pointing error decreases and the probability of outage decreases. On the other hand, when the value of ζ decreases, the effect of pointing error increases and consequently, the probability of outage increases. Moreover, the results show that as $\zeta \to \infty$, we are approaching a non-pointing error scenario. Furthermore, it is noteworthy that, the system diversity order is determine by the $\min\{\zeta^2, \alpha, \beta\}/2$. So, when the value of ζ^2 is less than that of α and β, it will affect diversity order of the system accordingly. However, when the value of ζ^2 is larger than that of α and β, it will affect just the coding gain of the system. In essence, an increase in ζ means that additional number of distributed RRHs and the associated RF users can communicate effectively via the backbone network to the BBU pool within an allowable latency.

Furthermore, in Fig. 6.3(b), we present results of varying the atmospheric turbulence parameters $\alpha \in (0.5, 0.6, 2.3, 4)$ and $\beta \in (0.5, 0.5, 0.9, 1.3)$ on the system outage performance. In the analysis, we assume a $\gamma_{th} = 5\ dB$ and $\zeta = 2.1$. We observe that, a decrease in the value of α or β leads to an increase in the detrimental effect of atmospheric turbulence. Consequently, the system performance is degraded. Also, we observe that the outage probability increases with an increase in the atmospheric turbulence strength and the performance of the system with σ_N^2=8 depicts the worst case scenario. For instance, to achieve an outage probability of 10^{-1}, with σ_N^2=1.21, about 20 dB is required. This subsequently increased to about 38 dB for the same outage probability when σ_N^2=7. The result demonstrates that system with low turbulence is relatively power efficient and has best performance. So, in essence, a decrease in the value of α or β or an increase in the value of σ_N^2 reduces the number of RRHs as well as the associated RF users that can be supported efficiently by the mobile fronthaul within an allowable latency.

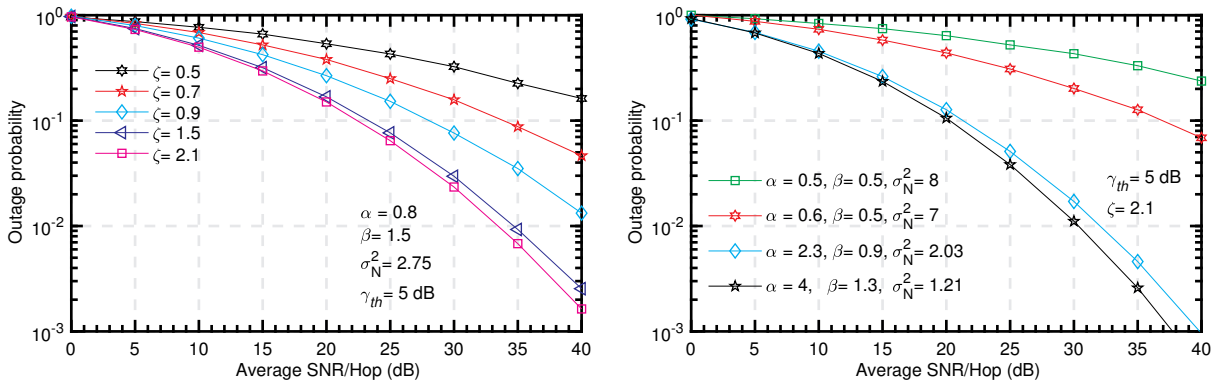

Figure 6.3: A dual-hop multiuser mixed RF/FSO wireless communication system (a) outage performance considering the impact of pointing errors at the FSO links, (b) outage performance considering different atmospheric conditions.

6.6.3 ASEP with ΓΓ-distributed Fading

Moreover, in Fig. 6.4(a), we show results of varying the channel parameters $\alpha \in (0.8, 1.8, 2.6)$ and β $(1.8, 2.6, 4)$ on the error probability performance of a dual-hop multiuser mixed RF/FSO wireless communication system. Also, we use $\zeta = 2.1$ and assume that the modulation-specific constant terms are equal. So, parameters a and b are equal to one (i.e. $a = b = 1$). This condition corresponds to a case of binary phase-shift keying modulation format. We observe that, an increase in the value of α or β leads to a decrease in the detrimental effect of atmospheric turbulence. Therefore, the system performance is enhanced. Also, we observe that the ASEP increases with an increase in the σ_N^2. For instance, to achieve an ASEP of 10^{-4}, with σ_N^2=0.73, about 22 dB is required. The value consequently increased to about 35 dB for the same ASEP when σ_N^2=2.5. The result shows that an increase in the σ_N^2 deteriorates the system performance.

6.6.4 Ergodic Channel Capacity with ΓΓ-Distributed Fading

Moreover, we study the effect of varying the channel parameters α (i.e. $\alpha = 15.7, 9.7, 5.7$) and β (i.e. $\beta = 6, 3, 3$) on the ergodic channel capacity of a dual-hop multiuser mixed RF/FSO wireless communication system for $\zeta = 2.1$. The plot of ergodic channel capacity is shown in Fig. 6.4(b). We observe that, an increase in the value of channel parameters leads to a decrease in the degradation caused by the atmospheric turbulence. Consequently, the system performance is enhanced and more RRHs can be supported efficiently. For instance, we observe that, to achieve a system capacity of 6 b/s/Hz with $\alpha = 5.7$ and $\beta = 3$, about 35 dB SNR/Hop is required whereas, for $\alpha = 15.7$ and $\beta = 6$, of the same capacity, about 25 dB SNR/Hop is required.

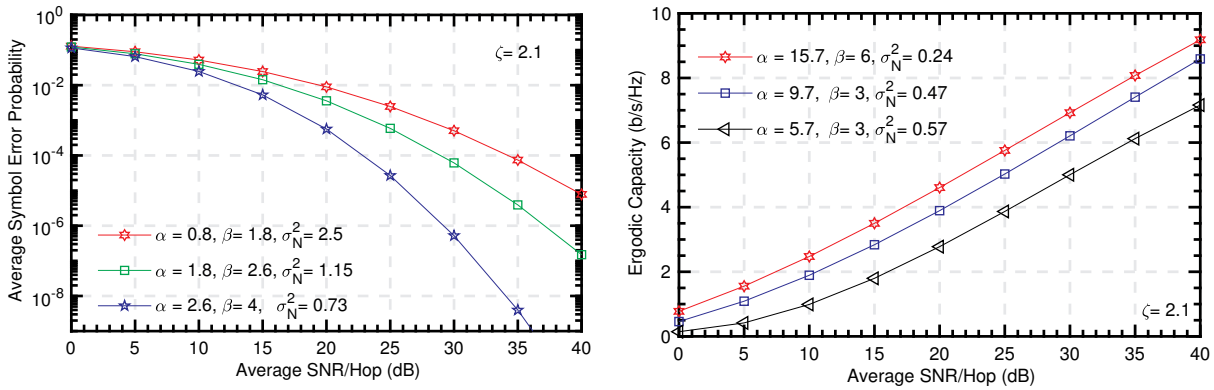

Figure 6.4: A dual-hop multiuser mixed RF/FSO wireless communication system (a) ASEP considering different atmospheric conditions (b) Ergodic channel capacity considering different atmospheric conditions.

6.7 Research Contributions

In this chapter, based on articles [26] and [225], considering the small-cell network architectures, we study multiuser mixed RF/FSO relay schemes as viable means of realizing optical-wireless convergence in dual-hop communication systems for the cloud-based RANs. We employ different performance metrics in order to demonstrate that the schemes are viable solutions for enhancing the wireless systems performance and efficiently addressing the last-mile transmission bottleneck. Furthermore, the schemes can be of great help in alleviating the associated stringent requirement by C-RAN backhaul/fronthaul as well as in the evolution towards an efficient backhaul/fronthaul for the 5G network. Moreover, we present simulation results to show the viability of mixed RF/FSO schemes deployment in the real-life scenarios.

6.8 Conclusion

In this chapter, we have presented a mixed RF/FSO dual-hop relay system as a feasible backhaul/fronthaul solution for the 5G cellular networks and beyond in which CC-RANs is envisaged to be implemented. Moreover, we have employed different performance metrics such as ASEP, e2e outage probability, and ergodic channel capacity in the study. In the analysis, we have assumed Rayleigh fading for the RF links. Also, we considered both $\mathcal{M}$-distributed fading and $\Gamma\Gamma$-distributed fading channels for the FSO link. In addition, we have studied the effect of atmospheric turbulence and pointing errors between the relay and the destination on the system performance. As a result, we have shown that, a decrease in the value of the effective number of large-scale or small-scale eddies of the scattering process reduces the total number of the RRHs as well as the associated RF users that can be efficiently supported by the mobile fronthaul within the permissible latency. Furthermore, we have demonstrated that, an increase in the ratio between the equivalent beam radius and the pointing error displacement standard deviation at the receiver means that, significant number of distributed RRHs can communicate effectively through the backbone network to the BBU pool within the specified latency. We have also presented results to show the advantages of diversity schemes in mitigating the system fading. The results presented can be beneficial in the system evaluation, optimization, and prediction of mixed RF/FSO dual-hop relay performance in the real-life scenarios deployment.

Chapter

Channel Characterization and Hybrid PON-FSO System

The FSO links are well known for the potential huge data rates. Nevertheless, the link reliability strongly dependent on the weather conditions. Consequently, accurate FSO channel measurements for different weather conditions are essential. This chapter is based on the experimental works that we reported in [145, 146, 169]. In the manuscripts, the performance of an FSO link subjected to a real atmospheric turbulence condition is experimentally investigated. The scintillation index σ_N^2 is measured from the channel samples so as to determine the degree of atmospheric turbulence and the subsequent effects on the FSO link quality. Furthermore, the C_n^2 can be calculated as explained in Chapter 3 on page 44. Consequently, experimental results on channel characterization of SISO FSO link that is based on channel measurements are present in this chapter. The histograms of the FSO channel samples and the atmospheric turbulence distribution fittings are presented together with the measured σ_N^2. In addition, the scintillation effects on the system performance are analyzed over different turbulence conditions. Moreover, we present a proof-of-concept gigabit-capable, long-reach, hybrid coherent PON and OWC systems. The hybrid schemes have the ability to support different applications over a shared optical fiber infrastructure.

7.1 Introduction

The proliferation of different mobile devices such as smartphones, laptops, and tablets contribute to high rate broadband connections per year. Additionally, in the recent years, various bandwidth-intensive applications and services also contribute to the tremendous growth [242–244]. Basically, there is a need for networks that can offer high-speed and improved-capacity system at relatively low cost [245]. As explained in Chapter 3 on page 44, FSO communication system is an appealing solution that combines the flexibility and mobility offered by RF networks with the high data rates provided by the optical systems [152, 186, 246, 247].

However, the FSO links are susceptible to atmospheric turbulence and local weather conditions [178, 245, 248–251].

Consequently, the system performance is hindered by the atmospheric effects that result in loss of spatial coherence, beam spreading, and temporal irradiance fluctuation which is known as scintillation [14, 146, 174, 247, 250, 252–254]. Therefore, a precise channel characterization is necessary for practical FSO link development. Moreover, it aids in determining the system performance over various transmission conditions [152]. Additionally, when a channel is accurately characterized, ergodic channel capacity can be determined as discussed in Chapter 3 on page 44 and Chapter 5 on page 78 [180, 255, 256].

There are various theoretical and experimental efforts in the literature for characterizing the FSO communication link [247]. In [255], closed-form expressions for the average capacity of MIMO FSO systems under ΓΓ fading channel were presented for an equal gain combining and maximum ratio combining diversity techniques. It was established that, the average capacity can be enhanced with the implementation of spatial diversity techniques. Also, [256] studied the effect of turbulence and weather conditions on the average channel capacity of FSO link using MIMO and aperture averaging techniques. It was shown that, as the number of transmit and receive apertures increase, the capacity increases regardless of the weather condition. Furthermore, in [167], the BER performance of FSO links with spatial diversity over log-normal atmospheric turbulence fading channels was considered with the assumption of independent and correlated channels among transceiver apertures. The results offered by the authors showed that, the FSO links with transmit and receive diversity can be denoted by equivalent SISO systems with suitable scaling in the channel variance.

Additionally, turbulence-induced fading in the FSO systems was defined with a double generalized gamma model in [257] with the pointing errors being considered. Also, performance measurements like the BER, the outage probability, and the ergodic capacity of the system were presented by employing unified closed-form expressions. Moreover, a MIMO FSO system that was based on Vertical-Bell Laboratories Layered Space-Time was presented in [258]. The authors established by simulation that, when the number of antenna increases, the channel capacity becomes higher and the error rate decreases. Moreover, the fluctuation of the optical signal, in the course of propagation in the FSO link was expressed by the log-normal and ΓΓ distribution models. Also, closed-form expressions for evaluating the average channel capacity of FSO were proposed in [259]. In addition, in [260], maximum likelihood estimation was used to characterize the log-normal-Rician turbulence model parameters, and the unknown parameters were evaluated using expectation-maximization algorithm. Also, an experimentally quantified channel model that was based on finite-state Markov chain which was derived for the distribution and the autocorrelation of the fading was proposed in [247].

In this chapter, we present FSO channel characterization through the channel gain measurement using a 54-meter (roundtrip), 10 Gbps outdoor link at 1548.51 nm wavelength. Moreover, based on the channel measurement, we propose closed-form expressions for estimating the ergodic channel capacity of MIMO FSO communication systems over atmospheric turbulence fading channels in Chapter 5 on page 78.

With the necessity for the FSO communication systems as well as the state-of-the-art on the subject matter being presented, in Section 7.2 on the next page experimental setup and results on channel measurement and characterization are discussed. Also, experimental setup and results on the real-time coherent PON OWC based on dual-polarization for the mobile backhaul/fronthaul are presented in Section 7.3 on page 105. Research contributions are discussed in Section 7.4 on page 107 and Section 7.5 on page 108 concludes this chapter.

7.2 Channel Measurement and Characterization

In the literature, there have been increase in the efforts on the experimental measurement based communication channel modeling. For instance, in [261], a link that operates at 1550 nm was employed for the estimation of fading distribution for a number of receiver aperture sizes. Using an unmodulated continuous-wave source, the authors compared the fitting parameters for the LN and the ΓΓ fading distributions based on the analytical model and experimental data as a function of receiver diameter. Moreover, using an unmodulated continuous-wave source at 1550 nm, FSO channel measurements were used to estimate the parameters for fading distributions in [262]. With the approach, the authors were able to jointly estimate parameters of the LN and the ΓΓ fading distributions as well as the noise. Also, in [263], without the presentation of channel model, channel measurements of attenuation on the FSO link that operates at 1550 nm were reported. Likewise, in [264] measurement results of a FSO link at 785 nm were reported.

In the following subsections, we present the experimental setup and results for the FSO channel gain measurement using a 54-meter, 10 Gbps outdoor link that operates at 1548.51 nm wavelength.

7.2.1 Experimental Setup

The experimental setup shown in Fig. 7.1 is employed in the channel measurement. The setup consist of a point-to-point FSO link that is based on IM/DD technique. The pattern generator uses a Pseudo Random Bit Sequence (PRBS) of length $2^{23}-1$ bits to generate a 10 Gb/s Non-Return-to-Zero (NRZ) signal. Also, the produced electrical signal is then injected into a JDSU Integrated Laser Mach Zehnder (ILMZ) drives at 1548.51 nm wavelength. A Standard Single-Mode Fiber (SSMF) is used to convey the optical output signal launched from the laser to 3 mm diameter collimator. The optical power at the input of collimator is set to 0 dBm. The collimated laser beam is subsequently transmitted over the FSO channel with a round trip length of 54 m. Figure 7.1 on the next page inset depicts an outdoor FSO setup employed in the measurement. The overall transmission distance is achieved when the optical signal from collimator 1 passes through the FSO channel to the mirror with a beam diameter of about 2 cm located at the other side of the link that is 27 m long, then, reflected back to the collimator 2 at the receiver with approximately its initial diameter. The collimator is made of concave mirror, in order to lessen beam scattering and considerably maximize the power transfer. The converged received optical signal at the receiver then focuses on the laser collimator which is coupled to the PD by the SSMF. The resulting optical signal is then converted into electrical signal using a 10 Gb/s PIN photodiode. The PIN is followed by a real-time sampling oscilloscope (Tektronix: DPO72004B) with a sample rate of 50 GS/s.

7.2.2 Experimental Results

The results of FSO channel samples collected from $9th$ - $20th$ November, 2015 for characterization are presented. The data obtained on $12th$ November 2015 at 01:45 pm and 09:30 pm are analyzed in this work. The recorded weather conditions are:

1. Scenario 1: 01:45 pm
   Temperature, 22 ^oC; wind, 6 mph; humidity, 69%; pressure, 1031 mb; visibility, 10 km; precipitation, 0 mm; and rain rate, 0%.

2. Scenario 2: 09:30 pm
   Temperature, 17 ^oC; wind, 4 mph; humidity, 80%; pressure, 1030 mb; visibility, 9 km; precipitation, 0 mm; and rain rate, 0%.

The FSO channel measurement is realized by injecting an unmodulated optical wave that emanates from the laser into the FSO channel. The FSO channel brings about a path loss with a mean value of 9 dB, for the setup and the atmospheric conditions. Using statistical means, the resultant signal detected and received by the real-time oscilloscope is analyzed offline using MATLAB®.

The characterization of the refractive-index structure parameter C_n^2 is achieved by fitting the nearest LN and the ΓΓ pdf curves to the pdf of the received data. The fittings are presented in Fig. 7.2. The scintillation index σ_N^2 is measured for the two scenarios considered. The

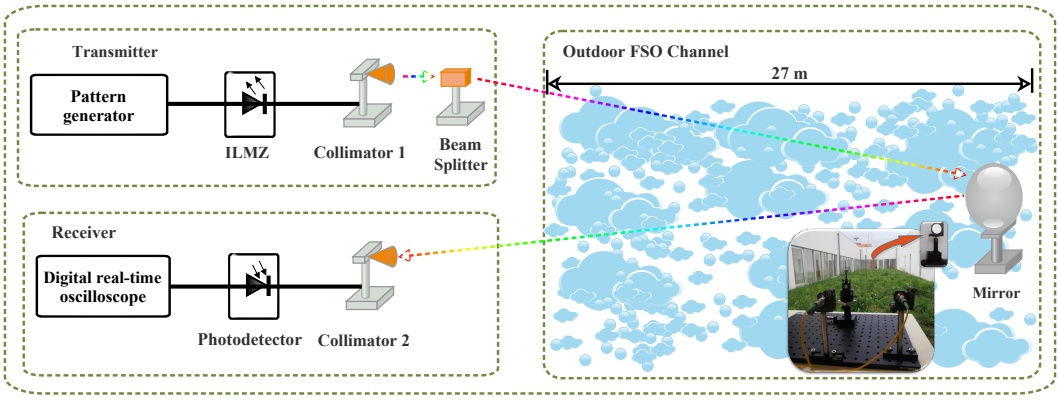

Figure 7.1: Experimental setup. The inset presents the picture of outdoor FSO setup, ILMZ: Integrated Laser Mach Zehnder.

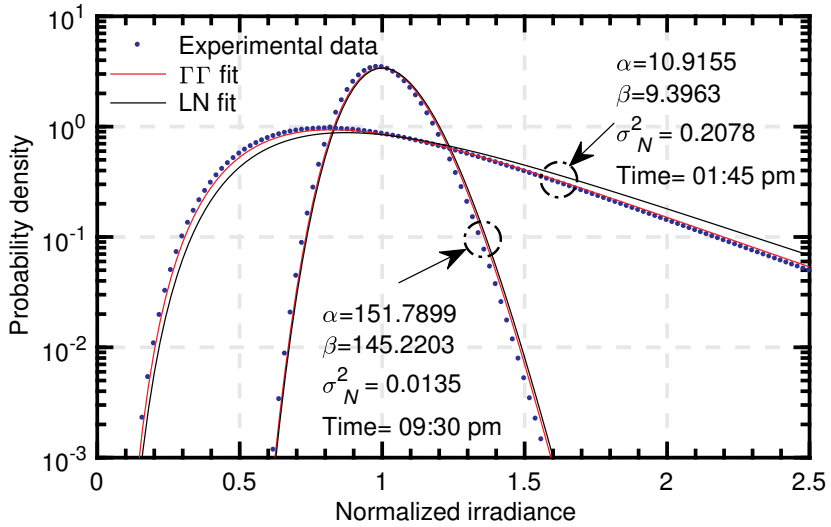

Figure 7.2: Histogram of normalized irradiance with log-normal and gamma-gamma fits under different scintillation index values.

values obtained are 0.0135 and 0.2078 for 09:30 pm and 01:45 pm, respectively. For the first scenario with $\sigma_N^2 = 0.0135$, the LN and the ΓΓ fit very well with the measured channel samples σ_N^2. However, when $\sigma_N^2 = 0.2078$, the LN fitting is loose and unable to give an accurate result for the fading model, whereas, the ΓΓ fitting still maintains a relatively better result for the fading model. This result shows that the LN model is unsuitable for the strong atmospheric fading characterization.

Furthermore, the estimated values of the refractive-index structure parameters C_n^2, are $6.7807 \times 10^{-16} m^{-2/3}$ ($\sigma_N^2 = 0.0135$) and $1.0864 \times 10^{-14} m^{-2/3}$ ($\sigma_N^2 = 0.2078$). Therefore, the first ($\sigma_N^2 = 0.2078$) and the second ($\sigma_N^2 = 0.0135$) scenarios correspond to the strong and weak turbulence regimes, respectively.

7.3 Real-Time Coherent PON OWC based on Dual-Polarization for the Mobile Backhaul/Fronthaul

In this section, a proof-of-concept gigabit-capable long-reach coherent PON and OWC systems with the ability to support different applications over a shared optical fiber infrastructure is experimentally implemented. This is in an effort to demonstrate the FSO application in certain areas in the mobile cellular systems in which physical connections by means of optical fiber cables are impractical or in rural area that lacks fiber infrastructure. Moreover, this is achieved by a reconfigurable real-time DSP reception of a Dual-Polarization Quadrature Phase Shift Keying (DP-QPSK) signal over the SSMF and FSO systems. It is noteworthy that, the system is validated by a commercial FPGA in order to have an open system whose components and protocols conform to standards and independent of a particular equipment vendor. In this analysis, we study signal transmission and reception over 100 km of SSMF as well as over a hybrid 100 km of SSMF plus 54 m outdoor FSO link. We are able to establish the lowest sampling rate that is necessary for digital coherent PON by employing four 1.25 Gsa/s ADCs with an electrical front-end receiver that offers just 1 GHz analog bandwidth. This is realized by implementing a phase and polarization diversity coherent receiver in conjunction with the DP-QPSK modulation formats. This technique is of high importance in order to relax the required electrical digital units at the ONU towards the RF rates. This scheme also helps in realizing the anticipated data rate for the next-generation coherent OAN for the 5G Mobile wireless networks.

7.3.1 Experimental Setup

The experimental setup depicted in Fig. 7.3(a) is used to validate the performance of a PON system with hybrid fiber and FSO link using Dual-Polarization (DP) signals. It is worth mentioning that, only the receiver DSP of the setup is estimated in real-time. At the OLT, the light from an External Cavity Laser (ECL) (<100 kHz linewidth) is injected into an IQ modulator (IQM). The wavelength λ is centered at ∼1549 nm. The IQM is driven by a 65 Gsa/s Arbitrary Waveform Generator (AWG) that generates 625 Mbaud signals from a $2^{12} - 1$ PRBS. The subsequent signal is then digitally filtered using a raised-cosine filter with 0.1 roll-off factor and 32-taps FIR resolution in addition to a simple 3-taps FIR pre-emphasis subsystem. The employed modulation formats is the differential DP-QPSK, providing 2.5 Gb/s per end-user. The obtained spectrum is shown in Fig. 7.3(b).

In an effort to emulate the DP system, this signal is divided into two using an optical

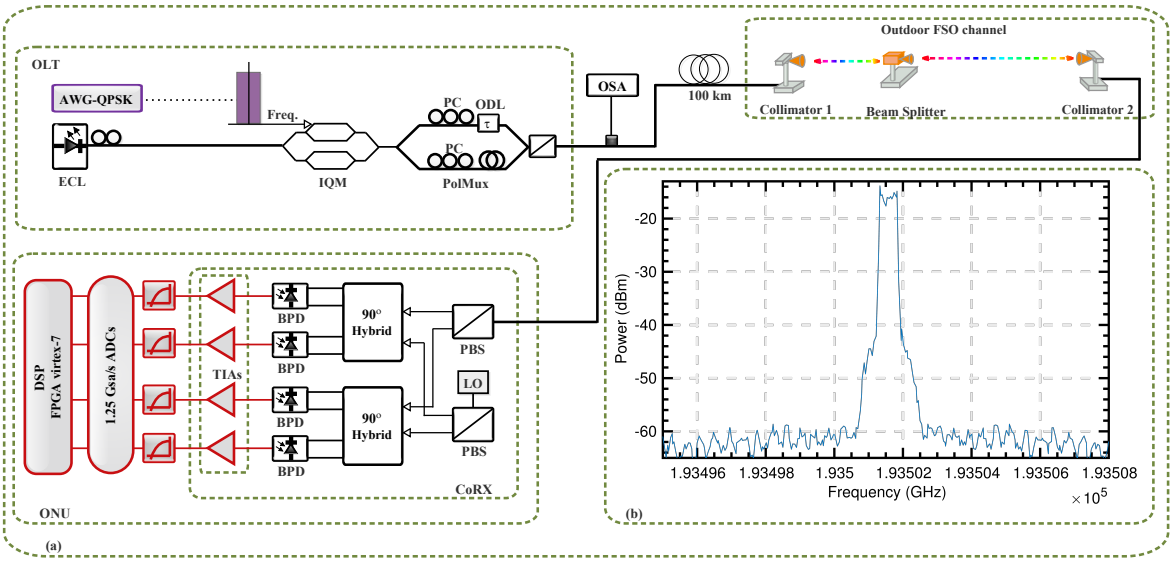

Figure 7.3: (a) Experimental setup for 20×625 Mbaud DP-QPSK signal; (b) Overall spectrum (PBS: polarization beam splitter; BPD: balanced photodetector; CoRX: coherent receiver).

splitter. Then, we applied a delay of 12 symbols to one of them for an effective decorrelation purposes. Afterward, both polarized signals are multiplexed orthogonally once again using a Polarization Beam Combiner (PBC). This implementation results in dual polarization of the signal. The optical power is managed using Variable Optical Attenuators (VOA). The subsequent signal is then propagated over 100 km of the SSMF and 54 m FSO. At the receiver side, the signal is coherently detected using a 4×90^o optical hybrid by means of a free-running ECL LO with about 100 kHz linewidth tuned to the center channel, λ. The optical signal is converted to an electrical domain using four balanced detectors (BD) and then amplified by TransImpedance Amplifiers (TIA). This results in the in-phase and quadrature components of each polarization. It is noteworthy that, only an output of the TIA is used. The signal is then filtered using 1 GHz low-pass filter and sampled by four 8-bit 1.25 Gsa/s ADCs. The digitalized signal is conveyed to a Virtex-7 FPGA, where the entire post-detection 8-bit DSP in real-time is implemented. The applied DSP is based on [265]. The BER is calculated in real-time by bit error counting, averaged between the two polarizations.

In addition, we consider the possibility of an outdoor FSO communication link as part of the system. The employed FSO link setup in this study is similar to that in Fig. 7.1 that we have discussed in Chapter 7 on page 101. The outdoor FSO link experiences a total loss of $\sim$ 8-9 dBm. At the collimator, the received signal is guided to an integrated phase- and polarization-diversity coherent receiver.

7.3.2 Experimental Results

Figure 7.4 on the next page illustrates receiver sensitivity in terms of BER measured for the DP-QPSK signal. The figure presents results for the Back-to-Back (B2B) and 100 km of fiber scenarios as well as 100 km plus 54 m FSO. The considered BER limit of 3.8×10^{-3} corresponds to the 7% Hard-Decision Forward Error Correction (HD-FEC). As shown Fig.

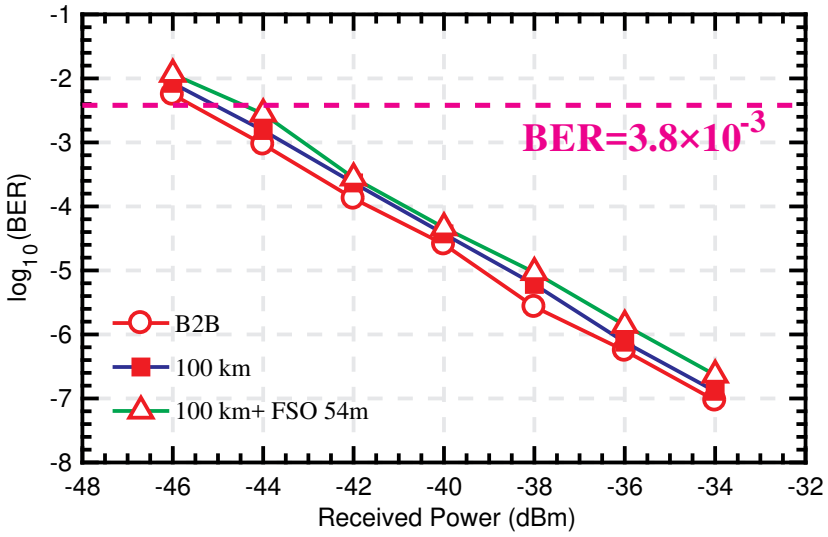

Figure 7.4: Receiver sensitivity in terms of BER measured for DP-QPSK signals.

7.4, there is no significant penalty between 100 km and 100 km plus FSO in real-time results.

7.4 Research Contributions

The contributions of this chapter based on channel characterization and hybrid PON-FSO system are enumerated in the following subsection.

7.4.1 First Contribution

According to [146] and [169], by experimental channel measurements, we characterized the SISO link. Furthermore, the scintillation effects on the system performance are analyzed over different turbulence conditions. Also, results that are useful for the adoption of adaptive modulation scheme are presented. Moreover, we extend the SISO FSO studies to diversity schemes and propose closed-form expressions for the evaluation of channel capacity of MIMO FSO communication systems over atmospheric turbulence fading channels as discussed in Chapter 5 on page 78.

7.4.2 Second Contribution

Based on the book chapter in [145], we present a proof-of-concept experiment on the transmission capabilities of a hybrid PON-FSO system. The experiment is in an effort to validate FSO application in specific areas in the mobile cellular networks where physical connections through optical fiber cables are inviable or in rural area that lacks fiber infrastructure. Furthermore, the implementation with a commercial FPGA encourages open system as well as open software standards.

7.5 Conclusion

In this chapter, we have presented experimental results on channel characterization of SISO FSO communication link based on the channel measurements. The histograms of the FSO channel samples along with the LN and the ΓΓ distribution fittings have been presented. Also, by varying the scintillation index, we have been able to demonstrate that the reliability of FSO system significantly depends on the weather conditions. In the proof-of-concept experiment, we study the transmission capabilities of a PON based on DP signal in terms of receiver sensitivity. This is implemented with the real-time ONU receiver that is emulated by a commercial FPGA. This helps in facilitating an open system and hence enables interoperability, portability, and open software standards. The transmissions over 100 km of SSMF, as well as over a hybrid 100 km of SSMF plus 54 m outdoor FSO link, are successfully realized considering 625 Mbaud DP-QPSK channel.

Chapter

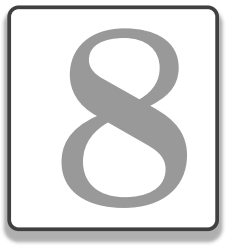

Conclusion

The 5G networks are envisioned to be heterogeneous communication systems that have the capabilities of supporting a number of advanced wireless technologies, services and applications. C-RAN is an attractive and feasible solution for efficient realization of the envisaged goals of the 5G network. This is as a result of its appealing features in terms of performance optimization and cost-effectiveness. However, the C-RAN architecture imposes stringent requirements on the fronthaul link in order to achieve seamless connectivity between the network elements. This is much more demanding with the implementation of cooperative techniques due to the huge amount of signaling initiations in the fronthaul by the intracell and intercell CoMPs. Consequently, the signaling limits the number of densely deployed RRHs that can access the same BBU pool at a time and eventually results in low system performance. High-bit rate and low-latency fronthaul aids larger-scale cooperative processing and networking. Therefore, this results in better utilization of the system resources. So, transmission and reception of digital radio signals require conforming standard interface to connect the RRHs with the BBU pool through an optical fiber.

There are a number of ways of achieving MFH in the C-RAN, nevertheless, the high-capacity and low latency requirements make optical fiber connections a promising solution. However, adoption of optical fiber for ultra-dense deployment of RRHs makes C-RAN employments less flexible and cost-intensive. This is still more demanding when trenching is necessary. There are different research efforts aiming at meeting the 5G RAN requirements with realistic MBH/MFH. A measure is to evolve the current MBH/MFH such as optical fiber, microwave, and copper, so as to meet the 5G network anticipations. Another method is to incorporate state-of-the-art wireless technologies for instance mm-wave and FSO into the network.

Furthermore, the transmission capacity will be constrained when wireless communications in microwave bands is implemented because of the limited available bandwidths. Also, the implementation of mm-wave would results in low dynamic range due to the associated free-space loss and atmospheric attenuation. In addition, in the C-RAN architecture, the fundamental means of distributing wireless signal in the MFH is to transmit digital baseband oversampled

IQ streams using CPRI or OBSAI interface. However, in addition to the strict control of jitter, synchronization, and latency that are obligatory, optical link based on these interfaces requires large bandwidth. This is due to the high resolution bits needed for the digitalization process of the RF samples. Therefore, this bandwidth inefficiency might limit or make them impractical for the next generation mobile system in which Massive MIMO antenna system is expected to be incorporated. In the following subsection, we present concluding remarks on means of optimizing the MFH for CC-RANs.

8.1 Concluding Remarks

This thesis has presented comprehensive overview of the key technologies, architectures, requirements, and challenges of the C-RAN MFH. Furthermore, some related open-ended issues have been studied and potential solutions on means of realizing an efficient C-RAN MFH for the NGNs have been effectively discussed. In addition, current fronthaul solutions and their limitations in the 5G cellular networks in which mm-wave and Massive MIMO technologies are envisaged to be integrated have been considered.

Furthermore, the thesis has presented potential modifications to address the bandwidth required for digital signal transportation in the MFH network. Also, different methods of realizing efficient MFHs, as well as technologies for access network performance enhancement, have been presented. We have also discussed schemes that can help in reducing the system complexity, cost, bandwidth requirement, and latency in the MFH. Moreover, a number of optical technologies that aid flexibility and multiple system operational functionalities in the MFH have been discoursed. Furthermore, the related technical challenges of their applications are deliberated. Likewise, capabilities of SDF for an efficient, automatic network management, and provisioning have been outlined.

In practice, the C-RAN architecture requires each RRH with dedicated connection to the centralized BBU pool and D-RoF based CPRI is the main method for distributing baseband samples in the C-RAN fronthaul. Nonetheless, in the 5G networks and beyond, huge number of RRHs may be deployed at locations that are very challenging to be reached by fiber. Consequently, dedicated wired links between individual RRH to the BBU may be impractical. So, optical wireless fronthaul solution can be a feasible complementary and/or alternative technology for better flexibility, high cost-efficiency, and easier deployment of the RRHs. As a result, FSO communication systems are applicable in specified areas within the mobile cellular networks where physical connections by optical fiber cables are impracticable or in the rural area with shortage of optical fiber infrastructure. These challenges prompted our research in OWC. Subsequently, we have presented various opportunities of OWC technologies implementations in different sectors of optical communication networks. Additionally, challenges of OWC applications have been presented. Moreover, we have presented simulation results on the atmospheric effects on RoFSO system.

Furthermore, FSO is a promising optical technology that can be employed for different application. However, the trade-off between the required high data rates and the limitations of atmospheric channel are the major challenges for reliable implementation of FSO technologies in the access networks. So, we have considered spatial diversity techniques for mitigating turbulence-induced fading in the FSO systems. In order to distinguish our contributions from others, we have derived simple and accurate approximate closed-form expressions for the error probability of the turbulence-induced FSO links with IM/DD. The approach helps

in preventing the associated analytical complexity of multi-dimensional numerical integration. It also serves as preventive measure for controlling the related upper limit truncation of the multi-dimensional numerical integration. Moreover, an additional significant contribution is that we have studied the effects of spatial correlation between the transmit apertures on the system performance and demonstrated that, realization of the anticipated diversity gains by the spatial diversity depends largely on effective separation between the apertures so as to alleviate the associated spatial correlation.

The spatial diversity techniques are good choices in mitigating turbulence-induced fading in the FSO systems. However, it should be noted that, for a multiple aperture system, performance estimations over different atmospheric turbulence conditions are computationally intensive. We have proposed novel adaptive multivariate precomputed statistical models and a power series representation based model for estimating the ergodic capacity of MIMO FSO system under generalized atmospheric turbulence channels. The models have a number of advantages such as high-accuracy, low memory requirement, fast, and stable operation. They also enhance modeling efficiency considerably without trade-off in accuracy nor complexity. Additionally, the proposed models can improve the speed by up to fifteen orders of magnitude and beyond without loss of fidelity compared to the existing models which are based on time-consuming numerical integration. In addition, the models are appropriate for real-time applications in the FSO system deployment for fast performance evaluation and system optimization.

Furthermore, as aforementioned, a realistic approach for turbulence-induced fading mitigation is spatial diversity technique in which multiple transmit/receive apertures are employed in order to create and exploit additional degrees of freedom in the spatial domain. The spatial diversity is an appealing technique for fading mitigation because of its typical redundancy. However, utilization of multiple apertures presents different challenges such as, an increase in the system complexity as well as cost. In addition, the distance between the apertures have to be large enough in order to inhibit detrimental effects of spatial correlation. A simplified way of implementing spatial diversity is the dual-hop relaying that is based on creating a virtual multiple-aperture system in order to realize advantages of the MIMO techniques. The dual-hop relaying implementation helps substantially in extending the network coverage area as well as improving the quality of the receive signal. Consequently, considering the small-cell network architectures, we have presented multiuser mixed RF/FSO relay schemes as feasible ways for realizing optical-wireless convergence in dual-hop communication systems for the cloud-based RANs. In addition, we have demonstrated that the schemes are viable solutions for wireless system performance optimization. Likewise, we have established that the schemes can efficiently address the last-mile transmission bottleneck and be of great help in alleviating the associated stringent requirements by C-RAN backhaul/fronthaul.

Moreover, since the FSO system performance is hindered by the temporal irradiance fluctuation, a precise channel characterization is necessary for practical FSO link deployment. Moreover, a well characterized channel aids in determining the system performance over various transmission conditions. Consequently, through experimental channel measurements, we have characterized the SISO FSO link. Similarly, based on the measurements, the scintillation effects on the system performance have been analyzed over different turbulence conditions for MIMO FSO communication systems. We have also presented a proof-of-concept experiment on the transmission capabilities of a hybrid PON-FSO system. The experiment is in an effort to validate the FSO application in sensitive or hazardous environments where the implementation of RF technology is not permitted. The idea is also relevant in the mobile cellular

networks where physical connections through optical fiber cables are unviable or in rural area that lacks fiber infrastructure. In addition, the system implementation on real-time ONU receiver that is emulated by a commercial FPGA enables an open system and hence supports interoperability, portability, and open software standards.

8.2 Future Work

There are still few years to the standardization of 5G networks and telecommunication industries, as well as academia, are still collaborating towards improving network performance and flexibility. This PhD work has addressed a number of research topics on optimization of MFH for the cloud RANs. In doing this, various directions have been investigated to ensure further capacity growth to be able to support the anticipated number of devices by the IoT. This section attempts to discuss several opening topics that are potential future research directions for the MFH performance optimization.

8.2.1 Link Adaptation Technology

In Chapter 3 on page 44, we discussed the implementation of adaptive modulation scheme for different operating conditions in order to enhance the system SE. The study can be extended by considering link adaptation technologies, such as Adaptive-Rate (AR) transmission and Automatic Repeat Request (ARQ). These technologies are important because there is no need for extra physical infrastructures for their implementation. A conventional design in which AR transmission and ARQ are separately implemented at the PHY layer and Data Link Control (DLC) layer can be adopted. In addition, a cross-layer design can be implemented so that PHY and DLC can be jointly integrated in order to improve the system performance over the atmospheric turbulence-induced fading. Furthermore, cross-layer optimization of the ARQ persistence level can be considered for the trade-off between the SE and the expected number of transmissions.

8.2.2 Multi-Hop High-Altitude Platform FSO Communication

The associated limited range of FSO system can be extended with multi-hop relaying as discussed in Chapter 6 on page 89. The link range of terrestrial FSO can further be improved with the help of High-Altitude Platform (HAP) such as Helios, CAPANINA, HAPCOS, and SkyNet that are normally deployed in the stratosphere. So, multi-hop HAP FSO communication integrates advantages of both satellite communication systems and terrestrial FSO links such as low transmission delay, high capacity, acceptable power consumption. The multi-hop HAP FSO communication system can be structured in such a way that the FSO is employed form the ground stations to the HAP station in the stratosphere. Furthermore, FSO links can be implemented between the serial multi-hop HAPs as well as for the downlink to the ground stations. Consequently, the FSO reach can be extended and more broadband data can be effectively transmitted.

Bibliography

[1] M. Ayyash, H. Elgala, A. Khreishah, V. Jungnickel, T. Little, S. Shao, M. Rahaim, D. Schulz, J. Hilt, and R. Freund, "Coexistence of WiFi and LiFi toward 5G: concepts, opportunities, and challenges," *IEEE Communications Magazine*, vol. 54, no. 2, pp. 64–71, February 2016.

[2] J. Wu, Z. Zhang, Y. Hong, and Y. Wen, "Cloud radio access network (C-RAN): a primer," *IEEE Network*, vol. 29, no. 1, pp. 35–41, Jan 2015.

[3] H. Dahrouj, A. Douik, O. Dhifallah, T. Y. Al-Naffouri, and M. S. Alouini, "Resource allocation in heterogeneous cloud radio access networks: advances and challenges," *IEEE Wireless Communications*, vol. 22, no. 3, pp. 66–73, June 2015.

[4] U. Siddique, H. Tabassum, E. Hossain, and D. I. Kim, "Wireless backhauling of 5G small cells: challenges and solution approaches," *IEEE Wireless Communications*, vol. 22, no. 5, pp. 22–31, October 2015.

[5] M. Peng and K. Zhang, "Recent advances in fog radio access networks: Performance analysis and radio resource allocation," *IEEE Access*, vol. 4, pp. 5003–5009, 2016.

[6] M. Peng, S. Yan, K. Zhang, and C. Wang, "Fog-computing-based radio access networks: issues and challenges," *IEEE Network*, vol. 30, no. 4, pp. 46–53, July 2016.

[7] C. Liu, L. Zhang, M. Zhu, J. Wang, L. Cheng, and G. K. Chang, "A novel multi-service small-cell cloud radio access network for mobile backhaul and computing based on radio-over-fiber technologies," *Journal of Lightwave Technology*, vol. 31, no. 17, pp. 2869–2875, Sept 2013.

[8] S. H. Park, O. Simeone, and S. S. Shitz, "Joint optimization of cloud and edge processing for fog radio access networks," *IEEE Transactions on Wireless Communications*, vol. 15, no. 11, pp. 7621–7632, Nov 2016.

[9] R. S. Oliveira, R. S. Oliveira, C. R. L. Francês, J. C. W. A. Costa, D. F. R. Viana, M. Lima, and A. Teixeira, "Analysis of the cost-effective digital radio over fiber system in the NG-PON2 context," in *Telecommunications Network Strategy and Planning Symposium (Networks), 2014 16th International*, Sept 2014, pp. 1–6.

[10] G.-K. Chang, C. Liu, and L. Zhang, "Architecture and applications of a versatile small-cell, multi-service cloud radio access network using radio-over-fiber technologies," in *2013 IEEE International Conference on Communications Workshops (ICC)*, June 2013, pp. 879–883.

[11] N. J. Gomes, P. Assimakopoulos, L. C. Vieira, and P. Sklikas, "Fiber link design considerations for cloud-radio access networks," in *2014 IEEE International Conference on Communications Workshops (ICC)*, June 2014, pp. 382–387.

[12] X. Liu, H. Zeng, N. Chand, and F. Effenberger, "Efficient mobile fronthaul via DSP-based channel aggregation," *Journal of Lightwave Technology*, vol. 34, no. 6, pp. 1556–1564, March 2016.

[13] P. P. Monteiro and A. Gameiro, "Convergence of optical and wireless technologies for 5G," in *Opportunities in 5G Networks: A Research and Development Perspective*, F. Hu, Ed. CRC Press: CRC Press, 2016, ch. 9, p. 179–215.

[14] I. Alimi, P. Monteiro, and A. Teixeira, "Analysis of atmospheric effects on RF signal transmission over the optical wireless communication links," in *XIII Symposium on Enabling Optical Networks and Sensors*, July 2016, pp. 35–38.

[15] K. Kazaura, P. Dat, A. Shah, T. Suzuki, K. Wakamori, M. Matsumoto, T. Higashino, K. Tsukamoto, and S. Komaki, "Studies on a next generation access technology using radio over free-space optic links," in *2008 The Second International Conference on Next Generation Mobile Applications, Services, and Technologies*, Sept 2008, pp. 317–324.

[16] P. Chanclou, A. Pizzinat, F. L. Clech, T. L. Reedeker, Y. Lagadec, F. Saliou, B. L. Guyader, L. Guillo, Q. Deniel, S. Gosselin, S. D. Le, T. Diallo, R. Brenot, F. Lelarge, L. Marazzi, P. Parolari, M. Martinelli, S. O'Dull, S. A. Gebrewold, D. Hillerkuss, J. Leuthold, G. Gavioli, and P. Galli, "Optical fiber solution for mobile fronthaul to achieve cloud radio access network," in *Future Network and Mobile Summit (FutureNetworkSummit), 2013*, July 2013, pp. 1–11.

[17] M. Nahas, A. Saadani, J. P. Charles, and Z. El-Bazzal, "Base stations evolution: Toward 4G technology," in *Telecommunications (ICT), 2012 19th International Conference on*, April 2012, pp. 1–6.

[18] A. Checko, H. L. Christiansen, Y. Yan, L. Scolari, G. Kardaras, M. S. Berger, and L. Dittmann, "Cloud RAN for Mobile Networks - A Technology Overview," *IEEE Communications Surveys & Tutorials*, vol. 17, no. 1, pp. 405–426, Firstquarter 2015.

[19] X. Rao and V. K. N. Lau, "Distributed fronthaul compression and joint signal recovery in cloud-RAN," *IEEE Transactions on Signal Processing*, vol. 63, no. 4, pp. 1056–1065, Feb 2015.

[20] *Understanding the basics of CPRI fronthaul technology*, EXFO Inc, October 2015, application note 310, [Online]. Available: http://www.exfo.com/search?q=Understanding%20the%20Basics%20of %20CPRI%20Fronthaul%20Technology.

[21] N. Saxena, A. Roy, and H. Kim, "Traffic-aware cloud RAN: a key for green 5G networks," *IEEE Journal on Selected Areas in Communications*, vol. 34, no. 4, pp. 1010–1021, April 2016.

[22] M. Peng, Y. Li, Z. Zhao, and C. Wang, "System architecture and key technologies for 5G heterogeneous cloud radio access networks," *IEEE Network*, vol. 29, no. 2, pp. 6–14, March 2015.

[23] A. de la Oliva, J. A. Hernandez, D. Larrabeiti, and A. Azcorra, "An overview of the CPRI specification and its application to C-RAN-based LTE scenarios," *IEEE Communications Magazine*, vol. 54, no. 2, pp. 152–159, February 2016.

[24] M. Y. Arslan, K. Sundaresan, and S. Rangarajan, "Software-defined networking in cellular radio access networks: potential and challenges," *IEEE Communications Magazine*, vol. 53, no. 1, pp. 150–156, January 2015.

[25] P. Mugen, V. Lau, Y. Wei, and W. Chonggang, "Cloud computing based radio access network," *China Communications*, vol. 12, no. 11, pp. 1–2, November 2015.

[26] I. A. Alimi, P. P. Monteiro, and A. L. Teixeira, "Outage probability of multiuser mixed RF/FSO relay schemes for heterogeneous cloud radio access networks (H-CRANs)," *Wireless Personal Communications*, vol. 95, no. 1, pp. 27–41, Jul 2017. [Online]. Available: https://doi.org/10.1007/s11277-017-4413-y

[27] S. C. Hung, H. Hsu, S. Y. Lien, and K. C. Chen, "Architecture harmonization between cloud radio access networks and fog networks," *IEEE Access*, vol. 3, pp. 3019–3034, 2015.

[28] C. Ran, S. Wang, and C. Wang, "Balancing backhaul load in heterogeneous cloud radio access networks," *IEEE Wireless Communications*, vol. 22, no. 3, pp. 42–48, June 2015.

[29] P. T. Dat, A. Kanno, and T. Kawanishi, "Radio-on-radio-over-fiber: efficient fronthauling for small cells and moving cells," *IEEE Wireless Communications*, vol. 22, no. 5, pp. 67–75, October 2015.

[30] N. Wang, E. Hossain, and V. K. Bhargava, "Backhauling 5G small cells: a radio resource management perspective," *IEEE Wireless Communications*, vol. 22, no. 5, pp. 41–49, October 2015.

[31] J. Bartelt, P. Rost, D. Wubben, J. Lessmann, B. Melis, and G. Fettweis, "Fronthaul and backhaul requirements of flexibly centralized radio access networks," *IEEE Wireless Communications*, vol. 22, no. 5, pp. 105–111, October 2015.

[32] *The LTE network architecture: A comprehensive tutorial*, Alcatel-Lucent, 2009, [Online]. Available: http://www.cse.unt.edu/ rdantu/FALL2013WIRELESSNETWORKS/ LTEAlcatelWhitePaper.pdf.

[33] S. Kuwano, J. Terada, and N. Yoshimoto, "Operator perspective on next-generation optical access for future radio access," in *2014 IEEE International Conference on Communications Workshops (ICC)*, June 2014, pp. 376–381.

[34] J. E. Mitchell, "Integrated wireless backhaul over optical access networks," *Journal of Lightwave Technology*, vol. 32, no. 20, pp. 3373–3382, Oct 2014.

[35] B. Haberland, F. Derakhshan, H. Grob-Lipski, R. Klotsche, W. Rehm, P. Schefczik, and M. Soellner, "Radio base stations in the cloud," *Bell Labs Technical Journal*, vol. 18, no. 1, pp. 129–152, June 2013.

[36] S. Park, C. B. Chae, and S. Bahk, "Large-scale antenna operation in heterogeneous cloud radio access networks: a partial centralization approach," *IEEE Wireless Communications*, vol. 22, no. 3, pp. 32–40, June 2015.

[37] L. F. Henning, S. Julião, A. S. R. Oliveira, P. P. Monteiro, and A. A. P. Pohl, "High spectral wavelength agnostic multicarrier D-RoF modem based on uncooled RSOA," *IEEE Photonics Technology Letters*, vol. 28, no. 9, pp. 1010–1013, May 2016.

[38] M. A. Marotta, N. Kaminski, I. Gomez-Miguelez, L. Z. Granville, J. Rochol, L. DaSilva, and C. B. Both, "Resource sharing in heterogeneous cloud radio access networks," *IEEE Wireless Communications*, vol. 22, no. 3, pp. 74–82, June 2015.

[39] M. C. R. Medeiros, R. Costa, H. A. Silva, P. Laurêncio, and P. P. Monteiro, "Cost effective hybrid dynamic radio access supported by radio over fiber," in *2015 17th International Conference on Transparent Optical Networks (ICTON)*, July 2015, pp. 1–4.

[40] P. J. Urban, G. C. Amaral, and J. P. von der Weid, "Fiber monitoring using a sub-carrier band in a sub-carrier multiplexed radio-over-fiber transmission system for applications in analog mobile fronthaul," *Journal of Lightwave Technology*, vol. 34, no. 13, pp. 3118–3125, July 2016.

[41] M. Peng, K. Zhang, J. Jiang, J. Wang, and W. Wang, "Energy-efficient resource assignment and power allocation in heterogeneous cloud radio access networks," *IEEE Transactions on Vehicular Technology*, vol. 64, no. 11, pp. 5275–5287, Nov 2015.

[42] B. P. Rimal, D. P. Van, and M. Maier, "Mobile edge computing empowered fiber-wireless access networks in the 5g era," *IEEE Communications Magazine*, vol. 55, no. 2, pp. 192–200, February 2017.

[43] Y. Yu, "Mobile edge computing towards 5g: Vision, recent progress, and open challenges," *China Communications*, vol. 13, no. Supplement2, pp. 89–99, January 2017.

[44] R. G. Stephen and R. Zhang, "Joint millimeter-wave fronthaul and OFDMA resource allocation in ultra-dense CRAN," *IEEE Transactions on Communications*, vol. 65, no. 3, pp. 1411–1423, March 2017.

[45] I. Alimi, P. Monteiro, and A. Teixeira, "Towards an efficient c-ran optical fronthaul for the future networks: A tutorial on technologies, requirements, challenges, and solutions," *In Press, IEEE Communications Surveys & Tutorials*, 2017.

[46] U. Dotsch, M. Doll, H. P. Mayer, F. Schaich, J. Segel, and P. Sehier, "Quantitative analysis of split base station processing and determination of advantageous architectures for LTE," *Bell Labs Technical Journal*, vol. 18, no. 1, pp. 105–128, June 2013.

[47] T. Pfeiffer, "Next generation mobile fronthaul and midhaul architectures [Invited]," *IEEE/OSA Journal of Optical Communications and Networking*, vol. 7, no. 11, pp. B38–B45, November 2015.

[48] A. Pizzinat, P. Chanclou, F. Saliou, and T. Diallo, "Things you should know about fronthaul," *Journal of Lightwave Technology*, vol. 33, no. 5, pp. 1077–1083, March 2015.

[49] *Open radio equipment Interface (ORI); Requirements for open radio equipment Interface (ORI) (Release 4)*, ETSI Group Specification, October 2014, rel. V4.1.1, [Online]. Available: http://www.etsi.org.

[50] *Common Public Radio Interface (CPRI); Interface Specification*, C. Parties, July 2013, rel. V6.1, [Online]. Available: http://www.cpri.info/spec.html.

[51] *Enabling C-RAN: The Case for OTN Mobile Fronthaul*, Microsemi, 2016, white paper PMC-2143908, Issue 2, [Online]. Available: https://www.microsemi.com/otn/otn-mobile-fronthaul/#white-papers.

[52] M. Paolini, "C-RAN and 5G take transport to new capacity and latency levels: Trends in backhaul, fronthaul, xhaul and mmW," Senza Fili, Tech. Rep., March 2016. [Online]. Available: http://content.rcrwireless.com/SenzaFili-backhaul-report

[53] *Mobile fronthaul as an enabler of centralized RAN: Featuring WDM-based optical transport*, Nokia, 2016, white paper, [Online]. Available: https://resources.ext.nokia.com/asset/192782.

[54] *Evolution to centralized RAN with mobile fronthaul: Technology overview*, Nokia, 2016, white paper, [Online]. Available: https://resources.ext.nokia.com/asset/192728.

[55] G. Heidari, C. D. Snyder, R. M. Rao, and Y. Shah, "Tutorial: designing to evolving LTE advanced pro and pre-5G requirements: Practical deployment considerations," Xilinx, Tech. Rep., January 2017. [Online]. Available: https://www.xilinx.com/publications/events/designcon/2017/tutorial-designing-evolving-lte-advanced-pro-andpre-5g-requirements.pdf

[56] N. J. Gomes, P. Chanclou, P. Turnbull, A. Magee, and V. Jungnickel, "Fronthaul evolution: From CPRI to Ethernet," *Optical Fiber Technology*, vol. 26, Part A, pp. 50 – 58, 2015, next Generation Access Networks. [Online]. Available: //www.sciencedirect.com/science/article/pii/S1068520015000942

[57] T. Pfeiffer, "Next generation mobile fronthaul architectures," in *Optical Fiber Communications Conference and Exhibition (OFC), 2015*, March 2015, pp. 1–3.

[58] *Mobile fronthaul for cloud-RAN deployment-efficient use of optical infrastructure for remote radio architectures*, Alcatel-Lucent, March 2014, [Online]. Available: http://www.tmcnet.com/tmc/whitepapers/documents/whitepapers/2014/10051-mobile-fronthaul-cloud-ran-deployment.pdf.

[59] R. S. Oliveira, R. S. Oliveira, C. R. L. Francês, J. C. W. A. Costa, D. F. R. Viana, M. Lima, and A. Teixeira, "Analysis of the cost-effective digital radio over fiber system in the NG-PON2 context," in *Telecommunications Network Strategy and Planning Symposium (Networks), 2014 16th International*, Sept 2014, pp. 1–6.

[60] *CPRI overview: Input requirements for CPRI*, CPRI, March 2015, [Online]. Available: http://www.ieee802.org/1/files/public/docs2015/liaison-CPRI_Tdoc _1124_presentation-0315.pdf.

[61] Y. Ma, X. Huo, J. Li, Xiaomu, and Jingwen, "Optical solutions for fronthaul application (invited)," in *2015 14th International Conference on Optical Communications and Networks (ICOCN)*, July 2015, pp. 1–3.

[62] X. Wang, S. Thota, M. Tornatore, H. S. Chung, H. H. Lee, S. Park, and B. Mukherjee, "Energy-efficient virtual base station formation in optical-access-enabled cloud-RAN," *IEEE Journal on Selected Areas in Communications*, vol. 34, no. 5, pp. 1130–1139, May 2016.

[63] "The benefits of cloud-RAN architecture in mobile network expansion," Fujitsu Network Communications Inc, white paper, 2014.

[64] R. T. Carlson and S. Paciorek, "Environmental qualification and field test results for the SONAbeam^{TM} 155 and 622," fSONA Communications Corp, Tech. Rep. [Online]. Available: http://www.fsona.com/tech/white_papers/tech_qual-test.pdf

[65] ITU-T, "ITU-T Recommendation G.692: Optical interfaces for multichannel systems with optical amplifiers," International Telecommunication Union, Tech. Rep., October 1998. [Online]. Available: https://www.itu.int/rec/T-REC-G.692-199810-I/en

[66] P. P. Monteiro and A. Gameiro, "Hybrid fibre infrastructures for cloud radio access networks," in *2014 16th International Conference on Transparent Optical Networks (ICTON)*, July 2014, pp. 1–4.

[67] L. Kazovsky, N. Cheng, W. Shaw, D. Gutierrez, and S. Wong, *Broadband optical access networks*. John Wiley & Sons, Inc, 2011.

[68] M. Rahman, C. M. Machuca, K. Grobe, and W. Kellerer, "Advantages of joint access network planning in dense populated areas," in *Networks and Optical Communications - (NOC), 2014 19th European Conference on*, June 2014, pp. 67–73.

[69] D. Nesset, "NG-PON2 technology and standards," *Journal of Lightwave Technology*, vol. 33, no. 5, pp. 1136–1143, March 2015.

[70] A. Shahpari, R. M. Ferreira, F. P. Guiomar, S. B. Amado, S. Ziaie, C. Rodrigues, J. D. Reis, A. N. Pinto, and A. L. Teixeira, "Real-time bidirectional coherent Nyquist UDWDM-PON coexisting with multiple deployed systems in Field-Trial," *Journal of Lightwave Technology*, vol. 34, no. 7, pp. 1643–1650, April 2016.

[71] M. Hajduczenia, H. J. A. D. Silva, and P. P. Monteiro, "Development of 10 Gb/s EPON in IEEE 802.3av," *IEEE Communications Magazine*, vol. 46, no. 7, pp. 40–47, July 2008.

[72] S. V. Pato, R. Meleiro, D. Fonseca, P. Andre, P. Monteiro, and H. Silva, "All-optical burst-mode power equalizer based on cascaded SOAs for 10-Gb/s EPONs," *IEEE Photonics Technology Letters*, vol. 20, no. 24, pp. 2078–2080, Dec 2008.

[73] P. P. Monteiro, D. Viana, J. da Silva, D. Riscado, M. Drummond, A. S. R. Oliveira, N. Silva, and P. Jesus, "Mobile fronthaul RoF transceivers for C-RAN applications," in *2015 17th International Conference on Transparent Optical Networks (ICTON)*, July 2015, pp. 1–4.

[74] Y. Luo, X. Zhou, F. Effenberger, X. Yan, G. Peng, Y. Qian, and Y. Ma, "Time- and wavelength-division multiplexed passive optical network (TWDM-PON) for next-generation PON stage 2 (NG-PON2)," *Journal of Lightwave Technology*, vol. 31, no. 4, pp. 587–593, Feb 2013.

[75] J. S. Wey, D. Nesset, M. Valvo, K. Grobe, H. Roberts, Y. Luo, and J. Smith, "Physical layer aspects of NG-PON2 standards- Part 1: Optical link design [Invited]," *IEEE/OSA Journal of Optical Communications and Networking*, vol. 8, no. 1, pp. 33–42, January 2016.

[76] R. S. Luis, A. Shahpari, J. D. Reis, R. Ferreira, Z. Vujicic, B. J. Puttnam, J. M. D. Mendinueta, M. Lima, M. Nakamura, Y. Kamio, N. Wada, and A. Teixeira, "Ultra high capacity self-homodyne PON with simplified ONU and burst-mode upstream," *IEEE Photonics Technology Letters*, vol. 26, no. 7, pp. 686–689, April 2014.

[77] T. Tashiro, S. Kuwano, J. Terada, T. Kawamura, N. Tanaka, S. Shigematsu, and N. Yoshimoto, "A novel DBA scheme for TDM-PON based mobile fronthaul," in *Optical Fiber Communications Conference and Exhibition (OFC), 2014*, March 2014, pp. 1–3.

[78] Z. Ghebretensae, K. Laraqui, S. Dahlfort, F. Ponzini, L. Giorgi, S. Stracca, J. Chen, Y. Li, J. Hansryd, and A. R. Pratt, "Transmission solutions and architectures for heterogeneous networks built as C-RANs," in *Communications and Networking in China (CHINACOM), 2012 7th International ICST Conference on*, Aug 2012, pp. 748–752.

[79] Y. Luo, H. Roberts, K. Grobe, M. Valvo, D. Nesset, K. Asaka, H. Rohde, J. Smith, J. S. Wey, and F. Effenberger, "Physical layer aspects of NG-PON2 standards- Part 2: System design and technology feasibility [Invited]," *IEEE/OSA Journal of Optical Communications and Networking*, vol. 8, no. 1, pp. 43–52, January 2016.

[80] D. Nesset, "PON roadmap [invited]," *IEEE/OSA Journal of Optical Communications and Networking*, vol. 9, no. 1, pp. A71–A76, Jan 2017.

[81] G. Vall-llosera, A. Rafel, N. Parkin, M. Angelou, D. Klonidis, I. Cano, M. Presi, G. Papastergiou, I. Tomkos, J. Prat, and E. Ciaramella, "COCONUT cost, power consumption and migration analysis: A route towards NG-PON3," in *2015 17th International Conference on Transparent Optical Networks (ICTON)*, July 2015, pp. 1–4.

[82] A. Császár, W. John, M. Kind, C. Meirosu, G. Pongrácz, D. Staessens, A. Takács, and F. J. Westphal, "Unifying cloud and carrier network: EU FP7 Project UNIFY," in *2013 IEEE/ACM 6th International Conference on Utility and Cloud Computing*, Dec 2013, pp. 452–457.

[83] B. Skubic, G. Bottari, A. Rostami, F. Cavaliere, and P. Öhlén, "Rethinking optical transport to pave the way for 5G and the networked society," *Journal of Lightwave Technology*, vol. 33, no. 5, pp. 1084–1091, March 2015.

[84] N. Shibata, T. Tashiro, S. Kuwano, N. Yuki, Y. Fukada, J. Terada, and A. Otaka, "Performance evaluation of mobile front-haul employing Ethernet- based TDM-PON with IQ data compression [Invited]," *IEEE/OSA Journal of Optical Communications and Networking*, vol. 7, no. 11, pp. B16–B22, November 2015.

[85] G. Anjos, J. Santos, A. Oliveira, P. Monteiro, D. Riscado, N. V. Silva, and P. Jesus, "Implementation and evaluation of a low latency and resource efficient compression method for digital radio transport of OFDM signals," in *2015 IEEE Globecom Workshops (GC Wkshps)*, Dec 2015, pp. 1–6.

[86] M. Peng, Y. Sun, X. Li, Z. Mao, and C. Wang, "Recent advances in cloud radio access networks: System architectures, key techniques, and open issues," *IEEE Communications Surveys Tutorials*, vol. 18, no. 3, pp. 2282–2308, thirdquarter 2016.

[87] *IEEE P1904.3 TF Radio over Ethernet update*, IEEE 802.1TSN, 2016, [Online]. Available: http://www.ieee802.org/1/files/public/docs2016/new-roe-status-rm-ieee1904dot3-0516-v00.pdf.

[88] T. Wan and P. Ashwood-Smith, "A performance study of CPRI over Ethernet with IEEE 802.1Qbu and 802.1Qbv enhancements," in *2015 IEEE Global Communications Conference (GLOBECOM)*, Dec 2015, pp. 1–6.

[89] C. J. Bernardos, A. D. Domenico, J. Ortin, P. Rost, and D. Wübben, "Challenges of designing jointly the backhaul and radio access network in a cloud-based mobile network," in *2013 Future Network Mobile Summit*, July 2013, pp. 1–10.

[90] M. Jaber, M. A. Imran, R. Tafazolli, and A. Tukmanov, "5G backhaul challenges and emerging research directions: A survey," *IEEE Access*, vol. 4, pp. 1743–1766, 2016.

[91] M. Gerasimenko, D. Moltchanov, R. Florea, S. Andreev, Y. Koucheryavy, N. Himayat, S. P. Yeh, and S. Talwar, "Cooperative radio resource management in heterogeneous cloud radio access networks," *IEEE Access*, vol. 3, pp. 397–406, 2015.

[92] D. Wake, A. Nkansah, and N. J. Gomes, "Radio over fiber link design for next generation wireless systems," *Journal of Lightwave Technology*, vol. 28, no. 16, pp. 2456–2464, Aug 2010.

[93] S.-H. Cho, H. Park, H. S. Chung, K. H. Doo, S. Lee, and J. H. Lee, "Cost-effective next generation mobile fronthaul architecture with multi-IF carrier transmission scheme," in *Optical Fiber Communications Conference and Exhibition (OFC), 2014*, March 2014, pp. 1–3.

[94] P. Almeida and H. Silva, "LTE signals transmission with modulation efficiency and robustness against chromatic dispersion improved based on DEMZM modulation in cloud-RoF access networks," in *2014 16th International Conference on Transparent Optical Networks (ICTON)*, July 2014, pp. 1–4.

[95] S. Lee, S. H. Cho, and J. H. Lee, "Future-proof optical-mobile converged access network based on integration of PON with RoF technologies," in *Microwave Photonics (MWP) and the 2014 9th Asia-Pacific Microwave Photonics Conference (APMP), 2014 International Topical Meeting on*, Oct 2014, pp. 409–411.

[96] T. Kawanishi, "Ultra high-speed fiber wireless transport," in *Optical Fiber Communications Conference and Exhibition (OFC), 2014*, March 2014, pp. 1–3.

[97] Z. Tang and S. Pan, "A full-duplex radio-over-fiber link based on a dual-polarization Mach-Zehnder modulator," *IEEE Photonics Technology Letters*, vol. 28, no. 8, pp. 852–855, April 2016.

[98] W. Ji and J. Chang, "The radio-on-fiber-wavelength-division-multiplexed-passive-optical network (WDM-RoF-PON) for wireless and wire layout with linearly-polarized dual-wavelength fiber laser and carrier reusing," *Optics and Laser Technology*, vol. 49, p. 301–306, July 2013.

[99] A. S. Gowda, A. R. Dhaini, L. G. Kazovsky, H. Yang, S. T. Abraha, and A. Ng'oma, "Towards green optical/wireless in-building networks: Radio-over-fiber," *Journal of Lightwave Technology*, vol. 32, no. 20, pp. 3545–3556, Oct 2014.

[100] C. Lim, Y. Yang, and A. Nirmalathas, "Transport schemes for fiber-wireless technology: Transmission performance and energy efficiency," *Photonics*, vol. 1, no. 2, pp. 67–83, April 2014. [Online]. Available: http://www.mdpi.com/2304-6732/1/2/67

[101] N. Gomes, P. Monteiro, and A. Gameiro, *Next generation wireless communications using radio over fiber*. Wiley, 2012. [Online]. Available: https://books.google.co.uk/books?id=YhntfBlyRtIC

[102] G. S. D. Gordon, M. J. Crisp, R. V. Penty, T. D. Wilkinson, and I. H. White, "Feasibility demonstration of a mode-division multiplexed MIMO-enabled radio-over-fiber distributed antenna system," *Journal of Lightwave Technology*, vol. 32, no. 20, pp. 3521–3528, Oct 2014.

[103] A. Nirmalathas, P. A. Gamage, C. Lim, D. Novak, and R. Waterhouse, "Digitized radio-over-fiber technologies for converged optical wireless access network," *Journal of Lightwave Technology*, vol. 28, no. 16, pp. 2366–2375, Aug 2010.

[104] S. Jang, G. Jo, J. Jung, B. Park, and S. Hong, "A digitized IF-over-fiber transmission based on low-pass delta-sigma modulation," *IEEE Photonics Technology Letters*, vol. 26, no. 24, pp. 2484–2487, Dec 2014.

[105] D. A. A. Mello, A. N. Barreto, F. A. Barbosa, C. Osorio, M. Fiorani, and P. Monti, "Spectrally efficient fronthaul architectures for a cost-effective 5G C-RAN," in *2016 18th International Conference on Transparent Optical Networks (ICTON)*, July 2016, pp. 1–5.

[106] J. Bae and J. Park, "An efficient algorithm for bandpass sampling of multiple RF signals," *IEEE Signal Processing Letters*, vol. 13, no. 4, pp. 193–196, April 2006.

[107] R. G. Lyons, *Understanding Digital Signal Processing (2Nd Edition)*. Upper Saddle River, NJ, USA: Prentice Hall PTR, 2004.

[108] F. Buchali, R. Dischler, and X. Liu, "Optical OFDM: A promising high-speed optical transport technology," *Bell Labs Technical Journal*, vol. 14, no. 1, pp. 125–146, Spring 2009.

[109] A. Cuenin and N. Engin, "Selective clipping and filtering: A low-EVM PAPR reduction scheme for OFDM standards," in *2016 IEEE 27th Annual International Symposium on Personal, Indoor, and Mobile Radio Communications (PIMRC)*, Sept 2016, pp. 1–6.

[110] U. Reimers, *DVB: The Family of International Standards for Digital Video Broadcasting*, ser. Signals and Communication Technology. Springer, 2005. [Online]. Available: https://books.google.pt/books?id=xL_Rq6qUvT0C

[111] T. Jiang, C. Ni, C. Ye, Y. Wu, and K. Luo, "A novel multi-block tone reservation scheme for PAPR reduction in OQAM-OFDM systems," *IEEE Transactions on Broadcasting*, vol. 61, no. 4, pp. 717–722, Dec 2015.

[112] Y. Yang, C. Lim, and A. . Nirmalathas, "Investigation on transport schemes for efficient high-frequency broadband OFDM transmission in fibre-wireless links," *Journal of Lightwave Technology*, vol. 32, no. 2, pp. 267–274, Jan 2014.

[113] C. Lim, Y. Yang, and A. Nirmalathas, "Transport strategies for broadband wireless signals distribution in fiber-wireless links," in *2014 OptoElectronics and Communication Conference and Australian Conference on Optical Fibre Technology*, July 2014, pp. 123–125.

[114] Q. Chen, J. He, R. Deng, M. Chen, F. Zhang, M. Dai, F. Long, and L. Chen, "Experimental research on adaptive 128/64QAM DFT-spread IFFT/FFT size efficient OFDM with a high SE in VLLC system," *IEEE Photonics Journal*, vol. 9, no. 1, pp. 1–8, Feb 2017.

[115] H. Golestaneh, F. A. Malekzadeh, and S. Boumaiza, "Three-way Doherty power amplifier for efficient amplification of wideband signals with extended PAPR," in *2014 IEEE Radio and Wireless Symposium (RWS)*, Jan 2014, pp. 136–138.

[116] X. Liu, H. Zeng, N. Chand, and F. Effenberger, "CPRI-compatible efficient mobile fronthaul transmission via equalized TDMA achieving 256 Gb/s CPRI-equivalent data rate in a single 10-GHz-bandwidth IM-DD channel," in *2016 Optical Fiber Communications Conference and Exhibition (OFC)*, March 2016, pp. 1–3.

[117] H. Dahrouj, A. Douik, F. Rayal, T. Y. Al-Naffouri, and M. S. Alouini, "Cost-effective hybrid RF/FSO backhaul solution for next generation wireless systems," *IEEE Wireless Communications*, vol. 22, no. 5, pp. 98–104, October 2015.

[118] C. l. I, Y. Yuan, J. Huang, S. Ma, C. Cui, and R. Duan, "Rethink fronthaul for soft RAN," *IEEE Communications Magazine*, vol. 53, no. 9, pp. 82–88, September 2015.

[119] C. L. I, J. Huang, Y. Yuan, S. Ma, and R. Duan, "NGFI, the xHaul," in *2015 IEEE Globecom Workshops (GC Wkshps)*, Dec 2015, pp. 1–6.

[120] K. Sundaresan, M. Y. Arslan, S. Singh, S. Rangarajan, and S. V. Krishnamurthy, "FluidNet: A flexible cloud-based radio access network for small cells," *IEEE/ACM Transactions on Networking*, vol. 24, no. 2, pp. 915–928, April 2016.

[121] *White Paper of Next Generation Fronthaul Interface*, China Mobile Research Institute, October 2015, white paper, [Online]. Available: http://labs.chinamobile.com/cran/wp-content/uploads/2015/09/NGFI-Whitepaper_EN_v1.0_201509291.pdf.

[122] T. Deiß, L. Cominardi, A. Garcia-Saavedra, P. Iovanna, G. Landi, X. Li, J. Mangues-Bafalluy, J. Núñez-Martínez, and A. de la Oliva, "Packet forwarding for heterogeneous technologies for integrated fronthaul/backhaul," in *2016 European Conference on Networks and Communications (EuCNC)*, June 2016, pp. 133–137.

[123] L. M. Contreras, C. J. Bernardos, A. de la Oliva, X. Costa-Pérez, and R. Guerzoni, "Orchestration of crosshaul slices from federated administrative domains," in *2016 European Conference on Networks and Communications (EuCNC)*, June 2016, pp. 220–224.

[124] X. Li, G. Landi, J. Núñez-Martínez, R. Casellas, S. González, C. F. Chiasserini, J. R. Sanchez, D. Siracusa, L. Goratti, D. Jimenez, and L. M. Contreras, "Innovations through 5G-crosshaul applications," in *2016 European Conference on Networks and Communications (EuCNC)*, June 2016, pp. 382–387.

[125] X. Costa-Perez, A. Garcia-Saavedra, X. Li, T. Deiss, A. de la Oliva, A. di Giglio, P. Iovanna, and A. Moored, "5G-crosshaul: An SDN/NFV integrated fronthaul/backhaul transport network architecture," *IEEE Wireless Communications*, vol. 24, no. 1, pp. 38–45, February 2017.

[126] L. Cheng, X. Liu, N. Chard, F. Effenberger, and G. K. Chang, "Experimental demonstration of sub-nyquist sampling for bandwidth- and hardware-efficient mobile fronthaul supporting 128 × 128 MIMO with 100-MHz OFDM signals," in *2016 Optical Fiber Communications Conference and Exhibition (OFC)*, March 2016, pp. 1–3.

[127] F. Lu, Y. C. Chi, M. Xu, L. Cheng, J. Wang, C. T. Tsai, G. R. Lin, and G. K. Chang, "Cost-effective bi-directional mobile fronthaul employing WRC-FPLD for beyond LTE-advanced services," in *2016 Optical Fiber Communications Conference and Exhibition (OFC)*, March 2016, pp. 1–3.

[128] L. Valcarenghi, K. Kondepu, A. Sgambelluri, F. Cugini, P. Castoldi, R. A. Morenilla, D. Larrabeiti, and B. Vermeulen, "SDN-controlled energy-efficient mobile fronthaul: An experimental evaluation in federated testbeds," in *2016 European Conference on Networks and Communications (EuCNC)*, June 2016, pp. 298–301.

[129] P. T. Dat, A. Kanno, N. Yamamoto, and T. Kawanishi, "Efficient mobile fronthaul for simultaneous transmission of 4G and future mobile signals," in *2016 21st OptoElectronics and Communications Conference (OECC) held jointly with 2016 International Conference on Photonics in Switching (PS)*, July 2016, pp. 1–3.

[130] P. J. Urban, G. Vall-llosera, E. Medeiros, and S. Dahlfort, "Fiber plant manager: an OTDR- and OTM-based PON monitoring system," *IEEE Communications Magazine*, vol. 51, no. 2, pp. S9–S15, February 2013.

[131] H. Schmuck, J. Hehmann, M. Straub, and T. Pfeiffer, "Embedded OTDR techniques for cost-efficient fibre monitoring in optical access networks," in *2006 European Conference on Optical Communications*, Sept 2006, pp. 1–2.

[132] D. V. Caballero, R. Almeida, P. Urban, J. Costa, J. von der Weid, and J. Chen, "SCM/WDM-PON with in-service baseband embedded OTDR monitoring," *Optics Communications*, vol. 356, pp. 250 – 255, 2015. [Online]. Available: http://www.sciencedirect.com/science/article/pii/S0030401815006884

[133] M. Sung, C. Han, S. H. Cho, H. S. Chung, S. M. Kim, and J. H. Lee, "Bandwidth efficient transmission of 96 LTE-A signals with 118-Gb/s CPRI-equivalent rate using 2-GHz frequency span and intermixing mitigation for mobile fronthaul," in *2016 International Conference on Information and Communication Technology Convergence (ICTC)*, Oct 2016, pp. 775–777.

[134] X. Liu, F. Effenberger, N. Chand, L. Zhou, and H. Lin, "Demonstration of bandwidth-efficient mobile fronthaul enabling seamless aggregation of 36 E-UTRA-like wireless signals in a single 1.1-GHz wavelength channel," in *2015 Optical Fiber Communications Conference and Exhibition (OFC)*, March 2015, pp. 1–3.

[135] F. Lu, M. Xu, L. Cheng, J. Wang, S. Shen, J. Zhang, and G. K. Chang, "Sub-band pre-distortion for PAPR reduction in spectral efficient 5G mobile fronthaul," *IEEE Photonics Technology Letters*, vol. 29, no. 1, pp. 122–125, Jan 2017.

[136] X. Liu, H. Zeng, N. Chand, and F. Effenberger, "Experimental demonstration of high-throughput low-latency mobile fronthaul supporting 48 20-MHz LTE signals with 59-Gb/s CPRI-equivalent rate and 2-μs processing latency," in *2015 European Conference on Optical Communication (ECOC)*, Sept 2015, pp. 1–3.

[137] X. Liu, H. Zeng, and F. Effenberger, "Bandwidth-efficient synchronous transmission of I/Q waveforms and control words via frequency-division multiplexing for mobile fronthaul," in *2015 IEEE Global Communications Conference (GLOBECOM)*, Dec 2015, pp. 1–6.

[138] H. Zeng, X. Liu, S. Megeed, N. Chand, and F. Effenberger, "Real-time demonstration of CPRI-compatible efficient mobile fronthaul using FPGA," *Journal of Lightwave Technology*, vol. PP, no. 99, pp. 1–1, 2017.

[139] N. Cheng, L. Zhou, X. Liu, and F. J. Effenberger, "Reflective crosstalk cancellation in self-seeded WDM PON for mobile fronthaul/backhaul," *Journal of Lightwave Technology*, vol. 34, no. 8, pp. 2056–2063, April 2016.

[140] M. Xu, J. H. Yan, J. Zhang, F. Lu, J. Wang, L. Cheng, D. Guidotti, and G. K. Chang, "Bidirectional fiber-wireless access technology for 5G mobile spectral aggregation and cell densification," *IEEE/OSA Journal of Optical Communications and Networking*, vol. 8, no. 12, pp. B104–B110, December 2016.

[141] S. H. Cho, H. S. Chung, C. Han, S. Lee, and J. H. Lee, "Experimental demonstrations of next generation cost-effective mobile fronthaul with IFoF technique," in *Optical Fiber Communications Conference and Exhibition (OFC), 2015*, March 2015, pp. 1–3.

[142] A. Caballero, S.-W. Wong, D. Zibar, L. G. Kazovsky, and I. T. Monroy, "Distributed MIMO antenna architecture for wireless-over-fiber backhaul with multicarrier optical phase modulation," in *Optical Fiber Communication Conference and Exposition*

(OFC/NFOEC), 2011 and the National Fiber Optic Engineers Conference, March 2011, pp. 1–3.

[143] C. B. Naila, K. Wakamori, M. Matsumoto, A. Bekkali, and K. Tsukamoto, "Transmission analysis of digital TV signals over a Radio-on-FSO channel," *IEEE Communications Magazine*, vol. 50, no. 8, pp. 137–144, August 2012.

[144] C. B. Naila, K. Wakamori, M. Matsumoto, and K. Tsukamoto, "Transmission analysis of digital TV signals over a radio-on-FSO channel," in *Kaleidoscope 2011: The Fully Networked Human? - Innovations for Future Networks and Services (K-2011), Proceedings of ITU*, Dec 2011, pp. 1–7.

[145] I. Alimi, A. Shahpari, A. Sousa, R. Ferreira, P. Monteiro, and A. Teixeira, "Challenges and opportunities of optical wireless communication technologies," in *Optical Communication Technology*, P. Pinho, Ed. Rijeka: InTech, 2017, ch. 02. [Online]. Available: http://dx.doi.org/10.5772/intechopen.69113

[146] I. Alimi, A. Shahpari, V. Ribeiro, N. Kumar, P. Monteiro, and A. Teixeira, "Optical wireless communication for future broadband access networks," in *2016 21st European Conference on Networks and Optical Communications (NOC)*, June 2016, pp. 124–128.

[147] C. Yu, L. Yu, Y. Wu, Y. He, and Q. Lu, "Uplink scheduling and link adaptation for narrowband internet of things systems," *IEEE Access*, vol. PP, no. 99, pp. 1–1, 2017.

[148] W. Ejaz, A. Anpalagan, M. A. Imran, M. Jo, M. Naeem, S. B. Qaisar, and W. Wang, "Internet of things (IoT) in 5G wireless communications," *IEEE Access*, vol. 4, pp. 10 310–10 314, 2016.

[149] G. Parca, A. Tavares, A. Shahpari, A. Teixeira, V. Carrozzo, and G. T. Beleffi, "FSO for broadband multi service delivery in future networks," in *2013 2nd International Workshop on Optical Wireless Communications (IWOW)*, Oct 2013, pp. 67–70.

[150] Z. Ghassemlooy, W. Popoola, and S. Rajbhandari, *Optical wireless communications: System and channel modelling with MATLAB®*. Taylor & Francis, 2012.

[151] Z. Ghassemlooy, S. Arnon, M. Uysal, Z. Xu, and J. Cheng, "Emerging optical wireless communications-advances and challenges," *IEEE Journal on Selected Areas in Communications*, vol. 33, no. 9, pp. 1738–1749, Sept 2015.

[152] M. A. Khalighi and M. Uysal, "Survey on free space optical communication: A communication theory perspective," *IEEE Communications Surveys & Tutorials*, vol. 16, no. 4, pp. 2231–2258, Fourthquarter 2014.

[153] S. Bloom, E. Korevaar, J. Schuster, and H. Willebrand, "Understanding the performance of free-space optics [Invited]," *J. Opt. Netw.*, vol. 2, no. 6, pp. 178–200, Jun 2003. [Online]. Available: http://jon.osa.org/abstract.cfm?URI=jon-2-6-178

[154] H. Kaushal and G. Kaddoum, "Optical communication in space: Challenges and mitigation techniques," *IEEE Communications Surveys & Tutorials*, vol. 19, no. 1, pp. 57–96, Firstquarter 2017.

[155] A. Sevincer, A. Bhattarai, M. Bilgi, M. Yuksel, and N. Pala, "LIGHTNETs: Smart LIGHTing and mobile optical wireless NETworks- A survey," *IEEE Communications Surveys & Tutorials*, vol. 15, no. 4, pp. 1620–1641, Fourth 2013.

[156] S. Rajagopal, R. D. Roberts, and S. K. Lim, "IEEE 802.15.7 visible light communication: modulation schemes and dimming support," *IEEE Communications Magazine*, vol. 50, no. 3, pp. 72–82, March 2012.

[157] K. Ying, Z. Yu, R. J. Baxley, H. Qian, G. K. Chang, and G. T. Zhou, "Nonlinear distortion mitigation in visible light communications," *IEEE Wireless Communications*, vol. 22, no. 2, pp. 36–45, April 2015.

[158] F. Yang and J. Gao, "Dimming control scheme with high power and spectrum efficiency for visible light communications," *IEEE Photonics Journal*, vol. 9, no. 1, pp. 1–12, Feb 2017.

[159] M. Wang, J. Wu, W. Yu, H. Wang, J. Li, J. Shi, and C. Luo, "Efficient coding modulation and seamless rate adaptation for visible light communications," *IEEE Wireless Communications*, vol. 22, no. 2, pp. 86–93, April 2015.

[160] *Visible light communication - VLC & PUREVLC^{TM}*, ANDY, Accessed: February 2017 [Online]. Available: http://andy96877.blogspot.pt/p/visible-light-communication-vlc-is-data.html.

[161] S. U. Jan, Y. D. Lee, and I. Koo, "Comparative analysis of DIPPM scheme for visible light communications," in *2015 International Conference on Emerging Technologies (ICET)*, Dec 2015, pp. 1–5.

[162] M. D'Amico, A. Leva, and B. Micheli, "Free-space optics communication systems: first results from a pilot field-trial in the surrounding area of Milan, Italy," *IEEE Microwave and Wireless Components Letters*, vol. 13, no. 8, pp. 305–307, Aug 2003.

[163] D.-Y. Song, Y.-S. Hurh, J.-W. Cho, J.-H. Lim, D.-W. Lee, J.-S. Lee, and Y. Chung, "4 × 10 Gb/s terrestrial optical free space transmission over 1.2 km using an EDFA preamplifier with 100 GHz channel spacing," *Opt. Express*, vol. 7, no. 8, pp. 280–284, Oct 2000. [Online]. Available: http://www.opticsexpress.org/abstract.cfm?URI=oe-7-8-280

[164] P. Bandera, "Defining a Common Standard for Evaluating and Comparing Free-Space Optical Products," fSONA Communications Corp, Tech. Rep. [Online]. Available: http://www.fsona.com/tech/white_papers/WHTPAP-Generalized_Link_Margin.pdf

[165] *Ultra-Low Latency Point-to-Point Wireless Bridge*, LightPointe, white paper, [Online]. Available: http://nebula.wsimg.com/793e82b2beac48cb90c347bd86776d12?AccessKeyId=C1431E109BF92B03DF85&disposition
=0&alloworigin=1.

[166] Z. Wang, W. D. Zhong, S. Fu, and C. Lin, "Performance comparison of different modulation formats over free-space optical (fso) turbulence links with space diversity reception technique," *IEEE Photonics Journal*, vol. 1, no. 6, pp. 277–285, Dec 2009.

[167] S. M. Navidpour, M. Uysal, and M. Kavehrad, "Ber performance of free-space optical transmission with spatial diversity," *IEEE Transactions on Wireless Communications*, vol. 6, no. 8, pp. 2813–2819, August 2007.

[168] I. A. Alimi, A. M. Abdalla, J. Rodriguez, P. P. Monteiro, and A. L. Teixeira, "Spatial interpolated lookup tables (LUTs) models for ergodic capacity of MIMO FSO systems," *IEEE Photonics Technology Letters*, vol. 29, no. 7, pp. 583–586, April 2017.

[169] I. Alimi, A. Shahpari, V. Ribeiro, A. Sousa, P. Monteiro, and A. Teixeira, "Channel characterization and empirical model for ergodic capacity of free-space optical communication link," *Optics Communications*, vol. 390, pp. 123 – 129, 2017. [Online]. Available: http://www.sciencedirect.com/science/article/pii/S0030401817300019

[170] A. Bekkali, C. B. Naila, K. Kazaura, K. Wakamori, and M. Matsumoto, "Transmission analysis of ofdm-based wireless services over turbulent radio-on-fso links modeled by gamma-gamma distribution," *IEEE Photonics Journal*, vol. 2, no. 3, pp. 510–520, June 2010.

[171] M. Al Naboulsi, H. Sizun, and F. de Fornel, "Fog attenuation prediction for optical and infrared waves," *Optical Engineering*, vol. 43, no. 2, pp. 319–329, 2004. [Online]. Available: http://dx.doi.org/10.1117/1.1637611

[172] A. A. Farid and S. Hranilovic, "Outage capacity optimization for free-space optical links with pointing errors," *Journal of Lightwave Technology*, vol. 25, no. 7, pp. 1702–1710, July 2007.

[173] H. G. Sandalidis, T. A. Tsiftsis, and G. K. Karagiannidis, "Optical wireless communications with heterodyne detection over turbulence channels with pointing errors," *Journal of Lightwave Technology*, vol. 27, no. 20, pp. 4440–4445, Oct 2009.

[174] L. Andrews and R. Phillips, *Laser beam propagation through random media*, ser. Press Monographs. SPIE Press, 2005.

[175] K. Kiasaleh, "Performance of APD-based, PPM free-space optical communication systems in atmospheric turbulence," *IEEE Transactions on Communications*, vol. 53, no. 9, pp. 1455–1461, Sept 2005.

[176] A. Jurado-Navas, J. M. Garrido-Balsells, J. F. Paris, and A. Puerta-Notario, "A unifying statistical model for atmospheric optical scintillation," J. Awrejcewicz, Ed. InTech, 2011, pp. 181–206.

[177] K. Yang, N. Yang, C. Xing, J. Wu, and Z. Zhang, "Space-time network coding with transmit antenna selection and maximal-ratio combining," *IEEE Transactions on Wireless Communications*, vol. 14, no. 4, pp. 2106–2117, April 2015.

[178] L. Yang, M. O. Hasna, and X. Gao, "Performance of mixed RF/FSO with variable gain over generalized atmospheric turbulence channels," *IEEE Journal on Selected Areas in Communications*, vol. 33, no. 9, pp. 1913–1924, Sept 2015.

[179] H. Samimi and M. Uysal, "End-to-end performance of mixed RF/FSO transmission systems," *IEEE/OSA Journal of Optical Communications and Networking*, vol. 5, no. 11, pp. 1139–1144, Nov 2013.

[180] J. Zhang, L. Dai, Y. Han, Y. Zhang, and Z. Wang, "On the ergodic capacity of MIMO free-space optical systems over turbulence channels," *IEEE Journal on Selected Areas in Communications*, vol. 33, no. 9, pp. 1925–1934, Sept 2015.

[181] C. L. Tran, T. A. Wysocki, A. Mertins, and J. Seberry, "Multiple-input multiple-output systems with space-time codes," in *Complex Orthogonal Space-Time Processing in Wireless Communications*. Springer-Verlag US: Springer, 2006, ch. 2, p. 9–58.

[182] K. P. Peppas, A. N. Stassinakis, G. K. Topalis, H. E. Nistazakis, and G. S. Tombras, "Average capacity of optical wireless communication systems over I-K atmospheric turbulence channels," *IEEE/OSA Journal of Optical Communications and Networking*, vol. 4, no. 12, pp. 1026–1032, Dec 2012.

[183] I. Alimi, A. Shahpari, P. Monteiro, and A. Teixeira, "Effects of diversity schemes and correlated channels on owc systems performance," *Journal of Modern Optics*, vol. 63, no. 21, pp. 2339–2347, 2017. [Online]. Available: http://dx.doi.org/10.1080/09500340.2016.1200684

[184] O. M. Hasan, M. Taha, and O. A. Sharkh, "Outage capacity and outage rate performance of mimo free-space optical system over strong turbulence channel," *Journal of Modern Optics*, vol. 63, no. 11, pp. 1106–1114, 2016. [Online]. Available: http://dx.doi.org/10.1080/09500340.2015.1112440

[185] A. ArockiaBazilRaj and U. Darusalam, "Performance improvement of terrestrial free-space optical communications by mitigating the focal-spot wandering," *Journal of Modern Optics*, vol. 63, no. 21, pp. 2339–2347, 2016. [Online]. Available: http://dx.doi.org/10.1080/09500340.2016.1200684

[186] A. Shahpari, A. Abdalla, R. Ferreira, G. Parca, J. D. Reis, M. Lima, V. Carrozzo, G. T. Beleffi, and A. Teixeira, "Ultra-high-capacity passive optical network systems with free-space optical communications," *Fiber and Integrated Optics*, vol. 25, no. 11, pp. 149–162, July 2014.

[187] M. Mirhosseini, B. Rodenburg, M. Malik, and R. W. Boyd, "Free-space communication through turbulence: a comparison of plane-wave and orbital-angular-momentum encodings," *Journal of Modern Optics*, vol. 61, no. 1, pp. 43–48, 2014. [Online]. Available: http://dx.doi.org/10.1080/09500340.2013.834084

[188] H. E. Nistazakis and G. S. Tombras, "On the use of wavelength and time diversity in optical wireless communication systems over gamma–gamma turbulence channels," *Optics & Laser Technology*, vol. 44, no. 7, pp. 2088 – 2094, 2012. [Online]. Available: http://www.sciencedirect.com/science/article/pii/S0030399212001314

[189] M. Safari and M. Uysal, "Do we really need ostbcs for free-space optical communication with direct detection?" *IEEE Transactions on Wireless Communications*, vol. 7, no. 11, pp. 4445–4448, November 2008.

[190] E. J. Lee and V. W. S. Chan, "Part 1: optical communication over the clear turbulent atmospheric channel using diversity," *IEEE Journal on Selected Areas in Communications*, vol. 22, no. 9, pp. 1896–1906, Nov 2004.

[191] S. G. Wilson, M. Brandt-Pearce, Q. Cao, and M. Baedke, "Optical repetition mimo transmission with multipulse ppm," *IEEE Journal on Selected Areas in Communications*, vol. 23, no. 9, pp. 1901–1910, Sept 2005.

[192] H. G. Sandalidis, "Coded free-space optical links over strong turbulence and misalignment fading channels," *IEEE Transactions on Communications*, vol. 59, no. 3, pp. 669–674, March 2011.

[193] N. D. Chatzidiamantis, M. Uysal, T. A. Tsiftsis, and G. K. Karagiannidis, "Iterative near maximum-likelihood sequence detection for mimo optical wireless systems," *Journal of Lightwave Technology*, vol. 28, no. 7, pp. 1064–1070, April 2010.

[194] X. Zhu and J. M. Kahn, "Markov chain model in maximum-likelihood sequence detection for free-space optical communication through atmospheric turbulence channels," *IEEE Transactions on Communications*, vol. 51, no. 3, pp. 509–516, March 2003.

[195] X. Zhu, J. M. Kahn, and J. Wang, "Mitigation of turbulence-induced scintillation noise in free-space optical links using temporal-domain detection techniques," *IEEE Photonics Technology Letters*, vol. 15, no. 4, pp. 623–625, April 2003.

[196] F. Xu, A. Khalighi, P. Caussé, and S. Bourennane, "Channel coding and time-diversity for optical wireless links," *Opt. Express*, vol. 17, no. 2, pp. 872–887, Jan 2009. [Online]. Available: http://www.opticsexpress.org/abstract.cfm?URI=oe-17-2-872

[197] T. A. Tsiftsis, H. G. Sandalidis, G. K. Karagiannidis, and M. Uysal, "Optical wireless links with spatial diversity over strong atmospheric turbulence channels," *IEEE Transactions on Wireless Communications*, vol. 8, no. 2, pp. 951–957, Feb 2009.

[198] L. Yang, X. Gao, and M. S. Alouini, "Performance analysis of free-space optical communication systems with multiuser diversity over atmospheric turbulence channels," *IEEE Photonics Journal*, vol. 6, no. 2, pp. 1–17, April 2014.

[199] J. Choi and D. J. Love, "Bounds on eigenvalues of a spatial correlation matrix," *IEEE Communications Letters*, vol. 18, no. 8, pp. 1391–1394, Aug 2014.

[200] H. Lim, Y. Jang, and D. Yoon, "Bounds for eigenvalues of spatial correlation matrices with the exponential model in mimo systems," *IEEE Transactions on Wireless Communications*, vol. 16, no. 2, pp. 1196–1204, Feb 2017.

[201] S. L. Loyka, "Channel capacity of mimo architecture using the exponential correlation matrix," *IEEE Communications Letters*, vol. 5, no. 9, pp. 369–371, Sept 2001.

[202] S. M. Alamouti, "A simple transmit diversity technique for wireless communications," *IEEE Journal on Selected Areas in Communications*, vol. 16, no. 8, pp. 1451–1458, Oct 1998.

[203] I. A. Alimi, K. F. Akingbade, J. J. Popoola, and M. O. Kolawole, "A hybrid coding technique for efficient bandwidth usage in conformity with IEEE 802.11 WLAN Standard," *International Journal of Electrical and Computer Engineering (IJECE)*, vol. 3, no. 5, pp. 593–602, October 2013.

[204] I. A. Alimi, J. J. Popoola, K. F. Akingbade, and M. O. Kolawole, "Performance analysis of bit-error-rate and channel capacity of MIMO communication systems over multipath fading channels," *International Journal of Informatics and Communication Technology (IJ-ICT)*, vol. 2, no. 2, pp. 57–63, July 2013.

[205] S. F. Liu, P. Reviriego, and J. A. Maestro, "Efficient majority logic fault detection with difference-set codes for memory applications," *IEEE Transactions on Very Large Scale Integration (VLSI) Systems*, vol. 20, no. 1, pp. 148–156, Jan 2012.

[206] H. Liu, R. Liao, Z. Wei, Z. Hou, and Y. Qiao, "Ber analysis of a hybrid modulation scheme based on ppm and msk subcarrier intensity modulation," *IEEE Photonics Journal*, vol. 7, no. 4, pp. 1–10, Aug 2015.

[207] K. P. Peppas and C. K. Datsikas, "Average symbol error probability of general-order rectangular quadrature amplitude modulation of optical wireless communication systems over atmospheric turbulence channels," *IEEE/OSA Journal of Optical Communications and Networking*, vol. 2, no. 2, pp. 102–110, February 2010.

[208] M. Qin, L. Chen, and W. Wang, "Generalized selection multiuser scheduling for the MIMO FSO communication system and its performance analysis," *IEEE Photonics Journal*, vol. 8, no. 5, pp. 1–9, Oct 2016.

[209] S. Amin, P. N. Landin, P. Händel, and D. Rönnow, "Behavioral modeling and linearization of crosstalk and memory effects in RF MIMO transmitters," *IEEE Trans. on Mic. The. and Tech.*, vol. 62, no. 4, pp. 810–823, April 2014.

[210] A. M. Abdalla and J. Rodriguez, "A new table based modelling of 28nm fully depleted silicon-on insulator (FDSOI)," in *2016 13th Int. Conf. on SMACD*, June 2016, pp. 1–4.

[211] D. Sarrut and J. Vandemeulebroucke, "B-LUT: Fast and low memory B-spline image interpolation," *Computer Methods and Programs in Biomedicine*, vol. 99, no. 2, pp. 172 – 178, 2010.

[212] B. M. Adams, *et al., DAKOTA*, Sandia National Laboratory, 2014.

[213] J.-P. Berrut and L. N. Trefethen, "Barycentric Lagrange interpolation," *SIAM Review*, vol. 46, no. 3, pp. 501–517, 2004.

[214] P. Henrici, "Barycentric formulas for interpolating trigonometric polynomials and their conjugates," *Numerische Mathematik*, vol. 33, no. 2, pp. 225–234, 1979.

[215] Q. Zhao and B. Wang, "Lebesgue constant minimizing bivariate barycentric rational interpolation," *Int. Jour. on App. Maths & Info. Sci.*, vol. 8, no. 1, pp. 187–192, Oct. 2013.

[216] H. T. Nguyen, A. Cuyt, and O. S. Celis, "Shape control in multivariate barycentric rational interpolation," in *Proc. CP1281, ICNAAM 2010*, vol. 1, 2010, pp. 543–548.

[217] H. Prautzsch, W. Boehm, and M. Paluszny, *Bézier and B-Spline techniques, ser. mathematics and visualization.* Springer, 2002.

[218] K. Zhou, L. Zheng, and F. Lin, "Image enlargement using symmetric B-spline basis on closed periodic zone," in *IEEE Inter. Conf. on Int. Comp. and Int. Systems*, vol. 4, Nov 2009, pp. 59–62.

[219] A. Abdelhafiz, L. Behjat, F. M. Ghannouchi, M. Helaoui, and O. Hammi, "A high-performance complexity reduced behavioral model and digital predistorter for MIMO systems with crosstalk," *IEEE Trans. on Comm.*, vol. 64, no. 5, pp. 1996–2004, May 2016.

[220] D. Saffar, N. Boulejfen, F. M. Ghannouchi, A. Gharsallah, and M. Helaoui, "Behavioral modeling of mimo nonlinear systems with multivariable polynomials," *IEEE Transactions on Microwave Theory and Techniques*, vol. 59, no. 11, pp. 2994–3003, Nov 2011.

[221] T. Eriksson and F. Norden, "Memory vector quantization by power series expansion [in speech coding]," in *Speech Coding, 2002, IEEE Workshop Proceedings.*, Oct 2002, pp. 141–143.

[222] B. Said-Houari, *Power Series Solution*. Cham: Springer International Publishing, 2015, pp. 125–140. [Online]. Available: http://dx.doi.org/10.1007/978-3-319-25735-8_5

[223] T. H. Cormen, C. E. Leiserson, R. L. Rivest, and C. Stein, *Introduction to algorithms*, 3rd ed. The MIT Press, 2009.

[224] H. Beigi, *Fundamentals of speaker recognition*. Springer Publishing Company, Incorporated, 2011.

[225] I. A. Alimi, P. P. Monteiro, and A. L. Teixeira, "Analysis of multiuser mixed rf/fso relay networks for performance improvements in cloud computing-based radio access networks (cc-rans)," *Optics Communications*, vol. 402, pp. 653 – 661, 2017. [Online]. Available: http://www.sciencedirect.com/science/article/pii/S0030401817305734

[226] M. Uysal, C. Capsoni, Z. Ghassemlooy, A. Boucouvalas, and E. Udvary, *Optical Wireless Communications: An Emerging Technology*, ser. Signals and Communication Technology. Springer International Publishing, 2016.

[227] H. Dahrouj, A. Douik, F. Rayal, T. Y. Al-Naffouri, and M. S. Alouini, "Cost-effective hybrid RF/FSO backhaul solution for next generation wireless systems," *IEEE Wireless Communications*, vol. 22, no. 5, pp. 98–104, October 2015.

[228] J. Zhang, L. Dai, Y. Zhang, and Z. Wang, "Unified performance analysis of mixed radio frequency/free-space optical dual-hop transmission systems," *Journal of Lightwave Technology*, vol. 33, no. 11, pp. 2286–2293, June 2015.

[229] I. S. Ansari, F. Yilmaz, and M. S. Alouini, "Impact of pointing errors on the performance of mixed RF/FSO dual-hop transmission systems," *IEEE Wireless Communications Letters*, vol. 2, no. 3, pp. 351–354, June 2013.

[230] H. Shen, J. Wang, W. Xu, Y. Rong, and C. Zhao, "A worst-case robust MMSE transceiver design for nonregenerative MIMO relaying," *IEEE Transactions on Wireless Communications*, vol. 13, no. 2, pp. 695–709, February 2014.

[231] E. Lee, J. Park, D. Han, and G. Yoon, "Performance analysis of the asymmetric dual-hop relay transmission with mixed RF/FSO links," *IEEE Photonics Technology Letters*, vol. 23, no. 21, pp. 1642–1644, Nov 2011.

[232] M. I. Petkovic, A. M. Cvetkovic, G. T. Djordjevic, and G. K. Karagiannidis, "Partial relay selection with outdated channel state estimation in mixed RF/FSO systems," *Journal of Lightwave Technology*, vol. 33, no. 13, pp. 2860–2867, July 2015.

[233] G. T. Djordjevic, M. I. Petkovic, A. M. Cvetkovic, and G. K. Karagiannidis, "Mixed RF/FSO relaying with outdated channel state information," *IEEE Journal on Selected Areas in Communications*, vol. 33, no. 9, pp. 1935–1948, Sept 2015.

[234] A. Jurado-Navas, J. M. Garrido-Balsells, J. F. Paris, M. Castillo-Vázquez, and A. Puerta-Notario, "Impact of pointing errors on the performance of generalized atmospheric optical channels," *Opt. Express*, vol. 20, no. 11, pp. 12 550–12 562, May 2012.

[235] A. M. Salhab, F. S. Al-Qahtani, R. M. Radaydeh, S. A. Zummo, and H. Alnuweiri, "Power allocation and performance of multiuser mixed RF/FSO relay networks with opportunistic scheduling and outdated channel information," *Journal of Lightwave Technology*, vol. 34, no. 13, pp. 3259–3272, July 2016.

[236] A. H. A. El-Malek, A. M. Salhab, S. A. Zummo, and M. S. Alouini, "Effect of rf interference on the security-reliability tradeoff analysis of multiuser mixed rf/fso relay networks with power allocation," *Journal of Lightwave Technology*, vol. 35, no. 9, pp. 1490–1505, May 2017.

[237] F. S. Al-Qahtani, A. H. A. El-Malek, I. S. Ansari, R. M. Radaydeh, and S. A. Zummo, "Outage analysis of mixed underlay cognitive rf mimo and fso relaying with interference reduction," *IEEE Photonics Journal*, vol. 9, no. 2, pp. 1–22, April 2017.

[238] K. P. Peppas, "Performance evaluation of triple-branch gsc diversity receivers over generalized-k fading channels," *IEEE Communications Letters*, vol. 13, no. 11, pp. 829–831, November 2009.

[239] N. C. Sagias, D. A. Zogas, and G. K. Karagiannidis, "Selection diversity receivers over nonidentical weibull fading channels," *IEEE Transactions on Vehicular Technology*, vol. 54, no. 6, pp. 2146–2151, Nov 2005.

[240] I. Trigui, I. Mechmeche, S. Affes, and A. Stéphenne, "Capacity and error rate analysis of cognitive MIMO AF relaying systems," *IEEE Wireless Communications Letters*, vol. 3, no. 6, pp. 665–668, Dec 2014.

[241] R. Boluda-Ruiz, A. García-Zambrana, B. Castillo-Vázquez, and C. Castillo-Vázquez, "Ergodic capacity analysis of decode-and-forward relay-assisted FSO systems over alpha-mu fading channels considering pointing errors," *IEEE Photonics Journal*, vol. 8, no. 1, pp. 1–11, Feb 2016.

[242] T. S. Rappaport, S. Sun, R. Mayzus, H. Zhao, Y. Azar, K. Wang, G. N. Wong, J. K. Schulz, M. Samimi, and F. Gutierrez, "Millimeter wave mobile communications for 5G cellular: It will work!" *IEEE Access*, vol. 1, pp. 335–349, 2013.

[243] J. G. Andrews, S. Buzzi, W. Choi, S. V. Hanly, A. Lozano, A. C. K. Soong, and J. C. Zhang, "What will 5G be?" *IEEE Journal on Selected Areas in Communications*, vol. 32, no. 6, pp. 1065–1082, June 2014.

[244] H. Mehrpouyan, M. R. Khanzadi, M. Matthaiou, A. M. Sayeed, R. Schober, and Y. Hua, "Improving bandwidth efficiency in E-band communication systems," *IEEE Communications Magazine*, vol. 52, no. 3, pp. 121–128, March 2014.

[245] K. Wakamori, K. Kazaura, and I. Oka, "Experiment on regional broadband network using free-space-optical communication systems," *Journal of Lightwave Technology*, vol. 25, no. 11, pp. 3265–3273, Nov 2007.

[246] A. Sousa, A. Shahpari, V. Ribeiro, M. Lima, and A. Teixeira, "Gigabit passive optical networks and CATV over hybrid bidirectional free space optics +20 km single mode fiber," *Microwave and Optical Technology Letters*, vol. 57, no. 12, pp. 2867–2871, 2015.

[247] A. Mostafa and S. Hranilovic, "Channel measurement and Markov modeling of an urban free-space optical link," *IEEE/OSA Journal of Optical Communications and Networking*, vol. 4, no. 10, pp. 836–846, Oct 2012.

[248] G. Parca, A. Shahpari, V. Carrozzo, G. M. Tosi Beleffi, and A. L. J. Teixeira, "Optical wireless transmission at 1.6-Tbit/s (16 × 100Gbit/s) for next-generation convergent urban infrastructures," *Optical Engineering*, vol. 52, no. 11, pp. 116 102–116 102, 2013. [Online]. Available: http://dx.doi.org/10.1117/1.OE.52.11.116102

[249] C. B. Naila, A. Bekkali, K. Wakamori, and M. Matsumoto, "Performance analysis of CDMA-based wireless services transmission over a turbulent RF-on-FSO channel," *IEEE/OSA Journal of Optical Communications and Networking*, vol. 3, no. 5, pp. 475–486, May 2011.

[250] H. E. Nistazakis, G. S. Tombras, A. D. Tsigopoulos, E. A. Karagianni, and M. E. Fafalios, "Capacity estimation of optical wireless communication systems over moderate to strong turbulence channels," *Journal of Communications and Networks*, vol. 11, no. 4, pp. 384–389, Aug 2009.

[251] M. A. Esmail, H. Fathallah, and M. S. Alouini, "Outdoor fso communications under fog: Attenuation modeling and performance evaluation," *IEEE Photonics Journal*, vol. 8, no. 4, pp. 1–22, Aug 2016.

[252] W. O. Popoola and Z. Ghassemlooy, "BPSK subcarrier intensity modulated free-space optical communications in atmospheric turbulence," *Journal of Lightwave Technology*, vol. 27, no. 8, pp. 967–973, April 2009.

[253] B. Epple, "Simplified channel model for simulation of free-space optical communications," *IEEE/OSA Journal of Optical Communications and Networking*, vol. 2, no. 5, pp. 293–304, May 2010.

[254] A. Mansour, R. Mesleh, and M. Abaza, "New challenges in wireless and free space optical communications," *Optics and Lasers in Engineering*, pp. –, 2016. [Online]. Available: http://www.sciencedirect.com/science/article/pii/S0143816616300252

[255] D. A. Luong and A. T. Pham, "Average capacity of MIMO free-space optical gamma-gamma fading channel," in *2014 IEEE International Conference on Communications (ICC)*, June 2014, pp. 3354–3358.

[256] P. Kaur, V. K. Jain, and S. Kar, "Capacity of free space optical links with spatial diversity and aperture averaging," in *Communications (QBSC), 2014 27th Biennial Symposium on*, June 2014, pp. 14–18.

[257] H. AlQuwaiee, I. S. Ansari, and M. S. Alouini, "On the performance of free-space optical communication systems over double generalized gamma channel," *IEEE Journal on Selected Areas in Communications*, vol. 33, no. 9, pp. 1829–1840, Sept 2015.

[258] M. Cao, H. Wang, K. Jia, and L. Hou, "Free space optical communication based on VBLAST," in *2010 Symposium on Photonics and Optoelectronics*, June 2010, pp. 1–4.

[259] H. E. Nistazakis, E. A. Karagianni, A. D. Tsigopoulos, M. E. Fafalios, and G. S. Tombras, "Average capacity of optical wireless communication systems over atmospheric turbulence channels," *Journal of Lightwave Technology*, vol. 27, no. 8, pp. 974–979, April 2009.

[260] L. Yang, J. Cheng, and J. F. Holzman, "Maximum likelihood estimation of the Lognormal-Rician FSO channel model," *IEEE Photonics Technology Letters*, vol. 27, no. 15, pp. 1656–1659, Aug 2015.

[261] F. S. Vetelino, C. Young, L. Andrews, and J. Recolons, "Aperture averaging effects on the probability density of irradiance fluctuations in moderate-to-strong turbulence," *Appl. Opt.*, vol. 46, no. 11, pp. 2099–2108, Apr 2007. [Online]. Available: http://ao.osa.org/abstract.cfm?URI=ao-46-11-2099

[262] A. Khatoon, W. G. Cowley, and N. Letzepis, "Channel measurement and estimation for free space optical communications," in *2011 Australian Communications Theory Workshop*, Jan 2011, pp. 112–117.

[263] F. S. Marzano, S. Mori, F. Frezza, P. Nocito, G. M. T. Beleffi, G. Incerti, E. Restuccia, and F. Consalvi, "Free-space optical high-speed link in the urban area of southern rome: Preliminary experimental set up and channel modelling," in *Proceedings of the 5th European Conference on Antennas and Propagation (EUCAP)*, April 2011, pp. 2737–2741.

[264] K. H. Kim, T. Higashino, K. Tsukamoto, and S. Komaki, "Optical fading analysis considering spectrum of optical scintillation in terrestrial free-space optical channel," in *2011 International Conference on Space Optical Systems and Applications (ICSOS)*, May 2011, pp. 58–66.

[265] R. M. Ferreira, A. Shahpari, J. D. Reis, and A. L. Teixeira, "Coherent UDWDM-PON with dual-polarization transceivers in real-time," *In Press, IEEE Photonics Technology Letters*, vol. 99, no. 1, June 2017.